

# **Molecular mechanisms controlling innate responses to injuries in plants**

**A thesis**

**Submitted in partial fulfilment of the requirements**

**of the degree of**

**Doctor of Philosophy**

**by**

**Anju P S**

**20213132**



**INDIAN INSTITUTE OF SCIENCE EDUCATION AND RESEARCH PUNE**

**2023**

*I dedicate this thesis to my parents*

## Declaration

I declare that this written submission represents my ideas in my own words and where others' ideas have been included, I have adequately cited and referenced the original sources. I also declare that I have adhered to all principles of academic honesty and integrity and have not misrepresented or fabricated or falsified any idea/data/fact/source in my submission. I understand that violation of the above will be cause for disciplinary action by the Institute and can also evoke penal action from the sources which have thus not been properly cited or from whom proper permission has not been taken when needed.

Place: IISER Pune

Date: 19<sup>th</sup> June 2023



Anju P S

20213132

## Certificate

Certified that the work incorporated in the thesis entitled “**Molecular mechanisms controlling innate responses to injuries in plants**” submitted by **Anju P S** was carried out by the candidate under my supervision. The work presented here or any part of it has not been included in any other thesis submitted previously for the award of any degree or diploma from any other University or institution.

Place: IISER Pune

Date: 19<sup>th</sup> June 2023



Dr Kalika Prasad

(Thesis supervisor)

## Copyright Statement

Parts of the data and the text presented in this thesis have been adapted from publications authored by Anju P Shanmukhan (given below). In every case, the representation is in compliance with the copyright policy and with prior permission from the publishers.

1. Shanmukhan, A. P., Mathew, M. M., Radhakrishnan, D., Aiyaz, M., & Prasad, K. (2020). Regrowing the damaged or lost body parts. *Current opinion in plant biology*, 53, 117-127.
2. Radhakrishnan, D., Shanmukhan, A. P., Kareem, A., Mathew, M. M., Varaparambathu, V., Aiyaz, M. & Prasad, K. (2021). Age, Wound Size and Position of Injury–Dependent Vascular Regeneration Assay in Growing Leaves. *Bio-protocol*, 11(9), e4010-e4010.
3. Radhakrishnan, D., Shanmukhan, A. P., Kareem, A., Aiyaz, M., Varapparambathu, V., Toms, A., Kerstens, M., Valsakumar, D., Landge, A. N., Shaji, A., Mathew, M. K., Sawchuk, M. G., Scarpella, E., Krizek, B. A., Efroni, I., Mähönen, A. P., Willemsen, V., Scheres, B., & Prasad, K. (2020). A coherent feed-forward loop drives vascular regeneration in damaged aerial organs of plants growing in a normal developmental context. *Development*, 147(6), 1–10. [Creative Commons Attribution License (CC BY)]
4. Shanmukhan, A. P., Mathew, M. M., Aiyaz, M., Varaparambathu, V., Kareem, A., Radhakrishnan, D., & Prasad, K. (2021). Regulation of touch-stimulated *de novo* root regeneration from Arabidopsis leaves. *Plant Physiology*, 187(1), 52-58.
5. Varapparambath, V., Mathew, M.M., Shanmukhan, A.P., Radhakrishnan, D., Kareem, A., Verma, S., Ramalho, J.J., Manoj, B., Vellandath, A.R., Aiyaz, M., Radha, R.K., Landge, A.N., Mahonen, A.P., Heisler, M.G., Weijers, D., Prasad, K. (2022). Mechanical conflict caused by a cell-wall-loosening enzyme activates *de novo* shoot regeneration. *Developmental Cell*, 57(17), pp.2063-2080.

### Research publications out of thesis work

1. **Shanmukhan, A. P.**, Mathew, M. M., Radhakrishnan, D., Aiyaz, M., & Prasad, K. (2020). Regrowing the damaged or lost body parts. *Current opinion in plant biology*, 53, 117-127.
2. Radhakrishnan, D.\*, **Shanmukhan, A. P.\***, Kareem, A., Aiyaz, M., Varapparambathu, V., Toms, A., Kerstens, M., Valsakumar, D., Landge, A. N., Shaji, A., Mathew, M. K., Sawchuk, M. G., Scarpella, E., Krizek, B. A., Efroni, I., Mähönen, A. P., Willemsen, V., Scheres, B., & Prasad, K. (2020). A coherent feed-forward loop drives vascular regeneration in damaged aerial organs of plants growing in a normal developmental context. *Development*, 147(6), 1–10. \*Equal contribution.  
[Featured on the cover of the journal, Editor’s pick for the summary and highlight of the issue, selected for highlight by *Plantae.org* (American Society of Plant Biologists)]
3. Radhakrishnan, D.\*, **Shanmukhan, A. P.\***, Kareem, A., Mathew, M. M., Varapparambathu, V., Aiyaz, M. & Prasad, K. (2021). Age, Wound Size and Position of Injury–Dependent Vascular Regeneration Assay in Growing Leaves. *Bio-protocol*, 11(9), e4010-e4010. \*Equal contribution
4. **Shanmukhan, A. P.**, Mathew, M. M., Aiyaz, M., Varapparambathu, V., Kareem, A., Radhakrishnan, D., & Prasad, K. (2021). Regulation of touch-stimulated *de novo* root regeneration from *Arabidopsis* leaves. *Plant Physiology*, 187(1), 52-58.  
[Selected as *Plant Physiology Article of the Week* by American Society of Plant Biologists (ASPB), selected as *Spotlight Author of the Week* selected by ASPB, selected for highlight by *Plantae.org* ASPB]
5. Varapparambath, V.\*, Mathew, M.M.\*, **Shanmukhan, A.P.\***, Radhakrishnan, D., Kareem, A., Verma, S., Ramalho, J.J., Manoj, B., Vellandath, A.R., Aiyaz, M., Radha, R.K., Landge, A.N., Mahonen, A.P., Heisler, M.G., Weijers, D., Prasad, K. (2022). Mechanical conflict caused by a cell-wall-loosening enzyme activates *de novo* shoot regeneration. *Developmental Cell*, 57(17), pp.2063-2080. \* Equal contribution  
[Featured Article, Featured on Cover Page, highlighted in Preview: Shoot meristem progenitors emerge from mechanical heterogeneities <https://doi.org/10.1016/j.devcel.2022.08.004> (Hamant, 2022), highlighted in Faculty Opinions: <https://facultyopinions.com/article/74229178>]
6. Mathew, M. M.\*, **Shanmukhan, A. P.\***, Varapparambath, V.\*, & Prasad, K. (2023). Protocol for real-time imaging, polar protein quantification, and targeted laser ablation of regenerating shoot progenitors in *Arabidopsis*. STAR protocols, 4(2), 102184.  
\* Equal contribution

## Acknowledgements

I am deeply grateful for all the experiences I had during the course of my Ph.D. I am thankful for my supervisor Dr Kalika Prasad for giving me an opportunity to work in his lab and explore interesting research questions. He gave me the opportunity to be a part of different projects, which helped me to appreciate each of them. He always encouraged me to ask, explore and think differently. His unwavering passion for research served as a constant source of inspiration for me, and I take pride in being his student. The trust he places in his students is admirable, which always helped me to perform at my best. He helped me to realise a lot more about myself personally and professionally. I have learned countless valuable lessons under his mentorship, often without even realizing it. Having the privilege to work in his lab for both my BSMS master project and PhD has been a rare and invaluable opportunity. I am grateful for his guidance.

I thank my Doctoral Committee members Dr Ravi Maruthachalam and Dr Jishy Varghese from IISER TVM and Research Advisory Committee members Dr Sunish Radhakrishnan and Dr Deepak Barua from IISER Pune for their valuable inputs and suggestions for my work.

I owe my sincere gratitude to our collaborators, Prof. Ben Scheres (Wageningen University, The Netherlands), Prof. Dolf Weijers (Wageningen University, The Netherlands), Prof. Ari Pekka Mähönen (University of Helsinki, Finland), Dr. Marcus Heisler (University of Sydney, Australia), Dr. Viola Willemsen (Wageningen University, The Netherlands), Prof. Anil Shaji (IISER-TVM), Dr. Enrico Scarpella (University of Alberta, Canada), Dr. Idan Efroni (Hebrew University of Jerusalem) and Prof. Ikram Blilou (King Abdullah University of Science and Technology) for their valuable contributions.

During my BSMS master's project in IISER TVM, I had the privilege to work with Dr. Kareem, the senior most PhD student in the lab. His guidance was invaluable during my final year of BSMS. I thank my senior Dr Kavya Durgaprasad, I admire the way she meticulously approach her work and the excitement in explaining her work. I am glad that I could help her in her manuscript preparation and I enjoyed drawing illustrations for her work. I am thankful to Dr Dhanya, who was my senior PhD, Master's project guide, friend and elder sister. I appreciate her for always being there to offer support whenever I needed it. I am glad that I

met Dr Mohammed Aiyaz, who is a postdoc in lab. I am happy that I worked with him for different projects, he is my colleague, guardian, travel companion and many more. I also want to acknowledge Vijina, who joined the lab for her PhD around the same time as me. Our mutual support throughout our journeys has been invaluable. She has been an exceptional friend and even a nurturing parental figure at times. I am grateful for the comfort and companionship we shared. I am grateful for the opportunity to work with Vijina and Mabel as well. I want to express my appreciation to Mabel, for being a wonderful junior, though we didn't had any distinction like that. It was a joy working with both of them and I cherish the memories we had together.

I extend my thanks to Abhijith, Raji, and Aanchal, who were JRFs in the lab, for their contributions. Additionally, I want to acknowledge all the BSMS students from IISER TVM and other project students who worked in the lab, including Madhujha, Vignesh, Kiran, Bejoy, Khaganshu, Archana, Hemamshu, Aswathy, Aleesha, Sandra, Midhun, Malavika and Parvathy. They are like my own children, and their presence made my time in the lab truly enjoyable. Being part of this team was a true blessing, and each individual played a role in making my experience in the lab enjoyable.

Our 'MGPB lab' was more than just a laboratory; it was a family. We stood together and worked as a team, and I cherish every moment we shared. Words cannot adequately express my gratitude to each of them. I also want to give special credit to Kalika for selecting the right people for the lab and his special way of mentoring created a bond between each of us. Although I didn't interact much, I am thankful to all the lab members in IISER Pune, including Akansha, Srijan, Ankita, Yamini, Saket, Yadhu, Shruti, and Harish. I am proud to be a part of this incredible team. I am happy that I could mentor Yamini for the vascular regeneration project. I appreciate her hardwork and the excitement to learn.

I extend my gratitude to the staff members at both IISER TVM and IISER Pune, including Sarika, Divya, Sandhya, Jijith, Naveen, Beena, Anil, Sayalee, Tushar, Ranjan, Swapnil, Sneha and Nayana, for their assistance. Their support has been invaluable. I would also like to thank my PhD batch mates and friends at IISER TVM, Anu, Sreelakshmi, Reshma, and Swetha, for their constant check-ins and support. Their friendship has made my journey more enjoyable.

I am thankful to CSIR for providing funding throughout my PhD, enabling me to pursue my research. I also express my gratitude to IISER TVM and IISER Pune for providing the necessary infrastructure and facilities that have been essential to my work.

As part of a collaboration, I had the opportunity to work in Ikram Blilou's lab at KAUST, Saudi Arabia for a few months. I am sincerely grateful to Ikram for treating me like her own daughter and extending a warm welcome to me. I am thankful for the excellent facilities and support provided for my work. I would like to express my gratitude to all the lab members I had the pleasure of meeting there, including Hemanshu, Shyam, Louai, Paula, Wouter, Tingting, Vinicius, Pepjin, Sunny, Gwen, Trang, Yasha, Tatiana, Catalina, and Jesse. Our time working in the lab, engaging in discussions, the lab trips we had, the iftar party, snorkeling adventures, and the night trips to Jeddah - all of these experiences were truly beautiful, and I am thankful for them.

I would also like to thank Naganand from Heribert Hirt's lab for assisting me with protein work. I have a great admiration for him as a person. Additionally, I express my gratitude to other lab members, including Prabhu, Sunitha, Waad, and Wiam. I am particularly thankful to Suja, a staff member, and her family for inviting me to their home and treating me delicious food. I am grateful for my housemates Elisabeth, May, Alexandra, and Lujaen, who made my stay abroad comfortable. I am especially thankful to May, for being an inspiration. I am glad that I met her. I am delighted to have made new friends during my time there, including Catalina, Elisabeth, Jesse, Waad, Somnath, Sunitha, Senzeni, Reshmi, Arto, Aadil, Monse, Abraham, Abdullah, Cesar, Camelo, Ted and Ahmed. I thank each and every one of them for their contribution to making my experience abroad enjoyable and for inspiring me to explore new things.

I am immensely grateful for Aleena, a friend I had the pleasure of meeting during my BSMS at IISER TVM. She is the coolest, sweetest and kindest person I ever met. I deeply admire her ability to find joy in the little things in life. She is truly one of the most precious gifts I have received, and I will forever cherish our friendship. I would also like to extend my gratitude to all my other friends, Sreelakshmi, Preethi, Lakshmy, Mahima, Anjana, Aswathi, Sujaya, Rutika, Shuhaib, Renil, Sreeja, Sumi, Arya, Anjali, Sheetal, Anand, Shivani, Ushma, and Archana. I apologize if I have unintentionally missed anyone's name. Each of them has played a significant role in my life, and I am thankful for their presence and friendship.

Lastly, I would like to sincerely thank my parents and my sister for their unwavering support, constant motivation, and inspiration. They have been by my side throughout my journey of pursuing my dreams and always supported my adventures. Their presence has been a source of strength for me, and I consider myself extremely fortunate to have them in my life. Overall, my PhD experience was enriched by the incredible people I met, and I am grateful to each and every one of them for their contributions.

**Anju P S**

## Synopsis

### Introduction

All multicellular organisms experience various kinds of injuries during their growth. Repair and regrowth of lost body parts is a general phenomenon across the kingdoms. Interestingly, some organisms can regenerate their lost body organs. Some notable examples are limb regeneration in Axolotl<sup>1</sup>, head and tail regeneration in Planaria<sup>2</sup>, head regeneration in *Hydra*<sup>3,4</sup> and root tip regeneration in *Arabidopsis*<sup>5</sup>. In animals, the repair mechanisms are lineage-specific, whereas, in plants, it is a universal phenomenon. Unlike animals, plants do not have specialised cells that can be recruited towards the site of injury as cell migration is not possible. Moreover, due to their sessile nature, they cannot escape from predators like mobile animals. Even with all these constraints, they display remarkable regeneration potential, ranging from single cell to whole organ regeneration<sup>5,6</sup>. This can be attributed to their remarkable developmental plasticity. They respond to various biotic and abiotic insults by healing or regrowing the damaged parts. It helps them to survive harsh environmental conditions and pathogens. Their ability to adapt and respond to abiotic and biotic factors to revive tissues and lost organs are widely exploited for various agricultural purposes. My work focuses on probing the mechanisms regulating innate regeneration responses to mechanical injuries in plants.

The main objectives of the thesis are:

1. To understand mechanism of tissue repair and regeneration in aerial organs of a growing plant.
2. Identification of key regulator for distinct regeneration response in a detached leaf.
3. To understand role of polar auxin transport mediated differential auxin distribution during *de novo* shoot regeneration.

### Contents of the thesis

#### Chapter 1

In their natural environment, plants are constantly exposed to multiple damages from biotic and abiotic stress factors. They repair these damages by local wound healing or organ regeneration. Unattended injuries can affect growth and survival of plants<sup>7,8</sup>. They exhibit remarkable regeneration capacity<sup>9</sup>. Upon mechanical injury, they undergo a series of processes such as wound perception, signalling, gene activation, cellular reprogramming and, wound

healing and tissue or organ restoration<sup>10</sup>. Innate regeneration responses can occur in a growing plant or in a detached organ of the plant<sup>9,11-14</sup>. Apart from the innate responses, plants can also respond to external hormonal conditions for *de novo* organogenesis<sup>15-18</sup>. In this chapter entitled '*Introduction*', I provide an overview of different natural regeneration responses upon injury exhibited in a growing plant and detached leaves as well as tissue culture mediated *de novo* shoot regeneration.

## **Chapter 2**

The second chapter of the thesis is titled: '*An assay to study tissue regeneration in growing leaves: Factors influencing vascular regeneration in leaves*'. In this chapter, I describe a novel vascular regeneration assay that was developed to investigate the regenerative responses occurring in the above-ground organs of plants. This assay is easy to learn and can be quickly executed using young growing seedlings. It allows to examine how plants naturally respond to injuries during their normal growth process. In this assay, an injury disconnecting the midvein of a leaf is created, which disrupts the transport of essential components, including photosynthates, necessary for plant growth. Following the injury, vascular strand is regenerated around the injured site, forming a D-shaped loop, reuniting the disconnected parental strand. The assay involves inducing injury in the vascular tissue of a leaf while the plant is actively growing. The vascular regeneration in leaves is influenced by several factors, including the size of the wound, the age of the plant, the location of the injury, and environmental conditions such as light availability. This chapter provides a comprehensive methodology detailing how to perform the vascular regeneration assay and discusses the various factors that influence the efficiency of regeneration. By utilizing this assay, researchers can effectively investigate tissue repair responses in growing plants, thereby expanding our understanding of plant regenerative processes.

## **Chapter 3**

The third chapter of the thesis is titled: '*A functionally conserved regulatory module confers universal regeneration potential to plants in response to mechanical injuries*'. In the work described in this chapter, I mimicked multiple injuries in plants that are likely to encounter during their growth, such as injuries in stem, leaves and excised explants. These injuries often disrupted the vascular tissue of stem and leaves. While the ability to regenerate vascular tissue in the wounded stem is known for a long, it was believed that injured leaves cannot repair the wound. Contrary to this notion, I find that local injuries in growing leaves can be repaired

without any support from artificial culture conditions. Through the study, a feed-forward loop involving two distinct plant-specific transcription factors *PLETHORA (PLT)* and *CUP SHAPED COTYLEDON 2 (CUC2)* was discovered. These transcription factors work coherently to enhance the production of auxin, in the vicinity of the wound by activating the auxin biosynthesis gene *YUCCA4 (YUC4)*. This localized hormonal environment establishes cell polarity and provides guidance for the reconnection of physically disconnected veins. Notably, the *PLT-CUC2* regulatory module is essential for vascular regeneration but is not involved in vein formation during normal developmental processes. Thus, this study differentiates tissue regeneration from the normal developmental program. This work not only expands our understanding of plant regenerative capabilities but also distinguishes the mechanisms involved in tissue regeneration from those governing normal development.

#### **Chapter 4**

The fourth chapter of the thesis is titled: '*Regulation of contact-stimulated de novo root regeneration from detached leaves*'. Unlike leaves growing in a normal developmental context, leaves detached from their plant body show a completely distinct regeneration response. The cut end of the leaf can either heal the wound by local cell proliferation or can regenerate a completely new organ such as the root. This largely depends on whether the cut end of a leaf is in contact with the solid or liquid surface. My study shows that the level of auxin is high in the cut end of the leaf which is in contact with a surface with respect to the cut end not in contact with any surface. Additionally, I also found that the *PLT* genes play an important role in this contact dependent regeneration response. Overall, the findings suggest that *de novo* root regeneration relies on a contact-driven regulatory module mediated by PLT, which operates independently from previously known regenerative or developmental pathways regulated by PLT.

#### **Chapter 5**

The fifth chapter of the thesis is titled: '*CUC2 mediated regulation of PIN1 localization during de novo shoot regeneration*'. Tissue culture-mediated regeneration allows researchers to explore the development of organ systems from cells lacking positional information. In this study, the emergence of shoots from callus was found to be asynchronous, with different types of progenitors identified: productive and pseudo progenitors. Productive progenitors could develop into shoot meristems, while pseudo progenitors could not. The distribution of the PIN1 protein, involved in auxin transport, differed between these progenitor types. Productive

progenitors displayed polar localization of PIN1, aiding in the export of auxin and maintaining a minimum level necessary for shoot initiation. Disruption of this auxin minimum formation inhibited shoot regeneration. Cell polarity and auxin distribution were identified as crucial factors in *de novo* shoot meristem regeneration, emphasizing the need for auxin minimum foci for successful progenitor formation and outgrowth. Deviations in auxin or cytokinin levels during progenitor formation can negatively impact shoot regeneration. The absence of the shoot promoting factor CUC2 reduces the number of progenitors formed and disrupts cell polarity. CUC2 regulates cell polarity by controlling the expression of XTH9 (*XYLOGLUCAN ENDOTRANSGLUCOSYLASE / HYDROLASE*) in the cells surrounding the progenitors. Precise timing and location of XTH9 expression are crucial for successful progression of progenitor to shoot meristem formation. CUC2-XTH9 axis regulates localization pattern of PIN1 non-cell autonomously. These findings provide insights into the regulatory mechanisms involved in shoot regeneration, specifically PIN1 polarity maintenance, and shed light on molecular factors governing the process.

## Conclusions

The study elucidates the intricate molecular mechanisms underlying tissue repair and regeneration in plants. The findings highlight the interdependent roles of transcription factors PLT and CUC2, along with the auxin biosynthesis gene YUC4, in cellular reprogramming, vascular regeneration, and wound repair in growing aerial organs. The study demonstrates the importance of a coherent feed-forward loop involving PLT, CUC2, and YUC4 in creating an optimal hormonal environment for tissue regeneration. Additionally, my study reveals that physical contact with a solid or liquid surface is a critical factor influencing regenerative responses in detached leaves, with *de novo* root regeneration occurring when the cut end of a leaf is in contact with a surface, while callus formation occurs when there is no contact. The study also highlights the significance of PIN1 polarity and auxin distribution in shoot progenitors during *de novo* shoot meristem formation, emphasizing the role of cell polarity in the self-organization of shoot meristems. Furthermore, the study investigates the effects of cytokinin levels on shoot regeneration and explores the regulation of PIN1 polarity by the XTH9 gene, which is regulated by CUC2.

My study highlights important role of the PLT-CUC2 regulatory module in different regenerative processes. Collectively, this regulatory module plays a vital physiological function by controlling PIN1 polarization and auxin distribution, enabling the successful

regeneration of plant tissues in response to mechanical injury in growing aerial organs or tissue culture-mediated shoot regeneration. Overall, the research provides insights into the regulatory mechanisms underlying tissue repair and regeneration in plants, contributing to our understanding of plant developmental plasticity.

## References

- (1) Spallanzani, A. Reproductions of the Legs in the Aquatic Salamander. *Essay Anim. Reprod. Lond. Becket Hondt* **1769**, 68–82.
- (2) Newmark, P. A.; Alvarado, A. S. Regeneration in Planaria. *E LS* **2001**.
- (3) Hoffmeister, S.; Schaller, H. C. A New Biochemical Marker for Foot-Specific Cell Differentiation in Hydra. *Wilhelm Roux Arch. Dev. Biol.* **1985**, *194*, 453–461.
- (4) Reddy, P. C.; Gungi, A.; Unni, M. Cellular and Molecular Mechanisms of Hydra Regeneration. *Evo-Devo Non-Model Species Cell Dev. Biol.* **2019**, 259–290.
- (5) Sena, G.; Wang, X.; Liu, H.-Y.; Hofhuis, H.; Birnbaum, K. D. Organ Regeneration Does Not Require a Functional Stem Cell Niche in Plants. *Nature* **2009**, *457* (7233), 1150–1153.
- (6) Mironova, V.; Xu, J. A Single-Cell View of Tissue Regeneration in Plants. *Curr. Opin. Plant Biol.* **2019**, *52*, 149–154.
- (7) Hau-Hsuan Hwang; Manda Yu; Erh-Min Lai. Agrobacterium-Mediated Plant Transformation: Biology and Applications. *Arab. Book* **2017**, 2017 (15). <https://doi.org/10.1199/tab.0186>.
- (8) Radhakrishnan, D.; Shanmukhan, A. P.; Kareem, A.; Aiyaz, M.; Varapparambathu, V.; Toms, A.; Kerstens, M.; Valsakumar, D.; Landge, A. N.; Shaji, A. A Coherent Feed-Forward Loop Drives Vascular Regeneration in Damaged Aerial Organs of Plants Growing in a Normal Developmental Context. *Development* **2020**, *147* (6), dev185710.
- (9) Mathew, M. M.; Prasad, K. Model Systems for Regeneration: Arabidopsis. *Development* **2021**, *148* (6), dev195347.
- (10) Shanmukhan, A. P.; Mathew, M. M.; Radhakrishnan, D.; Aiyaz, M.; Prasad, K. Regrowing the Damaged or Lost Body Parts. *Curr. Opin. Plant Biol.* **2020**, *53*, 117–127.
- (11) Chen, X.; Qu, Y.; Sheng, L.; Liu, J.; Huang, H.; Xu, L. A Simple Method Suitable to Study de Novo Root Organogenesis. *Front. Plant Sci.* **2014**, *5*, 208.
- (12) Durgaprasad, K.; Roy, M. V.; Venugopal, A.; Kareem, A.; Raj, K.; Willemsen, V.; Mähönen, A. P.; Scheres, B.; Prasad, K. Gradient Expression of Transcription Factor Imposes a Boundary on Organ Regeneration Potential in Plants. *Cell Rep.* **2019**, *29* (2), 453–463. e3.
- (13) Marhava, P.; Hoermayer, L.; Yoshida, S.; Marhavý, P.; Benková, E.; Friml, J. Re-Activation of Stem Cell Pathways for Pattern Restoration in Plant Wound Healing. *Cell* **2019**, *177* (4), 957–969. e13.
- (14) Mazur, E.; Benková, E.; Friml, J. Vascular Cambium Regeneration and Vessel Formation in Wounded Inflorescence Stems of Arabidopsis. *Sci. Rep.* **2016**, *6* (1), 1–15.

- (15) Gordon, S. P.; Heisler, M. G.; Reddy, G. V.; Ohno, C.; Das, P.; Meyerowitz, E. M. Pattern Formation during de Novo Assembly of the Arabidopsis Shoot Meristem. **2007**.
- (16) Kareem, A.; Durgaprasad, K.; Sugimoto, K.; Du, Y.; Pulianmackal, A. J.; Trivedi, Z. B.; Abhayadev, P. V.; Pinon, V.; Meyerowitz, E. M.; Scheres, B. PLETHORA Genes Control Regeneration by a Two-Step Mechanism. *Curr. Biol.* **2015**, *25* (8), 1017–1030.
- (17) Radhakrishnan, D.; Kareem, A.; Durgaprasad, K.; Sreeraj, E.; Sugimoto, K.; Prasad, K. Shoot Regeneration: A Journey from Acquisition of Competence to Completion. *Curr. Opin. Plant Biol.* **2018**, *41*, 23–31.
- (18) SKOOG, F.; MILLER, C. O. Chemical Regulation of Growth and Organ Formation in Plant Tissues Cultured in Vitro. *Symp. Soc. Exp. Biol.* **1957**, *11*, 118–130.

## Contents

Declaration.....	3
Certificate.....	4
Copyright Statement .....	5
Research publications out of thesis work.....	6
Acknowledgements.....	7
Synopsis .....	11
Contents .....	17
List of figures.....	21
List of abbreviations .....	23
Abstract.....	25
1. Introduction.....	26
1.1 Introduction.....	27
1.2 Innate regeneration responses in plants .....	27
1.2.1 Wound perception and signalling.....	28
1.2.2 Gene activation and cellular reprogramming.....	29
1.2.3 Wound healing and tissue or organ restoration on growing plants.....	32
1.2.4 <i>De novo</i> root regeneration from detached leaf.....	38
1.3 Tissue culture-mediated regeneration .....	39
2. An assay to study tissue regeneration in growing leaves: Factors influencing vascular regeneration in leaves .....	41
2.1 Introduction.....	42
2.2 Materials and Methods.....	43
2.2.1 Growth conditions.....	43
2.2.2 Seed sterilization and plating .....	43
2.2.3 Leaf incision.....	44
2.2.4 Sample decolourisation and clearing .....	46
2.2.5 Slide preparation .....	47
2.2.6 Brightfield imaging .....	47
2.2.7 Dark treatment experiment .....	48
2.2.8 Data analysis .....	48
2.3 Results.....	48

2.3.1	Vascular regeneration assay in leaves.....	48
2.3.2	Vascular regeneration depends on size of the injury and the age of the leaf.....	50
2.3.3	Vascular regeneration depends on the position of injury.....	54
2.3.4	Role of light in vascular regeneration in leaves.....	56
2.4	Discussion.....	58
3.	A functionally conserved regulatory module confers universal regeneration potential to plants in response to mechanical injuries.....	60
3.1	Introduction.....	61
3.2	Materials and Methods.....	62
3.2.1	Plant Materials and molecular cloning .....	62
3.2.2	Growth conditions.....	62
3.2.3	Seed sterilization and plating .....	62
3.2.4	Regeneration assays .....	62
3.2.5	Microscopic Imaging .....	64
3.2.6	qRT – PCR.....	64
3.2.7	Luciferase assay.....	65
3.2.8	ChIP-qPCR Analysis. ....	65
3.2.9	Constructs for molecular cloning.....	66
3.2.10	Decolourisation and tissue clearing for imaging vascular tissues .....	66
3.2.11	Oligonucleotide primers used for cloning and qRT PCR (5' ->3') .....	67
3.2.12	Numerical simulations of vascular regeneration.....	68
3.3	Results.....	74
3.3.1	<i>PLT</i> genes respond dynamically to mechanical injuries.....	74
3.3.2	<i>PLT</i> is required to activate innate regenerative responses to injuries in aerial organs growing in a normal developmental-context .....	81
3.3.3	<i>PLT</i> displays developmental-context sensitivity in regulating local cell proliferation response only vs tissue or organ regeneration in response to injury.....	90
3.3.4	<i>PLT</i> is sufficient for cellular reprogramming and its function is conserved across plant species .....	91
3.3.5	<i>PLT</i> directly activates <i>CUC2</i> expression to repair wounds and regenerate vascular tissue .....	95
3.3.6	<i>PLT-CUC2</i> module-dependent cell polarization is key to vascular regeneration. ....	101
3.3.7	<i>PLT</i> and <i>CUC2</i> activate the transcription of local auxin biosynthesis gene in a feedforward loop to repair wound and drive vascular regeneration .....	107
3.3.8	Dynamic response of early vascular markers during leaf vein regeneration .....	117

3.4 Discussion.....	119
4. Regulation of contact-stimulated de novo root regeneration from detached leaves.....	124
4.1 Introduction.....	125
4.2 Materials and methods.....	125
4.2.1 Growth conditions.....	125
4.2.2 Seed sterilization and plating.....	126
4.2.3 <i>De novo</i> root regeneration assay.....	126
4.2.4 Split plate experiment.....	126
4.2.5 Leaf pressed into media experiment.....	126
4.2.6 Agar block experiment.....	127
4.2.7 DNRR in water and soil.....	127
4.2.8 Quantification of auxin levels.....	127
4.2.9 Real-Time quantitative PCR (RT-qPCR).....	127
4.2.10 Plant materials.....	128
4.2.11 Confocal and brightfield imaging.....	128
4.2.12 Statistical analysis.....	129
4.3 Results.....	129
4.3.1 Leaves show distinct regeneration responses from the cut end.....	129
4.3.2 Identification of factors involved in distinct regeneration response in detached leaf.....	130
4.3.3 Contact stimulated increase in auxin level at the cut end of the petiole.....	132
4.3.4 PLT3, PLT5 and PLT7 are necessary as well as sufficient for contact-mediated DNRR.....	134
4.4 Discussion.....	142
5. CUC2 mediated regulation of PIN1 localization during de novo shoot regeneration ...	144
5.1 Introduction.....	145
5.2 Materials and Methods.....	146
5.2.1 Plant materials.....	146
5.2.2 Plasmid construction and molecular cloning.....	146
5.2.3 Plant growth conditions.....	148
5.2.4 Microscopic live imaging.....	148
5.2.5 Regeneration assay.....	149
5.2.6 Estradiol treatment for live imaging and regeneration assay.....	149
5.2.7 PIN1 polarity quantification.....	150

5.2.8 Auxin quantification .....	150
5.2.9 Statistical analysis.....	151
5.3 Results.....	151
5.3.1 Two distinct shoot progenitors are formed in the callus upon shoot inductive cues .....	151
5.3.2 The localization pattern of polarity proteins correlates with <i>de novo</i> shoot meristem formation.....	153
5.3.3 Specific localization of PIN1 promotes differential pattern of auxin distribution in productive progenitors and its surrounding cells .....	155
5.3.4 Excess of auxin in the callus impairs <i>de novo</i> shoot regeneration.....	157
5.3.5 CUC2 is required for the maintenance of PIN1 polarity in shoot progenitors .....	159
5.3.6 CUC2 regulates <i>XTH9</i> for maintaining PIN1 polarity in progenitors .....	160
5.3.7 <i>XTH9</i> shows differential expression patterns in productive and pseudo progenitors .....	160
5.3.8 <i>XTH9</i> regulates PIN1 polarity non cell autonomously in productive progenitors	164
5.3.9 Influence of cytokinin in <i>de novo</i> shoot regeneration.....	166
5.4 Discussion.....	168
6. Conclusion .....	171
7. References.....	175

## List of figures

Figure 1.1 Schematic illustration of tissue injuries and signalling in plants .....	30
Figure 1.2 Schematic diagram representing regeneration of specific cell types and tissues in the root tip .....	33
Figure 1.3 Various degrees of regeneration potential along the organ axis.....	35
Figure 1.4 Schematic diagram displaying wound repair and vascular regeneration in growing stem and leaf .....	36
Figure 1.5 Distinct regeneration response in detached leaf .....	39
Figure 1.6 Schematic representation of tissue culture-mediated shoot regeneration.....	40
Figure 2.1 Images demonstrating the site of the leaf incision .....	45
Figure 3.1 Schematic of each cell with the variables and parameters appearing in the mathematical model.....	68
Figure 3.2 Formation of veins in a grid of 50 by 50 cells.....	71
Figure 3.3 Formation of veins when there is a small incision .....	72
Figure 3.4 Development of veins when there is a large incision .....	73
Figure 3.5 No vein like patterns are formed without feedback.....	74
Figure 3.6 <i>PLT7</i> gene is locally induced after mechanical injury in inflorescence stem .....	75
Figure 3.7 <i>PLT3</i> , <i>PLT5</i> and <i>PLT7</i> genes are upregulated in response to injury in leaves.....	77
Figure 3.8 <i>PLT5</i> and <i>PLT3</i> genes are locally induced after mechanical injury in inflorescence stem.....	78
Figure 3.9 <i>PLT</i> show dynamic expression in excised explants during wound healing .....	79
Figure 3.10 Root and shoot stem cell regulators are not activated upon injury in growing leaves and stem .....	80
Figure 3.11 <i>PLT</i> genes are required for wound healing and vascular regeneration in growing inflorescence stem.....	82
Figure 4.1 Wound healing response and contact-dependent <i>de novo</i> root regeneration at the cut end of a detached leaf.....	130
Figure 4.2 Response of detached leaves when placed on different surfaces .....	131
Figure 4.3 Contact-dependent differential auxin response near the cut ends of detached leaves .....	133
Figure 4.4 Quantification of auxin levels at the cut ends of detached leaves placed on MS-agar medium.....	134
Figure 4.5 <i>PLT7</i> expression pattern in the cut end of leaf petiole.....	135
Figure 4.6 Expression pattern of <i>PLT3</i> and <i>PLT5</i> in cut ends of detached leaves .....	136
Figure 4.7 <i>PLTs</i> are necessary and sufficient for contact-mediated DNRR from the cut end of the detached leaves .....	137

Figure 4.8 Expression pattern of PLT1, PLT2 and CUC2 in the cut ends of detached leaves .....	139
Figure 4.9 Expression pattern of YUC4 in the cut ends of detached leaves.....	141
Figure 4.10 Expression pattern PME5 in cut ends of detached leaves .....	141
Figure 5.1 Schematic representation of progressive development of PIN1 (green) marked shoot progenitor to make <i>de novo</i> shoot apical meristem (SAM) .....	146
Figure 5.2 Different stages of PIN1 marked shoot progenitors .....	152
Figure 5.3 Time lapse for productive and pseudo-productive progenitor .....	153
Figure 5.4 Quantitative and qualitative analysis of PIN1 polarity in productive progenitors and pseudo-progenitors .....	154
Figure 5.5 Response of auxin sensor R2D2 in productive and pseudo-progenitor .....	156
Figure 5.6 Schematic representation of the role of PIN1 localization pattern in regulating auxin distribution during <i>de novo</i> shoot regeneration.....	157
Figure 5.7 Overexpression of auxin biosynthesis gene <i>YUC4</i> in the callus can abolish <i>de novo</i> shoot regeneration.....	158
Figure 5.8 CUC2 influence maintenance of PIN1 polarity in shoot progenitors.....	160
Figure 5.9 Expression pattern of XTH9 in productive progenitors .....	162
Figure 5.10 Expression pattern of XTH9 in pseudo progenitors .....	163
Figure 5.11 Downregulation of XTH9 affect PIN1 polarity and progenitor development ...	165
Figure 5.12 Overexpression of XTH9 affect PIN1 polarity and progenitor development ....	166
Figure 5.13 Effect of modulation of cytokinin levels on <i>de novo</i> shoot regeneration (preliminary data).....	167

## List of abbreviations

ACT - ACTIN	ROS – Reactive oxygen species
ANAC - <i>Arabidopsis</i> NAC domain containing protein	ERF - ETHYLENE RESPONSE FACTOR
ANT - AINTEGUMENTA	Est - Estradiol
AP2 - APETALA2	g - gram
<i>At</i> - <i>Arabidopsis thaliana</i>	GFP - Green Fluorescent Protein
ATHB8	GLR - Glutamate Receptor-Like
BLJ - BLUEJAY	GR - Glucocorticoid Receptor
CBF3 - C-REPEAT BINDING FACTOR 3	H - Hour
CEI - Cortex-Endodermis Initial	HAMP - Herbivore Associated Molecular Patterning
ChIP - Chromatin Immuno-precipitation	Hz - Hertz
CHX - cycloheximide	IPT5 - ISOPENTENYLTRANSFERASE 5
CIM - Callus Inducing Medium	JA - jasmonic acid
CKX3 - CYTOKININ OXIDASE 3	JKD - JACKDAW
Col - Columbia	LAF- Laminar Air Flow
CUC - CUP-SHAPED COTYLEDON	LBD - LATERAL ORGAN BOUNDARIES DOMAIN
CWI - cell wall integrity	LEI - Lateral Root Cap/Epidermis Initial
CYC - CYCLIN	mg - milligram
D - Day	mL - milliliter
daa – days after abrasion	mm - Millimetre
DAMP - Damage Associated Molecular Patterning	MS - Murashige and Skoog medium
DEG - Differentially expressed genes	<i>Os</i> - <i>Oryza sativa</i>
Dex - dexamethasone	OHP - Overhead Projector
DEX - Dexamethasone	PAMP - Pathogen Associated Molecular Patterning
DNRR - <i>de novo</i> root regeneration	PI - Propidium Iodide
dpc - days post cut	PID - PINOID
dpg - days post germination	PIN - PINFORMED
dpi - days post incision	PLT - PLETHORA
DR5 - Auxin responsive promoter	PME - PECTIN METHYL ESTERASE
dsRNAi - double-stranded RNA interference	PXY - PHLOEM INTERCALATED WITH XYLEM
eATP - extracellular ATP	
R2D2 - Ratiometric version of 2 D2's	

QC - quiescent centre  
qRT-PCR - Quantitative Real-Time  
Polymerase Chain Reaction  
RAM - Root Apical Meristem  
RAP - RELATED TO APETALA  
RBR - RETINOBLASTOMA-RELATED  
rcf - relative centrifugal force  
RNAi - RNA interference  
RNAseq - RNA sequencing  
ROI - Region of Interest  
RIM - root induction medium  
s.e.m - standard error of mean  
SAM - Shoot Apical Meristem  
SCR - SCARECROW  
SHR - SHORTROOT  
SIM - Shoot Induction Medium  
SMB - SOMBRERO  
TDIF - TRACHEARY ELEMENT  
DIFFERENTIATION INHIBITORY  
FACTOR  
TZ - trans-Zeatin  
UTR - Untranslated region  
UV - Ultra Violet  
WIND - WOUND INDUCED  
DEDIFFERENTIATION  
WOX - WUSCHEL-RELATED  
HOMEobox  
WT - WT  
WUS - WUSCHEL  
XTH - Xyloglucan endo transglucosylase/  
hydrolase  
YFP - Yellow Fluorescent Protein  
YUC - YUCCA  
 $\mu\text{g}$  - microgram  
 $\mu\text{L}$  - Microliter  
 $\mu\text{m}$  - Micrometre

## Abstract

All multicellular organisms experience various kinds of injuries during their growth. Repair and regrowth of lost body parts is a general phenomenon across the kingdoms. In animals, the repair mechanisms are lineage-specific, whereas, in plants, it is a universal phenomenon. The regeneration potential of plants can be attributed to their remarkable developmental plasticity. They respond to various biotic and abiotic insults by healing or regrowing the damaged parts. My work focuses on probing the mechanisms regulating innate regeneration responses to mechanical injuries in growing plant organs. For this, I have used the regeneration of specific cell types in wounded leaves as a model.

Forty years ago, Tsvi Sachs, using his classical experiments using the aerial part of the stem, proposed the auxin canalization model for vein formation. How auxin is channelized and how local auxin accumulation repairs the loss remained elusive. While the ability to regenerate vascular tissue in the wounded stem is known for a long, it was believed that injured leaves cannot repair the wound. Contrary to this notion, I find that local injuries in growing leaves can be repaired without any support from artificial culture conditions. Vascular regeneration in leaves is highly sensitive to the size of the wound, the age of the plant, the position of injury and environmental conditions such as light. My studies led to the discovery of a feed-forward loop where genes encoding two distinct plant-specific transcription factors act coherently to increase local auxin production in the vicinity of the wound. This local hormonal environment sets up cell polarity and guides the path of reunion between physically disconnected veins. Interestingly, this regulatory module is required for vascular regeneration but not for vein formation during normal development.

My studies distinguish the mechanisms between tissue regeneration and its normal developmental program. Unlike leaves growing in a normal developmental context, leaves detached from their plant body show a completely distinct regeneration. The cut end of the leaf can either heal the wound by local cell proliferation or can regenerate a completely new organ such as the root. This largely depends on whether the cut end of a leaf is in contact with the solid or liquid surface. Together, my studies provide a mechanistic framework of wound healing and tissue repair in response to mechanical injuries in aerial organs of plants.

# *Chapter 1*

## **Introduction**

Based on publication:

**Shanmukhan, A. P.**, Mathew, M. M., Radhakrishnan, D., Aiyaz, M., & Prasad, K. (2020).

Regrowing the damaged or lost body parts. *Current opinion in plant biology*, 53, 117-127.

## 1.1 Introduction

Regeneration is the process of repairing or replacing damaged body parts. Although all organisms possess the ability to regenerate, the efficiency of regeneration varies among different organisms. Hydra can regrow from both fragments when cut in halves<sup>1</sup>. They can also self-assemble to form a patterned body from a group of cells<sup>2</sup>. Axolotl can regenerate almost all parts of the body<sup>3</sup>. Catfish, lizards, and lobsters regenerate by forming blastema, which then further develops the lost body part<sup>4-8</sup>. But the regeneration capacity is limited for complex organisms. In higher animals, including humans, when a part of the liver is removed, it can be restored to its original size<sup>9-11</sup>. A zebrafish can replace a damaged or lost fin<sup>12,13</sup>. Planaria can generate an entire body even from a small piece of tissue<sup>14</sup>. Plants display an extraordinary ability to produce a new plant from any tissue or a single cell when appropriate inductive cues are provided. They can revive tissues and organs lost or damaged in injury, such as the regeneration of root tip in *Arabidopsis thaliana*<sup>15</sup>. Unlike animals, plants do not have a specialized group of cells for repair process when they encounter an injury. Their exceptional regeneration capacity is attributed to their plasticity mechanisms. The plasticity mechanism includes physiological, developmental, cellular, and epigenetic responses<sup>16</sup>. This helps them to survive harsh environmental conditions and pathogens. Their ability to adapt and respond to abiotic and biotic factors to revive tissues and lost organs is widely exploited for various agricultural purposes. The regeneration responses in plants can be broadly divided into two - innate regeneration responses and tissue culture-mediated regeneration responses.

## 1.2 Innate regeneration responses in plants

Plants encounter severe environmental stress by either biotic factors such as pathogens, nematodes, and herbivores or abiotic factors such as strong winds, abrasions, breakage, and incisions (Figure 1.1A). Plants efficiently respond to injury and often restore the lost organ. Unlike animals, plants cannot recruit specialized stem cells from other parts of the body to aid in wound healing as cell migration is absent. Instead, cells in the vicinity of the wound show remarkable plasticity and get reprogrammed to meet the urgent demand of repair, essential for their survival as unattended open wounds can lead to infections and eventually death<sup>17</sup>. So how do plants mount a timely response and restore the damaged tissues? They use a combination of electrical<sup>18</sup>, chemical<sup>19</sup>, mechanical<sup>20</sup>, and positional cues<sup>21,22</sup>. Regeneration at the wounded region occurs either by complete organ restoration or by replacing a few cells by cell division and differentiation<sup>23,24</sup>. However, the mechanism underlying wound perception, repair, and

re patterning in the context of a growing plant is yet to be fully explored. The sequential events that occur in response to local damages in growing plants include wound perception, signalling, gene activation, cellular reprogramming followed by wound healing and tissue or organ restoration.

### **1.2.1 Wound perception and signalling**

Wounding is the primary trigger for regeneration in plants and animals. But how do they detect the wound? In animals, stretched skin is disrupted by a wound causing the skin to retract. This mechanical alteration of the environment contributes to the mechanotactic guiding of specialised cells to the wound site and orchestrates their differentiation eventually culminating in wound healing<sup>25</sup>. However, plants adopt different mechanisms as cell migration is absent owing to their rigid cell walls.

Wounding alters the cell wall integrity (CWI) of the cells in the vicinity. The perception of this altered CWI by stretch-activated mechano-sensitive channels on the plasma membrane is a key event during wound detection<sup>26,27</sup>. Since the damaged cells lose turgor pressure, cells adjoining the damaged cells experience a sudden imbalance in stress and loss of initial radial alignment of microtubules thereby changing their mechanical properties<sup>28</sup>. In addition, DAMPs (Damage Associated Molecular Patterning) such as extracellular ATP (eATP), oligo galacturonic fragments (OG), glutamate and sucrose, Pathogen derived PAMPs (Pathogen Associated Molecular Patterning) and herbivore-derived HAMPs (Herbivore Associated Molecular Patterning) are released from damaged cells<sup>29-31</sup>. Thus, the altered CWI altered mechanical properties of adjacent cells, and a sudden increase in the extracellular concentration of sucrose, DAMPs, PAMPs, and HAMPs indicate tissue disruption in the vicinity. These probably act as the distress signals emanating from the damaged cell, which upon perception by the neighbouring cells trigger a secondary signal directing wound response. A local injury often elicits two kinds of responses: systemic immune response and healing response. eATPs and OGs trigger  $\text{Ca}^{2+}$  influx and ROS (Reactive oxygen species) production respectively, indicating their perception as an early event in plant wound signalling<sup>30</sup>. Perception of glutamate by ion channels of Glutamate Receptor-Like (GLR) protein elicits defense signal propagation by altering the cytosolic  $\text{Ca}^{2+}$  concentration, wherein defense signals are propagated as electrical signals. Cytosolic  $\text{Ca}^{2+}$  concentration, ROS, and electrical signals contribute to the trio signalling that supports both local and systemic immune responses<sup>31,32</sup>. PAMPs and HAMPs stimulate wound-induced synthesis of jasmonic acid

(JA)<sup>33</sup> that translocates from the damaged to the undamaged region where, the perception and subsequent JA signalling activate defense response<sup>34</sup>. Thus, DAMPs, PAMPs, HAMPs, calcium, ROS, and JA are involved in signalling networks that initiate systemic immune responses upon wounding. In addition to immune responses, wound healing, and regeneration are also elicited upon local injury. Calcium on entry into the cell acts as a master regulator of wound healing. A study by wounding epithelial tissue of *Drosophila* pupae via pulsed laser ablation, reports two sequential waves of calcium spreading into the neighbouring cells<sup>35</sup>. The occurrence of a similar pattern of calcium dynamics in shoot apical meristem of *Arabidopsis* where local cell ablation resulted in a calcium spike at the immediate vicinity and calcium wave propagating away from the site of injury, suggests the possibility of convergence of signalling from different damage mechanisms such as single-cell damage and tissue damage, on increasing cytosolic Ca<sup>2+</sup> concentration to regulate wound healing (Figure 1.1B)<sup>36</sup>. Likely, the sustained calcium spike in the immediate vicinity of the wound contributes to proliferation responses while the propagating calcium wave contributes to the immune responses.

Thus in plants, a rapid influx of calcium into the cell via stretch-activated mechano-sensitive ion channels, as well as the DAMPs, PAMPs, and HAMPs could probably stimulate a downstream signalling cascade which can alter the molecular and hormonal environment in the cells adjacent to the wound. Such hormonal and molecular alterations instrumental in reprogramming the cells in response to wounding will be discussed in the subsequent sections.

### **1.2.2 Gene activation and cellular reprogramming**

Cells adjoining the wound probably experience an abrupt loss of communication from cells that lie on the side of the wound. The communication loss from one side could cause the genes to disengage from the ongoing developmental regulatory network and become readily available to respond to distress signals emanating from the nearby damaged cell. The distress signals are perceived by the cells in the vicinity of a wound within seconds of injury. However, it takes hours to initiate regeneration responses.

Understanding the delay between the wound perception and regeneration initiation remains fragmentary. One of the prime focuses of most of the recent studies is exploring the activation of a variety of genes and hormonal upregulation in response to wounding. However, the temporal order of hormonal surge and gene activation where one can be causal for the other needs to be resolved. A rise in activation of various genes including stem cell regulators

accompanied by hormonal surge was reported in several experiments using cell ablation and excision studies in plants<sup>15,37</sup>. Molecular mechanisms that bring about an increase in gene activation and hormones can be partly attributed to epigenetic modifications in their loci. For example, an elegant study that demonstrates root regeneration from the shoot, reports the key role of epigenetic regulators in facilitating the activation of a hub of genes upon injury where, the wound-induced transient surge in JA upregulates auxin biosynthesis gene *via* histone methylation<sup>38</sup>.

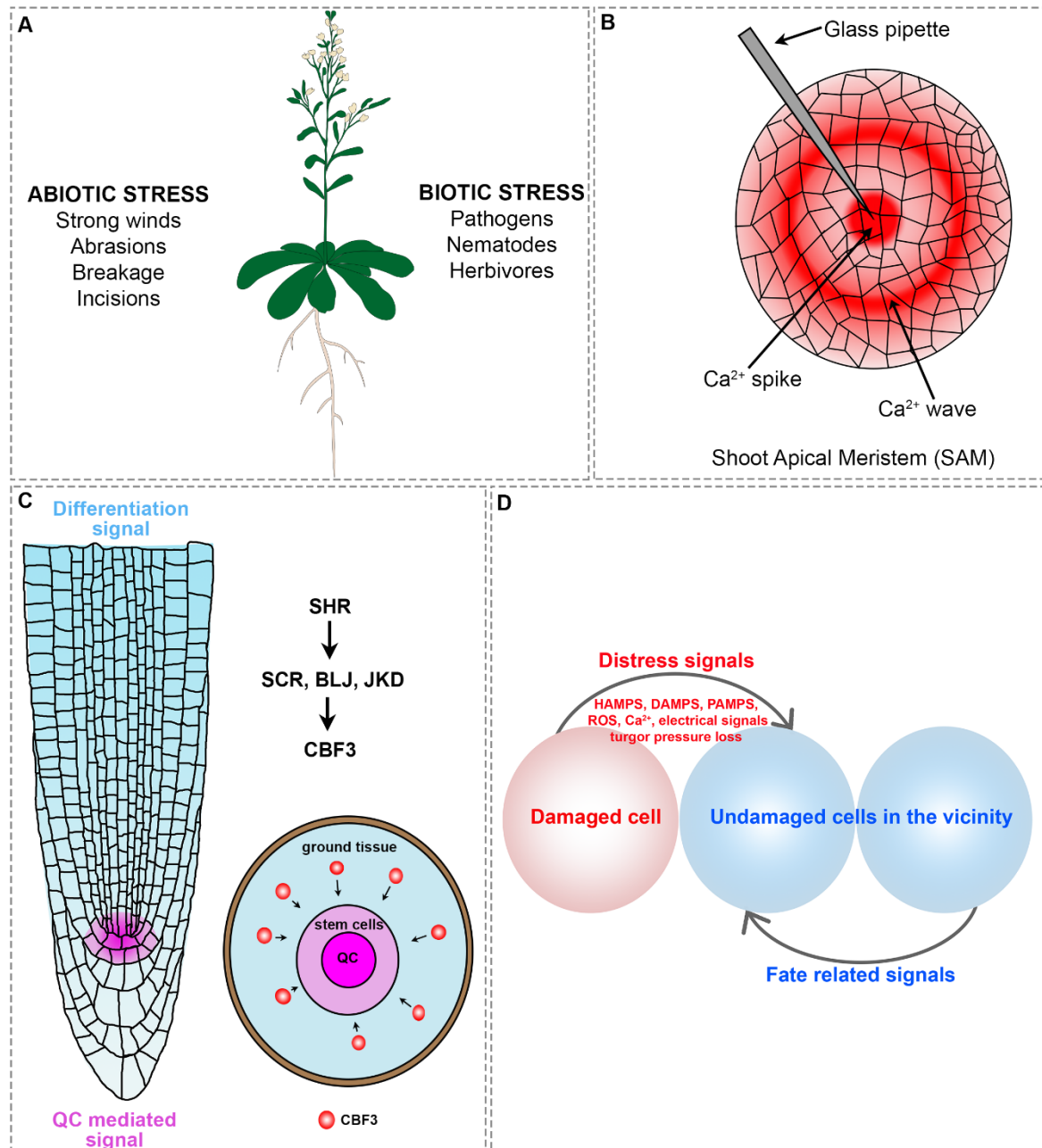


**Figure 1.1 Schematic illustration of tissue injuries and signalling in plants**

(A) Various biotic and abiotic factors inflict damage to aerial and underground plant parts during normal growth. (B) Local ablation of shoot apical meristem produces two kinds of calcium signals-

i)  $\text{Ca}^{2+}$  spike: cells in the immediate vicinity of the wound exhibit a surge in cytosolic  $\text{Ca}^{2+}$  ii)  $\text{Ca}^{2+}$  waves that are radiated away from damaged cells to undamaged cells<sup>36</sup>. (C) A growing root exhibits two kinds of positional signals. Differentiation signals released from mature cells of the root promote cell differentiation while the quiescent center (QC)-mediated signals inhibit differentiation-promoting signals<sup>39</sup>. Cross section of root showing ground tissue and stem cell niche where, transcription factor CBF3 moves out of ground tissue to maintain stem cell niche and to confer regeneration<sup>40</sup>. CBF3 is regulated by SCR, BLJ (BLUEJAY), and JKD (JACKDAW) which in turn are direct targets of SHR<sup>40,41</sup>. (D) Distress signals are released from damaged cells to the adjoining undamaged cells. These cells could also perceive fate-related signals from other neighbouring undamaged cells.

Laser ablation of root meristem cells indicates that a surge in auxin precedes the rise in gene activation. Laser ablation of quiescent center (QC) cells shifts the auxin response shootward during early hours post ablation and contributes to cell fate changes in adjoining cells *via* expression of root stem cell regulators *PLETHORA (PLT)*, *SHORTROOT (SHR)* and *SCARECROW(SCR)*<sup>37</sup>. Recent studies report the upregulation of stem cell regulators upon targeted ablation of cells of root meristem several hours post-ablation<sup>42</sup> suggesting that the initial rise in auxin promotes the build-up of root stem cell regulators after injury. However, whether the surge in auxin responses re-activates the cell fate determinants are yet to be established.

Root tip excision studies report an increase in auxin levels accompanied by activation of stem cell regulators in the neighbouring cells, but the temporal order of auxin surge and activation of stem cell regulators remain unknown<sup>15</sup>. Recent studies report a rapid accumulation of PLT2 near the cut site within a few hours, before any significant change in auxin response, while a higher auxin response by local auxin biosynthesis occurs relatively later, which drives root tip regeneration<sup>43,44</sup>. Corroborating with the fact that PLT2 activates local auxin biosynthesis gene *YUCCA3 (YUC3)* in the context of root development, it is likely that rapid burst of PLT2 builds up necessary auxin responses *via* local auxin biosynthesis in response to root tip excision<sup>45</sup>.

Very much in line with the role of PLT2 in root tip regeneration, other *PLTs (PLT3,5,7)* in shoot activates local auxin biosynthesis in a coherent feed-forward loop with *CUP SHAPED COTYLEDON 2 (CUC2)* thereby, contributing towards generating effective auxin response in wounded aerial organs<sup>46,47</sup>. Apart from a few studies, it remains unresolved whether the upregulation of hormones drives the surge in cell fate determinants or *vice versa* in other contexts of wound healing. Given ample evidence, it is highly unlikely that the interplay between hormones and cell fate determinants follows a linear relation. The mounting evidence during normal development suggests a regulatory feedback loop between the stem cell determinants and hormone responses in both aerial and underground organs. Presumably,

several such regulatory loops operate between the cell fate determinants and hormones upon injury, resulting in wound healing and organ regeneration.

### **1.2.3 Wound healing and tissue or organ restoration on growing plants**

Re-activation of a variety of genes in undamaged cells in the vicinity of the wound leads to regeneration. Depending on the nature of the injury and the context of damage, the regeneration responses are either confined to healing in the form of local cell proliferation or organ restoration. During normal plant development, the cell-to-cell communication in the growing organ directs its growth and patterning. For example, in the root, it is proposed that the QC signal inhibits the differentiation of contacting cells, while the positional signal for proper differentiation is conferred to them by more mature cells (Figure 1.1C)<sup>39</sup>. Such a signalling mechanism also operates in replacing damaged cells at the root tip<sup>21,39</sup>. Corroborating with this notion it can be proposed that distress signals from damaged cells reactivate the stem cell regulators in the contacting cells to trigger their proliferation and maintain them in an undifferentiated state whilst, neighbouring undamaged cells confer signals for differentiation (Figure 1.1D).

The displacement of QC towards the proximal part of root meristem upon QC ablation demonstrates the re-activation of root stem cell regulators (Figure 1.2B)<sup>37</sup>. In addition to QC, other injured cells of the root meristem can be replaced by positional cues emanating from the undamaged neighbouring cells<sup>21,39</sup>. Very much in line with these findings cell division by cells of inner cell files replaces ablated cells of outer cell files. This restorative cell division was highly compromised in mutants defective in stem cell maintenance (Figure 1.2C)<sup>42</sup>. A question arises whether injury-induced genes act autonomously or whether they can act non-cell autonomously as well during regeneration. Interestingly, a recent study shows that signals originate not only from QC but also from ground tissue wherein BIRD family genes regulate C-REPEAT BINDING FACTOR 3 (CBF3) which move out of the ground tissue and confer regeneration to stem cell niche (Figure 1.1C)<sup>40</sup>. Thus it is quite conceivable that pre-existing endogenous cue responds to injuries and drives the regeneration process.

What happens when part of an organ is lost in injury? Removal of root tip results in loss of stem cell niche. Interestingly, plants are capable of regenerating their missing root tip, suggesting a fully functional stem cell niche is not required for root tip regeneration<sup>15</sup>. Though, the root meristem harbours dividing cells, only a portion of it regenerate upon wounding, as the efficiency of root tip regeneration sharply decreases toward the proximal part of the meristem<sup>15,43</sup>. The non-uniform distribution of regeneration ability along the organ axis is not

only confined to plants but also other kingdoms, as zebrafish fin regeneration displays a similar pattern (Figure 1.3A)<sup>48</sup>. This raises an interesting question, what imposes the boundary on organ regeneration potential?

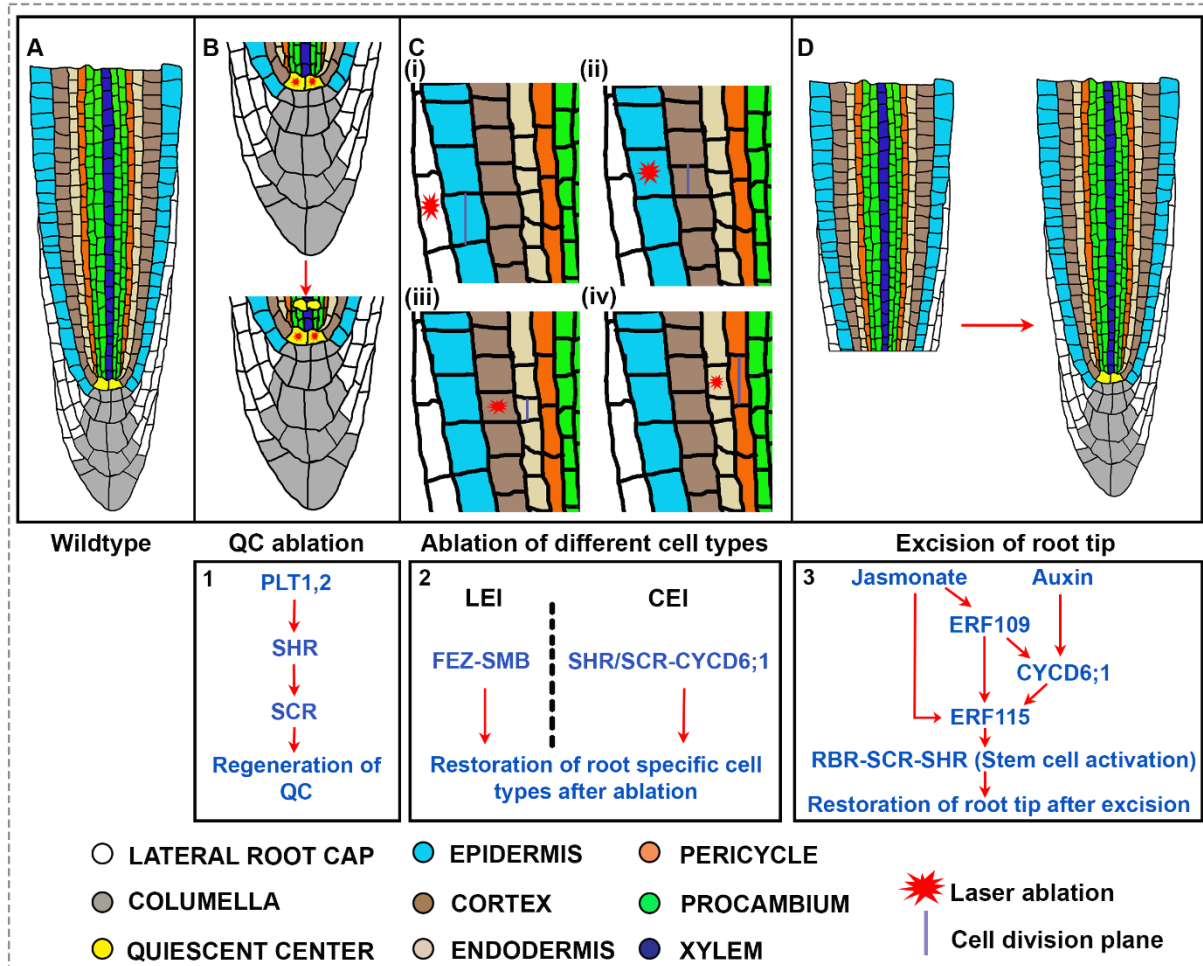


**Figure 1.2 Schematic diagram representing regeneration of specific cell types and tissues in the root tip**

(A) Wildtype (WT) root showing different cell files. (B) Root cell fate determinants (PLT, SCR, and SHR) help in the re-specification of the laser-ablated QC a few cell layers above the original site<sup>37</sup>. Box 1: The flow diagram represents the temporal order of activation of root cell fate determinants PLT1, PLT2, SHR, and SCR for QC regeneration. (C) Restorative cell division replacing the ablated (i) Lateral root cap cell, (ii) epidermal, (iii) cortical, (iv) endodermal cell of root meristem<sup>37,42</sup>. Box 2: Lateral Root Cap/Epidermis Initial (LEI) derived cells follow FEZ-SMB (SOMBRERO) pathway while, Cortex-Endodermis Initial (CEI) derived cells follow SHR/SCR-CYCD6;1 pathway to activate the restoration of ablated cells<sup>42</sup>. (D) In response to damage, JA and auxin activate a network of proteins leading to stem cell activation and restoration of the root tip. Box 3: Convergence of JA and auxin signalling leads to stem cell activation (RBR-SCR-SHR protein network) via ERF115, imperative for root tip restoration after excision<sup>49</sup>.

Recent discovery unravelled the existence of a regeneration competence zone attributed to a gradient-expressed transcription factor PLT2 in the root meristem, whose auto-activation guides regeneration (Figure 1.3B). Relatively higher expression of PLT2 in the competence

zone (distal end of meristem) contributes to high regeneration potential while a low level of PLT2 in the non-competence zone (proximal end of root meristem) impedes the regeneration ability. When the high and low expression domains of PLT2 are reversed, the regeneration potential also reverses accordingly without altering the meristem size. In multiple mutant combinations of redundant *plt*, transient downregulation of endogenous PLT2 in the competence zone leads to the cessation of regeneration. These findings explain why *plt1* and *plt2* mutants still exhibit regeneration where redundant PLTs can substitute this function<sup>15</sup>. In the WT, transient overexpression of PLT2 in differentiating cells of the non-competence zone confers the regeneration potential by upregulation of endogenous PLT2 expression. However, sustained PLT2 overexpression beyond a threshold that can increase the meristem length fails to restore root tip after excision, leaving only residual cell proliferation at the cut end. The findings demonstrate the dosage-dependent role of a gradient-expressed transcription factor in root tip regeneration. It also decouples the regeneration potential of an organ from its size as well as local cell proliferation response from complete organ restoration (Figure 1.3B)<sup>43</sup>. In addition to the internal cues, organ regeneration efficiency can be manipulated by external cues, as the proximal end of meristem that regenerates poorly exhibits efficient regeneration in response to weak electrical pulse and external auxin<sup>44,50</sup>.

The wealth of information on regeneration obtained from laboratory studies that mimic field conditions provides a better understanding of the molecular mechanisms dictating regeneration under natural growing conditions. Owing to the injury to roots imparted by nematodes, perennial woody plants evolve a greater adaptation as they remain rooted for a longer period than annual plants<sup>51</sup>. Single-cell ablation studies mimicking cyst nematode-mediated cell damage, reveal the protective effect of ethylene response genes against nematodes<sup>52</sup>. A recent study using both QC ablation and root tip excision as a model shows a rapid increase in JA and auxin which results in the activation of stem cell regulator *RBR* (*RETINOBLASTOMA-RELATED*) - *SCR* (*SCARECROW*) - *SHR* (*SHORTROOT*) through *ERF109* (*ETHYLENE RESPONSE FACTOR 109*), *ERF115* and *CYCD6;1* (*CYCLIND6;1*) enabling restoration of the root tip (Figure 1.2D). *ERF115* transcriptionally regulates *WOUND INDUCED DEDIFFERENTIATION* (*WIND1*) to promote root tip regeneration<sup>53,54</sup>. In addition to root tip regeneration and growth after nematode invasion, the JA pathway also promotes the reproductive success of the nematode<sup>49</sup>. Considering the mutually beneficial nature of this JA signalling, it can be presumed that the mechanism co-evolved in both plant and nematode.

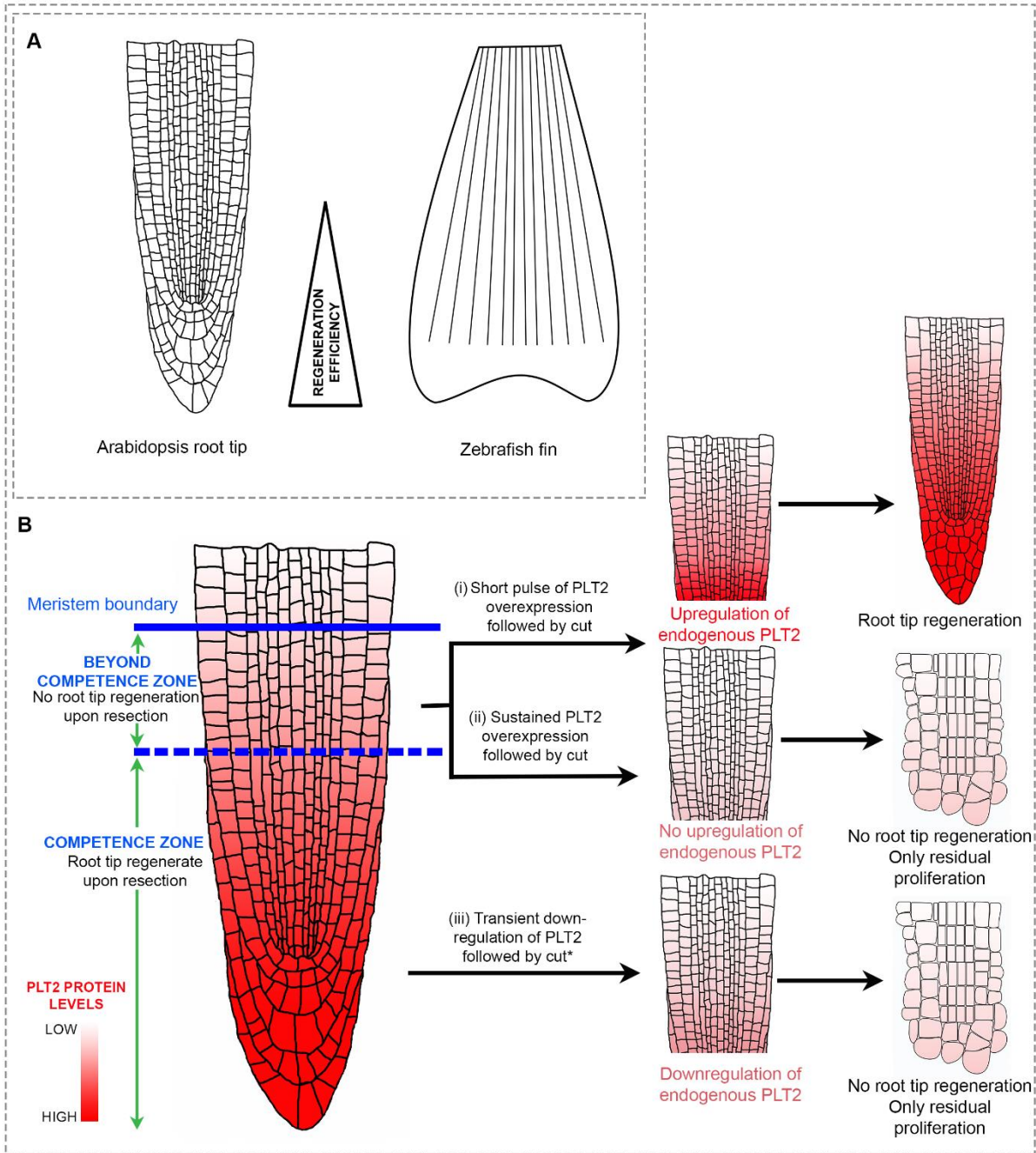


**Figure 1.3 Various degrees of regeneration potential along the organ axis**

(A) Regeneration efficiency is non-uniform along the proximo-distal axis in *Arabidopsis* root tip and Zebrafish fin<sup>15,43,48</sup>. (B) The schematic diagram represents a gradient expression of the PLT2 transcription factor in the root<sup>55</sup> and the effect of modulation of PLT2 expression level on root tip regeneration. \*Transient downregulation of PLT2 in the background of multiple *plt* mutant combinations<sup>43</sup>.

We know that in laboratory conditions, electrical pulse, and cell fate determinants influence root tip regeneration<sup>49,50</sup>. However, the relationship between the two is not yet established. Interpreting this relation can help in comprehending the molecular mechanisms driving root tip regeneration during nematode infection, as soil-dwelling fauna can impair the

intrinsic electrical signalling in roots<sup>56,57</sup>.

The elucidation of comprehensive mechanisms by which the underground plant organ responds to injuries makes one wonder if similar mechanisms operate in aerial organs as well. Local cell proliferation in the form of callus occurs upon partial incision<sup>46,58</sup>, girdling<sup>59–61</sup>, grafting<sup>62</sup>, and abrasion in stem<sup>47</sup> (Figure 1.4). Callus formed in response to wounding is a composite tissue arising from multiple cell types including cortex, pith, and vascular cell, but identification of its exact origin awaits cell lineage tracing<sup>46</sup>. Callus cells exhibit versatile nature, by virtue of which they can switch from one lineage to another for functional restoration. This is validated by the restoration of bark tissue from axial parenchyma-derived callus in response to girdling<sup>59</sup>.

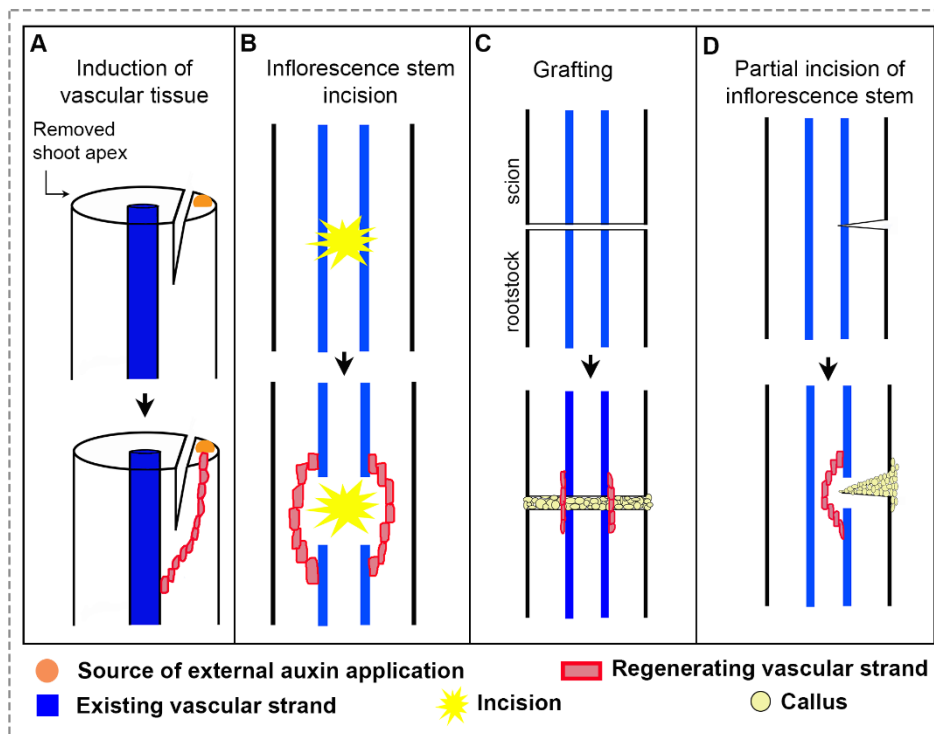


**Figure 1.4 Schematic diagram displaying wound repair and vascular regeneration in growing stem and leaf**

(A) New vascular strand forms from the site of external auxin application, on a flap of epicotyl tissue which is separated from the main vascular strand by a deep cut. The new vascular strand grows to unite with the existing vascular strand<sup>63</sup>. (B) In response to stem injury that disconnects vascular strands, newly regenerating vascular tissue around a damaged site reconnects to the parental strand<sup>64,65</sup>. (C) Callus formation between stock and scion is followed by vascular reunion during grafting<sup>62</sup>. (D) Regenerating vascular tissues circumvent the site of partial incision in the inflorescence stem and reconnect the parental strand<sup>47</sup>.

Callus acts as an adhesion material to seal the wound and provide immediate protection. In deeper wounds such as inflorescence stem incision or grafting where the vasculature has been cut off, callus formation is accompanied by the re-establishment of vascular continuity.

However, enhanced callus formation occurs when vascular continuity fails to re-establish, which compromises tissue regeneration. This draws attention to the inverse proportionality of callus formation to tissue restoration<sup>47,62,66</sup>. Therefore, tissue restoration is determined by the size of the wound, wherein the inability to regain vascular continuity in case of extensive damage can be attributed to the failure to establish optimum auxin flux<sup>67</sup>, as inferred from the canalization hypothesis proposed by Tsvi Sachs<sup>63,68</sup>.

Simple and elegant experiments by Tsvi Sachs in various plant species showed that vascular strands could be induced from mature parenchymatous tissues when the auxin flows from a source to a sink (Figure 1.4A). The growing leaves or site of external auxin application is the source while the sink is the end of the wounded tissue with a relatively lower level of auxin concentration. Regeneration requires the successful re-establishment of polar auxin transport from source to sink<sup>63,64,66,68,69</sup>. In comparison to dicots, monocots display relatively poor vascular regeneration efficiency<sup>70,71</sup> due to the absence of vascular cambium<sup>64,72</sup>. This is evident from the weak regeneration in the form of discontinuous strand formation in *Zea mays*. Moreover, injury in older internodes completely fails to regenerate<sup>73</sup>. The necessity of vascular continuity re-establishment during plant organ regeneration is analogous to the indispensable requirement of nerves in salamander limb regeneration<sup>74</sup>. Thus re-establishment of tissue continuity is instrumental for the functional restoration of the organ.

How does the tissue on either side of the wound recognize each other? Upon partial incision of the *Arabidopsis* inflorescence stem, auxin transport is disrupted, and the unequal distribution of auxin results in differential expression of many transcription factors on either side of the wound<sup>46</sup>. Such an asymmetrically localized expression of transcription factors such as *RAP2.6L* (*RELATED TO APETALA2.6L*) and *ANAC071* (*Arabidopsis* NAC domain containing protein 71) around the wound site is essential for tissue recognition to the direct vascular reunion<sup>46,75</sup>.

Though genes for regeneration in root and shoot are different, auxin surge in response to injury acts as a common regulatory module to drive regeneration in both cases. It seems auxin-driven tissue polarity, independent of auxin transporters, acts upstream of polar auxin transport and signalling to guide the path of vascular tissue formation in leaves<sup>76</sup>.

An organ is said to be restored only when it attains the appropriate shape and size pertaining to that particular developmental stage of the plant. This is evident from the restoration of the root tip and the re-establishment of vascular continuity. Thus it is plausible that the mechanism of organ restoration is tightly coupled with cellular differentiation and it

is likely to follow a normal developmental program.

#### 1.2.4 *De novo* root regeneration from detached leaf

What happens when an explant is detached from the plant body? When a leaf is excised from the plant, it gets completely disconnected from the parent plant and loses its positional cue. It heals the wounded area either by local cell proliferation in the form of callus or by *de novo* root regeneration (DNRR) from the cut end without the requirement of external hormonal cues (Figure 1.5). DNRR is widely used in agriculture for plant propagation<sup>77–86</sup>. Jasmonic acid (JA), ethylene, and ROS act as early wound signals for DNRR<sup>83,84,87,88</sup>. In response to injury, there is auxin accumulation at the wound site, in turn, activates root founder cell marker *WUSCHEL-RELATED HOMEODOMAIN11* (*WOX11*) in the procambial cells of the leaf<sup>89</sup>. The root founder cells give rise to root primordia with the activation of *LATERAL ORGAN BOUNDARIES DOMAIN16* (*LBD16*) and *WOX5*. Recent studies show that the genes *BLADE-ON-PETIOLE1/2* (*BOP1/2*), *PLETHORA* (*PLT1/2*), *PLT3*, *PLT5*, *PLT7*<sup>90,91</sup>, *CYCLINB1* (*CYCB1*)<sup>92,93</sup> and *ETHYLENE RESPONSE FACTOR 115* (*ERF115*) are required for DNRR from leaf explants<sup>94,95</sup>.

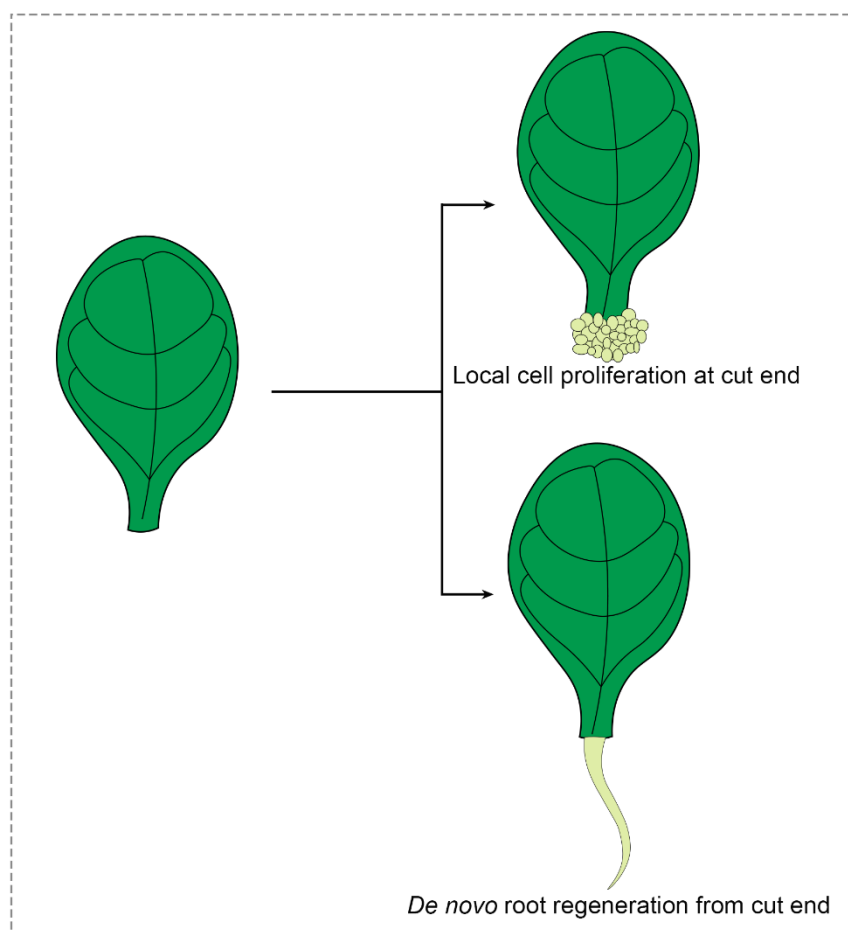


### **Figure 1.5 Distinct regeneration response in detached leaf**

A detached leaf produces two kind of regeneration response from the cut end - (i) Local cell proliferation and (ii) DNRR

### **1.3 Tissue culture-mediated regeneration**

Apart from the innate responses to injuries, plants have an exceptional ability to regrow an entire body plan when appropriate external cues such as hormones and culture conditions are provided. The tissue culture method of regeneration is an age-old technique widely used to propagate plants. Shoot organogenesis through the tissue culture method is possible through the either indirect or direct mode of regeneration (Figure 1.6). The indirect mode of shoot regeneration involves an intermediate callus formation stage before shoot organogenesis. For this, any part of the plant, called explant, is incubated in auxin rich callus induction medium (CIM) to attain pluripotency for regeneration. The pluripotent callus is then transferred to a cytokinin-rich shoot induction medium (SIM) and incubated for several days for shoot formation. In the direct mode of regeneration, the explant is incubated in cytokinin-rich media to form shoots. In this process, the differentiated tissue undergoes transdifferentiation to acquire a new fate. For example, direct shoot regeneration from lateral root primordia. Once the shoot is formed, it is transferred to the root induction medium (RIM) to form a complete plant.

The indirect *de novo* shoot formation from the mass of the callus requires self-organization of the cells that are precursors for shoot formation. Not all pluripotent callus cells can produce shoot. Only a few groups of cells can eventually form a shoot. The shoot precursor cells are termed shoot progenitors. These shoot progenitors can further develop into shoot meristem and eventually forms a complete shoot. PINFORMED1 (PIN1), a polar auxin efflux carrier marks the regenerating shoot progenitors<sup>96,97</sup>. The stochastic nature of shoot progenitor formation implies the heterogeneity of callus cells. Also, the expression pattern of key shoot regulatory genes is not uniform throughout the callus<sup>96-99</sup>. These studies show that strict spatiotemporal regulation is required for successful shoot regeneration. As embryonic or post-embryonic positional cues are absent in this context, it is interesting to understand how only a few cells in the pool of pluripotent callus cells decide among themselves to form a shoot.

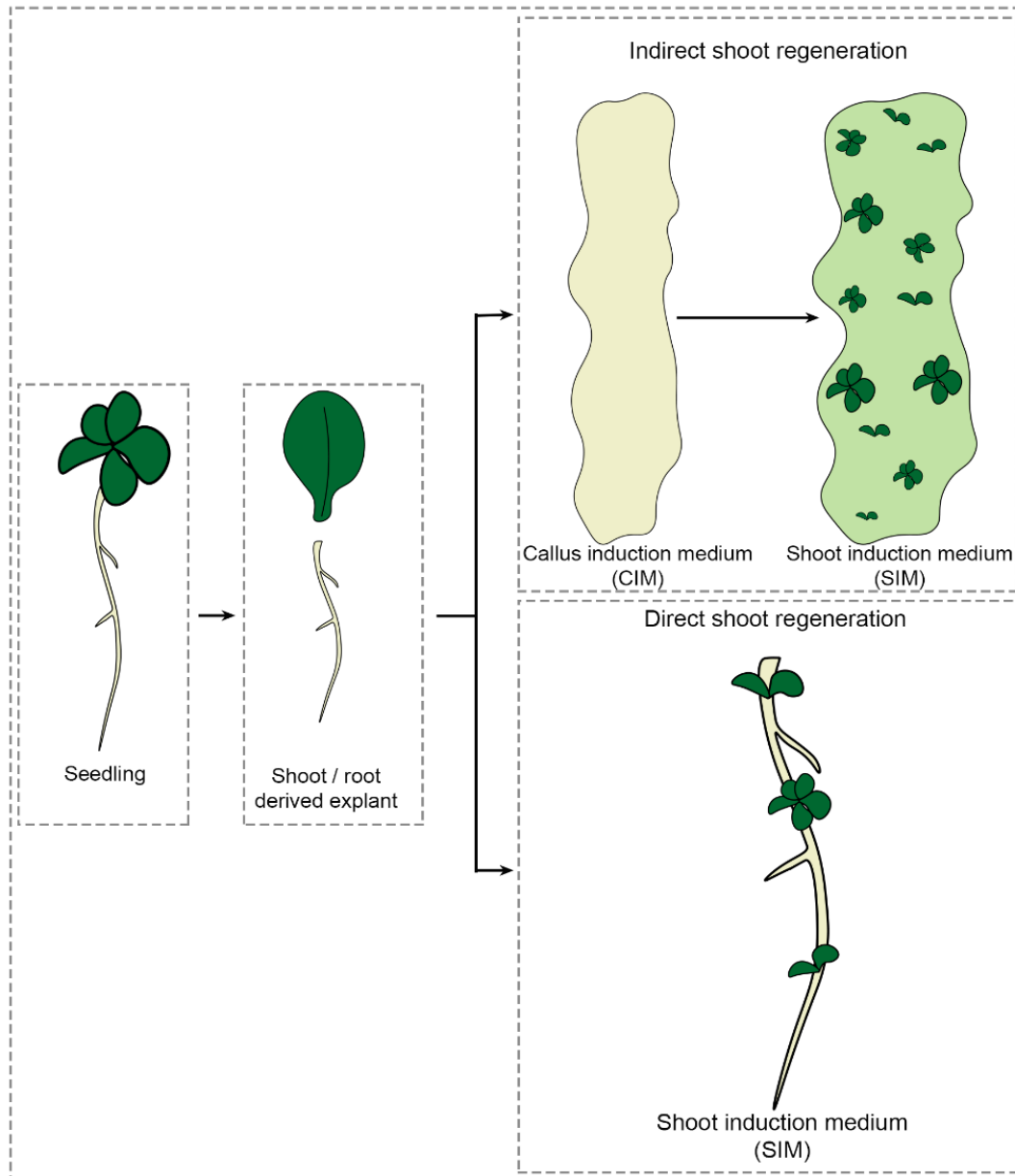


**Figure 1.6 Schematic representation of tissue culture-mediated shoot regeneration**

## *Chapter 2*

# **An assay to study tissue regeneration in growing leaves: Factors influencing vascular regeneration in leaves**

Part of the work described in this chapter is published in:

Radhakrishnan, D.\*, **Shanmukhan, A. P.\***, Kareem, A., Mathew, M. M., Varaparambathu, V., Aiyaz, M. & Prasad, K. (2021). Age, Wound Size and Position of Injury–Dependent Vascular Regeneration Assay in Growing Leaves. *Bio-protocol*, 11(9), e4010-e4010.

\*Equal contribution

## 2.1 Introduction

Plants frequently experience injuries caused by various living (biotic) and non-living (abiotic) factors. These injuries can have detrimental effects on plant immunity, growth, and overall survival if not properly addressed<sup>47,100</sup>. However, plants have evolved a remarkable ability to respond to such wounds through various regenerative processes. These processes range from local cell proliferation for wound healing to complete organ regeneration, such as the regrowth of root tips<sup>23,101</sup>. While numerous studies have investigated the mechanisms underlying regenerative responses in plants, only a few have focused on the regeneration potential of above-ground organs<sup>43,53,97</sup>. Consequently, despite the vulnerability of above-ground organs, particularly leaves, to injuries, there is a scarcity of data regarding their recovery and regenerative capabilities. Despite the crucial role leaves play in plant physiology, research on their regenerative potential has been limited<sup>101,102</sup>.

The vascular network in *Arabidopsis* leaves comprises a complex arrangement of veins that transport water, nutrients, and hormones throughout the leaf<sup>103</sup>. The leaf vasculature consists of two main types of veins - midvein and lateral veins. The midvein acts as the primary conduit for nutrient and water transport, extending from the leaf base to the leaf tip and branching out into smaller veins as it reaches towards the leaf margins. Lateral veins emerge from the midvein and form a hierarchical pattern, connecting the midvein to the leaf periphery. These veins play a crucial role in distributing resources to different regions and supporting leaf growth and function<sup>103</sup>. The arrangement and density of veins in *Arabidopsis* leaves vary depending on leaf type and developmental stage. In mature leaves, the vascular network forms a dense mesh-like pattern that optimizes resource distribution and facilitates efficient gas exchange<sup>103</sup>. Vein development in *Arabidopsis* involves the coordination of genetic and environmental factors. Genetic regulatory pathways control the specification and differentiation of vein cell types, while hormones such as auxin contribute to vein patterning and branching<sup>103,104</sup>.

Damage to the midvein requires immediate repair to restore substance transport and promote leaf and branch growth<sup>47,105</sup>. To study how the injuries are repaired, particularly in their vasculature, it is crucial to develop reliable vascular regeneration assays. While such assays have been well-established for aerial plant parts like the stem and inflorescence stalk, they have remained unexplored for leaf vasculature. In our recent research, we successfully established a novel vascular regeneration assay in growing leaves and unravelled the underlying molecular mechanism. In this chapter, a detailed step-by-step method for

conducting the leaf incision and regeneration assay is described to study leaf vascular regeneration. By employing micro-surgical perturbations, brightfield microscopy, and other experimental techniques, we also demonstrate that the success rate of regeneration is influenced by factors such as leaf age, the position of the injury, and the size of the wound. This vascular regeneration assay is easily mastered and serves as an efficient and rapid approach for investigating the mechanisms underlying vascular regeneration in growing leaves. Additionally, the assay can be readily combined with various cellular and molecular biology techniques, allowing for a comprehensive exploration of the topic.

In this study, we demonstrate that the capacity for vascular regeneration in leaves is influenced by the size of the injury, the age of the leaf explant, and the position of the injury along the proximodistal axis of the leaf. This vascular regeneration assay is simple, reproducible, and can be performed using readily available laboratory equipments. It provides a valuable tool for investigating the molecular players and mechanisms involved in wound-induced responses and regeneration within the context of normal developmental processes. The assay allows for real-time confocal imaging and facilitates the use of molecular techniques, such as quantitative real-time PCR, on injured leaves. This approach is particularly useful for studying the interdependence of vein patterning mechanisms during development and vein regeneration.

## **2.2 Materials and Methods**

### **2.2.1 Growth conditions**

*Arabidopsis thaliana* (Columbia ecotype) were used for the experiment. Seeds were subjected to surface sterilization (See section 2.2.2 for details) and were placed on half-strength Murashige-Skoog (MS) medium with a pH of 5.7, supplemented with 1% agar. The growth conditions included a temperature of 22°C, a relative humidity of 70%, and continuous white light with an intensity of 45mol/m<sup>2</sup>/s. Growth chamber used: Percival, AR-100L3 model.

### **2.2.2 Seed sterilization and plating**

To achieve proper sterilization of seeds, it is essential to perform the procedure in a sterile environment inside a laminar airflow hood (LAF). Prior to the sterilization process, the workspace and instruments (micropipettes, tip boxes, and reagent bottles) is thoroughly cleaned with 70% ethanol and exposed to UV irradiation. Hands were cleaned with soap and wiped with 70% ethanol before initiating any *in vitro* culture. The following methodology

outlines the process for liquid surface sterilization and plating of seeds:

1. The wildtype (WT) seeds are transferred into a 1.5 ml microcentrifuge tube. The number of seeds are limited to 300 per tube to ensure effective sterilization. Additionally, debris such as leftover silique pieces are removed from the collected seeds.
2. 1 ml of 70% ethanol is added to the microcentrifuge tube containing the seeds and shaken for two to three minutes.
3. After a brief spin at 4,226g (rcf), the ethanol is carefully removed from the microcentrifuge tube.
4. 1 ml of 0.8% sodium hypochlorite (made from 4% commercial sodium hypochlorite) is added to the tube containing the seeds and the contents are shaken for two to three minutes. Step 3 was repeated to remove the sodium hypochlorite.
5. The seeds are washed 5-7 times with 1ml of sterile, autoclaved water each time. This helps to remove any residual sodium hypochlorite.
6. The seeds are stratified by placing them in 1ml of sterile, autoclaved water and keeping them at 4°C for two days. This cold treatment enhances germination.
7. Using a 1 ml pipette, approximately 25 seeds are transferred onto the MS Agar medium. The seeds are arranged in a row, ensuring a minimum distance of 0.5cm between each seed. Note: It is important to avoid placing the seeds too close together to facilitate easier incision during subsequent steps.
8. The Petri plates (sterile disposable square Petri dishes with dimensions of 120mm x 120mm, for example, Himedia model: PW050-1) are placed in a vertical position inside a growth chamber with a temperature of 22°C and relative humidity of 70%, and continuous white light (24 hours) as the light source. Note: Depending on the experimental requirements, the assay can also be performed under long-day or short-day conditions using 5-day-old plants.

### **2.2.3 Leaf incision**

1. Before performing the leaf incision, necessary precautions are taken to minimize contamination by wearing gloves and a face mask. The surface of the Zeiss Stemi 2000 dissection microscope is cleaned with 70% ethanol to ensure a sterile working area. Prior to making the incision, the tweezers are immersed in 70% ethanol and dried for a few

minutes. To avoid multiple openings of the plate and potential contamination, it is advisable to perform the incision on the same day.

2. To perform the incision, the plate containing 5-day-old seedlings is opened under a dissection microscope to confirm their age. Due to asynchronous germination, the age of the seedlings may not be uniform. The number of days post-germination (dpg) is used to determine the age of the seedlings, with 0 days marked as the first day of radicle emergence. It is important to perform the incision when the seedlings are at the desired stage of development to ensure uniformity. The wounded seedlings can be separated from the healthy ones to maintain consistency. The age of the seedlings is critical as very young seedlings may be severely damaged during the process, while older seedlings exhibit reduced regeneration efficiency. The optimal age for incision is typically between 4 to 6 dpg (Figure 2.2).
3. The leaf that is facing the lid of the Petri dish is chosen for the incision among the initial pair of leaves (true leaves) for better accessibility. Using the pointed tip of Dumont tweezers (model: Style 5), an incision is made on the lower abaxial surface of the first pair of leaves at the junction between the petiole and the basal end of the lamina (Figure 2.1, 2.2A). The region right above the first lateral vein (counted from the base of the leaf) exhibits the highest regeneration efficiency compared to other locations along the proximodistal axis of the midvein (Figure 2.3). Enough force has to be applied to pierce the vascular tissue adjacent to the leaf's abaxial surface without damaging the adaxial surface. This step is crucial as extensive damage that creates a gap larger than 400 $\mu$ m between the parental vascular strands cannot be repaired (Radhakrishnan et al., 2020) (Figure 2.2P).

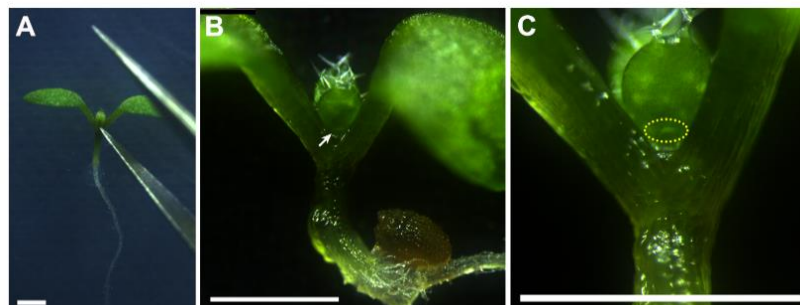


**Figure 2.1 Images demonstrating the site of the leaf incision**

(A) Leaf incision is performed in 5dpg seedlings using a fine tweezer as demonstrated in the image. (B and C) The white arrow (B) and the yellow dotted circle (C) mark the site of the incision at the basal end of a young leaf. Note the light green discoloration at the site of injury (C). Scale bars: 1mm.

4. After making the incision, the plates are sealed and placed vertically in a growth chamber set at a temperature of 22°C under continuous light conditions.
5. Four days after the incision (dpi), the wounded leaf was gently cut at the petiole using Vannas scissors (Micro-Vannas scissors, straight, Ted Pella, model: 1340). The cut leaf is transferred to a small round Petri dish containing 15% ethanol. A 35mm round Petri dish (Himedia, catalogue number: PW050) can be used for treating 20 to 30 leaves with 2-3 ml of 15% ethanol. If working with multiple sample types, 6-well plates can be utilized.

Note: During the decolorizing process, it is important not to touch the injured leaves as it may cause additional harm. The use of forceps or a sterile 200-L micro tip help to restrict plant movement by holding the cotyledon or hypocotyl. This prevents the plant from sinking into the medium due to the force of the incision.

#### **2.2.4 Sample decolourisation and clearing**

1. After a 15-minute incubation in 15% ethanol, the ethanol is carefully drained using a micropipette, taking care not to harm the samples.

Note: Initially, the leaves may float on the surface of the solvent. The leaves are gently immersed using a paintbrush with tiny bristles.

2. Successive treatments of 50%, 70%, and 96% ethanol for 15 minutes each are provided. These treatments gradually dehydrate the tissue. After discarding the 96% ethanol, the leaves are incubated in 100% ethanol for 12 hours for further dehydration of the tissues and remove chlorophyll pigmentation.
3. For rehydration, the samples are successively incubated for 15 minutes in 96%, 70%, 50%, and 15% ethanol.
4. After removing the ethanol, a newly made clearing solution is prepared using chloral hydrate (Sigma-Aldrich, catalogue number: 23100), distilled water, and 100% glycerol (Sigma-Aldrich, catalogue number: G5516) in the ratio of 8g:3mL:1mL. The clearing solution is added to the samples. The samples are incubated in the clearing solution for at least 3 hours before mounting them on slides for brightfield imaging.

Note: Increasing the duration of clearing can significantly improve contrast in brightfield imaging.

### **2.2.5 Slide preparation**

After clearing the leaves and incubating them in the clearing solution, these steps are followed for mounting the cleared leaves on slides:

1. The cleared leaves are carefully picked up with a paintbrush from the clearing solution and is placed on a fresh slide (Labtech) with its adaxial surface facing up. If any leaves are curled, they are gently opened with the paintbrush without causing any damage.
2. A coverslip (Corning, model: 2850-22) is placed carefully over the sample, ensuring that it covers the leaf completely.
3. Depending on the size of the leaves, a single coverslip can accommodate several leaves, typically 6-9.
4. The spaces between the mounted leaves are filled by adding a small amount of the clearing solution from the corner of the mounted coverslip. A 200  $\mu$ L pipette tip is used for this purpose.

### **2.2.6 Brightfield imaging**

To image the site of the incision and assess the regeneration of vascular strands, the guidelines are followed using a Leica TCS SP5 II confocal microscope:

1. Appropriate imaging mode is chosen: Brightfield mode is selected for initial determination of regeneration in cleared samples. For higher-resolution imaging of regenerating xylem components, confocal mode is used.
2. The microscope parameters used as follows:
  - a. Laser: Argon laser or DPSS 561.
  - b. Laser power: 30%.
  - c. Scan speed: 200 Hz.
  - d. Line average: 2.
  - e. Pixel size: 1024 x 1024
3. The slide with cleared sample is placed on the microscope stage, ensuring that the area of interest, specifically the regenerating vascular strand, is in the field of view.
4. High-resolution images of the regenerating vascular strand is captured using the confocal microscope. The focus and settings are adjusted as needed to obtain clear and

detailed images.

5. The acquired images are examined to evaluate the regeneration of vascular strands. The characteristic appearance of xylem components joined end to end, indicate effective regeneration. D-loop formation is identified where the regenerating vein joins the cut ends of the midvein, or the connection of one cut end to a lateral vein.

Note: Incisions performed away from the junction of the first lateral vein when examining age-dependent regeneration is excluded for methodological consistency. Only incisions with a distance between the detached parental strands less than 400 $\mu$ m is scored as successful regeneration. Proper clearing and mounting procedures are followed for the leaf samples, and the clearing solution is prepared freshly as needed. This ensures optimal sample preparation for brightfield and confocal microscopy.

### **2.2.7 Dark treatment experiment**

For dark treatment experiment, the plates with injured plants were immediately covered using aluminium foil and placed in the growth chamber. After the treatment, the aluminium foil was removed and the plants were further grown in normal light conditions.

### **2.2.8 Data analysis**

The R program was used to conduct the statistical analysis. Using Pearson's  $\chi^2$  test, the acquired data were statistically evaluated.

## **2.3 Results**

### **2.3.1 Vascular regeneration assay in leaves**

The first pair of young leaves, which had formed the midvein but not the lateral veins, were injured to maintain developmental uniformity (Figure 2.2, 2.3). The injuries were performed on 5dpg old leaves with length approximately 500 $\mu$ m (measured from leaf tip to base of the lamina). The injuries were designed to either (i) damage the midvein without creating an opening or (ii) completely disconnect the midvein, resulting in a gap between the vascular strands. In both cases, the cells surrounding the midvein experienced mechanical disturbances caused by the pressure applied by a needle.

In WT leaves, both types of injuries were repaired. In case (i), where the break was incomplete, the injured midvein underwent repair, and new vascular cells regenerated to restore the physiological connection (Figure 2.2, 2.3). In case (ii), where there was a complete

disconnection, we observed regeneration of vascular tissue predominantly in the cut end of the upper vascular strand. The regenerating vascular cells bypassed the damaged area and reconnected with the lower half of the midvein, forming a "D-loop" around the wound site, similar to the vascular regeneration observed in the stem of pea plants by Sachs<sup>64</sup>. Alternatively, the regenerating cells formed a new connection with the nearest lateral vein (Figure 2.2, 2.3F, G). The lower vascular strand, which did not regenerate, degenerated after residual proliferation at the cut end (Figure 2.3B', J).

We closely monitored the process of vascular regeneration from the time of injury to distinguish between the regenerating vascular strands originating from the cut end of the midvein versus recruiting pre-existing lateral veins that developed during leaf growth (Figure 2.3A-C, A'-C'). Importantly, vascular regeneration was rarely observed when the injury created a wider hole in the leaf blade exceeding 400 $\mu$ m between the cut ends of the midvein (Figure 2.2, 2.3H, I). Such injuries resulted in the formation of unorganized mass of cells without proper vascular regeneration (Figure 2.3H).

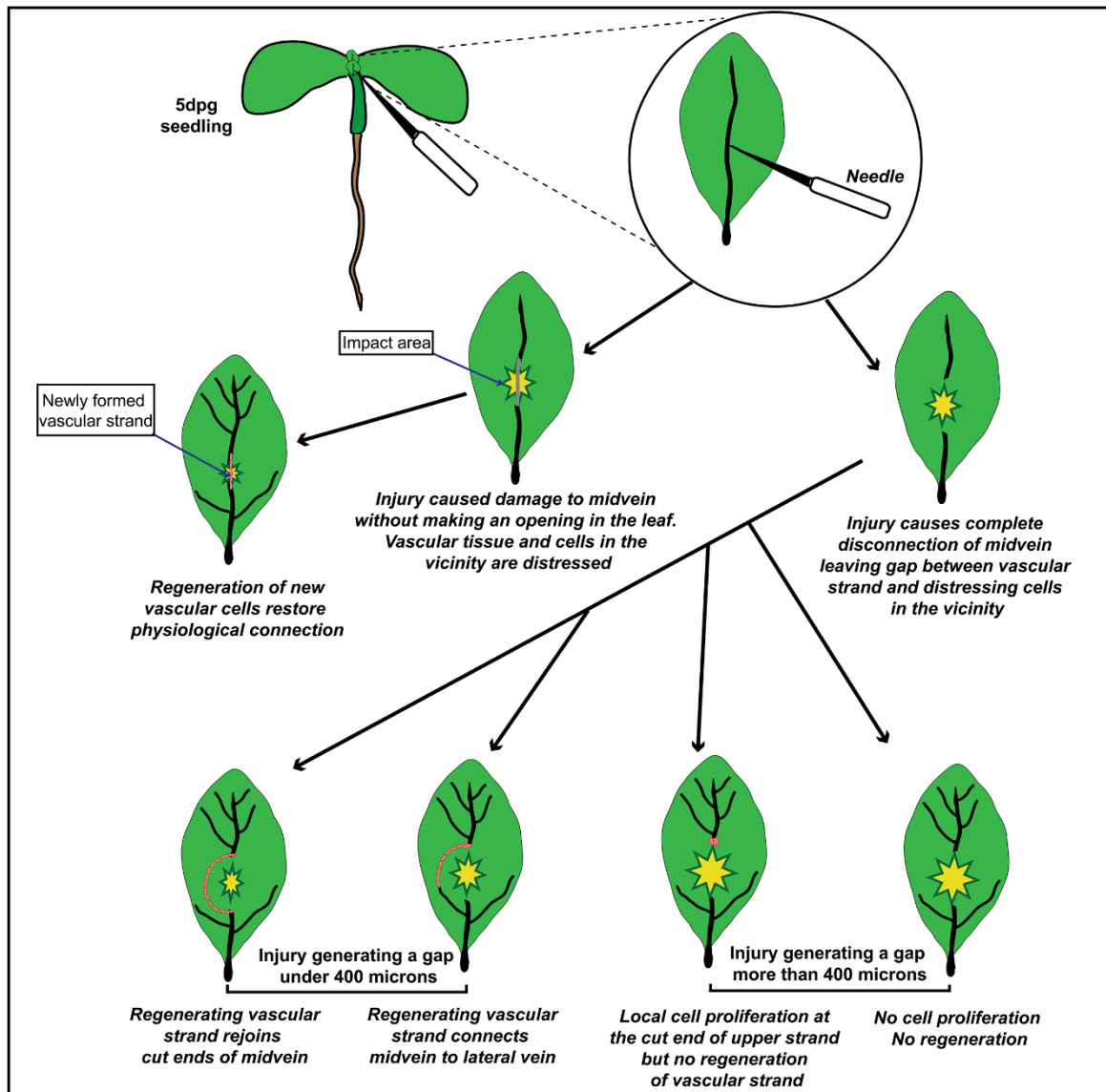


**Figure 2.2 Schematic representation showing vascular regeneration in response to injury in the midvein of growing leaf**

### 2.3.2 Vascular regeneration depends on size of the injury and the age of the leaf

Although regeneration in plants has been extensively studied, leaf regeneration and local wound repair have received far less attention<sup>101,102</sup>. We outline a thorough step-by-step procedure for a new assay for leaf vascular regeneration that may be used to examine how the midvein regenerates in response to local damage (Refer section 2.2.3). Our study has demonstrated that regenerated vascular strands can connect disconnected ends of the midvein that results in a gap of  $< 400\mu\text{m}$  (measured after 4 days post-injury and after sample clearing)<sup>47</sup>. The newly formed vasculature can either join the detached strands or connect to the closest lateral vein (Figure 2.2). In any case, the reconnection ensures that the vascular network of the leaf is restored, as well as communication between the leaf and the rest of the

plant body. The leaf vascular tissue cannot be functionally restored if there is substantial damage that results in a gap bigger than 400 $\mu$ m (Figure 2.2P)<sup>47</sup>. By using a computational model based on the canalization hypothesis of vein formation in leaves, the wound-size dependency of vascular regeneration was thus recapitulated *in silico*<sup>106</sup> (Refer chapter 3). The canalization theory<sup>66</sup> proposes that a positive feedback between auxin flux and auxin conductivity results in a channelized auxin flow, which in turn promotes the differentiation of vascular tissue.

Stages of vascular regeneration in leaves with incision

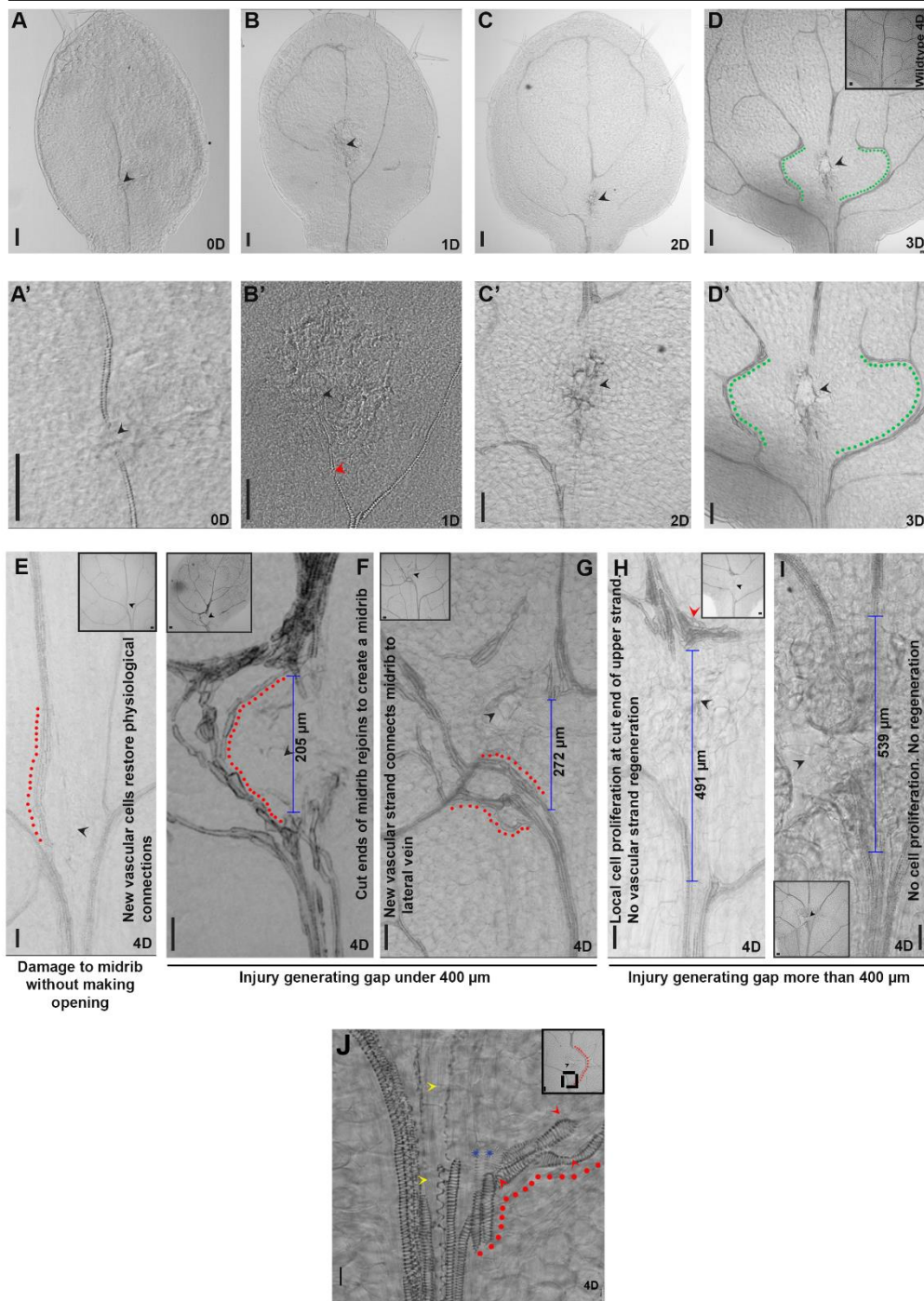


**Figure 2.3 Vascular regeneration in response to injury in growing leaves**

(A) Incision (black arrow) in midvein of 5 dpg old WT leaf. Note that only midvein is differentiated at this stage. (B) WT leaf with incision (black arrowhead) on midvein 1 day post injury. (C) WT leaf with incision (black arrowhead) on midvein 2 day post injury. (D) WT leaf with incision (black arrowhead) on the midvein 3 days post injury. New vascular cells form between lateral veins creating a venation pattern which does not occur in uninjured WT leaf (inset). (A'-D') Zoomed in images of corresponding panels from (A-D) showing site of incision. (E-I) Responses to midvein injury in growing leaf. (E) Regeneration of new vascular cells (red dotted line) restore physiological connection in midvein when incision does not create an opening in the leaf. Red scale bar depicts distance between distressed ends of midvein. (F) Regenerating vascular strands (red dotted lines) rejoin disconnected ends of midvein by

creating a D shaped loop (distance marked by scale bar) (G) Regenerating vascular strands rejoin lower cut end of midvein to lateral vein (distance of connection marked by scale bar). (H) Local cell proliferation (red arrow) at the cut end of upper strand but no regeneration of vascular strands. (I) No vascular cell proliferation or regeneration due to extensive area of damage creating opening in the leaf. (J) Zoomed in image shows lower cut end of midvein, two days post leaf incision. Yellow arrowheads mark degenerating vascular strands at lower cut end of midvein. Blue star marks initiation of procambium differentiation into vascular cells while red arrow heads mark end to end attached differentiated xylem vessel elements formed in response to injury. Scale bars represent 50  $\mu\text{m}$ .

The computational model shows that the size of the opening (simulating a wound-induced gap) generated in a matrix of cells (similar to a leaf blade) is in fact necessary for the creation of a new vascular strand, which is in agreement with our experimental findings (Figure 2.3, please refer to chapter 3 for modelling). The model also suggests that the disruption of auxin flow and concentration caused by the bigger wound may be responsible for the failure of vascular regeneration following significant injury. Such a disruption would limit the effective differentiation of the regenerated vascular strands and interfere with the correct auxin channelization. Our findings suggest that wound size sensitivity of the healing process is conserved in plants in addition to animal cells and unicellular *Dictyostelium*<sup>107</sup>.

After demonstrating that vascular regeneration is wound-size dependent, we next looked at whether the regeneration response is age dependent. Progressive ageing is linked to diminished regeneration capabilities in many higher animals<sup>108</sup>. We made the incision in plants aged 3-10 dpg in order to investigate how age controls the regeneration response in leaves. It was difficult to incise 3 dpg leaves as it caused excessive damage to the small leaves. While making an incision, the leaves frequently got detached from the plant. In comparison, the regeneration efficiency of the leaves of 3 dpg plants was lower than that of 5 dpg plants (Figure 2.4A,C,I). The most suitable period for examining vascular regeneration in leaves is between 4-6 dpg, when plants have the maximum regeneration efficiency (Figure 2.4B-D, I). The regeneration efficiency dropped sharply, with leaves of 10 dpg plants entirely failing to regenerate (Figure 2.4F-I), even though it is simpler to make incisions in older and bigger leaves. It is important to note that vascular regeneration was hampered in these older leaves even when the injury-induced gap was smaller than 400 $\mu\text{m}$  (Figure 2.3F-I); consequently, our observations imply that vascular regeneration efficacy declines with age of the leaf and size of injury in wounded plants.

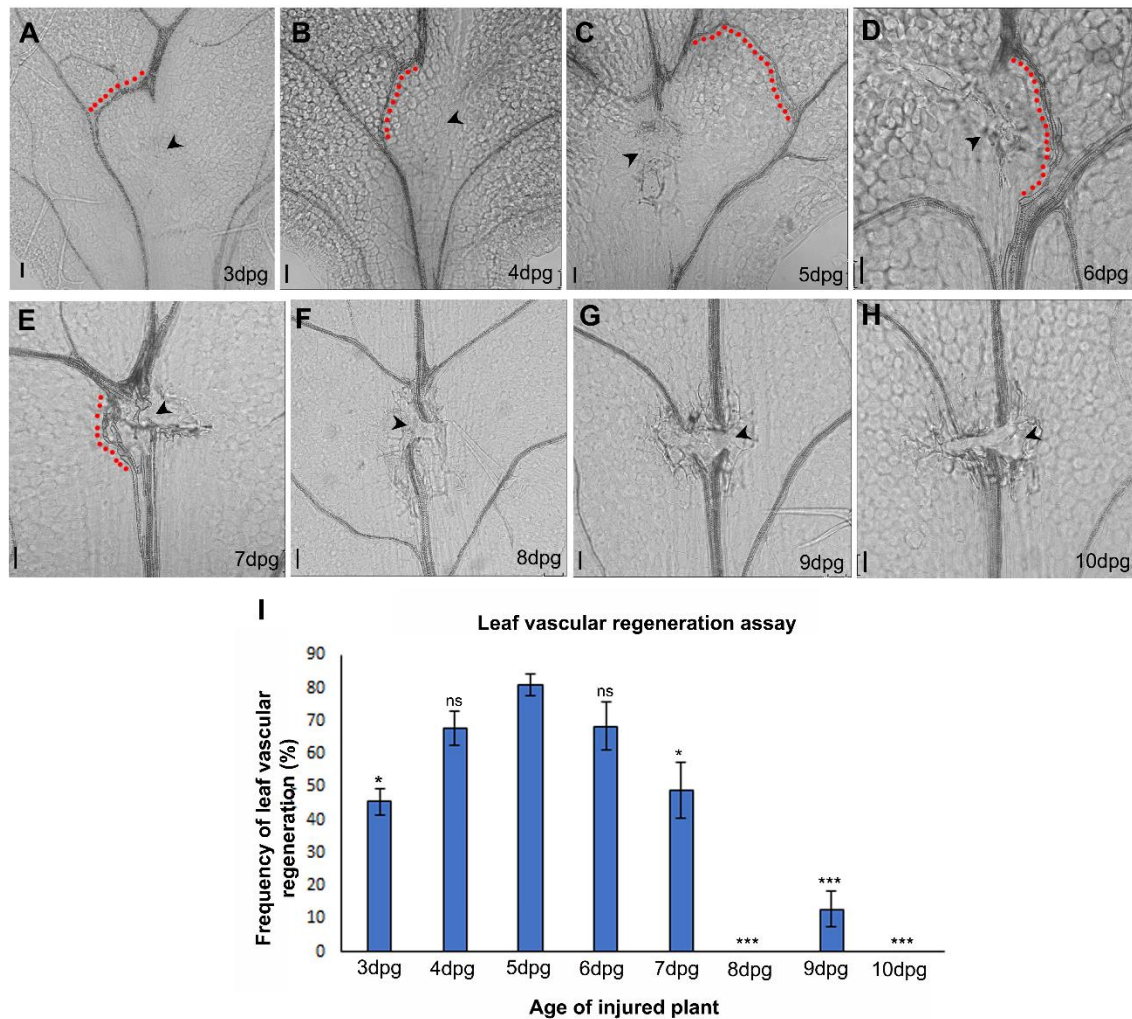


### Figure 2.4 Leaf vascular regeneration upon midvein injury depends on the age of the injured leaf

(A-I) Regeneration responses in leaves injured at different ages were observed as follows:- 3 dpg (A) (\* $P = 0.016$ ,  $n = 24$ ), 4 dpg (B) ( $P = 0.426$ , not significant (ns),  $n = 45$ ), 5 dpg (C) ( $n = 20$ ), 6 dpg (D) ( $P = 0.605$ , not significant (ns),  $n = 40$ ), 7 dpg (E) (\* $P = 0.03$ ,  $n = 34$ ), 8 dpg (F) (\*\* $P = 1.6 \times 10^{-12}$ ,  $n = 43$ ), 9 dpg (G) (\*\* $P = 2.405 \times 10^{-9}$ ,  $n = 52$ ), and 10 dpg (H) (\*\* $P = 4.8 \times 10^{-8}$ ,  $n = 21$ ). Statistical analysis was done using Pearson's  $\chi^2$  test. Note that the 3-7 dpg leaves are capable of reconnecting their disconnected vasculature but the regeneration efficiency declines with the progressive aging of the leaves. The regenerating vasculature is indicated by the red dots. The black arrowheads indicate the site of injury. (I) Graph depicting the frequency of vascular regeneration in leaves injured at different ages. Scale bar: 50 $\mu$ m. Error bars represent s.e.m.

### 2.3.3 Vascular regeneration depends on the position of injury

We then looked at how the location of the incision on the growing leaf affected the vein regeneration efficiency. Regeneration studies in plants and animals have shown that the competence to regenerate in response to injury can vary even within a specific organ<sup>43,48</sup>. We made incisions along the leaf blade at several positions, including the petiole of the leaf, the basal end of the midvein (proximal to the plant body axis), the apical end of the midvein (distal to the plant body axis), and the lateral veins (Figure 2.5A, C-F). The midvein

between first and second lateral veins, namely at the basal end of the midvein, showed the greatest regeneration frequency (Figure 2.5B, D). In response to damage, the petiole also demonstrated a higher rate of regeneration and frequently caused the creation of numerous strands (Figure 2.5B, C). However, when the leaf is removed from the petiole during sample collection, occasionally good samples are lost because the incision site and regenerated vascular strand is harmed. We found that when other places were injured, the apical regions of midvein and the lateral veins, there was a significant decrease in regeneration efficiency (Figure 2.5B, E–G).

Overall, our findings indicate that the size of the wound, the age of the injured leaf, and the position of the incision all influence the extent to which a leaf can regenerate its vascular system.

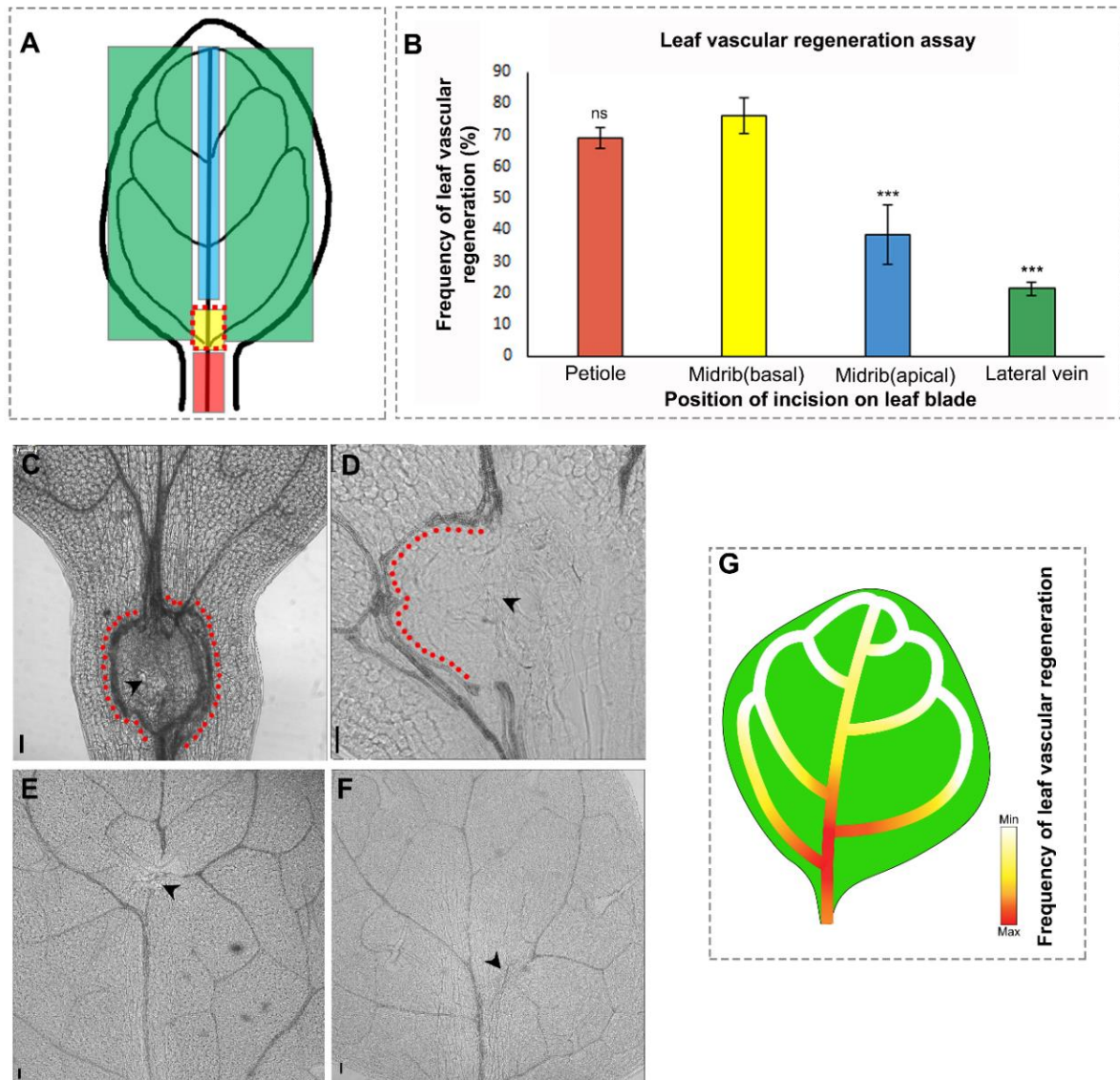


**Figure 2.5 Vascular regeneration depends on the position of injury in the leaf**

(A) Schematic depicting the positions of incision on the leaf blade and petiole. (B) The frequency of vascular regeneration at different positions (represented by coloured boxes in (A)) in the leaf is represented by the same colour bars in the graph (B) Petiole ( $n = 21$ ,  $P = 0.95$ , not significant (*ns*)), basal correct position ( $n = 45$ ), midvein upper end ( $n = 42$ ,  $***P = 0.0009$ ), lateral vein ( $n = 21$ ,  $***P = 0.0002$ ). (C-F) Images showing the incision to the vasculature in the petiole (C), the base of the midvein (D), the apical region of the midvein (E), and the lateral vein (F). Note the multiple-strand formation upon injury in the petiole (C). The red dots indicate regenerated vascular strands and the black arrowheads represent the site of the incision. Scale bar:  $50\mu\text{m}$ . (G) Gradient represents the efficiency of vascular regeneration along the leaf blade with maximum regeneration (represented by red) at the base of the midvein. Lateral veins and the distal end of the midvein exhibit reduced regeneration frequency. Error bars represent s.e.m.

### 2.3.4 Role of light in vascular regeneration in leaves

Light plays a crucial role in the growth and development of leaves, influencing various physiological and morphological processes. As a primary source of energy, light is essential

for photosynthesis, which is responsible for the synthesis of carbohydrates necessary for leaf growth<sup>109</sup>. Moreover, light acts as an environmental cue that regulates leaf development. It affects the synthesis and distribution of plant hormones, such as auxin and cytokinin, which control leaf expansion, shape, and orientation<sup>110</sup>. Light also triggers photomorphogenic responses, leading to changes in leaf morphology, including leaf expansion, chlorophyll production, stomatal development, and branching<sup>111</sup>. Furthermore, light quality and quantity influence various aspects of leaf architecture, such as leaf colouration, vein formation, and overall leaf shape<sup>112</sup>. Overall, light serves as a fundamental factor in leaf growth and development, providing energy for photosynthesis and acting as a key regulator of hormonal and morphological processes.

We investigated the role of light in vascular regeneration, injured leaves were subjected to various durations of dark treatment. The efficiency of vascular regeneration gradually decreased with longer periods of dark treatment (Figure 2.6A, preliminary data). This suggests that light plays a critical role in the regeneration of vascular tissue in leaves. Prolonged exposure to darkness have detrimental effects on normal leaf growth and vein development. The leaves treated in dark for more than 2 days were smaller, and the vein development was also affected. Additionally, these leaves showed reduced deposition of lignin in their veins and a halt in vein development (Figure 2.6B-G), emphasizing the crucial role of light in these processes. The results imply that light availability and duration are important factors to consider when studying and promoting successful vascular regeneration in plant leaves.

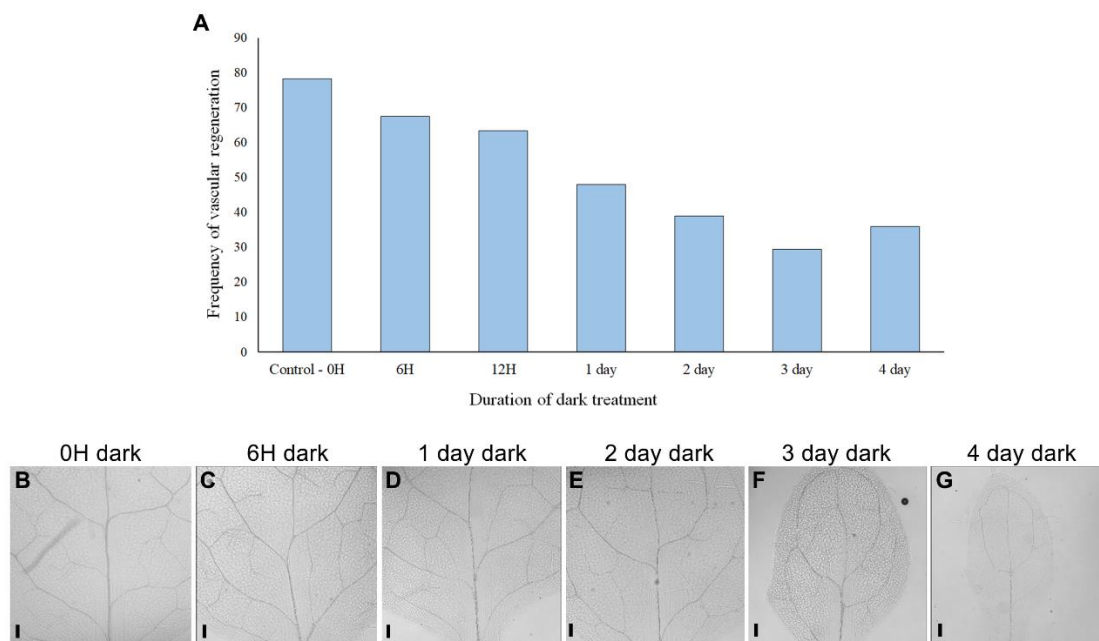


**Figure 2.6 Dark treatment after injury reduces leaf vascular regeneration efficiency**

(A) Graph representing frequency of vascular regeneration in leaves upon different durations of dark treatment (preliminary data). (B-G) Leaf vascular pattern in uninjured leaves upon different duration of dark treatment followed by light. (B) Control with no dark treatment, (C) 6H dark treatment, (D) 1 day dark treatment, (E) 2 day dark treatment, (F) 3 day dark treatment, (G) 4 day dark treatment. All the treatments were done on 4 day old plants. Scale bar: 50 $\mu$ m.

## 2.4 Discussion

During their growth, plants are susceptible to various types of injuries caused by both living (biotic) and non-living (abiotic) factors. However, plants possess a remarkable ability to repair themselves and resume their growth. Understanding the mechanisms behind their self-healing processes is of great importance. Most of the studies on plant regeneration were focused on roots due the simplicity of conducting regeneration experiments on roots. In our study, we developed a rapid approach to investigate vascular regeneration in growing plant leaves.

Our findings indicate that leaves aged between 4 and 6 days after germination (dpg) exhibit a more efficient response to smaller wounds inflicted at the junction of the first lateral vein near the base of the leaf blade, provided that the wound size is less than 400 $\mu$ m (measured four days after injury on cleared samples). However, as the leaf ages, it becomes less capable of repairing wounds even if they are smaller than 400 $\mu$ m. We also observed that the location of the damage influences vein regeneration. Therefore, for examining regeneration in different plant species using this approach, we recommend standardizing the procedure based on the aforementioned requirements.

The efficiency of vascular regeneration in injured leaves gradually decreases with prolonged exposure to darkness, indicating the dependence of this regenerative process on light cues. Understanding the mechanisms by which light influences these processes can provide valuable insights for enhancing regenerative capacities in plants and optimizing their growth and development in various environmental conditions. Further research in this area will contribute to a more comprehensive understanding of plant regeneration and its implications for agriculture and ecological restoration efforts.

Although the assay may initially appear laborious, with practice, it can be performed quickly and proficiently on a large number of samples. The experiment is accessible to the wider scientific community due to its brief duration (data can be obtained 5 days after damage) and lack of requirement of specialised equipment. Moreover, this approach can be combined with various cellular and molecular biology techniques with minimal standardization, as demonstrated previously<sup>47</sup>, thereby enhancing its significance.

## *Chapter 3*

# **A functionally conserved regulatory module confers universal regeneration potential to plants in response to mechanical injuries**

Part of the work described in this chapter is published in:

Radhakrishnan, D.\* , **Shanmukhan, A. P.\***, Kareem, A., Aiyaz, M., Varapparambathu, V., Toms, A., Kerstens, M., Valsakumar, D., Landge, A. N., Shaji, A., Mathew, M. K., Sawchuk, M. G., Scarpella, E., Krizek, B. A., Efroni, I., Mähönen, A. P., Willemsen, V., Scheres, B., & Prasad, K. (2020). A coherent feed-forward loop drives vascular regeneration in damaged aerial organs of plants growing in a normal developmental context. *Development*, 147(6), 1–10.

Radhakrishnan, D.\* , **Shanmukhan, A. P.\***, Kareem, A., Mathew, M. M., Varaparambathu, V., Aiyaz, M. & Prasad, K. (2021). Age, Wound Size and Position of Injury–Dependent Vascular Regeneration Assay in Growing Leaves. *Bio-protocol*, 11(9), e4010-e4010.

\*Equal contribution

### 3.1 Introduction

Both plants and animals have the ability to trigger regenerative responses when they are subjected to tissue damage. Regenerative responses can either be restricted to local healing in the form of cell proliferation alone or, in some cases, lead to regeneration of the tissue or organ<sup>23,24</sup>. In addition to their innate ability to regenerate organs *in vivo*, plants exhibit a remarkable capability to regenerate an entire plant from excised tissue in *in vitro* through a two-step process where acquisition of pluripotency can be separated from organ differentiation<sup>23,97,98</sup>.

Plants have evolved strategies to repair tissues damaged by environmental insults such as pathogen attacks, herbivory and abiotic factors like wind. Though both above ground and below ground plant organs have the machinery to activate innate regenerative responses, local wound repair in response to tissue damage is largely studied in the stem and developing root tips. While the consequences of partial ablation in the leaf, namely wound induced long distance leaf-to-leaf and leaf-to-root signalling are known, the ability of growing leaves to repair the vein injury remains to be determined<sup>102,113,114</sup>. In roots, regeneration of root meristems lost upon resection follows embryonic patterning events and involves embryo-specific genes. Regeneration of specific root cell types lost in ablation requires root cell-fate determinants<sup>115,116</sup>. At the shoot tip, positional cues drive regeneration of leaf primordia in response to injuries<sup>117</sup>.

Wounds in other parts of the plant can also be repaired, restoring damaged tissue. Studies on regeneration of vascular tissues in the stem and root of multiple plant species have revealed role for the plant hormone auxin<sup>64,68,118,119</sup>. Healing processes also come into play during tissue union in grafting and in healing incisions made in stems<sup>62,120–123</sup>. Cellular, molecular and hormonal interactions at the wound site coordinate the wound healing process and restore vascular tissues to reinstate physiological competence<sup>62,75,120–123</sup>. Response to injuries are seen not only in growing plants but also in detached organs that can either regenerate roots by activating *WOX* genes or form callus-like growth at the cut surface by activating wound induced factors such as *WIND1*<sup>78,94,124,125</sup>.

Although there have been studies investigating specific regeneration processes in particular plant parts or excised organs, there is currently a lack of comprehensive research on the molecular mechanisms underlying wound repair and tissue regeneration across the plant body, particularly in organs growing in their normal developmental context. Importantly, how

wound repair in a tissue compares with its normal tissue developmental programs remains largely unknown. In this study, we demonstrate the essential role of members from the *PLETHORA (PLT)* / *AINTEGUMENTA (ANT)* gene family in activating innate responses to injuries encountered by growing aerial plant parts. We show that *PLT* genes, acting through the embryonic symmetry determinant *CUP-SHAPED COTYLEDON2 (CUC2)*, but not through root or shoot stem cell regulators, are involved in the repair of wounds and the regeneration of vascular tissue in damaged aerial organs that are growing in their normal developmental context. Additionally, we reveal that the *PLT-CUC2* module controls local auxin biosynthesis and cell polarization, which are essential for driving vascular regeneration in aerial organs. Strikingly, the necessity of the *PLT-CUC2* module specifically for vascular regeneration, rather than vascular development, separates the ability of the tissue to repair wounds independent of its normal developmental program.

## **3.2 Materials and Methods**

### **3.2.1 Plant Materials and molecular cloning**

In this study, the WT used was *Arabidopsis thaliana* ecotype Columbia (Col-0). Mutant lines used in the study, such as *plt3;plt5-2*, *plt3;plt7*, *plt3;plt7* double mutants, *plt3-1;plt5-2;plt7* triple mutant<sup>90</sup>, *pid-14* single mutant, *pid;wag1;wag2* triple mutant<sup>126</sup>, *yuc1;yuc4* double mutant<sup>127</sup>, *plt3;plt7;ant-4* triple mutant<sup>128</sup>, *cuc2-1* and *cuc2-3* single mutants, and *cuc1-5;cuc2-3* double mutant<sup>129,130</sup> (ABRC), have been previously described. WT; *pPXY-erYFP* and WT; *pWOX4-erYFP* was received from Prof. Ari Pekka Mahonen. The Multisite Gateway recombination cloning system (Invitrogen) with the pCAMBIA 1300 destination vector was employed for cloning the constructs. These constructs were then introduced into C58 by electroporation and subsequently transformed into *Arabidopsis* using the floral dip method<sup>131</sup>.

### **3.2.2 Growth conditions**

Please refer section 2.2.1 in Chapter 2.

### **3.2.3 Seed sterilization and plating**

Please refer section 2.2.2 in Chapter 2.

### **3.2.4 Regeneration assays**

For the wound-induced natural regeneration experiments, the plants were grown on hormone-free MS agar medium (Sigma) under the specified growth conditions. To investigate

wound repair and vascular regeneration in the growing inflorescence, three-week-old seedlings were selected. Using a sterile razor blade and under a dissection microscope (Zeiss), the inflorescence stem region between the rosette leaves and the first or second cauline leaves were subjected to either peeling of tissue layers (inflorescence abrasion) or partial incision (perpendicular partial cut) through the vascular tissues (inflorescence incision). The observations were recorded four days after the injury.

In the leaf vascular regeneration assay (Please refer chapter 2 for detailed methodology), one of the first pair of leaves with fully developed midvein of a 4-5 dpg old seedling was injured. A sharp incision was made at the basal part of the leaf blade using fine pointed sterile tweezers. Incisions made elsewhere were not considered for scoring. The incisions were made from the abaxial surface of the leaf. The injured plants were allowed to grow for an additional four days, while being protected from further damage. After four days, the injured leaves were collected without causing any damage to the leaf blade using Vannas straight scissors. The leaf tissue was cleared using chloral hydrate, and brightfield images were obtained to assess the outcomes of regeneration. Successful regeneration outcomes were scored when newly formed vascular strands connected the cut ends of the midvein to form a D-shaped loop or when they connected one of the cut ends of the midvein to a lateral vein, identified by the distinct morphology of end-to-end arranged xylem elements.

To study *de novo* root regeneration (DNRR) and healing in response to wounding in excised organs, explants of leaves, roots, and hypocotyls were collected from nine-day-old seedlings and placed on hormone-free MS agar medium. For DNRR, leaves were placed on the plate with the abaxial side facing the medium so that the cut end of the petiole contacted the medium. For callus formation, leaves were placed in the opposite manner, with the cut end of the petiole facing away from the medium. Callus formation and root formation from leaves were assessed after six days and 14 days, respectively. Callus formation at the cut end of hypocotyls and root was assessed 12 days after the cut. All plates for regeneration experiments were incubated vertically in a plant growth chamber at 22°C and 70% relative humidity under continuous white light with an intensity of 45  $\mu\text{mol}/\text{m}^2 \text{ s}$ .

Data analysis was conducted using Pearson's  $\chi^2$  test for the regeneration assay and Welch two-sample test for qRT-PCR data analysis. Holm-Bonferroni correction was performed for multiple analyses using the Pearson's  $\chi^2$  test.

### 3.2.5 Microscopic Imaging

Bright-field and confocal laser-scanning microscopy imaging techniques were employed following the previously described methods<sup>97</sup>. For bright-field imaging of vascular regeneration in incised leaves, a Leica TCS SP5 II inverted confocal microscope and an Olympus BX63F microscope were used in brightfield mode. Prior to imaging, the leaf samples were cleared according to the procedure described in chapter 2.

Confocal imaging of leaves and thick samples was conducted using a Leica TCS SP5 II upright microscope. To enhance visualization of cell boundaries in root, hypocotyl, and callus samples, staining with 10 µg/mL propidium iodide (Sigma) was performed. Images were acquired using different objectives, including a 10x air objective, 20x oil immersion objective, 20x air objective, and 40x oil immersion objective. The acquired images were processed and reconstructed from z stacks using Leica LAS-AF software. Image compilation was performed using Adobe Photoshop CS6. It is noted that all image panels represent z stacks unless specified otherwise.

### 3.2.6 qRT – PCR

For qRT-PCR analysis, inflorescence abrasion was performed on both the WT (Columbia ecotype) and *plt3;plt5-2;plt7* triple mutant plants. After four days, the injured part of the inflorescence was collected and used for RNA extraction. In the case of leaf injury, complete seedlings excluding the roots were used for qPCR analysis. Additionally, the expression of *PLT5* and *PLT7* genes was induced in WT plants expressing *35S::PLT5-GR* and *35S::PLT7-GR* constructs. Following inflorescence abrasion, the entire plants were transferred to MS plates containing 20µM dexamethasone (DEX), and liquid MS medium with DEX was flooded onto the plate. For the mock treatment, MS medium supplemented with only DMSO was used, and for flooding, liquid MS medium supplemented with DMSO was used. The wounded inflorescence samples were collected at 4 hours or 8 hours after treatment for RNA extraction. The transcript level in the control sample was always normalized to 1.

Total RNA was extracted from the samples using the Nucleospin Plant RNA extraction kit (MN) and treated with on-column DNase following the manufacturer's instructions. cDNA synthesis was performed using a High-Capacity cDNA Reverse Transcription kit (Applied Biosystems) with 1µg of total RNA. qRT-PCR was conducted in a 25µL reaction volume containing 12.5µL SYBR Green PCR master mix (Takara), 100nM gene-specific primers, and 100 ng cDNA on the CFX96 Touch™ Real-Time PCR Detection System. Three independent

biological replicates were used, and each biological sample was tested in technical triplicate. *ACTIN2* (*ACT2*) was used as the reference gene for normalization. The relative gene expression was calculated as fold-change ( $-\Delta\Delta CT$ ) compared to the control<sup>97</sup>.

### 3.2.7 Luciferase assay

The luciferase assay was conducted following the protocol outlined in the study by Diaz-Trivino et al., 2017<sup>132</sup>.

### 3.2.8 ChIP-qPCR Analysis.

The ChIP (Chromatin Immunoprecipitation) assay was carried out according to the protocol described in the study by Yamaguchi *et al.*, (2014)<sup>133</sup>. Five-day-old proliferating callus tissues derived from roots of *PLT5::PLT5-vYFP* and *plt3;plt5-2;plt7* were cross-linked with 1% formaldehyde. The tissues were weighed (600mg fresh weight) and subjected to cross-linking to preserve the protein-DNA interactions. The cross-linked tissues were lysed, and the chromatin was extracted. The extracted chromatin was immunoprecipitated using an anti-GFP antibody (5 $\mu$ L per sample) (Clontech). After immunoprecipitation, several washing steps were performed to remove non-specifically bound proteins and DNA fragments. After immunoprecipitation, several washing steps were performed to remove non-specifically bound proteins and DNA fragments and the DNA further purified by using PCR Purification Kit (Qiagen). qPCR was performed using SYBR Premix (Clontech) to determine the PLT5 protein occupancy on *CUC2* promoter region. The relative fold enrichment of *CUC2* DNA was calculated by comparing the enrichment in the *PLT5::PLT5-vYFP* sample to the *plt3;plt5-2;plt7* sample. The expression levels of the *ACTIN 7* (*ACT7*) gene were used as a normalization control between the samples. The ChIP-qPCR reactions were performed in triplicates to ensure the accuracy and reliability of the results.

Note: It's important to consult the original study by Yamaguchi et al. (2014)<sup>133</sup> for a detailed and comprehensive understanding of the ChIP protocol, as it may contain specific parameters, conditions, and additional steps not mentioned here.

The primers used for ChIP qPCR are listed in the table below

Primer	Sequence
CUC2-ChIP #1_F	ACATTTTTGGGTGGGAAAT
CUC2-ChIP #1_R	AGAGAAGATATTTATGCTGCCT

CUC2-ChIP #2_F	GATTTGCAACCTGTA ACTTC
CUC2-ChIP #2_R	TGTCAGCACAGTACATGATT
CUC2-ChIP #3_F	TCTTCTCTACGACTTTCTGG
CUC2-ChIP #3_R	TAAGAAGAAAGATCTAAAGCTTTTG
ACT7-ChIP_F	CGTTTCGCTTTCCTTAGTGTTAGCT
ACT7-ChIP_R	AGCGAACGGATCTAGAGACTCACCTTG

### 3.2.9 Constructs for molecular cloning

The construct *pWUS::3xVENUS-tWUS* was generated by combining 5.744kb of *WUS* upstream regulatory sequences, 3xVENUS, and 1.635kb of *WUS* 3'UTR<sup>133</sup>. For the *PLT5::YUC4-YFP* construct, 5.6kb of *PLT5* upstream regulatory elements and a 1.93kb fragment of the *YUC4* gene, including introns and exons, were fused with YFP in the pCAMBIA destination vector<sup>127</sup>. Previous studies described translational fusion constructs such as *PLT1::PLT1-vYFP*, *PLT2::PLT2-vYFP*, *PLT3::PLT3-vYFP*, *PLT5::PLT5-vYFP*, and *PLT7::PLT7-vYFP*<sup>55,90</sup>. The constructs *35S::PLT5-GR*, *35S::PLT7-GR*, *pCUC2::3xVENUS*, and *35S::CUC2-3AT* have also been previously reported<sup>97</sup>. To rescue regeneration in *plt3;plt5-2;plt7* mutants, *OsPLT2* (LOC\_Os06g44750.1) was inserted under the *Arabidopsis* *PLT5* promoter and tagged with vYFP<sup>90</sup>. Please refer to the respective references for more detailed information.

### 3.2.10 Decolourisation and tissue clearing for imaging vascular tissues

To visualize the regeneration of vascular strands, the injured leaf and inflorescence stem were carefully removed from the growing seedling at different time intervals after incision, using Vannas straight scissors. Prior to chlorophyll removal, a longitudinal cut was made through the injured area of the excised inflorescence stem using a razor blade, allowing the regenerating vascular strands in the thick inflorescence tissues to be exposed. Both the leaf and inflorescence stem underwent a dehydration process, during which chlorophyll was bleached. This was achieved by sequentially immersing the samples in ethanol solutions of increasing concentrations: 15%, 50%, 70%, and 96%, for 15 minutes each. Subsequently, the samples were soaked in absolute ethanol overnight (12 hours) for complete dehydration. To rehydrate the samples, they were transferred from 100% ethanol to lower concentrations of ethanol (96%, 70%, 50%, and finally 15%), in reverse order, with 15 minutes of incubation at each

concentration. Following rehydration, the samples were incubated in a freshly prepared clearing solution composed of 8g chloral hydrate, 1mL 100% glycerol, and 3mL distilled water, for a period of 2-3 hours. The cleared samples were then mounted on slides using the clearing solution, ensuring that the adaxial surface of the leaf and the exposed cut surface of the inflorescence stem faced upward. Careful placement of the coverslip was done to prevent the formation of bubbles and curling of the tissues. Please refer to chapter 2 for detailed protocol.

### 3.2.11 Oligonucleotide primers used for cloning and qRT PCR (5'->3')

Additional primers used in this study have been previously described<sup>97</sup>.

Primer	Sequence
qRT-PLT5-FP	CTACTCCGGTGGACACTCGT
qRT-PLT5-RP	CGTTCTTCTTCGGAGTAGGC
qRT-PLT7-FP	TTTCCTCGGTGATTCCTTTG
qRT-PLT7-RP	TGACGTGGATCGTAGAATGG
qRT-PID-FP	AGATTTTATGCCGCCGAAGTTC
qRT-PID-RP	AGTCGGAGCATAGAGAGAGGTC
qRT-YUC4-FP	TCCATAATATTAGCGACTGGGTA
qRT-YUC4-RP	CCCTTCTCTCCTTTCCATCC
pWUS-FP	CGGCTTTAAAGCATGTATATTACACTCAT
pWUS-RP	TGTGTGTTTGATTCGACTTTTGTTCAC
pCUC2 LUCR-FP	GGGGACAAGTTTGTACAAAAAAGCAGGCTttaaattctacattttgttgg
pCUC2 LUCR-RP	GGGGACCACTTTGTACAAGAAAGCTGGGTtgttttgaagaagaa gataaa
pATHB8-FP	GGGGACAACCTTTGTATAGAAAAGTTGTTCGGATAAACC AATTTTCAAATG
pATHB8-RP	GGGGACTGCTTTTTTGTACAACTTGTCTTTGATCCTCT CCGATCT

gATHB8-FP	GGGGACAAGTTTGTACAAAAAAGCAGGCTGTATGGGA GGAGGAAGCAATAATAGTCA
gATHB8-RP	GGGGACCACTTTGTACAAGAAAGCTGGGTTTATAAAAG ACCAGTTGAGGAACATGAAGC

### 3.2.12 Numerical simulations of vascular regeneration

The numerical simulations were performed by Dr Anil Shaji, IISER Thiruvananthapuram. The *in-silico* investigations aimed to gain a quantitative and qualitative understanding of the relationship between vascular regeneration and wound size, as observed in our experiments. To achieve this, we utilized a widely studied mathematical model that incorporates the feedback between auxin, its flux, and active transport<sup>134</sup>. We chose not to make any modifications to the model in order to maintain focus on understanding the experimental observations, rather than exploring the potential consequences of such modifications. Figure 3.1 schematically represents the variables and parameters associated with each cell in the model.

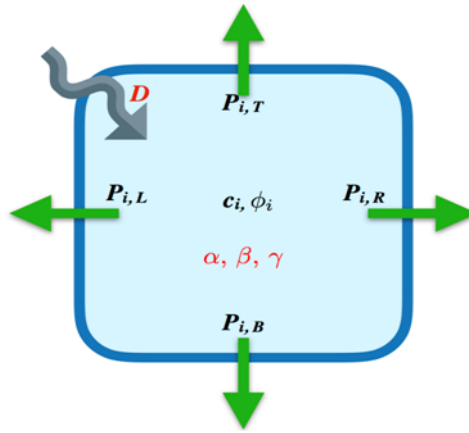


**Figure 3.1 Schematic of each cell with the variables and parameters appearing in the mathematical model**

The individual cells are modelled as rectangular or square units and shown in the figure is the  $i^{th}$  cell from a large grid. The concentration of auxin in this cell is labelled as  $c_i$  and  $\phi_i$  denotes the total flux of auxin through the  $i^{th}$  cell. Net auxin efflux corresponds to  $\phi_i$  having positive values while negative values of  $\phi_i$  corresponds to net auxin influx. The total flux is the sum of the fluxes through all four sides of the square cell:

$$\Phi_i = \Phi_{i,L} + \Phi_{i,R} + \Phi_{i,B} + \Phi_{i,T}, \quad (1)$$

where, the subscripts  $L$ ,  $R$ ,  $B$  and  $T$  stand for fluxes to/from the left, right, bottom and top respectively. The positive feedback between the concentration and flux of auxin and the efflux carriers (and their polarity) is encoded in the active transport coefficients  $P_{i,L}$ ,  $P_{i,R}$ ,  $P_{i,B}$ , and  $P_{i,T}$  associated with the four walls of the  $i^{th}$  cell. In addition to facilitated diffusion, ordinary diffusion of auxin across the four cell walls controlled by the diffusion constant  $D$  is also present. The auxin flux across each of the walls is then given by:

$$\Phi_{i,X} = D(c_i - c_j) + P_{i,X}c_i - P_{j,X'}c_j \quad (2)$$

where, subscripts  $X$  and  $X'$  can take on values  $L$ ,  $R$ ,  $B$  or  $T$ . In the equation above,  $c_j$  is the concentration of auxin in the adjacent cell on the appropriate side. For instance, if we are considering the flux to/from the left for the  $i^{th}$  cell, then  $c_j$  is the concentration of auxin in the cell immediately to the left of the one under consideration. In this case the subscript  $X'$  in  $P_{i,X'}$  takes the value  $R$  since the net flux to/from the left for the  $i^{th}$  cell also depends on the flux of auxin to/from the right for the cell immediately to the left of the one under consideration.

The active transport coefficients are also variables in the model that change in response to the auxin flux. This positive feedback loop is governed by the equation,

$$dP_{i,X}/dt = \alpha \Phi_{i,X}^2 \Theta(\Phi_{i,X}) + \beta - \gamma P_{i,X} \quad (3)$$

where,  $\alpha$ ,  $\beta$  and  $\gamma$  are constants that are tunable parameters in the model. Here  $\alpha$  controls the positive nonlinear feedback that auxin the flux  $\Phi_{i,X}$  has on the transport coefficient. This parameter is relevant only when there is efflux and  $\Phi_{i,X}$  is positive since the term is multiplied by the Heaviside step function  $\Theta(x)$  which is zero when  $x$  is negative and has unit value when  $x$  is positive. The parameter  $\beta$  controls the background production of efflux carriers and  $\gamma$  is the rate of decay of the same.

The concentration of auxin in each cell is governed by the equation:

$$dc_i/dt = \sigma - \sum_{X=L,R,B,T} \Phi_{i,X} \quad (4)$$

where,  $\sigma$  is the intrinsic auxin production rate in each cell. The negative sign before the second term in the equation above appears because we have taken auxin efflux to correspond to positive values of  $\Phi_{i,X}$ .

Where  $\sigma$  is the intrinsic auxin production rate in each cell. The negative sign before the second term in the equation above appears because we have taken auxin efflux to correspond to positive values of  $\Phi_{i,x}$ . We run our numerical simulations on a 50 by 50 grid of square cells using Matlab. It does not matter whether the cells are square or rectangular since all that matters is that each cell has four neighbours. Initially, each of the cells is assigned random small values for both  $c_i$  and  $\Phi_{i,x}$ . An auxin sink is present at the bottom boundary of the grid so that there is no flux from below for the bottom-most row of cells. However flux to the bottom  $\Phi_{i,B} > 0$  is allowed for these cells so that they can dump auxin into the sink. The left and right sides of the grid have hard wall boundary conditions so that no flux of auxin to or from the left is allowed for the left-most column of cells and no flux to or from the right is allowed for the right-most column of cells. Similarly, for all except two cells in the top row, the flux of auxin to or from above is not allowed. At two locations along the top row that divides the 50-cell long array into almost equal thirds, two sources of auxin are introduced. For these two cells, the influx of auxin from the top is fixed at a constant value.

Numerical integration of the set of equations describing the model proceeds as follows. Starting from the random distribution of the values fluxes and concentration of auxin, the active transport coefficients  $P_{i,x}$  associated with each cell are updated according to equation (3). Using the updated values of  $P_{i,x}$  the fluxes and concentrations associated with each cell are updated using equations (2) and (4) respectively. A small time step of 0.05 in arbitrary units is used for the numerical propagation of the system of equations. For all the simulations done, we have chosen  $\beta = \gamma = 0.0005$ , keeping the intrinsic production and decay of auxin efflux carriers relatively low in all cells. There is no intrinsic rate of production of auxin since  $\alpha = 0$  in all our numerical runs. The diffusion constant is kept at  $D = 0.3$ . In Figure 3.3, the result of integrating the equations through 24000 time steps is shown with the feedback coefficient that regulates the production of efflux carriers in response to increased auxin flux ( $\alpha$ ) is set to the value 0.05. We see that, as reported earlier as well, this system of equations leads to the formation of a vein-like structure through which the flow of auxin is canalized.

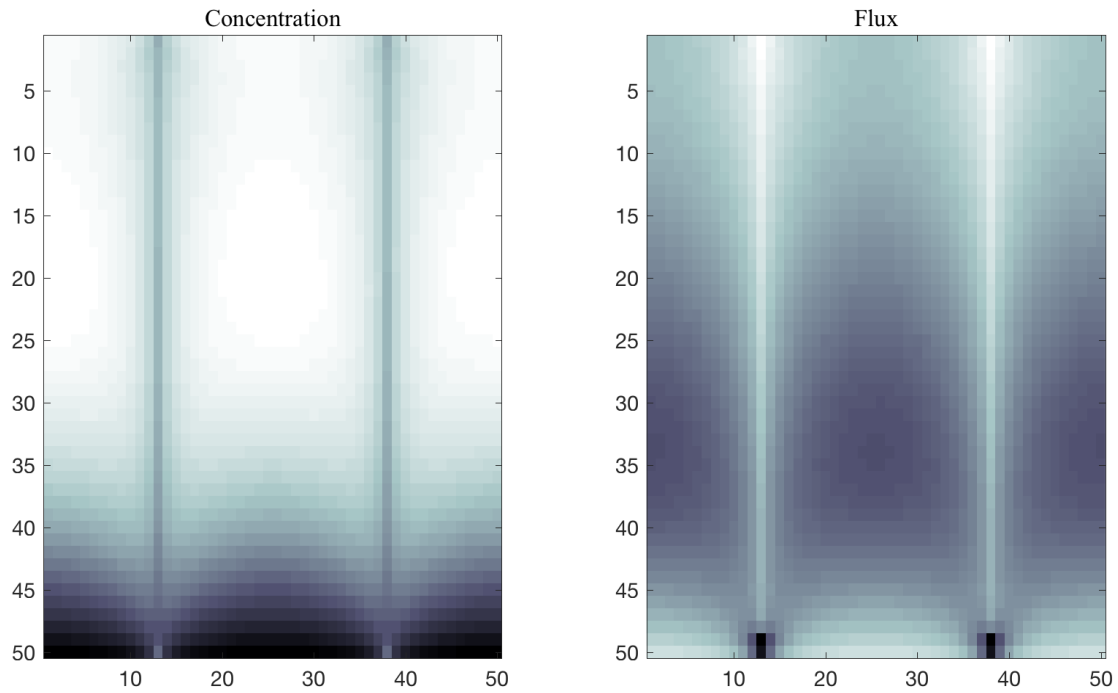


**Figure 3.2 Formation of veins in a grid of 50 by 50 cells**

In Figure 3.2, the panel on the left shows the deviation of the concentration of auxin in each cell from the average. The panel on the right shows the deviation in the total flux of auxin through each cell from the average value. The total flux is computed using equation (1) and the averages as computed across all the cells. In the panel on the left, dark areas correspond to low auxin concentrations relative to the mean and the bright areas correspond to high concentrations relative to the mean. The clearly demarcated vertical lines of cells that start at the locations of the auxin sources can be identified with the veins. Since auxin is being drained quickly in these cells and auxin does not accumulate, we see that the concentration of auxin in the location of the veins is low as expected.

It may be noted that the duration of integration up to 24000 times steps is chosen so that the vein formation has sufficient time to complete connecting the sources at the top to the sink at the bottom. The integration time is long enough to produce a steady pattern. However the integration cannot be continued much beyond the point after the vein that is dynamically formed connects to the sink. This is because the sink is much stronger than the source and it will drain substantial amount of auxin from the system bringing the concentration down to the level of numerical errors very quickly.

The panel on the right shows the auxin flux. Here dark areas correspond to higher auxin efflux relative to the mean and brighter areas show cells into which there is a net auxin influx.

As expected, cells with net auxin influx mark the veins. However the lower tip of the veins that have just made contact with the sink show high auxin efflux. At shorter integration time, the same pattern is seen at the tip of the vein that is forming, which shows that accumulated auxin at the growing tip leads to an up-regulation of the efflux carriers at the tip.

We next computed what happens when some of the cells in the path of one of the veins (vascular strand on the right in the images) that are formed are removed to simulate the effect of a small incision. A small incision that is 4 cells wide and 2 cells tall was introduced both after the initial formation of the veins as well as before they are formed. Since no qualitative difference is found in the final result, we present the results when the incision is made before the veins develop so that problems associated with very low concentrations of auxin that arise after one of the veins has made contact with the sink are avoided. The result of the numerical simulation is shown in figure 3.3.

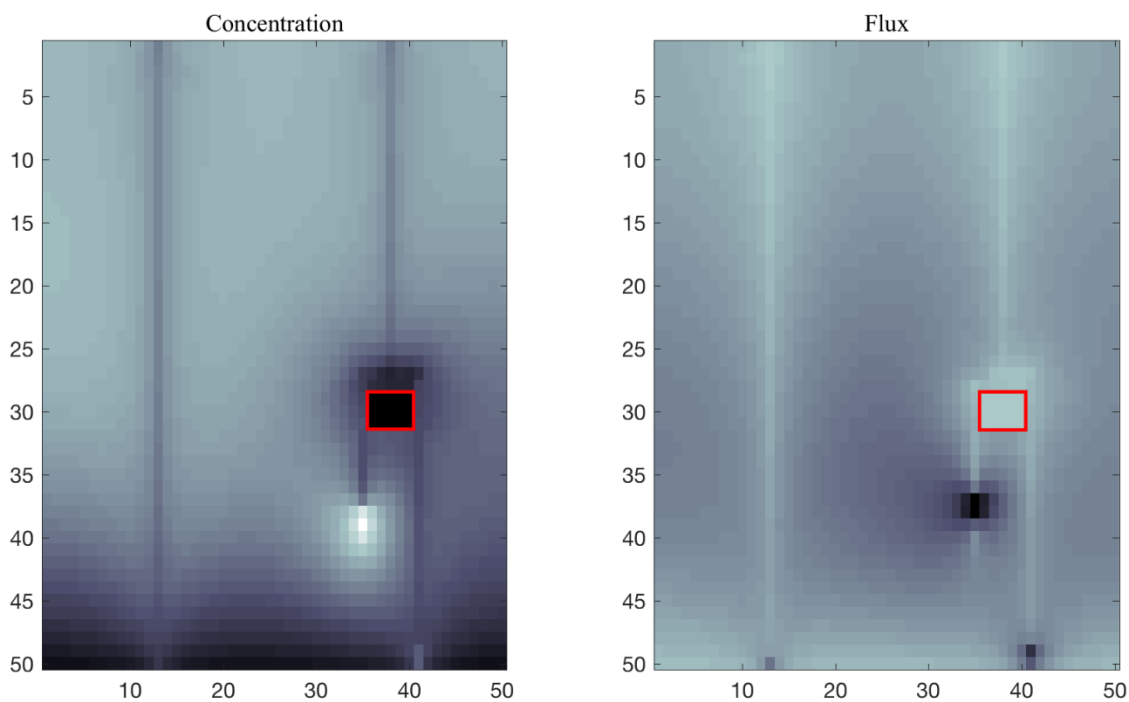


**Figure 3.3 Formation of veins when there is a small incision**

The boundary conditions set for solving the equations along the edges of the incision are such that there is no flux of auxin into or from the region where the cells have been removed. Red rectangle marks site of incision. We see that the dynamically formed veins find a path around the small incision and out of the two arms that develop around the incision; one finds its way down to the sink. Once one of the arms reaches the sink, the continued drain of auxin slows down and eventually stops the development of the second arm.

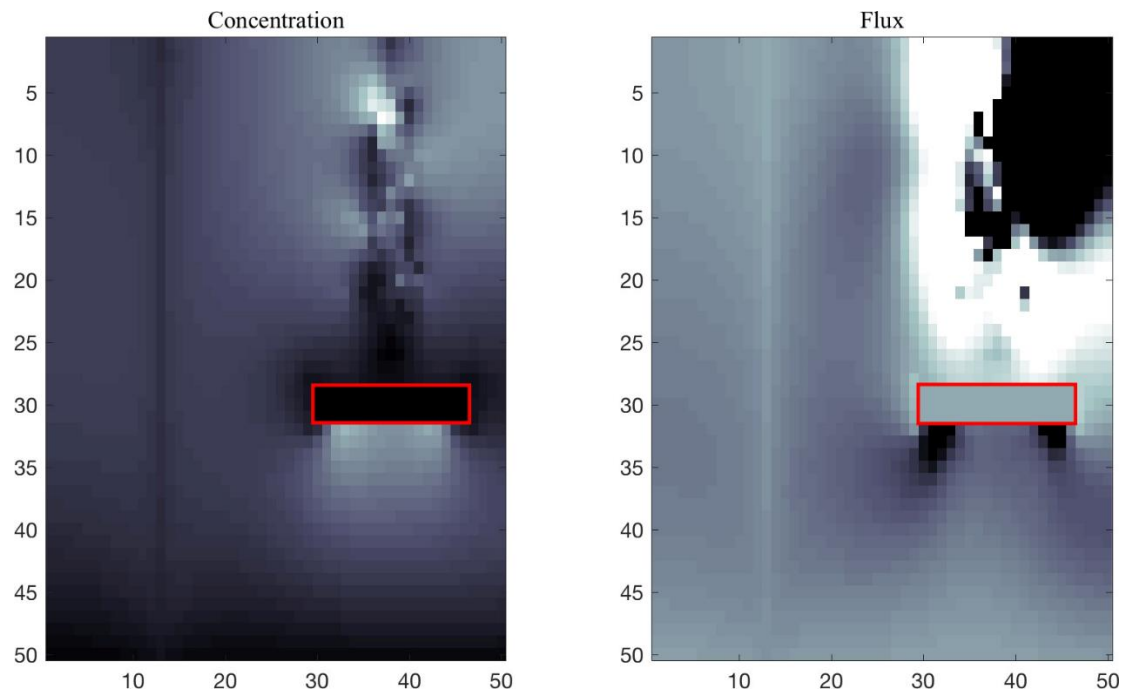


**Figure 3.4 Development of veins when there is a large incision**

The sink in the realistic case can be another branching vein that has continuous connectivity to the base of the leaf. The feedback control between the auxin flux and the active transport coefficients mimic the relationship between auxin flow and polarized PIN proteins. The numerical model shows that this feedback mechanism can indeed navigate around small incisions and regenerate the vascular tissue (Figure 3.14A, B). Red rectangle marks site of incision.

Figure 3.4 shows the development pattern at 24000 time steps when the incision is made much wider at 16 cells wide by 2 cells tall. The feedback mechanism is unable to navigate around the large incision and form a link to the sink. In some isolated cases, a connection to the already formed vein to the left is seen but in general within the time window through which the equations can be numerically integrated without proliferation of numerical errors, the development of the vein is more often than not completely curtailed by the large incision. This is again in support of the observations made in the leaf incision experiments (Figure 3.14C, D).

The pattern of veins produced is relatively robust even if the parameter values are changed provided they are changed proportionately. Increasing or decreasing one of the parameters alone can change the pattern drastically. A pertinent control case is when  $\alpha$ , which is the parameter that controls the feedback between auxin flux and active transport (efflux carriers) is set to zero. As seen from Figure 3.5, no vein like patterns develop in this case.

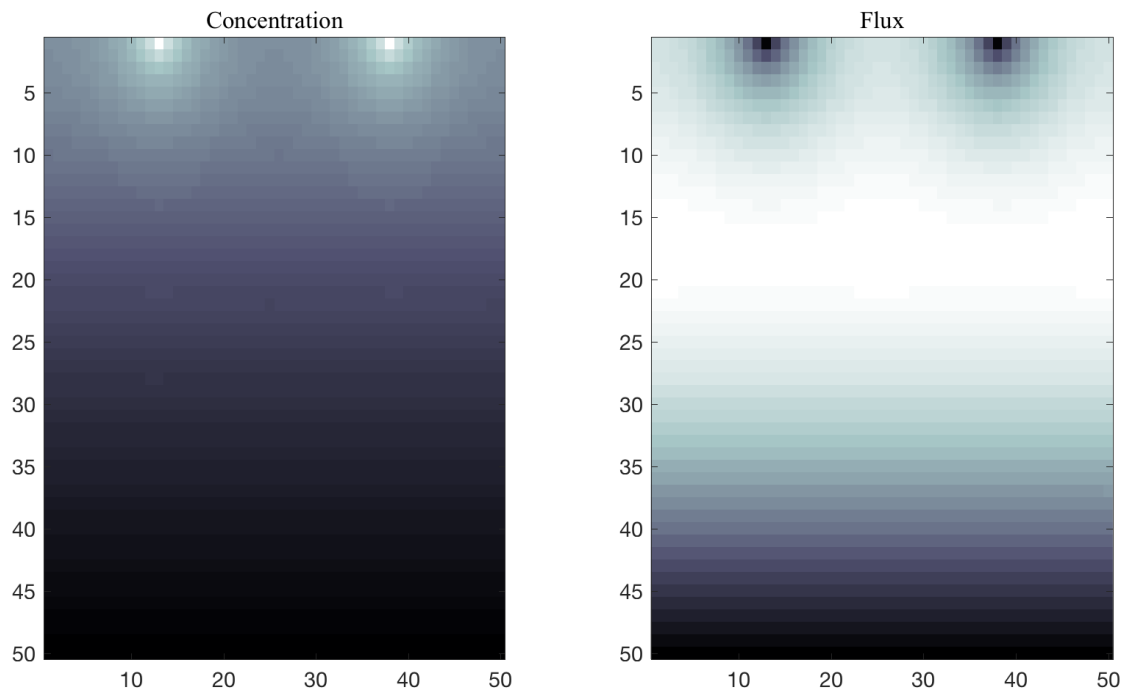


**Figure 3.5 No vein like patterns are formed without feedback**

We see that the numerical modelling yields results that closely follow what is observed as response to injury to the vascular tissue in leaves. The last case also shows that when the feedback between auxin flux and concentration/polarity of efflux carriers is broken or inhibited it leads to defects in vein formation.

### 3.3 Results

#### 3.3.1 *PLT* genes respond dynamically to mechanical injuries

*PLT3*, *PLT5*, and *PLT7* are plant-specific transcription factors (will be referred as *PLT* from here on). *PLT* is essential for tissue-culture-mediated *in vitro* shoot regeneration. *PLT* regulated root stem cell regulators establish pluripotency in callus and *PLT* regulated shoot stem cell regulators and shoot promoting factors acting in response to external hormonal cues are necessary for the regeneration of the complete plant body<sup>97</sup>.

To investigate the role of *PLT* in repairing damaged organs without external hormonal cues, we examined the expression patterns of *PLT* in response to various types of mechanical injuries that commonly occur during plant growth. These injuries included local abrasions in the stem, partial incisions (half broken stem), and midvein injuries in the leaf blade, all of which were performed without detaching any organ.

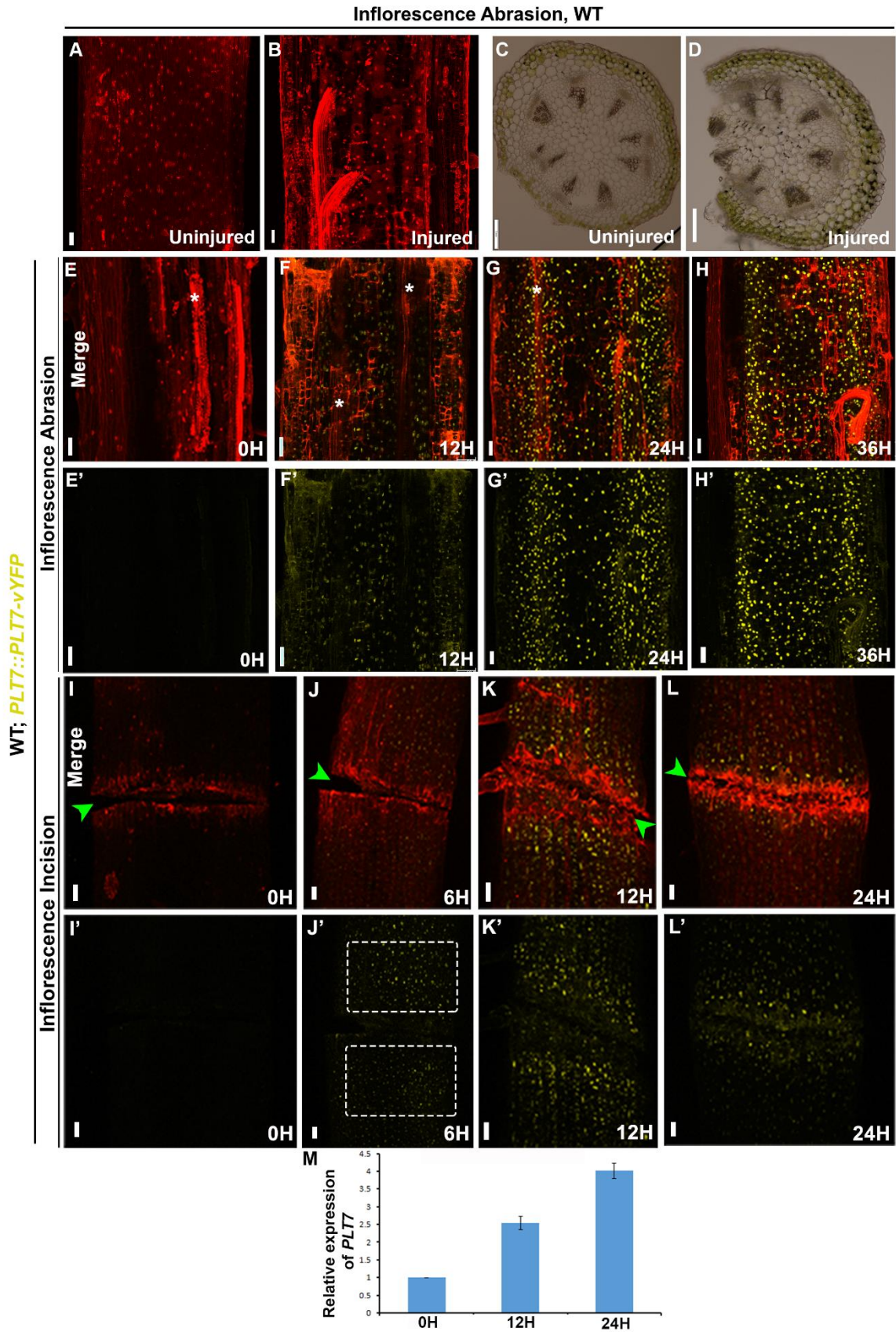


**Figure 3.6 *PLT7* gene is locally induced after mechanical injury in inflorescence stem**  
 (A-D) Inflorescence stem damage: impact on epidermal and vascular tissues. (A, C) intact inflorescence

stem. (B, D) sections revealing damage to the epidermis, sub-epidermal layers, and vascular tissue following inflorescence stem abrasion. (A, B) Longitudinal sections. (C, D) Transverse sections. (E-L') Expression of *PLT7::PLT7-vYFP* (yellow) after inflorescence abrasion (E-H') and partial incision (indicated by green arrowheads) (I-L'). White asterisks indicate vascular tissue. White dotted rectangle in J' highlights the upregulation of PLT7 expression at the upper end of the incision. E'-H' and I'-L' represent the YFP channel for E-H and I-L, respectively. (M) Transcript levels of *PLT7* in WT plants upon partial incision in the inflorescence stem: Injured segments of the inflorescence stem, encompassing the narrow domain on either side of the incision, were collected at 0H, 12H, and 24H. Expression levels were normalized to *ACTIN2*. Error bars represent s.e.m. from three independent biological replicates. Panels represent different samples at each time point. Red signal: propidium iodide staining. The brightness of the YFP signal was increased in J' for better visibility. H represents hours after injury. WT: wildtype, scale bar: 50µm.

Upon inflicting a local abrasion that damaged the epidermal and sub-epidermal layers, including the vascular tissue in the inflorescence, we observed an upregulation of PLT7 expression as indicated by the *PLT7::PLT7-vYFP* reporter 12 hours post-injury, before any visible signs of regeneration response (Figure 3.6A-D). The expression of PLT7 peaked at 36 hours (Figure 3.6E-H, E'-H'). Similarly, in response to partial incision of the inflorescence stem, we observed upregulated *PLT7::PLT7-vYFP* expression at both ends of the incised stem, with relatively higher expression in the upper end after 6 hours (Figure 3.6I, I', J, J'). This high level of expression continued for 12 hours (Figure 3.6K, K'). Notably, at 12 hours, the upregulated expression extended beyond the partial slit, and at 24 hours, it was confined to a narrower domain in the vicinity of the partial slit in the inflorescence (Figure 3.6K, K', L, L'). Consistent with the protein expression patterns, the transcript levels of *PLT7*, measured in partially incised inflorescence segments encompassing the narrow domain on either side of the wound, remained upregulated until 24 hours (Figure 3.6M).

In a similar manner, when the midvein of a growing leaf blade was wounded, cells in the surrounding area exhibited notable upregulation of *PLT7::PLT7-vYFP* expression 12 hours post injury (Figure 3.7A-D). Moreover, *PLT3::PLT3-vYFP* and *PLT5::PLT5-vYFP* showed expression patterns similar to *PLT7::PLT7-vYFP*, although with some differences in their activation timing and spatial distribution upon injuries in leaves and inflorescence stem of growing plant (Figure 3.7E-L, 3.8).

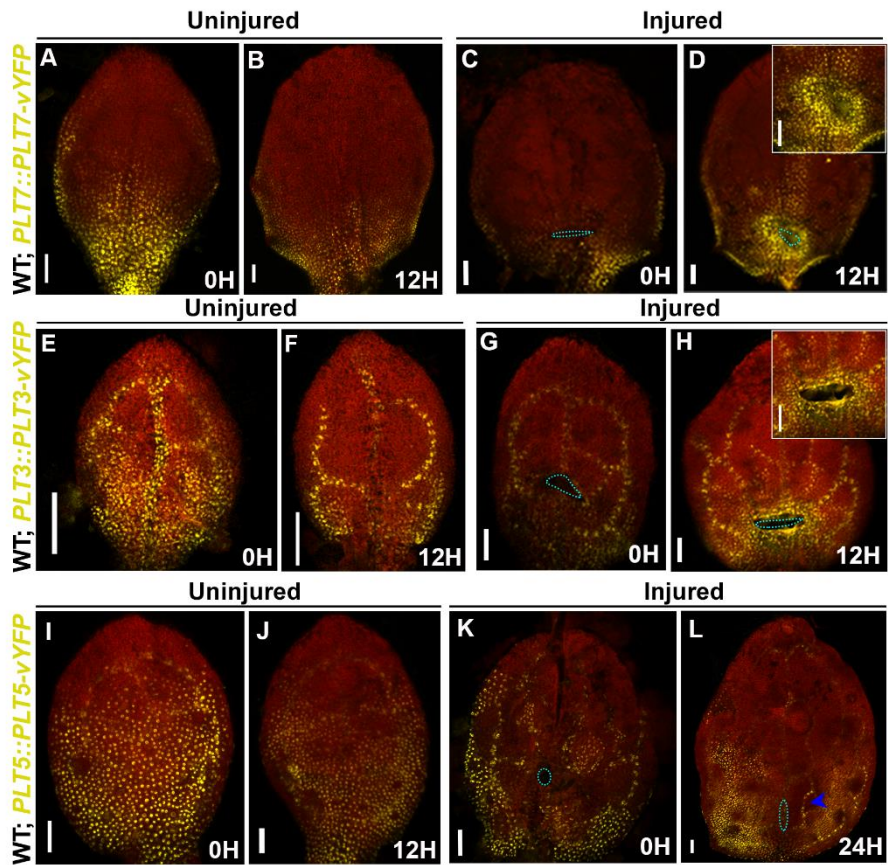


**Figure 3.7 *PLT3*, *PLT5* and *PLT7* genes are upregulated in response to injury in leaves**

(A-D) Expression of *PLT7::PLT7-vYFP* (yellow) in uninjured and injured leaves. Upregulation of *PLT7::PLT7-vYFP* observed near the wound site (insets) following leaf incision (blue dotted area indicates the incision site). (E-H) Expression of *PLT3::PLT3-vYFP* (yellow) in uninjured and injured leaves. (I-L) Expression of *PLT5::PLT5-vYFP* (yellow) in uninjured and injured leaves. The panels represent different samples at each time point. Red signal represents chlorophyll autofluorescence. H represents hours after injury. WT: wildtype, scale bars: 50µm.

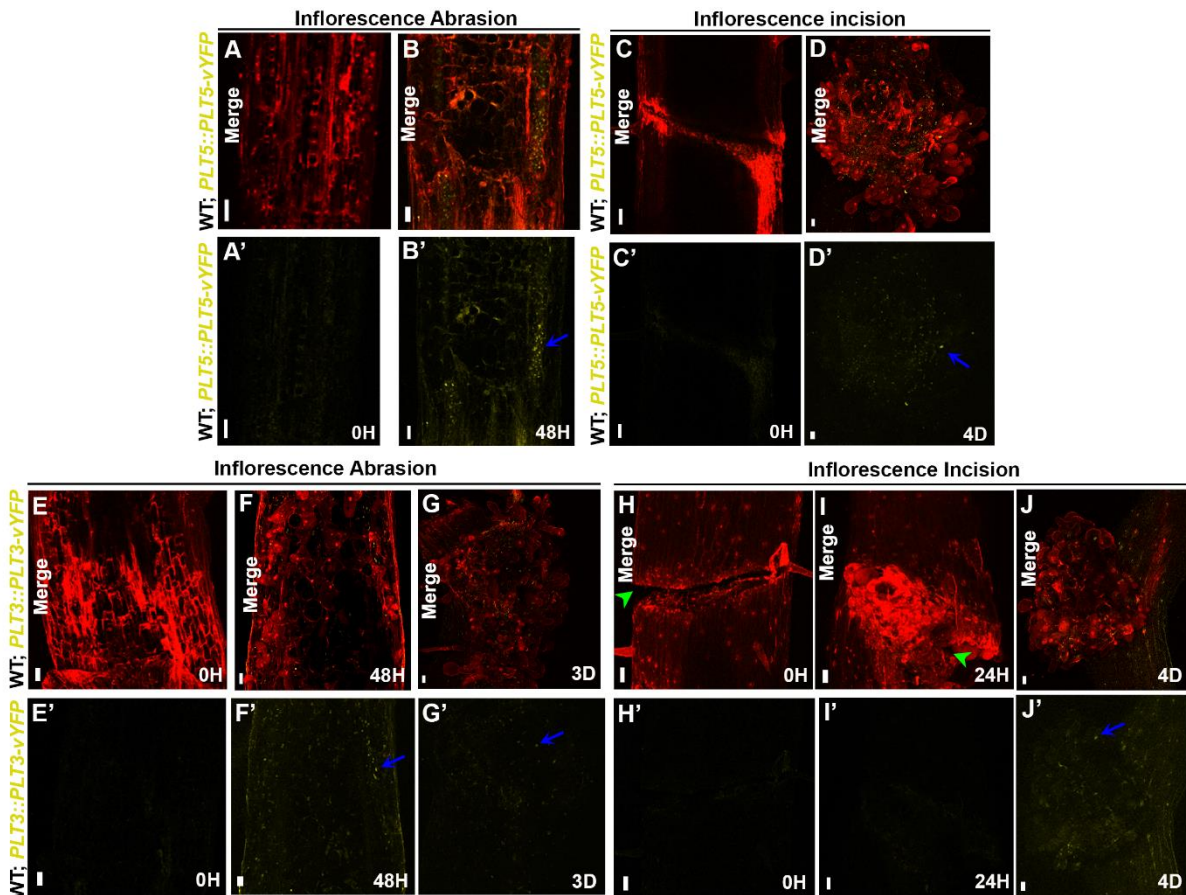


**Figure 3.8** *PLT5* and *PLT3* genes are locally induced after mechanical injury in inflorescence stem

(A-D') Expression of *PLT5::PLT5-vYFP* in response to inflorescence stem abrasion and partial incision. Note the upregulation of *PLT5::PLT5-vYFP* in wounded vascular tissue (B', blue arrow) and in callus formation (D'). (E-J') Expression of *PLT3::PLT3-vYFP* in response to inflorescence stem abrasion and partial incision. Weak expression (blue arrow) is observed in sub-epidermal tissues (F') and in callus formation (G' and J'). (E'-G' and H'-J'). Maximum intensity projection of z-stack in YFP channel. Red colour represents propidium iodide staining. Green arrowheads indicate partial incision in the inflorescence stem. Blue arrows highlight *PLT3* or *PLT5* expression in response to injury. Each panel represents a different sample at each time point. WT: wildtype, Scale bar: 50µm. H: hours post-injury, D: days post-injury.

Furthermore, *PLT7::PLT7-vYFP*, *PLT3::PLT3-vYFP*, and *PLT5::PLT5-vYFP* also responded to injuries when organs such as hypocotyl, leaf, and root were detached from plants. We observed their expression in the vascular tissue, in the callus formed at the cut end, as well as in the regenerating root emerging from the cut end of the leaf (Figure 3.9, Chapter 4). These findings suggest that *PLT3*, *PLT5*, and *PLT7* transcription factors are upregulated in response to various types of injuries in aerial organs of growing plant.

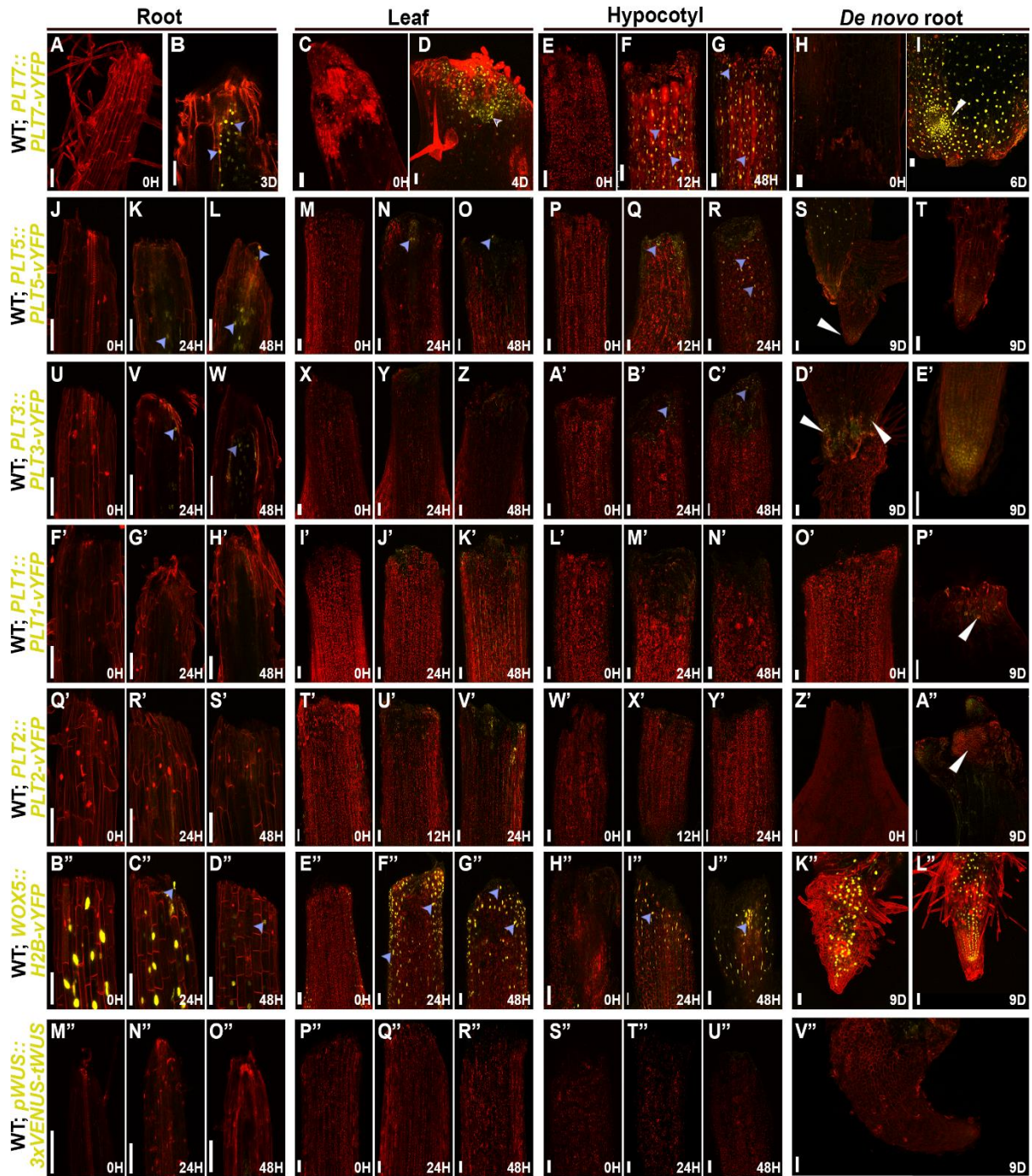


**Figure 3.9** *PLT* show dynamic expression in excised explants during wound healing

(A-I) Expression of *PLT7::PLT7-vYFP* observed in excised root (A,B), leaf (C,D), and hypocotyl (E-G), as well as during *de novo* root formation from the cut end of leaf petiole (H,I). Blue arrowheads indicate expression in response to wounding. (J-T) Expression of *PLT5::PLT5-vYFP* observed in excised root (J-L), leaf (M-O), hypocotyl (P-R), and during *de novo* root formation (S,T). White arrowhead marks root primordia. (U-E') Expression of *PLT3::PLT3-vYFP* observed in excised root (U-W), hypocotyl (A'-C'), and during *de novo* root formation from the cut end of leaf petiole (D',E'). *PLT3-YFP* was rarely detected (refer chapter 4 for *PLT3* expression in cut end of leaf) in excised leaf (X-Z). (F'-O') No expression of *PLT1::PLT1-vYFP* observed in excised explants. (P') Expression of *PLT1::PLT1-vYFP* (white arrowhead) observed in the cut end of the leaf during *de novo* root formation. (Q'-Z') No expression of *PLT2::PLT2-vYFP* observed in excised explants. (A'') Expression of

*PLT2::PLT2::vYFP* (white arrowhead) observed in root primordia during *de novo* root formation from excised leaf. (B''-J'') Expression of *WOX5::H2B-vYFP* observed in excised root (B''-D''), excised leaf (E''-G''), excised hypocotyl (H''-J''). (D'') *WOX5::H2B-vYFP* expression (arrow) is downregulated in excised root at 48 hours. (J'') Increased expression of *WOX5::H2B-vYFP* at 48 hours observed in the vascular strand at the cut end of hypocotyl. (K'', L'') Expression of *WOX5::H2B-vYFP* during *de novo* root formation. (M''-V'') No expression of *WUS::3xVENUS-tWUS* observed in excised explants. Scale bars represent 50  $\mu$ m. Red colour in A-D, J-L, U-W, F'-H', Q'-S', B''-D'', and M''-O'' represents propidium iodide staining, while in the rest it represents chlorophyll autofluorescence. All images are maximum projections of z stacks, except B, K, L, V, W, G', and H' which represent a subset of layers to show expression in internal tissues. Blue arrowheads mark expression in response to injury, while white arrowheads mark root primordia. Brightness and contrast have been adjusted in autofluorescence channels for clarity of the cut part. WT: wildtype.

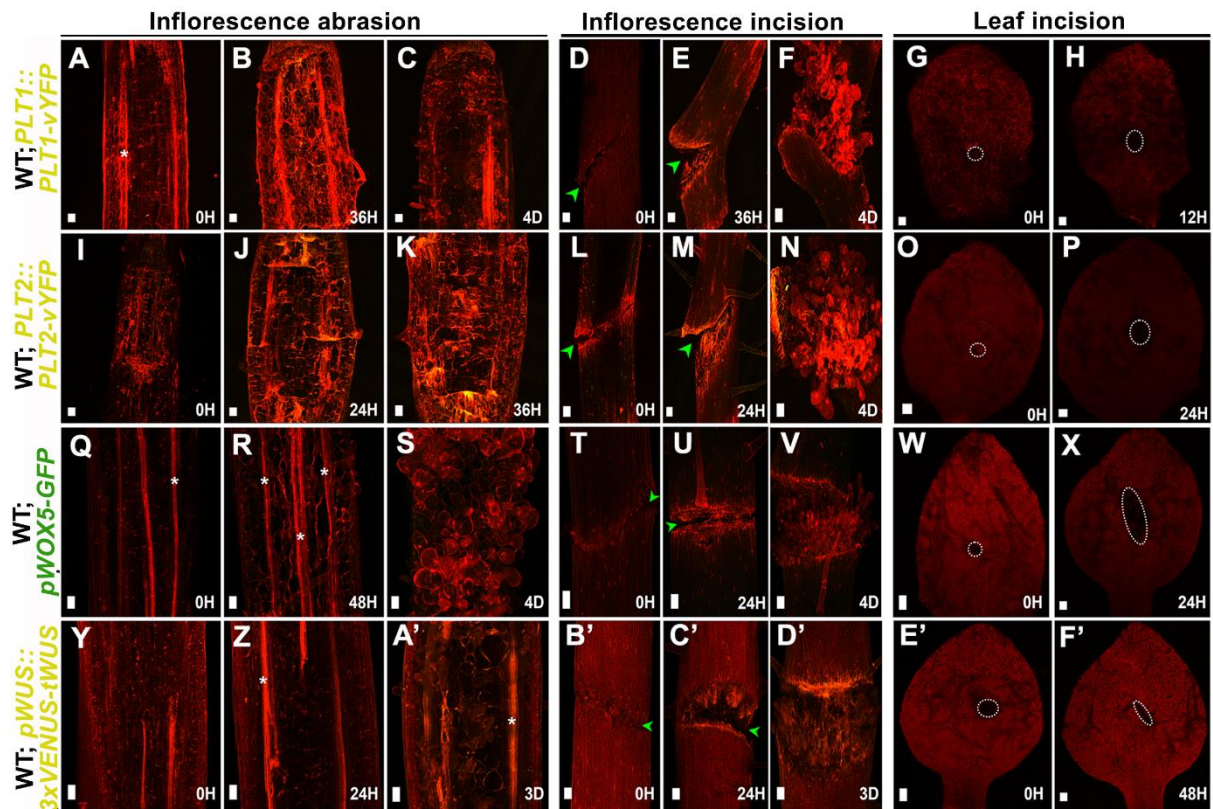


**Figure 3.10 Root and shoot stem cell regulators are not activated upon injury in growing leaves and stem**

(A-F') Lack of expression of *PLT1::PLT1-vYFP*, *PLT2::PLT2-vYFP*, *WOX5::GFP*, and *WUS::3xVENUS-tWUS* following injury in growing aerial organs. Red colour in all leaf incision panels is due to autofluorescence, while it represents propidium iodide staining in the rest. Green arrowheads mark the site of partial incision in the inflorescence stem. White asterisks represent vascular tissue exposed by inflorescence abrasion. H: hours post injury, D: days post injury, Scale bars represent 50  $\mu$ m.

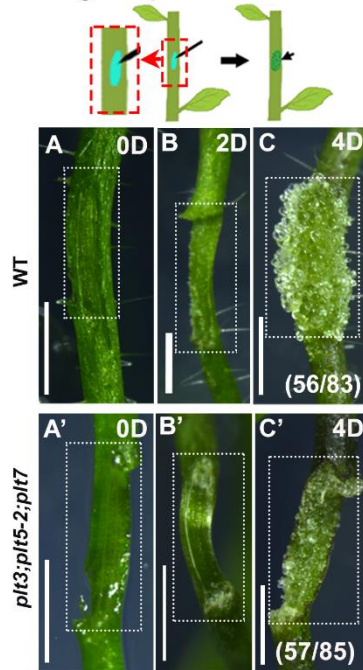
### **3.3.2 *PLT* is required to activate innate regenerative responses to injuries in aerial organs growing in a normal developmental-context**

Considering that aerial organs of growing plants experience significant wear and tear, it is important to investigate the role of *PLT* in regulating wound repair and tissue regeneration. Therefore, our study aimed to examine the involvement of *PLT* in controlling these processes in aerial organs, specifically in stems and leaves, within the normal developmental context of *Arabidopsis*.

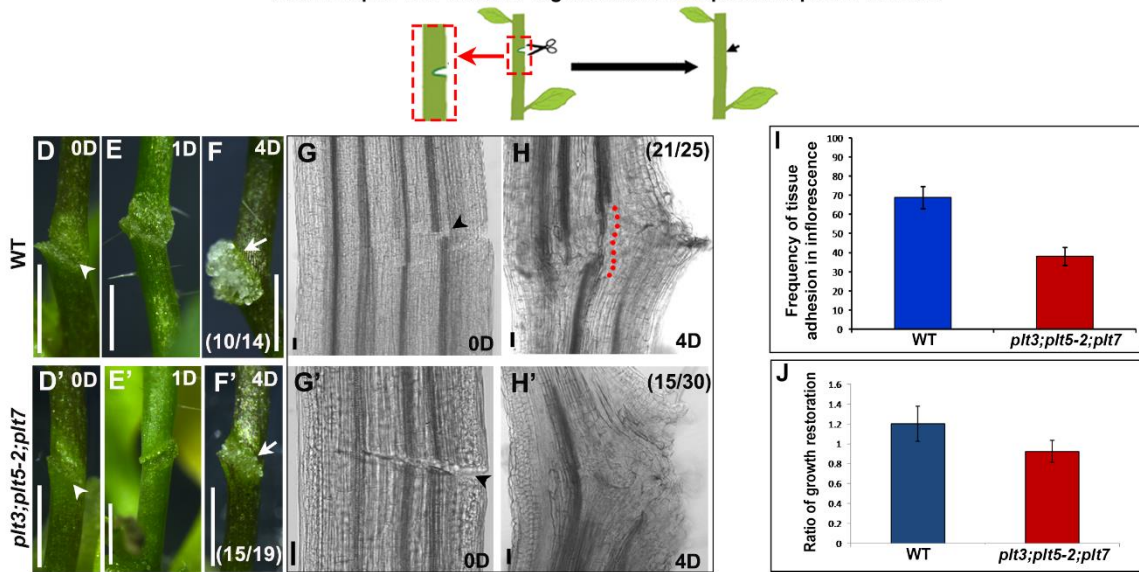
#### 3.3.2.1 Wound repair and vascular regeneration in inflorescence stem

To mimic physical abrasion, we locally damaged specific tissue layers, including the epidermis, sub-epidermal layers, and vascular tissue, in the growing inflorescence stem of both WT and *plt3;plt5-2;plt7* mutant plants (Figure 3.11A, A'). In WT plants, a healing response was observed at 2 days after abrasion (2daa), where a visible mass of proliferating cells, resembling callus-like growth, was present throughout the wound (Figure 3.11B, C). By 4daa, this callus-like growth completely covered and sealed the wound, allowing the inflorescence stems to resume their growth (Figure 3.11B, C). In contrast, the injured *plt3;plt5-2;plt7* inflorescence showed a significantly reduced healing response compared to the WT (Figure 3.11A'-C'). The wound sealing process was incomplete in the triple mutant, and a prominent callus-like growth was not formed. These impaired wound repair phenotypes were fully penetrant in the mutant plants. Notably, the impaired response was specific to the injured inflorescence and did not affect the development of uninjured mutant stems (Figure 3.16K, L).

Wound healing in response to inflorescence abrasion



Wound repair and vascular regeneration in response to partial incision



K Vascular regeneration assay

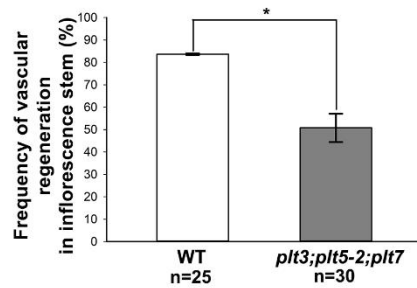


Figure 3.11 *PLT* genes are required for wound healing and vascular regeneration in growing inflorescence stem

(A-C') Schematics above A-C represent inflorescence stem abrasion (red rectangle; cyan indicates wounded region) and wound healing response (arrow). (A, A') Abrasion (dotted rectangles) in inflorescence stems of WT (A) and *plt3;plt5-2;plt7* (A') on 0D after injury. (B, B', C, C') Reduced wound healing response (dotted rectangles indicate the area of cell proliferation) in *plt3;plt5-2;plt7* (B', C') compared with WT (B, C) on 2D and 4D after injury. (D-H, D'-H', K) Partial incision in inflorescence stem. (D, D') Partial incision (white arrowheads) in inflorescence stems of WT (D) and *plt3;plt5-2;plt7* (D') on 0D after injury. (E, F, E', F') Compromised callus formation (white arrows) in inflorescence stems of *plt3;plt5-2;plt7* (E', F') compared with WT (E, F). (G, G') Disruption of vascular tissue (black arrowheads) by partial incision in inflorescence stems of WT (G) and *plt3;plt5-2;plt7* (G'). (H, H') Vascular strands regenerate in WT inflorescence stems (H) but fail to regenerate in ~49% of *plt3;plt5-2;plt7* stems (H'). Schematics above F-H indicate partial incision on inflorescence stem (red rectangle) and wound healing response. Black arrow indicates site of wound healing. (I) More callus formation in WT 24 hours following inflorescence incision leading to increased frequency of tissue adhesion in WT as compared to *plt3;plt5-2;plt7* (E'). (J) Graph representing growth restoration in WT and *plt3;plt5-2;plt7* post partial incision in inflorescence. (K) Frequency of vascular regeneration in response to partial incision in the inflorescence stems of WT and *plt3;plt5-2;plt7* (\* $P=0.033$ ; Pearson's  $\chi^2$  test). Error bars represent s.e.m. In image panels, sample numbers are shown in parentheses. Scale bars: 1 mm (A-F'); 50  $\mu\text{m}$  (G, G', H, H'). D, days after injury. WT: wildtype.

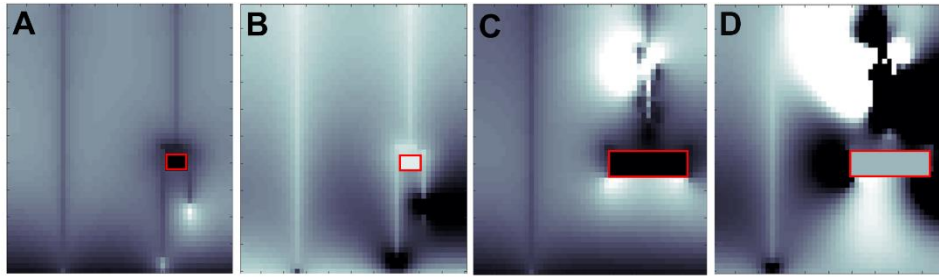
Next, we inflicted an injury by creating a partial slit in the inflorescence stem of both WT and *plt3;plt5-2;plt7* mutant plants, causing disruption to the connections of both vascular and ground tissues. (Figure 3.11D-K). Within 24 hours of the incision, we observed adhesion of the wounded parts in the WT inflorescence stem (Figure 3.11E, E', I). Subsequently, there was evidence of cell proliferation, indicated by visibly swollen tissues at the cut ends, followed by the regeneration of vascular tissues at 4 days after the cut (4dac) (Figure 3.11G). The restoration of physiological function was demonstrated by the development of new flowers and siliques (Figure 3.11H). In contrast to the WT, where the wound was completely healed by the 4<sup>th</sup> day, the *plt* triple mutant exhibited a severely reduced callus-like growth at the wound site and failed to regenerate vascular tissue (Figure 3.11D-H, D'-H', K).

These findings highlight the crucial role of PLT in initiating the healing response, characterized by callus-like growth and vascular regeneration, to repair and restore damaged tissue in the growing inflorescence stem.

### 3.3.2.2 Vascular regeneration in a growing leaf

Vascular tissue connects the growing lateral organ such as leaf to the stem. Unlike the cylindrical and unbranched vascular strands found in the stem, the vascular system in *Arabidopsis* leaves consists of intricate networks of veins that transport water, nutrients, and hormones. It includes the midvein, which runs centrally along the leaf, and lateral veins that branch out from it. The arrangement and density of veins vary based on leaf type and developmental stage<sup>135</sup>.

To explore the relationship between the development of leaf veins and their ability to repair wounds, we conducted experiments involving the midvein of young WT leaf blades (Please refer chapter 2 for more details). Next, we sought the possible mechanistic basis of the effects of wound size on vascular regeneration. Towards this end, we employed a computational modelling approach and examined if vascular regeneration in response to injury can be recapitulated *in silico* by implementing a canalisation model proposed for leaf vascular tissue development<sup>136</sup>. According to the canalisation approach, positive feedback between auxin flux and PIN1 polarization leads to channelized auxin flow, that in turn, promotes the differentiation of vascular tissue in the stem<sup>119</sup>. As a proof-of-concept we combined an existing mathematical model of leaf vascular tissue development<sup>136</sup> with our experimental data and examined if re-establishment of feedback regulation between auxin flux and PIN1 polarization is key to drive vascular regeneration in a growing leaf<sup>134,136,137</sup>. Equations governing the mathematical model and other relevant details are presented in the methods section of this chapter. On an array of rectangular cells, a pair of localized auxin sources are introduced at the top edge of the array. In the presence of feedback regulation in the system of equations, two distinct channels of high auxin flux emerged from the locations of the sources and connected down to the bottom end of the array of cells which acted as an auxin sink. (Section 3.2.10 in Materials and methods). The formation of these structures was consistent with previous numerical studies of the same model<sup>136</sup>. We next mimicked the vascular injury *in silico* by creating either a narrow or a wide gap interrupting one of the two vein like structures within the matrix (Figure 3.12, Section 3.2.10 in Materials and methods). In the presence of continued auxin supply from the apical source, a new vascular strand formed from the upper end of the narrower gap and connected to the lower end of the array (Figure 3.12A, B, Section 3.2.10 in Materials and methods). Conversely, with a wider gap no new strand like structures formed (Figure 3.12B, C, Section 3.2.10 in Materials and methods). This was presumably because diffusion of auxin over a larger area did not allow the activation of feedback regulation between auxin flux and PIN polarization that was strong enough to result in channelized auxin flow. Furthermore, veins were not formed when the feedback regulation between PIN proteins and auxin was turned off (Section 3.2.10 in Materials and methods). Thus computational modelling recapitulated the effects of wound size on vascular regeneration (Please see Section 3.2.10 in Materials and methods for the details of numeric and *in silico* simulation).



Simulations done by Anil Shaji, School of Physics, IISER TVM,  
Biological parameters quantified and given by Anju P S

**Figure 3.12 Numerical simulation of mathematical model shows the effect of wound size on leaf vascular regeneration**

(A-D) Numerical simulation of mathematical model incorporating positive feedback between auxin flux and PIN1 shows the effect of wound size on leaf vascular regeneration. In a grid of cells, two apical auxin sources are introduced. Auxin flux is initiated in the downward direction from both sources and the flux is canalized by the positive feedback between the flux and PIN1. A rectangular region where cells have been removed from the grid, representing the wound, intercepts one of the two channels. The red box in panels (A-D) marks this region and the panels show a snapshot of the dynamics taken at the instant when auxin flux is established from top to bottom through the control channel on the left. (A, B) correspond to a small wound while (C, D) correspond to a larger one. In A and C the auxin concentration is shown with brighter areas representing higher concentrations while B and D shows the flux, with brighter areas representing higher flux. Concentration, as expected, is low where the flux is high and high flux channels correspond to regions where vascular regeneration has occurred. A path to the bottom of the grid is established in the case of small wounds but such a path does not form when the wound is larger.

To avoid variations in extent and form of damage among samples, we restricted our analysis to leaf blade injuries that completely disconnected the midvein leaving a gap well under 400 $\mu$ m between the cut ends in various genetic backgrounds described here onwards. In WT plants, approximately 80% of the injured leaves were able to regenerate vascular strands, effectively reconnecting the lateral veins to the midvein. However, in *plt3;plt5-2;plt7* mutant plants, only around 45% of the injured leaves were capable of regenerating vascular tissue, while the remaining leaves failed to generate any new vascular strands (Figure 3.13A-E). In non-regenerating mutant leaves, the lateral veins were unable to establish connections near the wound site (Figure 3.13B', H). Instead, we observed an unorganized mass of proliferating cells at the wound site, primarily at the cut ends of the upper vascular strands and on the epidermis. These leaves exhibited poor growth and failed to develop properly (Figure 3.13H, H').

### Vascular regeneration in response to injury in growing leaf

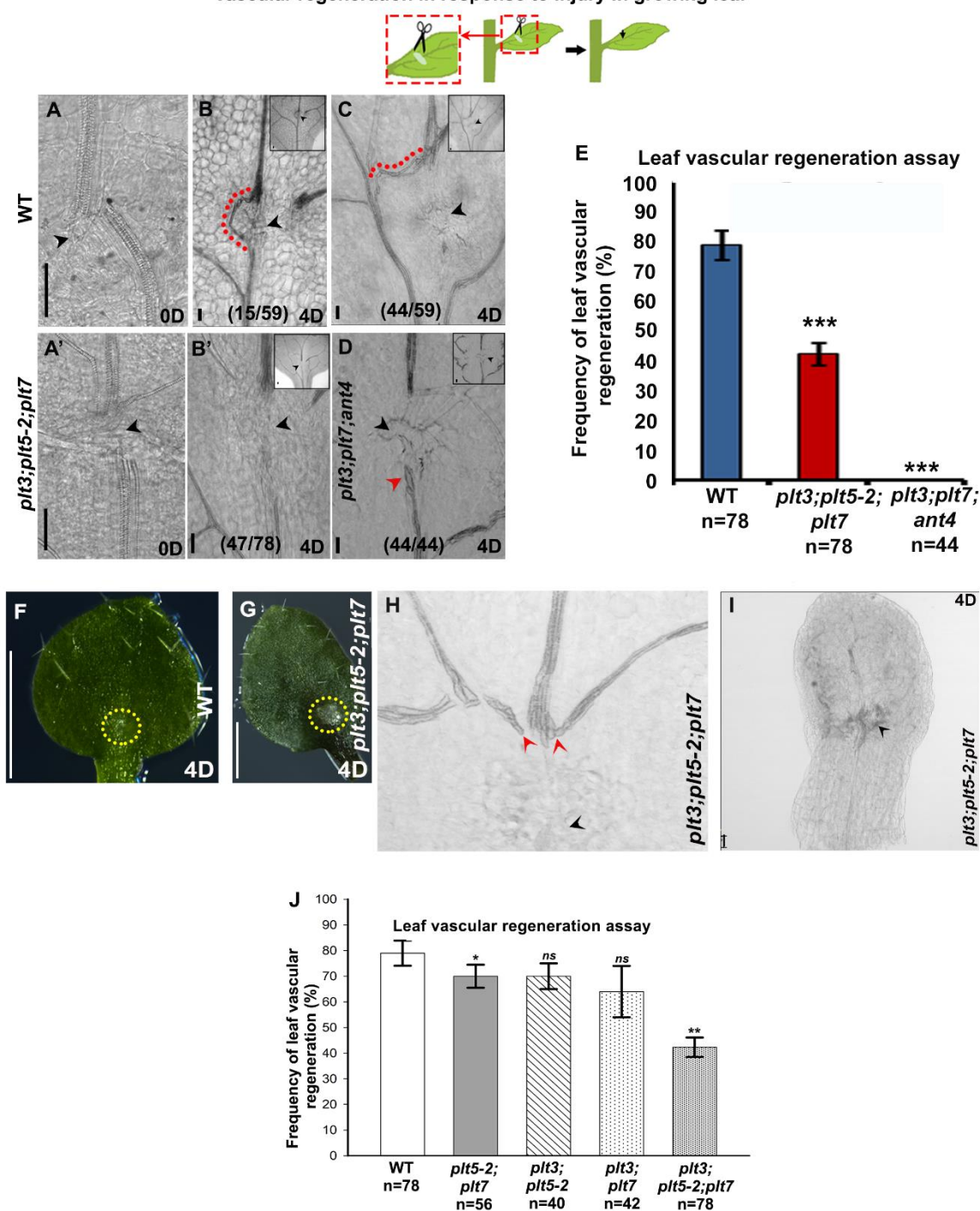


**Figure 3.13** *PLT* activates innate regenerative responses to injuries in aerial organs growing in the normal developmental context

(A-D) Vascular strand regeneration in growing leaf. (A, A') Incision (black arrowhead) in the midvein of WT (A) and *plt3;plt5-2;plt7* (A') growing leaf. (B) Vascular strand regeneration (red dotted line) in WT leaf bypassing wounded area and connecting cut ends of midvein. (C) New vascular strand (arrow in rectangle and red dotted line) connecting damaged upper end of midvein to lateral vein. (H', J) Vascular strand failed to regenerate in *plt3;plt5-2;plt7* (B') and *plt3;plt7;ant4* (D) mutant leaves in response to midvein injury. Red arrowhead in (D) marks proliferating cells at the lower cut end of midvein. Black arrowhead in represent site of leaf incision. Insets show zoomed out images of site of injury marked by black arrows. (E) Frequency of leaf vascular regeneration in WT, *plt3;plt5-2;plt7*

(\*\*\* $P=1.211 \times 10^{-15}$ ) and *plt3; plt7; ant-4* mutants (\*\*\* $P=7.707 \times 10^{-13}$ ). (F-I) Response of *plt3;plt5-2;plt7* mutant leaf after incision (F) No local cell proliferation was observed on WT leaf surface, (G). Proliferation in epidermis (G) and vascular strand (H) (red arrowhead) of *plt3;plt5-2;plt7* following leaf incision (site of incision marked by yellow dotted circle/ black arrowhead). (I) Following incision, many of the *plt3;plt5-2;plt7* mutant leaves display stunted growth and slower development. Black arrowhead: site of incision. Scale bar represents 1 mm in F and G and 50  $\mu\text{m}$  in others. Error bar represents s.e.m. WT: wildtype.

Importantly, uninjured *plt3;plt5-2;plt7* mutant plants did not exhibit any defect in leaf venation pattern or vascular development in the formation of closed vein loops compared to WT plants<sup>47</sup>. However, they were severely impaired in their ability to regenerate vascular tissue (Figure 3.13E, 3.14A, B). Regarding leaf morphology, we did not observe any defects in the initial pair of leaves. However, a few of the later arising leaves displayed subtle changes at their margins (Figure 3.14). Among the different combinations of double mutants, *plt3;plt5-2* and *plt5;plt7* double mutants did not show any apparent defects in leaf vascular regeneration compared to WT plants. Around 70% of the mutant leaves in these combinations were able to regenerate vascular strands in response to midvein injury (Figure 3.15A).

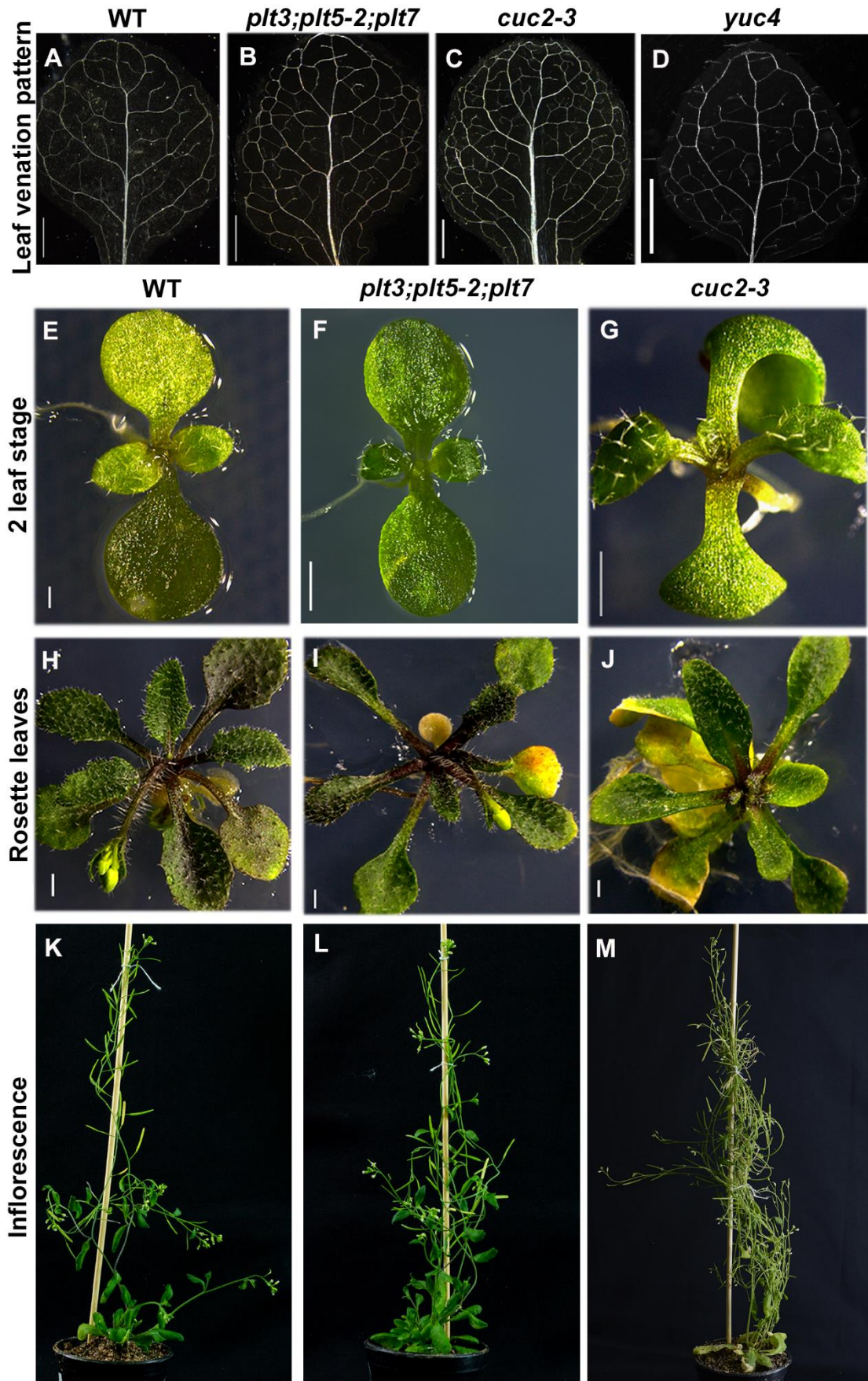


### Figure 3.14 Venation pattern in leaf and developmental stages

(A-D) Venation pattern of *plt3;plt5-2;plt7* (B) and *cuc2-3* (C) mutant does not show any change in leaf vascular pattern and vascular tissue development as compared to WT (A). (D) Venation pattern of *yuc4* mutant showing no defect in the formation of midvein and lateral veins. (E-M) *plt3;plt5-2;plt7* and *cuc2-3* mutants grow comparable to WT. WT: wildtype.

The closely related *AINTEGUMENTA* (*ANT*) gene marks stem cells of root vascular cambium and acts redundantly with *PLT3* and *PLT7* during plant development<sup>128,138</sup>. *ANT* is strongly expressed in the vascular tissue of young leaves (Figure 3.15B). We therefore examined vascular regeneration in *plt3;plt7;ant-4* triple mutant plants in response to midvein injury. Strikingly, none of the tested *plt3;plt7;ant-4* seedlings regenerated vascular tissues demonstrating an essential role of *ANT* with *PLT3* and *PLT7* in vascular regeneration (Figure 3.13E, 3.15C). Due to the severe shoot phenotypes observed in *plt3;plt7;ant-4* mutants, where only leaves but no stem were produced, we selected the *plt3;plt5-2;plt7* mutant for further investigation as it developed normal leaves and an inflorescence similar to WT plants<sup>90,128</sup>.

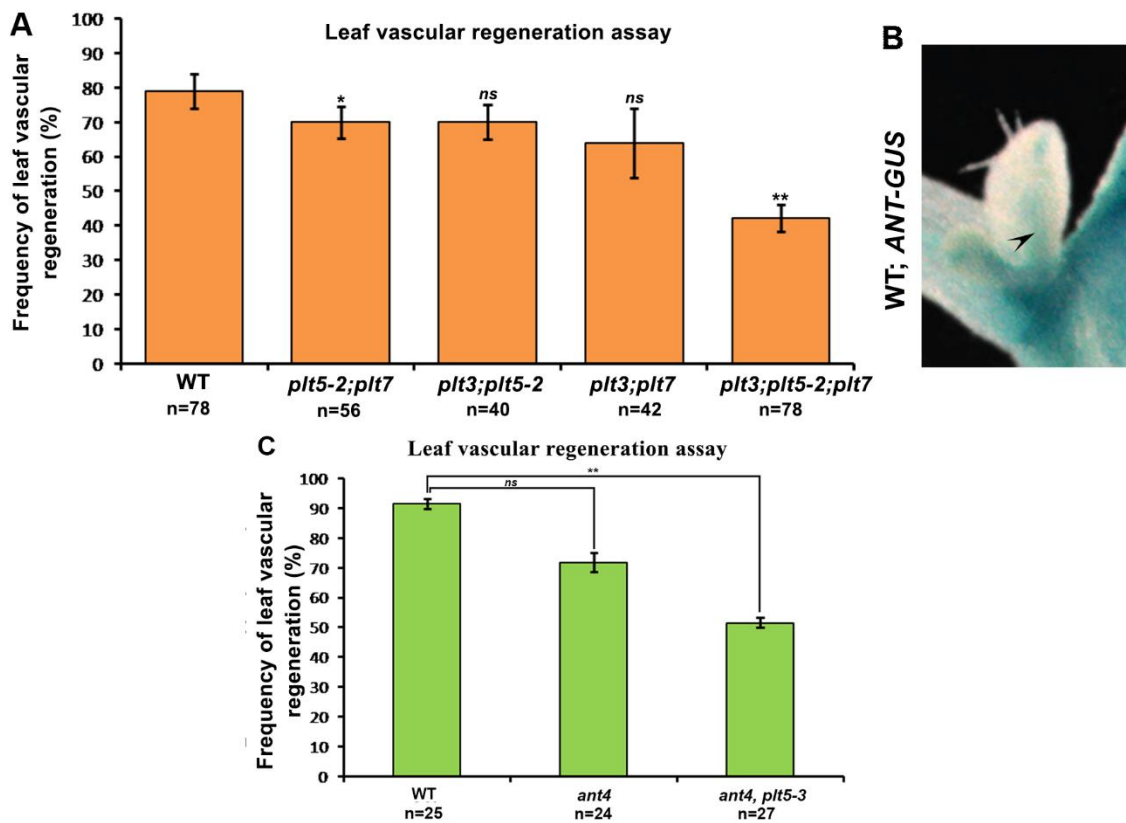


### Figure 3.15 Leaf vascular regeneration and expression of *ANT*

(A) Frequency of leaf vascular regeneration in WT, *plt* double mutants and *plt3;plt5-2;plt7* triple mutants (\* $P=0.025$ ; \*\* $P=0.008$ ; ns,  $p>0.05$ ) (WT\_n=78, *plt5-2;plt7*\_n=56, *plt3;plt5-2*\_n=40, *plt3;plt7*\_n=42, *plt3;plt5-2;plt7*\_n=78). (B) Expression of *ANT* in leaf vasculature (black arrow). (C) Frequency of leaf vascular regeneration in WT, *ant4* mutant and *ant4;plt5-3* double mutant (ns,  $P>0.05$ ; \*\* $P=0.004$ ) (WT\_n=25, *ant4*\_n=24, *ant4;plt5-3*\_n=27). WT: wildtype.

### 3.3.3 *PLT* displays developmental-context sensitivity in regulating local cell proliferation response only vs tissue or organ regeneration in response to injury

The *plt3;plt5-2;plt7* mutant exhibited a decreased healing response in the damaged inflorescence stem, as indicated by reduced callus-like growth. However, noticeable cell proliferation was observed in the damaged leaf (Figure 3.13B', F-H). Unlike the reduced callus-like growth observed in excised organs, callus formation remained unaffected in the *plt3;plt5-2;plt7* mutant leaves after incision (Figure 3.13F, G, 3.18). These findings distinguish the local cell proliferation response from the regeneration of vascular tissues or organs, suggesting that the role of *PLT* genes cannot be generalized as regulators of callus formation in response to injuries (Figure 3.17). Taken together, our study reveals a previously unrecognised role of *PLT* and *ANT* in repairing damaged tissues during the plant growth.

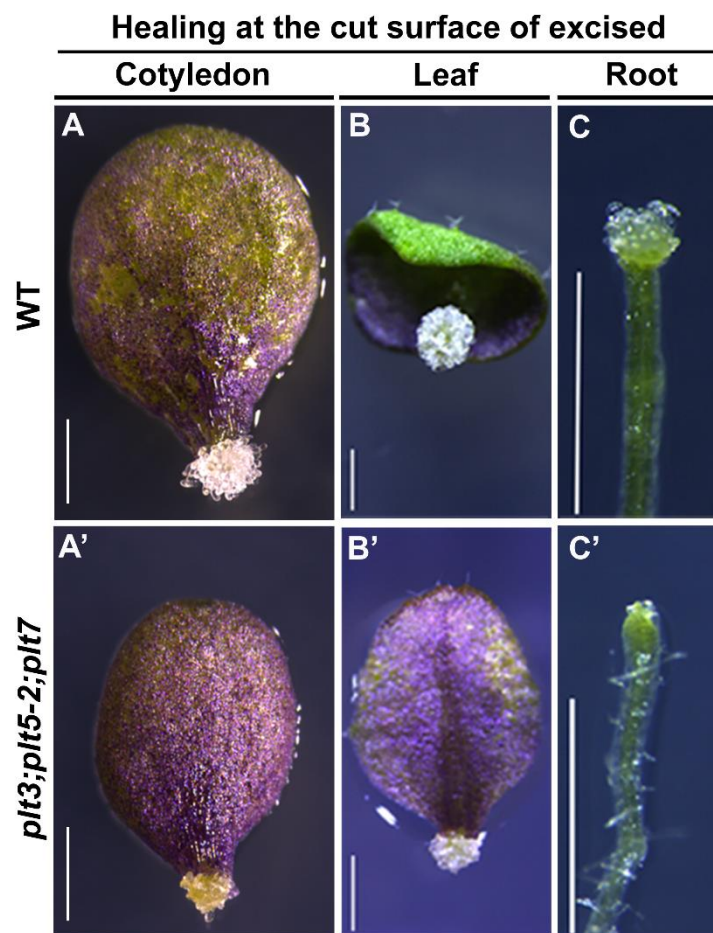


**Figure 3.16 *PLT* are required for wound healing response in excised explants**

(A, A') Excised cotyledon of WT (A) shows more callus formation at cut end as compared to *plt3*, *plt5-2*, *plt7* (A'), 9 day post cut (dpc). (B, B') Reduced callus formation at the wound site in leaf of *plt3;plt5-2;plt7* (B') as compared to WT (B) on 7dpc. (C, C') Reduced callus formation at the wound site in root of *plt3;plt5-2;plt7* (C') as compared to WT (C) on 15 dpc. Scale bar represents 1mm. WT: wildtype.

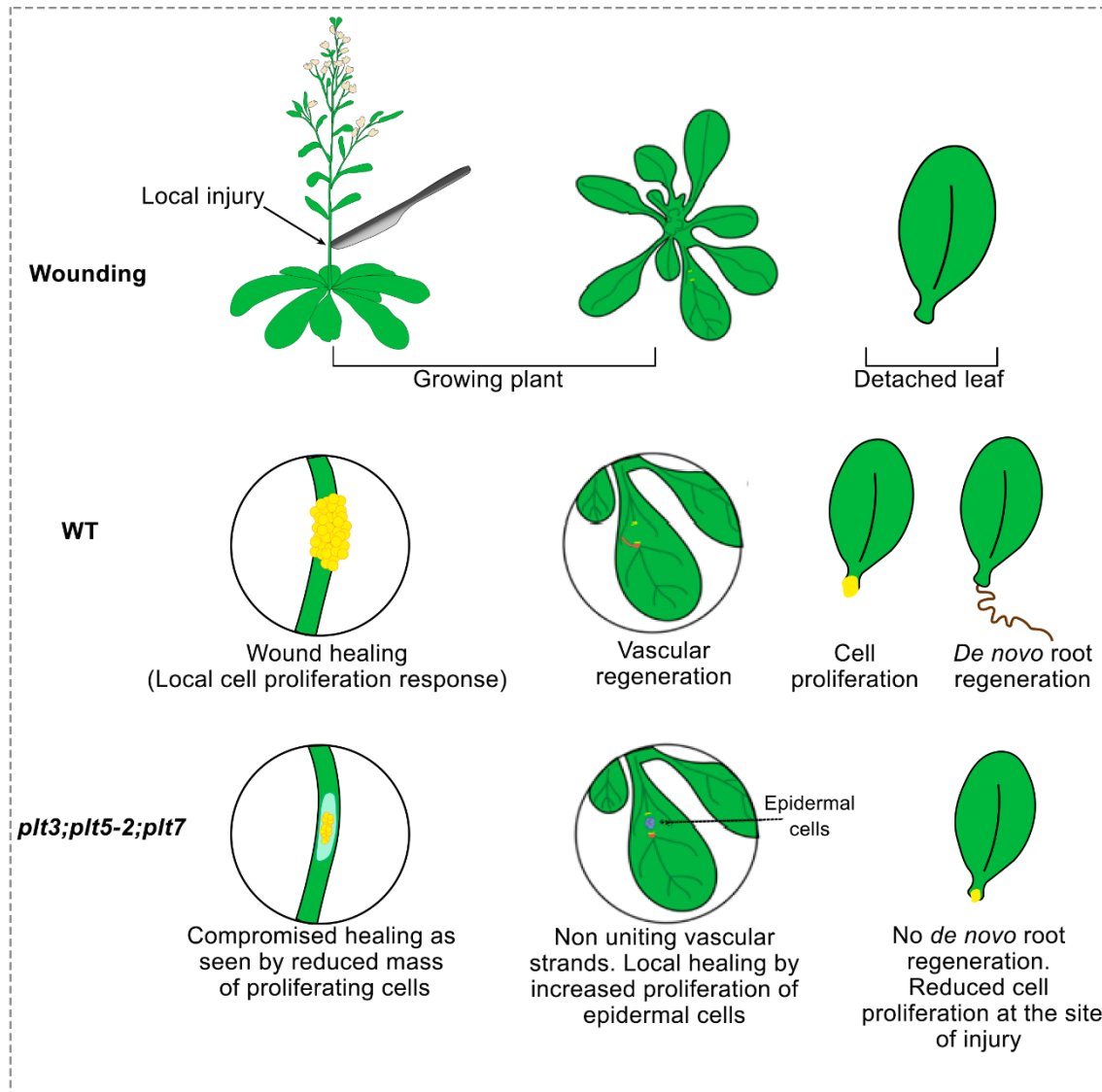


**Figure 3.17 *PLT* displays developmental context sensitivity in regulating local cell proliferation versus tissue or organ regeneration in response to injury**

### **3.3.4 *PLT* is sufficient for cellular reprogramming and its function is conserved across plant species**

We next examined if *PLT* is sufficient to activate cellular reprogramming. Inducible ectopic overexpression of *PLT7* (*35S::PLT7-GR*) or *PLT5* (*35S::PLT5-GR*) was sufficient to activate multiple distinct fates in growing seedling such as callus-like growth (mimicking local healing response), ectopic leaf, a complete shoot from petiole and ectopic root formation (mimicking tissue/organ regeneration responses) (Figure 3.18). While ectopic callus-like outgrowth, new leaves and new shoots were commonly observed, ectopic roots were only observed rarely (Figure 3.18F). These ectopic organs originated from the vascular tissue of a growing leaf (Figure 3.18J). Our data establish that *PLT* is capable of inducing multiple organ

programs in a context dependent manner and can promote wound induced responses (Figure 3.18, 3.19). These data demonstrate that *PLT* is sufficient for cellular reprogramming.

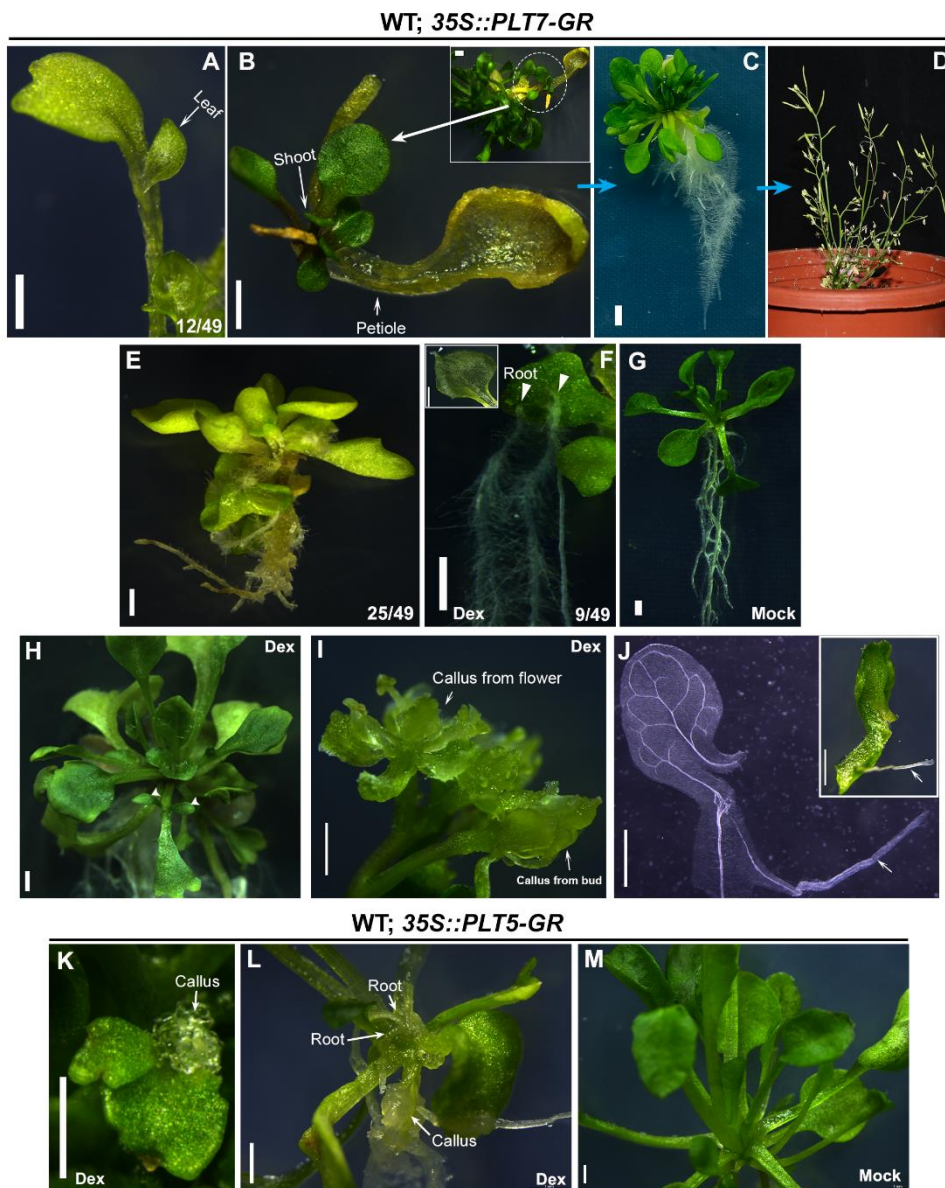


**Figure 3.18** *PLT* is sufficient for cellular reprogramming in growing plants and detached organs

(A) Ectopic formation of leaf (white arrowheads) from the petiole of growing seedling upon inducible overexpression of *PLT7* in WT. (B-D) Stages of growth of ectopic plant induced from the petiole of growing seedling upon overexpression of *35S::PLT7-GR* in WT. (B) Multiple leaves arise ectopically to form a shoot. B (inset): the plant to which the petiole (dotted circle) was attached. (C) Formation of rosette leaves in ectopically induced plant. (D) Formation of flowers and siliques in ectopically formed fertile plant. (E-G) Overexpression of *35S::PLT7-GR* in WT triggered ectopic formation of callus (white arrows) from root (E). (F) Roots formed from leaf (white arrowhead). (G) No ectopic structures were observed in mock treated seedling of WT; *35S::PLT7-GR*. (H) Ectopic formation of leaf (white arrowheads) from the petiole of growing seedling upon inducible overexpression of *PLT7* in WT. (I) Ectopic formation of callus from inflorescence upon inducible overexpression of *35S::PLT7-GR*. (J) Ectopic formation of root from vascular tissue of leaf upon overexpression of *35S::PLT7:GR*. Inset shows the leaf with emerging root. (K-M) *PLT5* overexpression phenotypes in growing plants. (K)

Ectopic callus formation, (L) root formation from shoot meristem, callus from hypocotyl. (M) Mock treated seedling (control). Scale bar: 1mm. WT: wildtype.

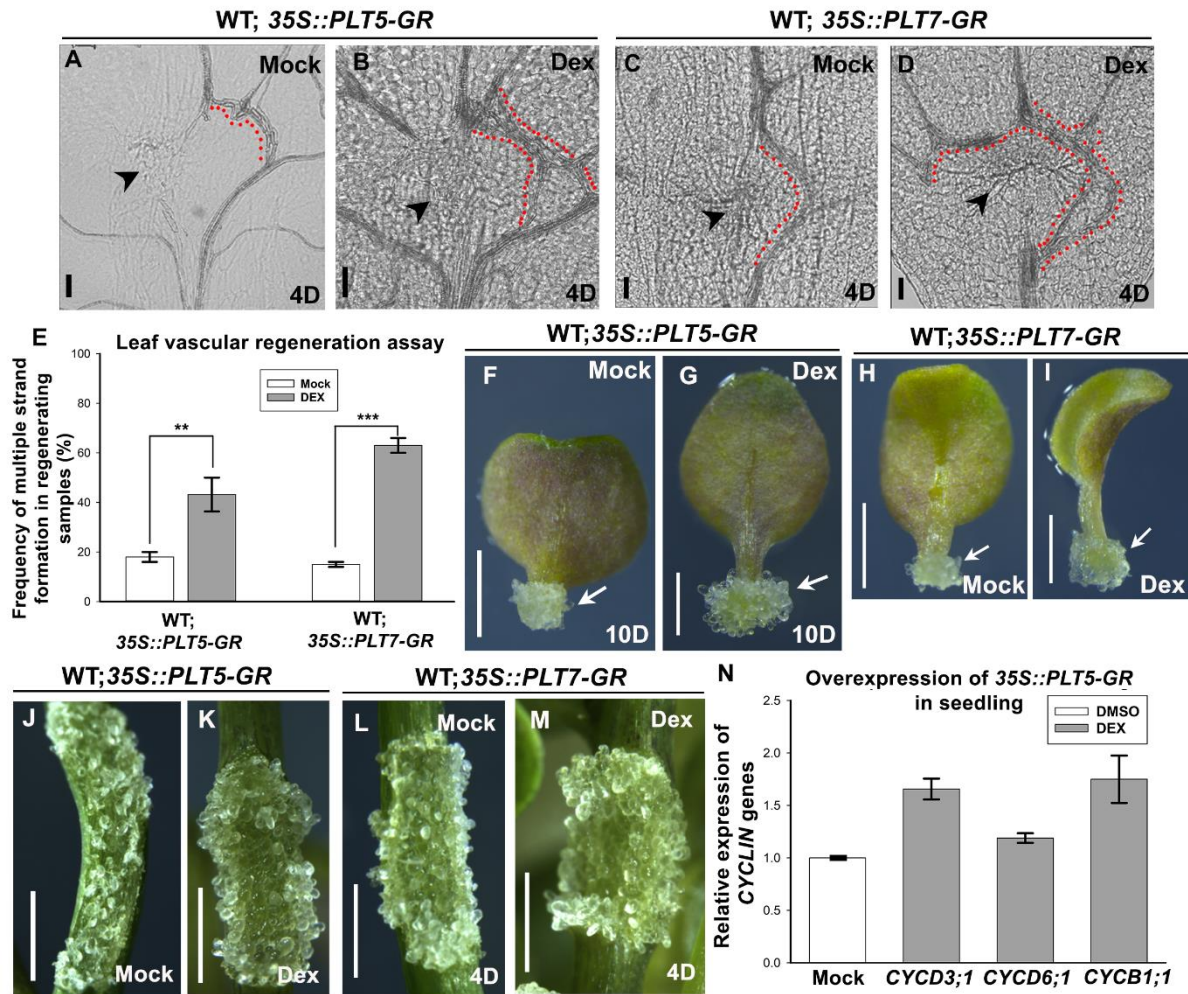
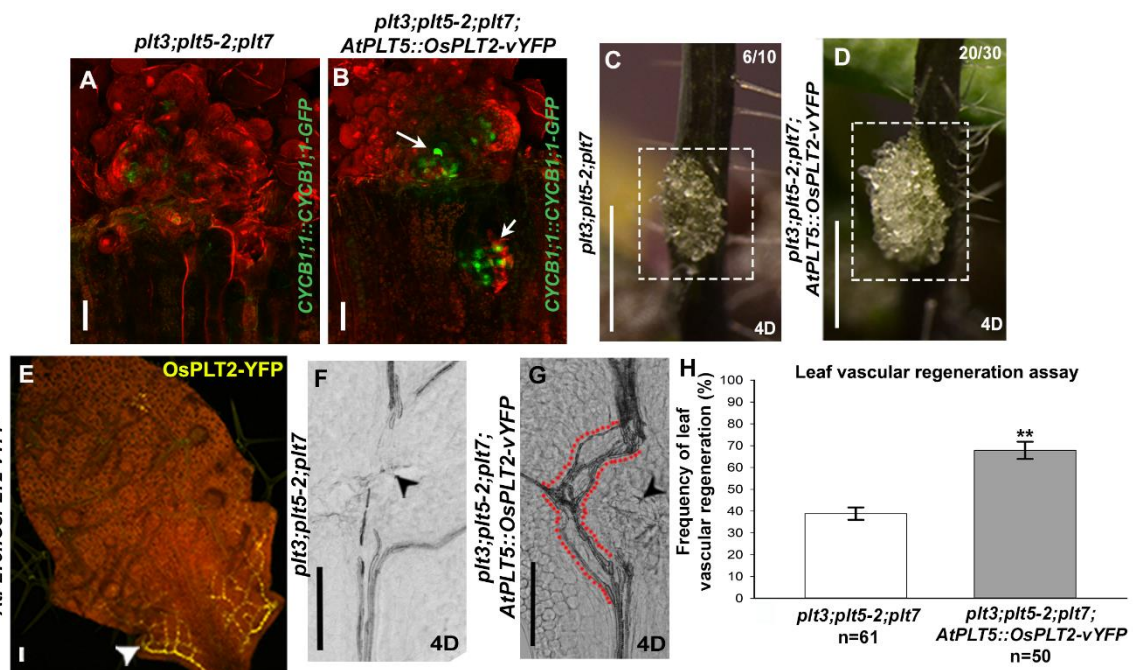


**Figure 3.19** *PLT* genes are sufficient for vascular regeneration and wound repair

(A-E) Overexpression of 35S::PLT5-GR and 35S::PLT7-GR promotes multiple vascular strand formation upon leaf incision (E) Graph representing increase in frequency of vascular strand formation upon overexpression of 35S::PLT5-GR and 35S::PLT7-GR during vascular regeneration in response to midvein incision (Pearson's  $\chi^2$  test; \*\* $P=0.007$ ; \*\*\* $P=1.2 \times 10^{-5}$ ). (F, G) Increased callus formation (white arrow) from cut end of leaf on ectopic induction of 35S::PLT5-GR (G) as compared to control (F). (G, H) Overexpression of 35S::PLT7-GR enhances callus formation from cut end of the leaf upon induction (H) compared to uninduced leaves (G). (J-M) Increased callus formation on the surface of inflorescence stem following abrasion upon induction of 35S::PLT5-GR and 35S::PLT7-GR. (N) Expression of *CYCLIN* genes in response to overexpression of 35S::PLT5-GR in growing seedlings. Expression levels are normalized to *ACTIN2*. Error bar represents s.e.m. from three independent biological replicates. Red dotted lines indicate regenerated vascular strands. Dex: dexamethasone. Error bars represent s.e.m. Scale bar: 1mm (F-M), 50 $\mu$ m (A-D), D: days after injury. WT: wildtype.

Our studies revealed that *PLT* plays a crucial role in the process of cellular reprogramming during wound healing in *Arabidopsis*. We further investigated the potential of *PLT*-like genes from other plant species in promoting regeneration. Rice is a morphologically

diversified monocot plant, while *Arabidopsis* is a dicot. Interestingly, expression of a rice *PLT*-like gene *OsPLT2* under the *Arabidopsis PLT5* promoter in a *plt3;plt5-2;plt7* mutant (*plt3;plt5-2;plt7; AtPLT5::OsPLT2-YFP*) healed damaged *Arabidopsis plt* triple mutant inflorescence by inducing cell proliferation as evident from up-regulated expression of cell cycle progression markers (Figure 3.19A-D). Additionally, *OsPLT2-YFP* successfully rescued the defects in leaf vascular regeneration observed in the *plt3;plt5-2;plt7* mutant, suggesting that it functions as a functional homolog of *Arabidopsis PLT* (Figure 3.20F-H). Notably, *OsPLT2* was capable of activating wound repair both in the damaged inflorescence and leaf of the *Arabidopsis plt* triple mutant (Figure 3.20A-H). These findings indicate that the role of the rice *PLT*-like gene in regeneration is conserved across different plant species.



Images by Vijina VP and Anju P S

**Figure 3.20 Rice *PLT* gene can rescue regeneration defect in *plt* triple mutant**

(A,B) *plt3;plt5-2;plt7* barely shows any cell proliferation marked by cell cycle progression marker *CYCB1:1::CYCB1:1-GFP* as compared to strong expression detected in clusters of actively dividing cells forming callus in response to inflorescence abrasion in *plt3;plt5-2;plt7; AtPLT5::OsPLT2-vYFP*. Confocal imaging was performed only for GFP excitation and emission detection. (C, D) Only residual cell proliferation response is observed in *plt3;plt5-2;plt7* (C) unlike extensive callus like growth observed in *plt3;plt5-2;plt7; AtPLT5::OsPLT2-vYFP* in response to inflorescence abrasion (D). Dotted rectangle encloses area of callus formation upon inflorescence abrasion. (E) Expression of *AtPLT5::OsPLT2-YFP* in vascular tissue (white arrowhead) of *plt3;plt5-2;plt7* leaf. (F-H) *AtPLT5::OsPLT2-vYFP* rescues vascular tissue regeneration in response to leaf incision (black arrowheads) in *plt3;plt5-2;plt7; AtPLT5::OsPLT2-vYFP* (G) while *plt3;plt5-2;plt7* (F) failed to regenerate. Red dotted lines represent new vascular strands connecting cut end of midvein. (H) Rescue of vascular tissue regeneration in response to leaf incision in *plt3;plt5-2;plt7; AtPLT5::OsPLT2-vYFP* (\*\* $P=0.004$ ; Pearson's  $\chi^2$  test) compared with *plt3;plt5-2;plt7* leaves, of which ~61% failed to

regenerate. Error bars represent s.e.m. Scale bar: 50 $\mu$ m. WT: wildtype.

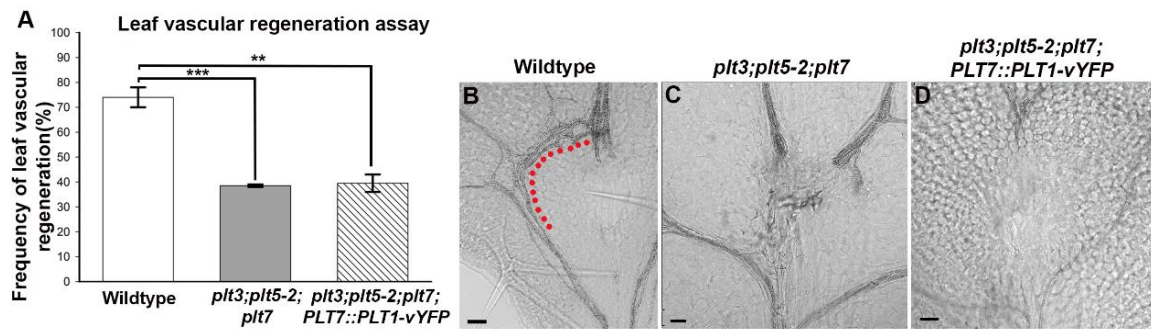


**Figure 3.21 Overexpression of PLT1 under heterologous promoter in *plt* triple mutant cannot rescue vascular regeneration defect**

(A) Leaf vascular regeneration in WT, *plt3;plt5-2;plt7* (Pearson's  $\chi^2$  test; \*\*\**P*-value = 0.0003109) and *plt3;plt5-2;plt7; PLT7::PLT1-vYFP* (Pearson's  $\chi^2$  test; \*\**P*-value = 0.003007). (B-D) Representative images of WT (B), *plt3;plt5-2;plt7*(C) and *plt3;plt5-2;plt7; PLT7::PLT1-vYFP* (D) leaves 4 days after injury. Scale bar: 50 $\mu$ m. Error bar represent s.e.m. WT: wildtype.

### 3.3.5 *PLT* directly activates *CUC2* expression to repair wounds and regenerate vascular tissue

Having established that *PLT* regulates wound repair and vascular regeneration in damaged aerial parts of the plant, we next sought to define the mechanisms underlying this regulation. Previously we had shown that *PLT* directs tissue-culture-mediated *in vitro* shoot regeneration by activating root stem cell regulators and, shoot stem cell regulator *CUC2* in a two-step mechanism where the second step, shoot promoting activity of *CUC2*, is dependent on root stem cell regulators, *PLT1*, *PLT2* and *SCARECROW (SCR)*<sup>97</sup>.

However, in the context of wound repair in growing aerial organs, we found no evidence suggesting the participation of root stem cell regulators (Figure 3.10, 3.21). Nevertheless, *CUC2* remains an intriguing candidate for involvement in wound repair in growing aerial organs. It is important to note that *CUC2* is implicated in the regulation of leaf margin development by directing PIN1 polarity and the resultant auxin distribution<sup>130,139</sup>. However, the role of *CUC2* in wound repair and vascular regeneration has not been explored. Therefore, we aimed to investigate whether *CUC2* responds to mechanical injury and whether *PLT* acts through *CUC2* to facilitate wound repair.

To investigate the expression pattern of *CUC2* upon injury, we utilized reporter lines containing *pCUC2::3xVENUS* and *CUC2::CUC2-vYFP* constructs, where the same *CUC2* promoter was used for both transcriptional and translational fusions. The expression pattern

observed with *pCUC2::3xVENUS*, which includes an expanded domain of expression compared to *CUC2::CUC2-vYFP*, can largely be attributed to the *3xVENUS* component. Both reporter fusions were able to recapitulate the previously reported expression of *CUC2* at the leaf margin<sup>130,139</sup> (Figure 3.22A, B).

In response to midvein damage in WT plants, both *pCUC2::3xVENUS* and *CUC2::CUC2-vYFP* expression were upregulated proximal to the wound site 12 hours after injury, followed by a broader domain of enhanced expression after 24 hours (Figure 3.22 C-E, F-H). In contrast, there was no upregulation of the reporter near the wound site in *plt3;plt5-2;plt7* mutant plants (Figure 3.22 C'-E', F'-H'). Similar patterns of changes were also observed at the transcript level in response to midvein injury (12 hours post injury) (Figure 3.22I). Additionally, in the damaged inflorescence stem, *CUC2* transcripts were reduced in *plt3;plt5-2;plt7* mutants compared to WT plants (Figure 3.22J).

Furthermore, upon inducible overexpression of PLT5 (*35S::PLT5-GR*) or PLT7 (*35S::PLT7-GR*) in injured leaves, *CUC2* transcripts were rapidly increased, even in the presence of the translation inhibitor cycloheximide, suggesting direct activation of *CUC2* transcription by PLT5 and PLT7 (Figure 3.23A, B). Consistent with these observations, our ChIP assay revealed that PLT5 binds to the *CUC2* promoter (Figure 3.23C, D), and DAP Seq analysis identified the binding of PLT7 to the *CUC2* promoter (Figure 3.23E). Moreover, transient transfection of constructs containing PLT5 or PLT7 proteins and a *CUC2* promoter-driven Luciferase reporter in *Nicotiana* leaves induced reporter gene expression, demonstrating that PLT5 and PLT7 can directly activate *CUC2* transcription (Figure 3.23F).

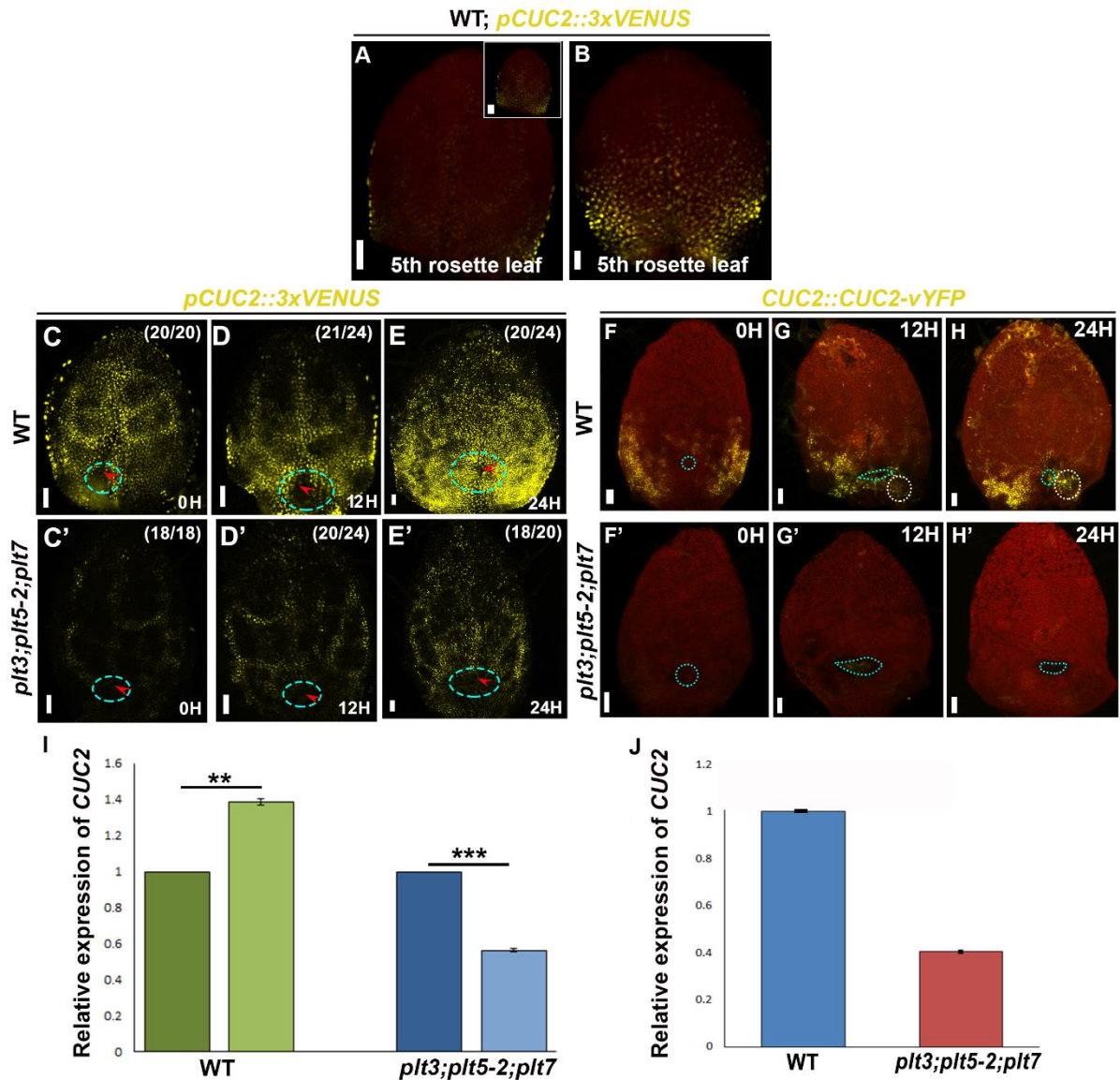


**Figure 3.22 CUC2 expression in response to injury in WT and *plt* mutant**

(A) Single optical section showing expression of *pCUC2::3xVENUS* in the leaf margin of fifth rosette leaf. Inset in (A) represents stacked image of the same leaf. (B) *pCUC2::3xVENUS* expression is absent from the hydathode and higher in the leaf sinus as reported previously<sup>130,139</sup>. Except (A) and (B) (5th rosette leaves), all other panels represent leaves belonging to 1st pair of rosette leaves. (C-E, C'-E') Reduced expression of *pCUC2::3xVENUS* (yellow) in *plt3;plt5-2;plt7* (C'-E') compared with WT (C-E) in response to injury. Red arrowheads denote incision site and dashed circles enclose leaf tissue in the vicinity of the wound showing upregulation of *pCUC2::3xVENUS* in WT but not in *plt3;plt5-2;plt7*. Sample numbers are shown in parentheses (numerator, number of samples showing the expression represented in the image panel; denominator, total number of samples analysed). (F, F') *plt3;plt5-2;plt7* shows reduced expression of *CUC2::CUC2-vYFP* as compared to WT. (G, H, G', H') Upon incision WT (G,H) shows expanded domain of expression of *CUC2::CUC2-vYFP* unlike *plt3;plt5-2;plt7* (G', H'). White dotted circle marks upregulation of YFP expression near wounded area. Blue dotted line marks incision. (I) Upregulation of CUC2 transcript in injured WT leaf at 12 h post injury as compared to control uninjured WT leaves. Downregulation of CUC2 transcript in injured *plt3;plt5-2;plt7* leaves as compared to control uninjured *plt3;plt5-2;plt7* leaves. (Welch's two-sample *t*-test; \*\* $P=0.002$ ; \*\*\* $P=0.0004$ ), (J) Relative expression levels (qRT-PCR) of CUC2 in injured *plt3;plt5-2;plt7* mutant inflorescence segments compared with WT (4 dpi). Expression levels in (I) and (J) are normalized to

*ACTIN2*. Error bar represents s.e.m. from three independent biological replicates. Scale bar: 50µm. WT: wildtype.

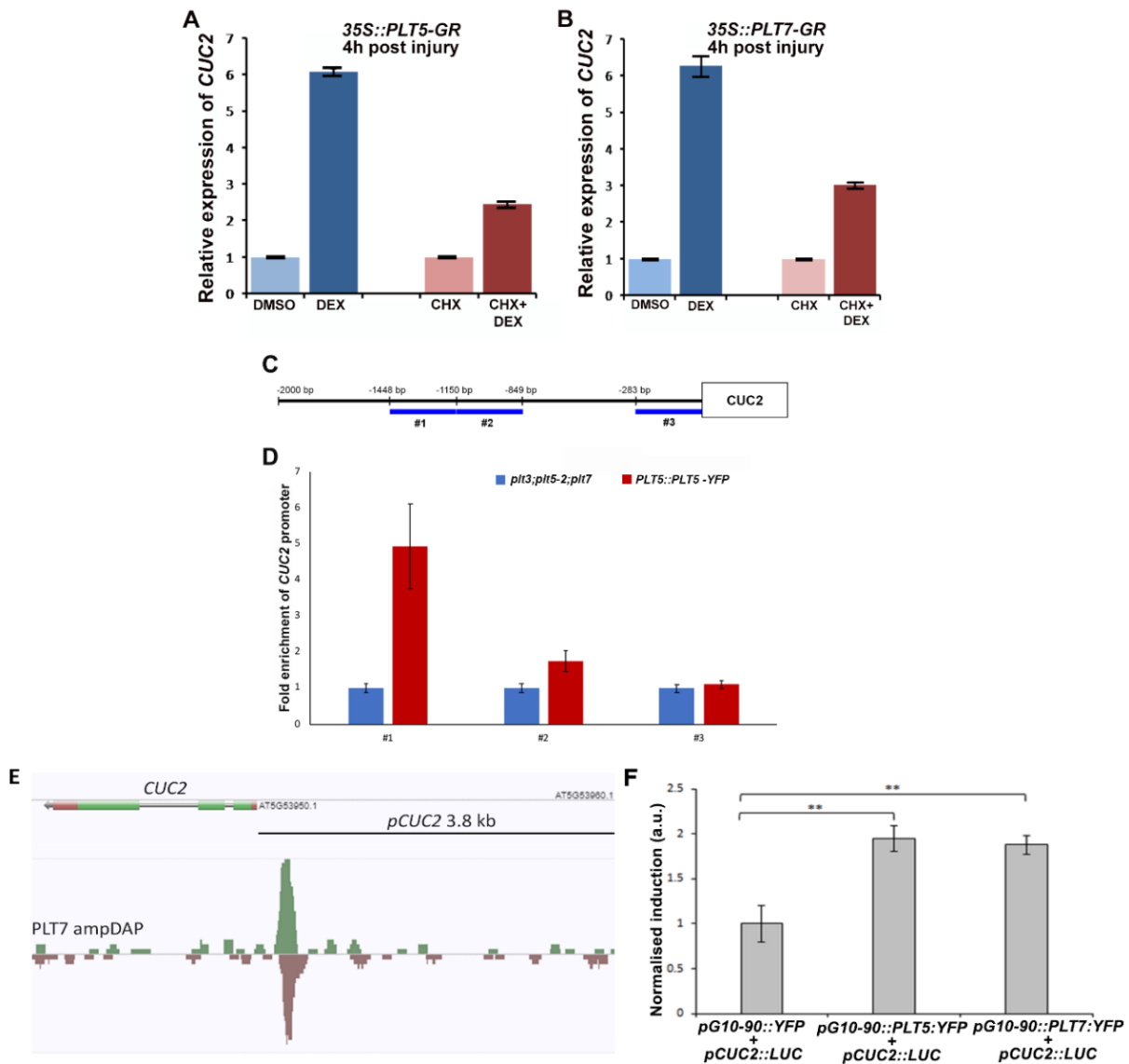


### Figure 3.23 PLTs can directly activate CUC2 transcription

(A) Transcript level of *CUC2* upon induction of PLT5 with DEX treatment and with cycloheximide treatment. (B) Rapid upregulation of *CUC2* (qRT-PCR) in injured tissue upon induction of 35S::PLT7-GR. Expression levels in A and B are normalised to *ACTIN2*. Error bars represent s.e.m. from three independent biological replicates. (C) ChIP-qPCR analysis: ChIP-qPCR experiment in callus tissues shows direct binding of PLT5 fusion protein to the *CUC2* promoter. (D) The results are shown as fold enrichment relative to *plt3;plt5-2;plt7* loss of function mutant. A strong binding of PLT5 is noticed at the fragment #1 (-1150 to -1448 bp) followed by a weak binding at #2 (-849 to -1149 bp) and no significant binding at the fragment #3 (-1 to -283 bp) of the upstream sequence of *CUC2*. Error bars show the standard error of the ChIP-qPCR reactions performed in triplicates. (E) PLT7 binds the *CUC2* promoter (<http://neomorph.salk.edu/>). Indicated region shows *pCUC2*, which was used in the luciferase reporter assay. (F) PLT5 and PLT7 induce *pCUC2* in a luciferase reporter assay 2 days post-inoculation in *Nicotiana*. \*\* $P < 0.01$  (Mann-Whitney U one-tailed test). Six biological replicates each with three technical replicates were performed. Error bars represent s.e.m.

As molecular data suggests that *CUC2* acts downstream of *PLT*, we investigated the requirement of *CUC2* activity for the wound repair function of *PLT*, we performed inducible ectopic overexpression of *PLT5* in *cuc2-3* mutant tissues (*cuc2-3; 35S::PLT5-GR*). Strikingly, we observed that the overexpression of *PLT5* failed to promote wound repair at the damaged ends of *cuc2-3* mutant tissues. The compromised wound repair observed at the cut ends of *cuc2-3* remained unaffected by *PLT5* overexpression, in contrast to WT where *PLT5* overexpression (*WT; 35S::PLT5-GR*) enhanced wound repair at the cut ends (Figure 3.24). These findings provide compelling evidence that *PLT* requires *CUC2* activity to effectively repair the wound.

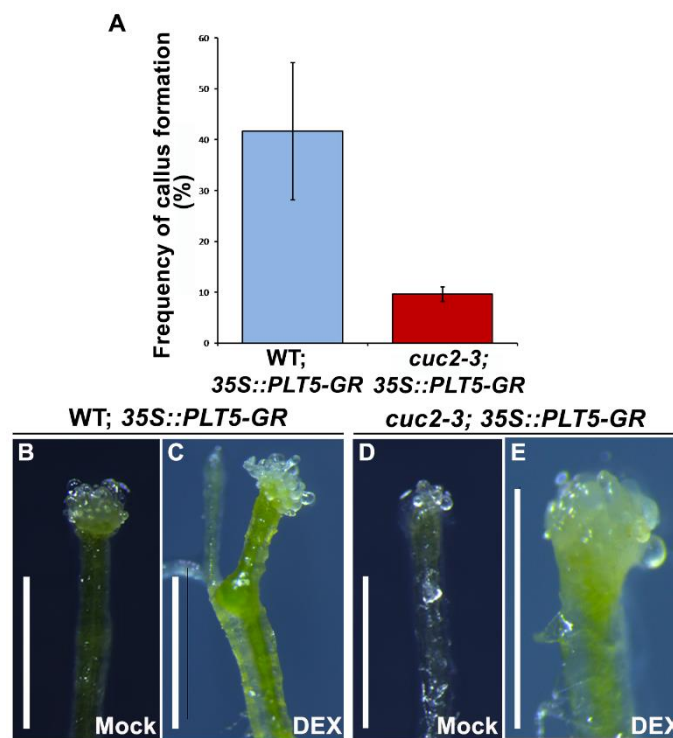


**Figure 3.24** *PLT* acts through *CUC2* to repair the wound

(A) Frequency refers to the number of excised organs showing callus formation at the cut end. In addition to frequency, the extent of callus formation was also reduced in *cuc2-3; 35S::PLT5-GR*. (B,C) WT; 35S::PLT5-GR upon DEX induction (C) shows increased extent of callus formation unlike in mock treated control (B). (D,E) *cuc2-3; 35S::PLT5-GR* upon DEX induction (E) shows no increase in extent of callus formation as compared to mock treated control (D). Scale bar: 1mm, WT: wildtype.

We examined the involvement of *CUC2* in leaf vascular regeneration by examining loss-of-function mutants (Figure 3.25A). Strikingly, both the recessive mutant *cuc2-3* and the dominant mutant *cuc2-1* exhibited a significant impairment in vascular regeneration. Around 71% of *cuc2-3* mutant leaves and 81% of *cuc2-1* mutant leaves failed to undergo vascular regeneration upon midvein injury (Figure 3.25A). Importantly, it is worth noting that the loss of *CUC2* function did not affect the development of midvein or lateral veins compared to WT leaves (Figure 3.14C).

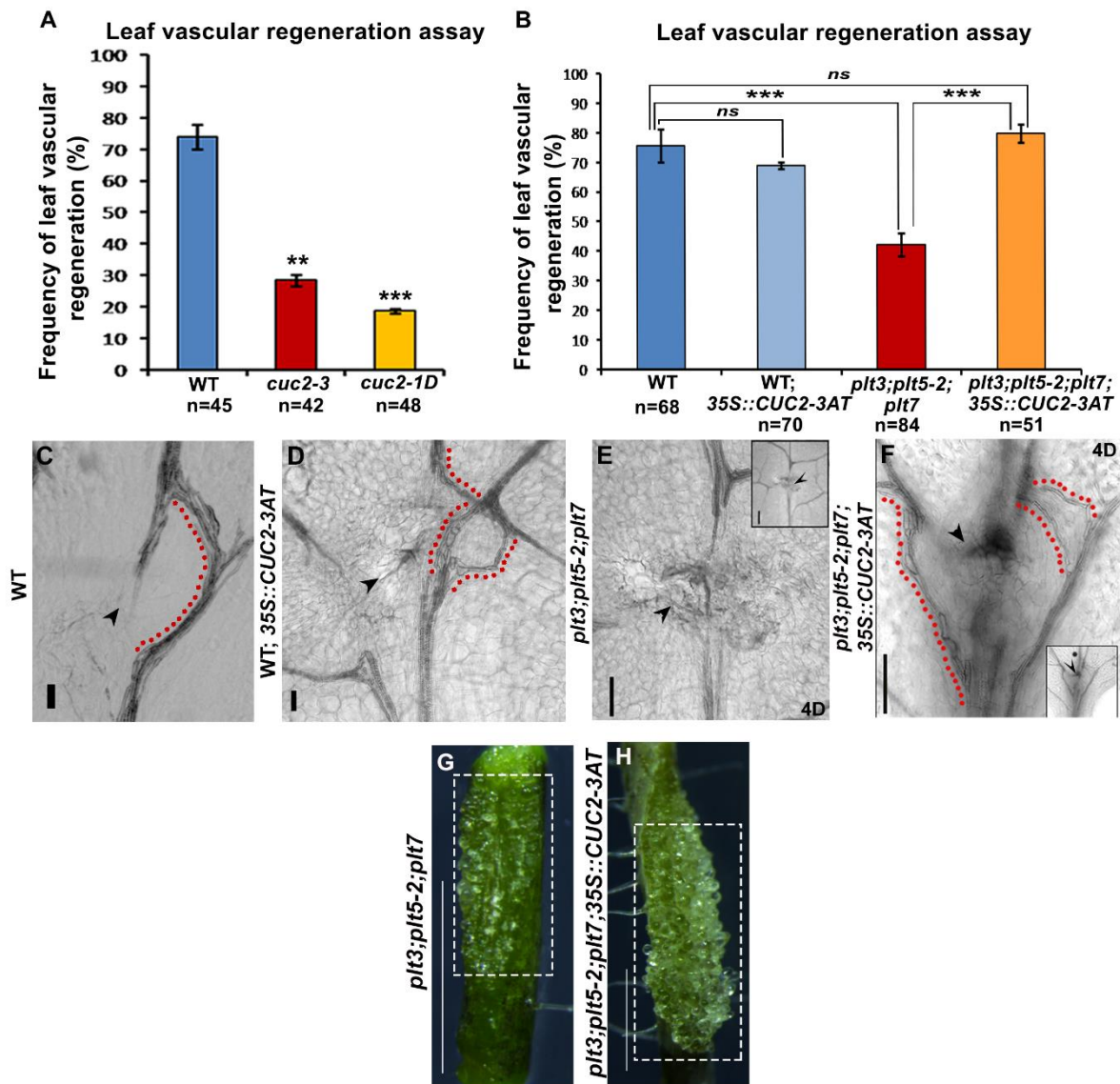


**Figure 3.25 PLT acts through *CUC2* to repair wound and to regenerate vascular tissue**

(A) Frequency of leaf vascular regeneration in *cuc2-3* (recessive) (\*\* $P = 0.007$ ), *cuc2-1D* (dominant) (\*\* $P = 0.0005$ ) mutants as compared to WT. (B) Frequency of leaf vascular regeneration in WT, WT; 35S::*CUC2-3AT* (ns;  $P = 0.65$ ), *plt3;plt5-2;plt7* (\*\* $P = 9.9 \times 10^{-5}$ ) and *plt3;plt5-2;plt7; 35S::CUC2-3AT* (\*\* $P = 4.7 \times 10^{-6}$ ). (C, D) Vascular tissue regeneration in WT. Note the increased vascular proliferation and regeneration (yellow dotted lines) of multiple vascular strands generating multiple reunion points in WT; 35S::*CUC2-3AT* (D) unlike in WT (C). Black arrow indicate site of incision. (E, F) Vascular tissue regeneration is rescued in *plt3;plt5-2;plt7; 35S::CUC2-3AT* (F) as compared to *plt3;plt5-2;plt7* (E) in response to leaf incision (black arrowhead). Note the increased vascular proliferation and regeneration of multiple vascular strands (red dotted lines) generating multiple reunion points in *plt3;plt5-2;plt7; 35S::CUC2-3AT* (F) unlike in *plt3;plt5-2;plt7* (E). (G, H) Ectopic overexpression of *CUC2* in *plt3;plt5-2;plt7* (H) enhances local cell proliferation and wound healing response upon inflorescence abrasion (enclosed in dotted rectangle) as compared to *plt3;plt5-2;plt7* (G). Scale bar: 1mm (G, H), 50 $\mu$ m (C-F). Error bars represent s.e.m. WT: wildtype.

Subsequently, we investigated whether overexpression of *CUC2* could rescue the vascular regeneration defect in *plt3;plt5-2;plt7* mutant leaves. Strikingly, the restoration of regeneration efficiency (including the timing and reunion of vascular strands) and frequency

was achieved upon *CUC2* overexpression in *plt3;plt5-2;plt7* mutants, reaching the levels observed in WT plants. The mutant plants exhibited the regeneration and reunion of new vascular strands four days post injury (4 dpi), similar to the pattern seen in WT plants (Figure 3.25C-F). Moreover, the repair process in locally wounded *plt3;plt5-2;plt7* inflorescence stems was also rescued by *CUC2* overexpression (Figure 3.25G, H). Collectively, our findings provide compelling evidence that PLT directly activates the transcription of *CUC2* in response to injury, and the *PLT-CUC2* module plays a vital role in the repair of damaged leaf and stem tissues, but not for their normal development (Figure 3.14).

### **3.3.6 *PLT-CUC2* module-dependent cell polarization is key to vascular regeneration**

To gain a deeper understanding of vascular regeneration in developing leaves, particularly in terms of *in vivo* process, we aimed to investigate the cellular mechanisms regulated by the *PLT* transcription module. During vascular regeneration, the regenerating tissue or organ needs to undergo polarized growth in order to restore its original size and shape. Additionally, the polarized growth of vascular strands and their reunion are crucial for the proper functioning of the regenerated tissue after injury. Our *in silico* simulations suggest a wound size-sensitive re-establishment of cell polarity with respect to PIN polarization is key to driving vascular regeneration in a leaf (Figure 3.12A-D, see materials and methods).

To explore this further, we examined the localization of PIN1, a protein involved in auxin transport, in response to midvein injury in the leaf blade. Prior to wounding, we observed the expression of *PINI::PINI-GFP* primarily in the procambium cells towards the basal end of young leaves in both WT and mutant plants (Figure 3.26A, B). Following injury, we observed an increased accumulation of PIN1-GFP near the wound sites in both WT and mutant plants (Figure 3.26C-J').

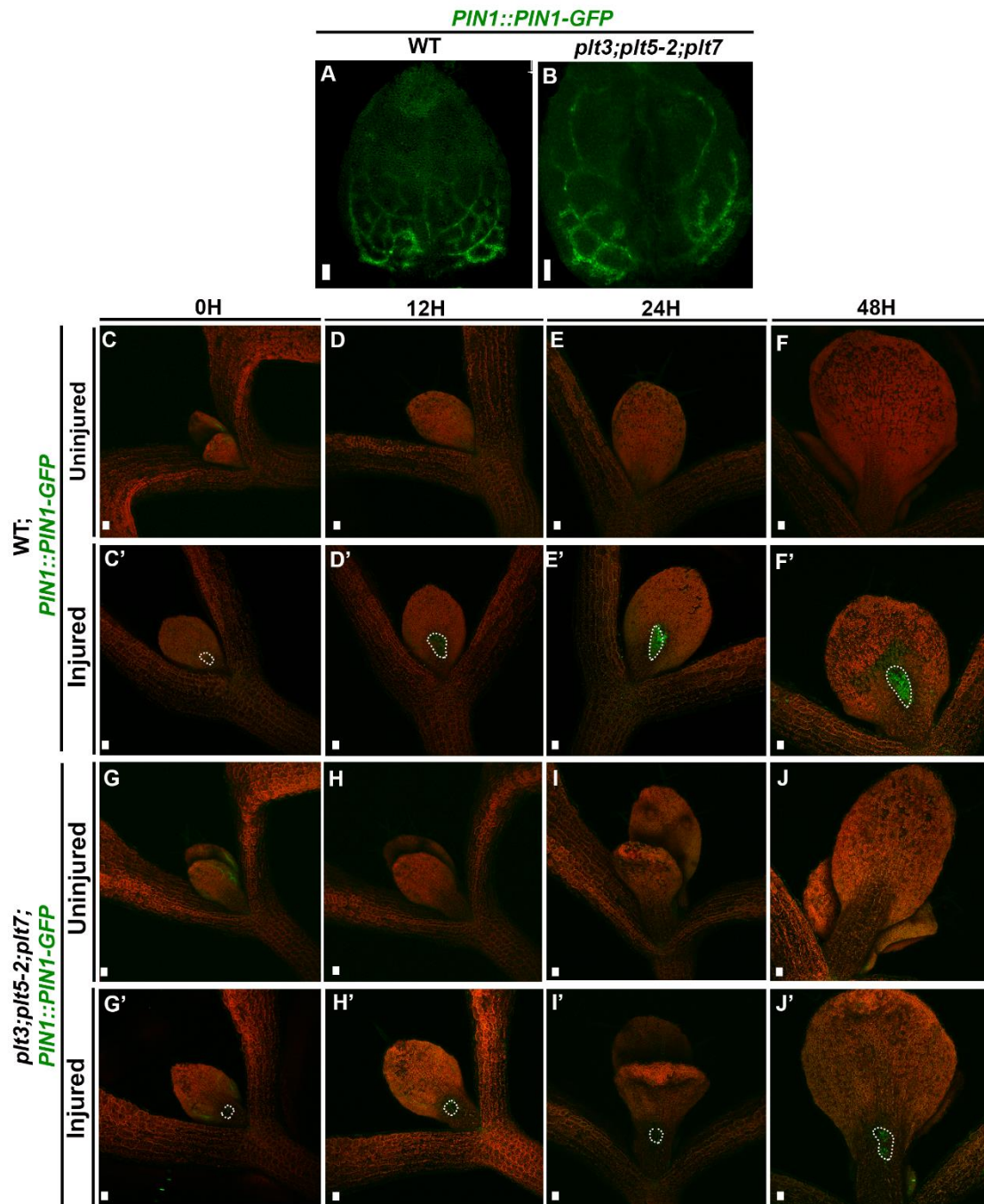


**Figure 3.26 PIN1 expression is not defective in *plt* mutant during normal development**

(A, B) *PIN1::PIN1-GFP* expression in undamaged leaves of WT (A) and *plt3;plt5-2;plt7* (B). PIN1 expression is visible in the basal part of the leaves in both WT and *plt3;plt5-2;plt7*. (C-J') Confocal time lapse images showing expression of *PIN1::PIN1-GFP* in WT (C-F') and *plt3;plt5-2;plt7* (G-J'). (C-F) and (G-J) represent uninjured leaves while the remaining represent injured leaves in which injured areas are marked by white dotted lines. Scale bar: 50  $\mu$ m. H: hour, WT: wildtype.

To examine the localization of PIN1-GFP in regenerating vascular cells, we generated transgenic lines containing both *PIN1::PIN1-GFP* and *ATHB8::ATHB8-YFP* constructs. The ATHB8-YFP marker specifically labels developing procambium cells in the leaf (Scarpella et

al., 2004). In 4-day-old leaves, we observed the expression of both PIN1-GFP and ATHB8-YFP in the developing procambium region (Figure 3.27A, A', B, B').

Within the first 12 hours following incision, we did not observe regenerating vascular cells expressing both PIN1-GFP and ATHB8-YFP near the wound site (Figure 3.27C, C'). However, after 24 hours, regenerating procambium cells that exhibited polarized PIN1-GFP and ATHB8-YFP were observed near the wound in the WT plants (Figure 3.27D). In contrast, in the *plt3;plt5-2;plt7* mutant plants, we did not observe regenerating procambium cells expressing both polarized PIN1-GFP and ATHB8-YFP near the wound even after 24 hours, indicating a failure to re-establish PIN1 polarity in the cells surrounding the damaged site in the mutant (Figure 3.27D'). These findings suggest that the inability to re-establish polar auxin transport within 24 hours may contribute to impaired vascular regeneration in the *plt* triple mutant.

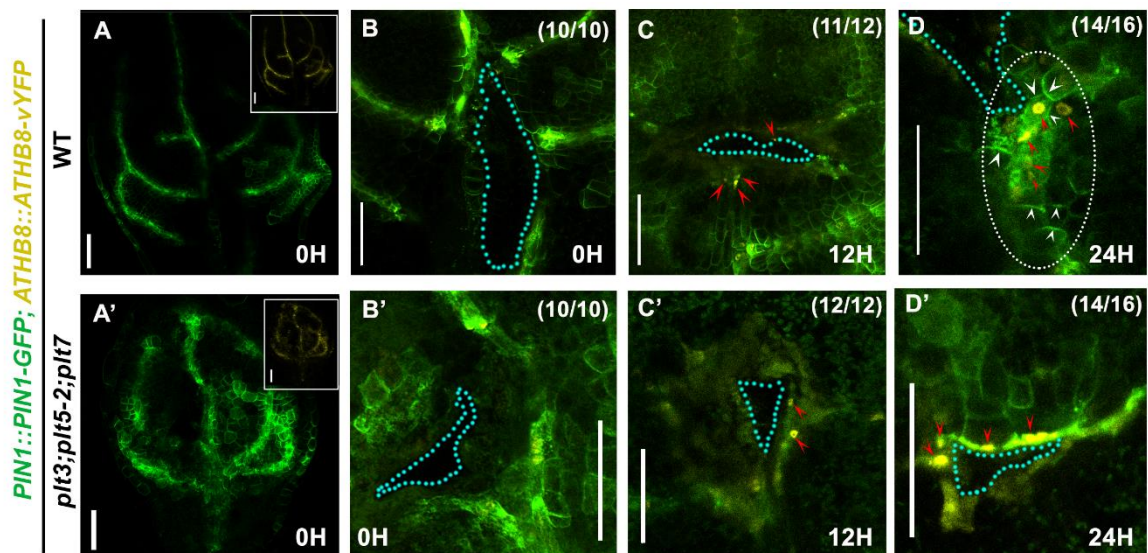


**Figure 3.27 PLT-CUC2 regulatory axis re-specifies early vascular cell fate and guides the polarized vein path for regeneration in leaf**

(A, B) Expression of *PIN1::PIN1-GFP* and *ATHB8::ATHB8-vYFP* in WT leaf. Inset in A shows single channel YFP expression of *ATHB8*. (A', B') Expression of *PIN1::PIN1-GFP* and *ATHB8::ATHB8-vYFP* in *plt3;plt5-2;plt7* leaf. Inset in A shows single channel YFP expression of *ATHB8*. (C, C') No expression of PIN1 is detected in the immediate vicinity of the wound at 12H in both WT and *plt3;plt5-2;plt7*. Red arrows indicate presence of pre-existing *ATHB8* near the wounded area. (D, D') Expression of polarized *PIN1::PIN1-GFP* and *ATHB8::ATHB8-vYFP* are detected in the regenerating cells (hexagonal shape of developing procambium) of WT (dotted rectangle) (D). However PIN1 polarization is absent in *plt3;plt5-2;plt7*. Only pre-existing expression of PIN1 and *ATHB8* are visible near the damaged region. White arrow mark PIN1 polarity direction in cells. Scale bar: 50 μm. H: hours post injury. WT: wildtype.

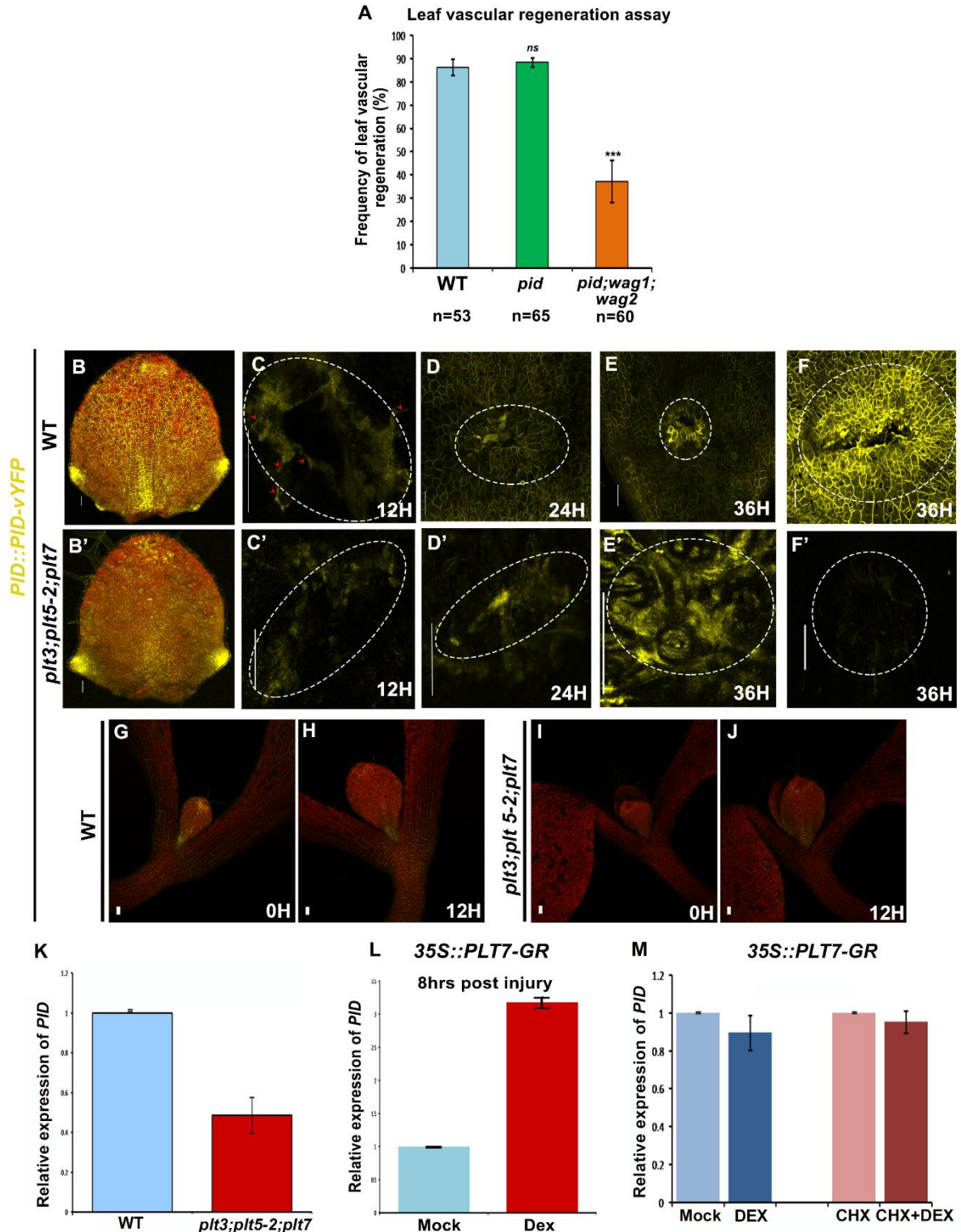


**Figure 3.28 PLT regulates *PID* expression and localization during vascular regeneration in leaves**

(A) Leaf vascular regeneration in WT, *pid* (ns; 0.63) and *pid; wag1; wag2* (\*\*\*) following leaf incision. (B, B') *PID::PID-vYFP* expression in undamaged leaves of WT (B) and *plt3;plt5-2;plt7* (B'). (C-F, C'-F') *PID::PID-vYFP* expression in WT (C-F) and *plt3;plt5-2;plt7* (C'-F') leaves post incision (neighbouring cells surrounding the wound are encircled in dashed lines). Red arrowheads in (C) mark membrane localized *PID*. Note that WT (C-F) shows an upregulation and relocalization of *PID* on the membrane of cells in the vicinity of the wound unlike in *plt3;plt5-2;plt7* (C'-F'). (G-J) Real

time confocal images showing expression of *PID::PID-YFP* in WT (G,H) and in *plt3;plt5-2;plt7* (I,J) uninjured leaves. (K) *PID* transcript level in WT and *plt3;plt5-2;plt7* injured inflorescence segments. (L) Upregulation of *PID* transcript levels in injured tissue after 8 hours of DEX induction, measured by qRT-PCR. (M) *PID* transcript level is not increased in WT uninjured leaf upon DEX induction and DEX+cycloheximide (CHX) after 4H. Expression levels in K-M are normalized to *ACTIN2*. Error bar represents s.e.m from three independent biological replicates. Scale bar: 50µm, H: hour, WT: wildtype.

In support of this concept, impaired vascular regeneration was observed in the *pid;wag1;wag2* triple mutant, which lacks the polar auxin transport regulators AGC3 kinases<sup>126</sup> (Figure 3.28A). To investigate whether PLT regulates the expression of *PID* in response to injury, we examined the expression and localization of *PID* in *plt* triple mutant leaves compared to WT. Unlike PIN1, which exhibited protein delocalization without significant changes in expression levels, both the expression and localization of *PID* were deregulated in damaged *plt* triple mutant leaves (Figure 3.28B-J). *PID* transcripts were reduced in damaged *plt3;plt5-2;plt7* tissues and increased upon PLT7-GR induction (Figure 3.28K, L). The upregulation of *PID* expression was observed after 8 hours of DEX induction, but this increase was not observed in the presence of the translation inhibitor cycloheximide, suggesting that *PID* may not be a direct target of PLT (Figure 3.28L, M).

To investigate the effect of disrupted auxin flow in *plt3;plt5-2;plt7* mutant leaves on auxin response patterns, we examined the auxin reporter *pDR5::3xVENUS-N7* in both WT and mutant plants. Prior to injury, no differences in auxin response distribution patterns or levels were observed between the two genotypes in leaves (Figure 3.29A-G, G'). In the WT, we detected an increase in *pDR5::3xVENUS-N7* signal in the vascular tissue proximal to the wound at 12 hours post injury (Figure 3.29I-K), followed by localized auxin response near the wound at 48 hours (Figure 3.29L, M). In contrast, the *plt3;plt5-2;plt7* mutant did not exhibit enhanced *pDR5::3xVENUS-N7* signal in the vascular tissue or confined expression in response to injury (Figure 3.29H'-K'). The DR5 signal remained dispersed throughout the leaf lamina even at 48 hours (Figure 3.29N, O). The altered auxin response specifically in the damaged mutant leaf, but no changes in the distribution patterns or levels of auxin response in uninjured normal developing mutant leaves compared to WT, further substantiate the specific role of *PLT* in the response to injury rather than the normal development of leaf vascular tissue.

*pDR5rev::3XVENUS-N7*

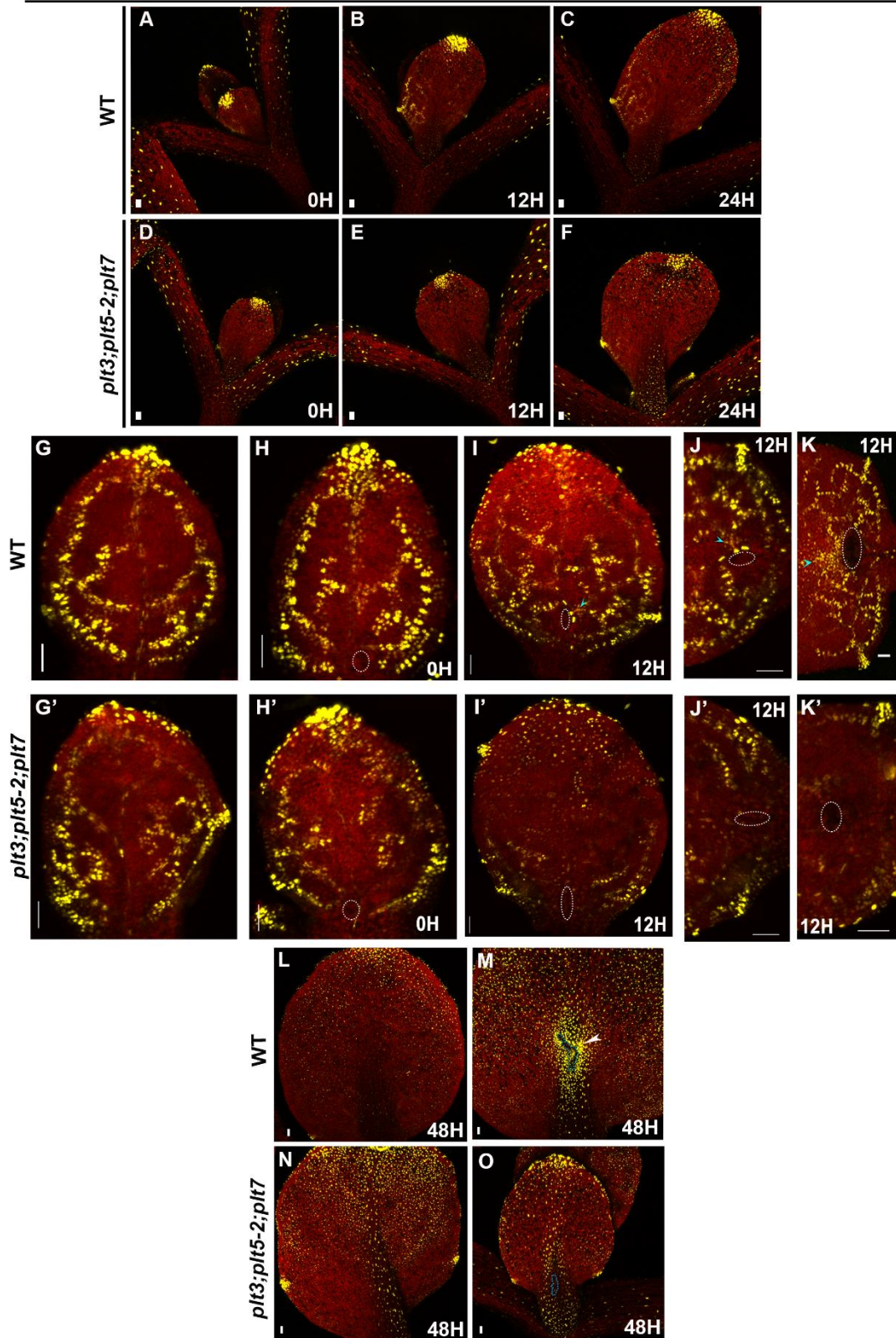


**Figure 3.29** *PLT* genes regulate auxin response during vascular regeneration

(A-F) Real time confocal images showing expression of *pDR5rev::3xVENUS-N7* in WT (A-C) and *plt3;plt5-2;plt7* (D-F) uninjured leaves. (G,G') *pDR5::3xVENUS-N7* expression in undamaged leaves of WT (G) and *plt3;plt5-2;plt7* (G'). (H-K, H'-K') *pDR5::3xVENUS-N7* expression in WT (H-K) and

*plt3;plt5-2;plt7* (H'-K') leaves post incision (dotted circle marks damaged area). Note the upregulation of *pDR5::3xVENUS-N7* in vascular tissue proximal to the wound (marked by blue arrowheads) in WT (I-K) unlike in *plt3;plt5-2;plt7* (I'-K'). J and J' represent zoomed in images of basal end of leaves in I and I' respectively. K and K' represent zoomed in images of another pair of leaf showing similar response to wounding. (L-O) Real time confocal images showing expression of *pDR5rev::3xVENUS-N7* in WT (L,M) and *plt3;plt5-2;plt7* (N,O) leaves. Blue dotted area encloses damage caused by incision. White arrowhead marks upregulation and confined expression of *DR5-VENUS* around site of injury in WT leaf (M) as compared to mutant (O). Scale bar: 50µm. Red colour represent chlorophyll autofluorescence. WT: wildtype.

### 3.3.7 PLT and CUC2 activate the transcription of local auxin biosynthesis gene in a feedforward loop to repair wound and drive vascular regeneration

So far our data showed that both, PIN polarization and auxin response was lost in the *plt* triple mutant. Since auxin and PIN polarization act in a positive feedback loop, it is hard to discern, at this stage whether the lack of effective auxin response near wound site caused the loss of PIN polarization or *vice-versa*. We therefore searched for additional factors that could contribute towards generating an effective auxin response. To gain further insights into factors contributing to an effective auxin response, we explored the involvement of local auxin biosynthesis. Interestingly, the expression of the auxin biosynthesis gene *YUC4* was upregulated in response to midvein injury (12 hours post-injury) in growing WT leaves, but not in *plt3;plt5-2;plt7* leaves. *YUC4* transcripts were reduced in the mutant following leaf injury (Figure 3.30A, B). Additionally, *YUC4* expression was reduced in the damaged *plt3;plt5-2;plt7* inflorescence segment (Figure 3.30B). In contrast, injured tissues exhibited rapid increase in *YUC4* transcripts upon induction of *PLT5-GR* and *PLT7-GR*, even in the presence of the translation inhibitor cycloheximide, indicating direct activation of *YUC4* by PLT (Figure 3.30C). Given that molecular data suggests *YUC4* acts downstream of PLT, we investigated whether PLT requires *YUC4* activity to initiate cellular reprogramming. Remarkably, inducible overexpression of PLT5 or PLT7 failed to induce ectopic cellular reprogramming in the *yuc4;yuc1* mutant background (*yuc4;yuc1; 35S::PLT5-GR* or *yuc4;yuc1; 35S::PLT7-GR*), unlike in the WT background (WT; *35S::PLT5-GR* or WT; *35S::PLT7-GR*) (Figure 3.30E, F). Similarly, overexpression of PLT5 or PLT7 did not promote wound repair at the damaged end, demonstrating that PLT acts through *YUC4* during reprogramming and wound repair (Figure 3.30).

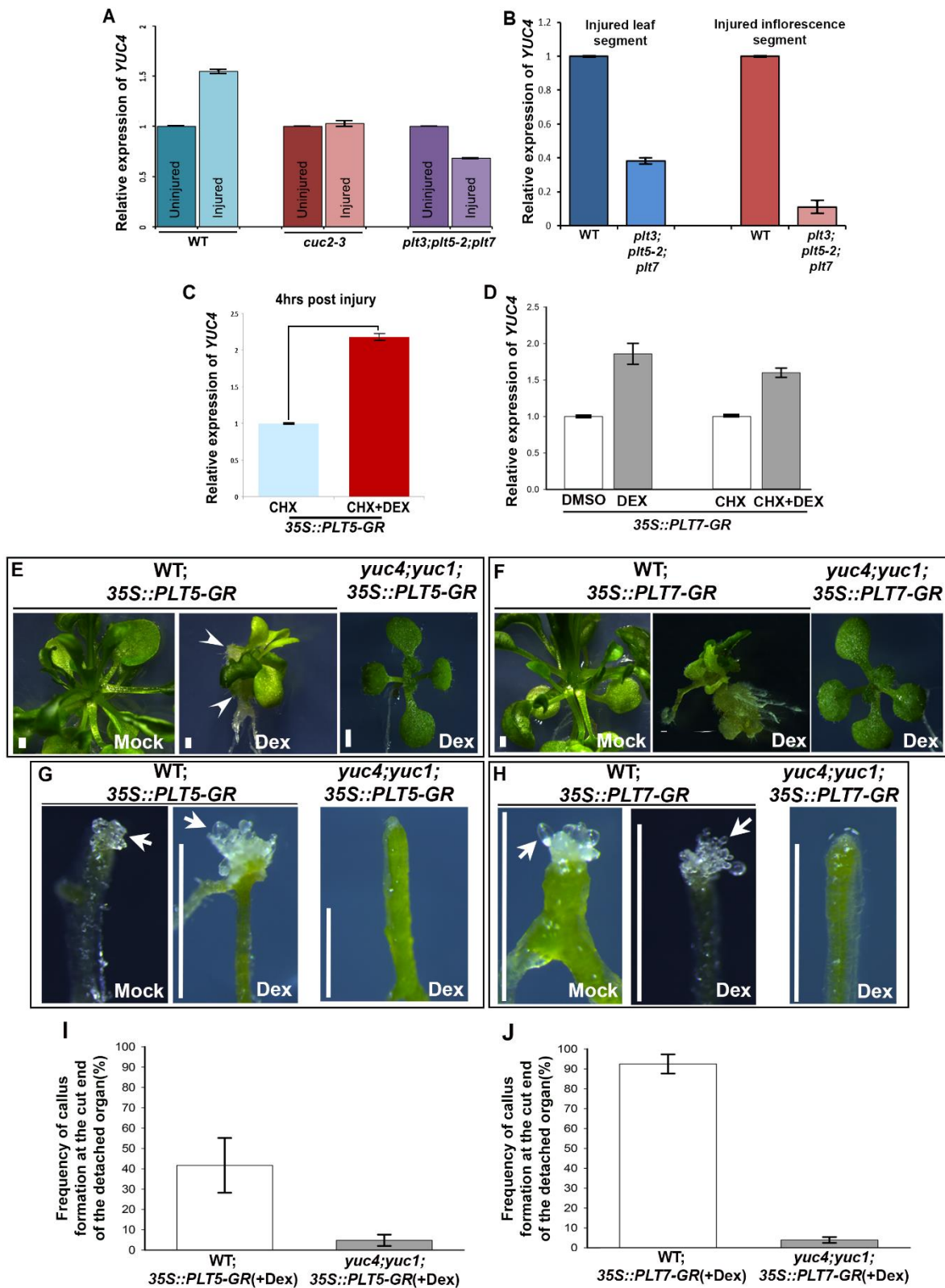


**Figure 3.30** *YUC4* is activated upon injury and PLT acts through *YUC4* during reprogramming and wound repair

(A) The levels of *YUC4* transcripts were analyzed using qRT-PCR in both injured and uninjured leaves of WT, *cuc2-1D*, and *plt3;plt5-2;plt7* plants. (*ns*, not significant,  $P=0.45$ ;  $**P=0.001$ ,  $***P=0.0002$ ; Welch's two-sample t-test). (B) The transcript levels of *YUC4* were analyzed in both injured and

uninjured leaf and inflorescence stem segments of both WT and *plt3;plt5-2;plt7* mutant plants using qRT-PCR. The error bars in the data represent the standard error of the mean (s.e.m.) of 3 independent biological replicates. (C) The transcript levels of *YUC4* were found to be upregulated in injured leaves when *35S::PLT5-GR* was induced with cycloheximide (CHX) treatment, as determined by qRT-PCR analysis (\*\**P*=0.0008; Welch's two-sample t-test). Expression level in A-C is normalized to *ACTIN2*. (D) Transcript level of *YUC4* upon induction of *35S::PLT7-GR* with DEX treatment and with cycloheximide treatment at 4 hours post injury. Expression levels are normalized to *ACTIN2*. Error bar represents s.e.m. from three independent biological replicates. (E) Growing seedlings of WT; *35S::PLT5-GR* upon DEX induction shows callus formation (arrowheads) from shoot and root leading to stunted growth of the plant, unlike mock treated control, which does not show any ectopic phenotypes. However *yuc4;yuc1; 35S::PLT5-GR* does not show any cellular reprogramming even upon DEX induction. (F) Growing seedlings of WT; *35S::PLT7-GR* upon DEX induction shows callus formation (arrowhead) from hypocotyl and root leading to stunted growth of the plant, unlike mock treated control, which does not show any ectopic phenotypes. However *yuc4;yuc1; 35S::PLT7-GR* does not show any cellular reprogramming even upon DEX induction. (G) WT; *35S::PLT5-GR* upon DEX induction (n=15/20) shows increased extent of callus formation unlike in mock treated control of detached organ (n=10/13). However *yuc4;yuc1; 35S::PLT5-GR* (n=20/20) shows barely any callus formation upon DEX induction. (H) WT; *35S::PLT7-GR* upon DEX induction (n=9/10) shows increased extent of callus formation unlike in mock treated control of detached organ (n=7/11). However *yuc4;yuc1; 35S::PLT7-GR* (n=14/15) rarely shows callus formation upon DEX induction. (I, J) Frequency refers to the number of excised organs showing callus formation at the cut end. In addition to frequency, the extent of callus formation at the wounded end of detached organ was extremely reduced in *yuc4;yuc1* as compared to WT upon DEX induction of *35S::PLT5-GR* (I) and *35S::PLT7-GR* (J). Scale bar: 1mm. Error bar represents s.e.m.

To explore the potential contribution of *CUC2* in regulating local auxin biosynthesis in response to injury, we investigated *YUC4* expression in *cuc2* single mutant. We found that *YUC4* transcripts were not upregulated in response to midvein injury in the *cuc2* mutant (Figure 3.30A). Conversely, *YUC4* transcript levels were rapidly increased upon induction of *CUC2-GR*, even in the presence of the translation inhibitor cycloheximide, indicating direct activation of *YUC4* expression by *CUC2* (Figure 3.31A). This inference aligns with the identification of *CUC2* binding to the *YUC4* promoter through DAP Seq analysis (Figure 3.31B)<sup>140</sup>.

Furthermore, we investigated whether, similar to *PLT*, *CUC2* requires downstream *YUC4* activity to promote vascular regeneration. Ectopic overexpression of *CUC2* resulted in the promotion of vascular regeneration and the regeneration of multiple vascular strands in WT plants (WT; *35S::CUC2-3AT*) (Figure 3.31C). In contrast, ectopic overexpression of *CUC2* failed to induce the regeneration of multiple vascular strands from the wound site in the *yuc4;yuc1* mutant (*yuc4;yuc1; 35S::CUC2-3AT*) (Figure 3.31D-F). Injured leaves in *yuc4;yuc1; 35S::CUC2-3AT* seedlings either did not regenerate any vascular strand or occasionally displayed a single file of regenerating vascular cells, similar to the observations in *yuc4;yuc1* mutants (Figure 3.31D-F). These findings demonstrate that, like *PLT*, *CUC2* acts through *YUC4* to promote wound repair and vascular regeneration.

In summary, our data suggests that, in addition to PLT, CUC2 can also activate *YUC4* expression during wound repair, indicating the presence of a regulatory feedforward loop controlling local auxin biosynthesis. Moreover, we found that *PLT5-GR* can moderately activate *YUC4* expression after 4 hours of induction, even in the genetic background where the function of *CUC2* and the redundantly acting *CUC1* is lost (in damaged *cuc1-5; cuc2-3* tissues) (Figure 3.31G). Additionally, the overexpression of *PLT5* or *PLT7* in the *cuc2-3* mutant partially rescued the vascular regeneration defect (Figure 3.31H), further supporting the notion that increased *YUC4* transcripts in damaged leaves of the WT are the result of independent activation by *PLT5* and *CUC2* in a feedforward loop during tissue regeneration.

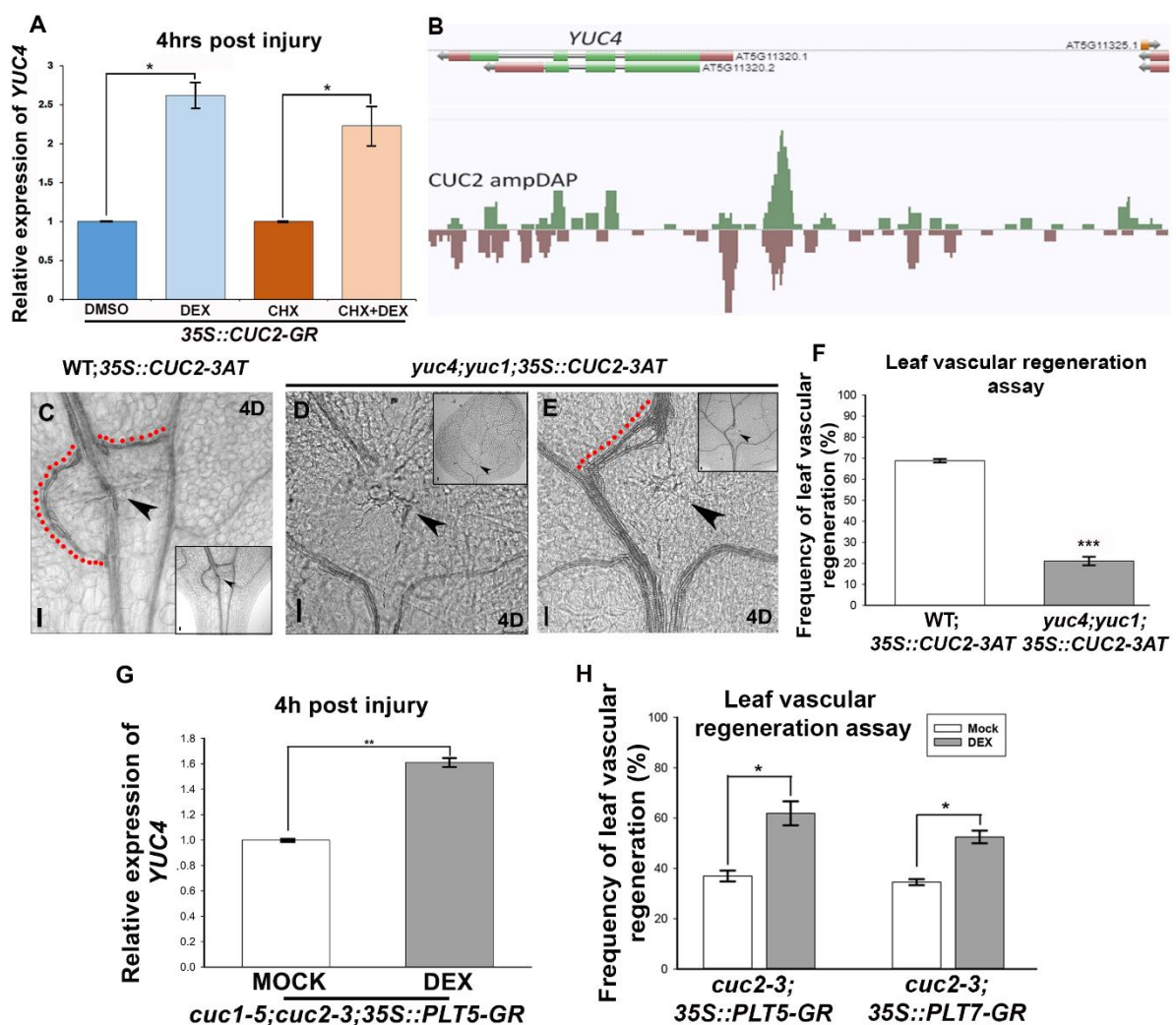


**Figure 3.31 PLT and CUC2 activates YUC4 during vascular regeneration**

(A) The transcript levels of *YUC4* were found to be upregulated in injured leaves upon induction of *35S::CUC2-GR*, with and without CHX treatment. Statistical analysis using Welch's two-sample t-test indicated a significant difference (\* $P < 0.05$ ). (B) DAP-seq analysis revealed that CUC2 binds to the promoter region of *YUC4*, providing evidence of a direct interaction. (C-F) Ectopic overexpression of CUC2 in WT; *35S::CUC2-3AT* resulted in the generation of multiple vascular strands from the wound site (C), unlike in the *yuc4;yuc1; 35S::CUC2-3AT* (D, E). (F) The frequency of leaf vascular

regeneration was compared between WT; *35S::CUC2-3AT* and *yuc4;yuc1; 35S::CUC2-3AT*. A highly significant difference was observed ( $***P = 2 \times 10^{-6}$ ). (G) The transcript levels of *YUC4* were measured in *cuc1-5;cuc2-3* upon induction of *35S::PLT5-GR* using qRT-PCR. The data, normalized to *ACTIN2*, revealed a significant increase in *YUC4* expression ( $**P = 0.0032$ ; Welch's two-sample t-test). (H) The frequency of leaf vascular regeneration was assessed upon overexpression of *35S::PLT5-GR* and *35S::PLT7-GR* in the *cuc2-3* mutant. Pearson's  $\chi^2$  test was performed to analyze the data. Scale bar: 50 $\mu$ m. The error bars represent the standard error of the mean (s.e.m.).

We further sought genetic evidence for the feedforward regulatory interaction between *PLT* and *CUC2*, we conducted analyses of their genetic interaction. Remarkably, we observed a synergistic interaction between *PLT* and *CUC2* during wound repair and vascular regeneration. The cumulative loss of *PLT* and *CUC2* function in the *plt3;plt5-2;plt7;cuc2-3* mutant resulted in severely compromised wound repair at the cut end of detached plant organs, in comparison to the *plt3;plt5-2;plt7* or *cuc2-3* single mutants. In the *plt3;plt5-2;plt7;cuc2-3* mutant, the frequency of wound repair was dramatically reduced, and there were scarce proliferating callus-like cells at the damaged ends of the organs (Figure 3.32). In the *plt3;plt5-2;plt7;cuc2-3* mutant, there was a more pronounced reduction in the transcript level of *YUC4* compared to either the *plt3;plt5-2;plt7* or *cuc2-3* mutant<sup>47</sup>. Additionally, we observed increased sensitivity to midvein injury in leaves of seedlings heterozygous for *plt* and *cuc2* alleles, *plt3+/-;plt5-2+/-;plt7+/-;cuc2-3+/-*, compared to *plt3+/-;plt5-2+/-;plt7+/-* or *cuc2-3+/-* (Table 1). These findings provide strong support for the regulation of *YUC4* expression by *PLT* and *CUC2* in a feedforward loop during wound repair and vascular regeneration.

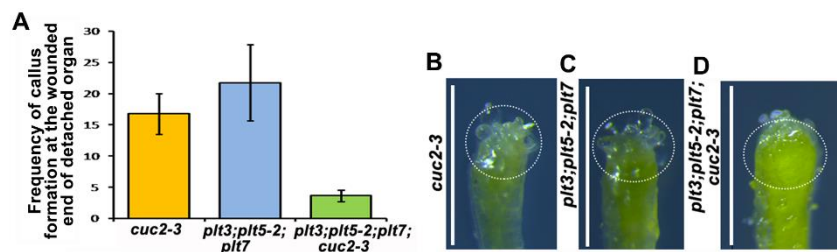


**Figure 3.32 Synergistic role of *PLT* and *CUC2* during wound repair and vascular regeneration**

(A) The number of excised organs that exhibited callus formation at cut ends. (B-D) The extent of callus formation was assessed in *plt3;plt5-2;plt7;cuc2-3* (D), *cuc2-3*, and *plt3;plt5-2;plt7*. The *plt3;plt5-2;plt7;cuc2-3* mutant exhibited a drastic reduction in both frequency and extent of callus formation compared to *cuc2-3* and *plt3;plt5-2;plt7*, which displayed moderate callus formation. The circles mark the cut ends of the explant. Scale bar: 1mm.

Genotype	Frequency of leaf vascular regeneration (%)
<i>plt3<sup>+/-</sup>;plt5-2<sup>+/-</sup>;plt7<sup>+/-</sup></i>	70.52
<i>cuc2-3<sup>+/-</sup></i>	71.66
<i>plt3<sup>+/-</sup>;plt5-2<sup>+/-</sup>; plt7<sup>+/-</sup>;cuc2-3<sup>+/-</sup></i>	36.80

**Table 3.1 Synergistic interaction between PLT and CUC2 during vascular regeneration**

In line with the crucial role of *YUC4* expression activation, approximately 40% of *yuc4* single mutant leaves and 87% of *yuc1;yuc4* double mutant leaves exhibited a failure to regenerate vascular tissue in response to midvein injury (Figure 3.33A-D). Importantly, the *yuc4* single mutant did not exhibit any defects in midvein and lateral vein development, and the leaf venation pattern appeared similar to that of the WT (Figure 3.14A, D). However, the double mutant displayed an altered vascular pattern characterized by open loops and vein fragments on the lamina (Figure 3.17C). In the rare cases where regeneration occurred in *yuc4;yuc1* mutant leaves, multiple partially regenerated strands were observed, but they were unable to reconnect with the parental strands, indicating a disruption in the proper guidance of regenerating veins in the mutant (Figure 3.33D). Finally, we asked if reconstitution of *YUC4* expression in *plt3;plt5-2;plt7* and *cuc2-1* mutants can rescue their vascular regeneration defects. The reconstitution of *YUC4* expression within the endogenous *PLT5* domain (*PLT5::YUC4-YFP*) in *plt3;plt5-2;plt7* and *cuc2-1* mutants rescued the vascular regeneration defects observed in injured leaves to a greater extent (Figure 3.33F-M). Remarkably, the reconstitution of *YUC4* expression in the *cuc1-5;cuc2-3* mutant (*cuc1-5;cuc2-3; PLT5::YUC4-YFP*), which typically exhibits only cup-shaped cotyledons but lacks leaf or stem development, resulted in the restoration of post-embryonic development with fully developed rosette leaves and could activate regeneration responses (Figure 3.34). These findings provide compelling evidence for the functional significance of the *PLT-CUC2* module-dependent activation of local auxin biosynthesis in controlling vascular regeneration processes.

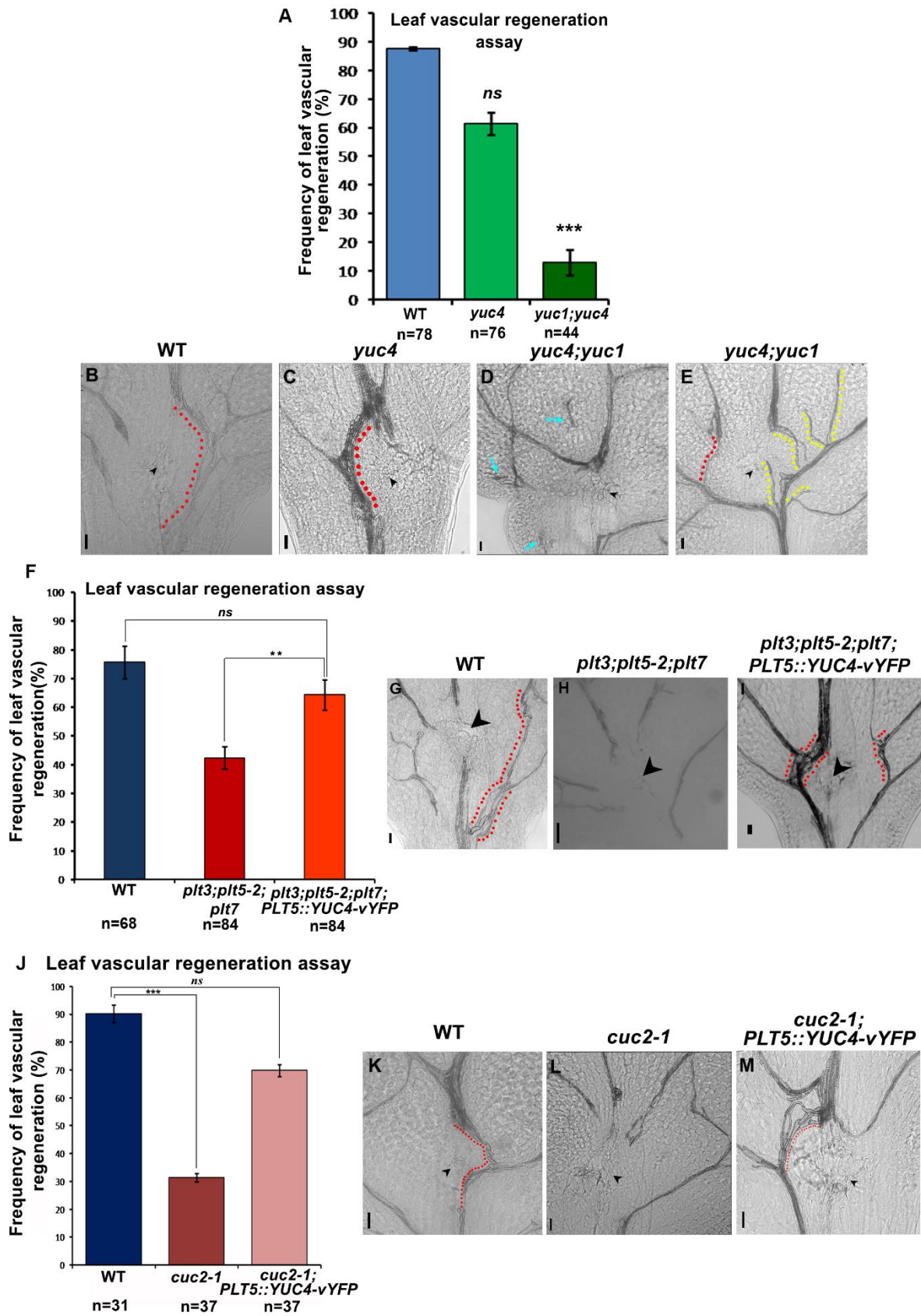


**Figure 3.33** PLT and CUC2 dependent hormonal environment drives vascular regeneration in leaf

(A) The percentage of leaf vascular regeneration in WT, *yuc4*, and *yuc4;yuc1*. No significant difference

between WT and *yuc4* (not significant,  $P=0.8$ ). However, a highly significant difference was observed in *yuc4;yuc1* ( $***P=1.02\times 10^{-6}$ ; Pearson's  $\chi^2$  test). (B-E) Leaf vascular regeneration was observed in WT (B), *yuc4* (C), and *yuc4;yuc1* (D, E) mutants. The red dotted line indicates vascular reconnection, the yellow dotted line represents incomplete connection, blue arrows denote fragments of vascular strands, and the black arrowhead marks the site of incision. (F) The frequency of leaf vascular regeneration was compared between WT, *plt3;plt5-2;plt7*, and *plt3;plt5-2;plt7; PLT5::YUC4-vYFP* ( $**P=0.0087$ ). (G-I) Vascular strand regeneration was examined in WT (G), *plt3;plt5-2;plt7* (H), and *plt3;plt5-2;plt7; PLT5::YUC4-vYFP* (I). Vascular strands failed to regenerate in *plt3;plt5-2;plt7* (H). (J-M) Reconstitution of the local auxin biosynthesis gene in the PLT5 domain rescued leaf vascular regeneration in the *cuc2-1* mutant. ( $***P=4.11\times 10^{-6}$ ; *ns*, not significant,  $P=0.08$ ). Vascular strands failed to regenerate in *cuc2-1D* (L) compared to WT (K). However, the vascular regeneration defect was rescued in *cuc2-1D; PLT5::YUC4-vYFP* (M). Black arrowheads indicate the site of leaf incision, and red dotted lines mark regenerated vascular strands. The error bars represent the standard error of the mean (s.e.m.). Scale bar: 50 $\mu$ m. D: days post injury.

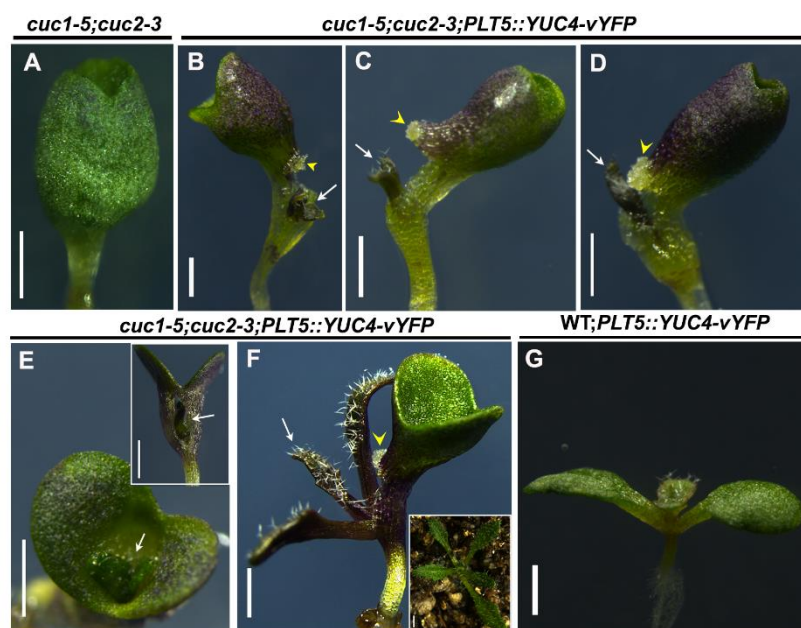


**Figure 3.34 Rescue of post-embryonic development defect in *cuc1-5; cuc2-3* mutant by YUC4**

(A) *cuc1-5;cuc2-3* mutant with cup shaped cotyledon. None of the plants produced shoot ( $n=80$ ). (B-F) When the local auxin biosynthesis gene *YUC4* was reintroduced into the PLT5 domain, it rescued post-embryonic development, resulting in the formation of fully developed leaves (white arrows). Among the 48 plants with cup-shaped cotyledons, 20 plants produced shoots from the base of the cotyledon. The callus formed at the base of the cotyledon due to the emergence of the shoot is marked by yellow arrowheads. (G) The WT plant expressing *PLT5::YUC4-vYFP* showed normal shoot formation. Scale bar: 1mm.

In summary, our findings discover a new role of *PLT-CUC2* module in wound repair and vascular regeneration and provide deep mechanistic understanding of the *PLT-CUC2* regulatory axis. In our study, several lines of evidence demonstrate that activation of *CUC2* transcription by PLT is a key regulatory mechanism of wound repair and vascular regeneration.

(i) PLT binds to *CUC2* promoter and directly activates the transcription of *CUC2*.

(ii) PLT requires downstream CUC2 activity during wound repair as ectopic PLT over expression fails to promote wound repair in *cuc2-3* mutant.

(iii) Reconstitution of CUC2 expression under heterologous promoter in *plt* triple mutant rescues the vascular regeneration defect.

Our studies not only identify the *PLT-CUC2* regulatory axis but also reveal the mechanism by which *PLT-CUC2* module drives vascular regeneration. PLT and CUC2 activate the transcription of local auxin biosynthesis gene in a feedforward loop to drive vascular regeneration. We provide multiple lines of compelling evidence for this mechanism.

(i) Both, PLT and CUC2 require downstream *YUC4* activity as ectopic over expression of PLT as well as of CUC2 fails to trigger cellular reprogramming in *yuc4;yuc1* mutant.

(ii) Reconstitution of *YUC4* expression under heterologous promoter in *plt* triple mutant as well as in *cuc2-1* mutant rescue the vascular regeneration defects.

(iii) PLT and CUC2 act synergistically to repair the damaged tissues.

Taken together our study reveals *PLT-CUC2* regulatory module driven generation of the optimal hormonal environment as a key underlying mechanism of wound repair and vascular regeneration in aerial organs that are growing in a normal developmental context.

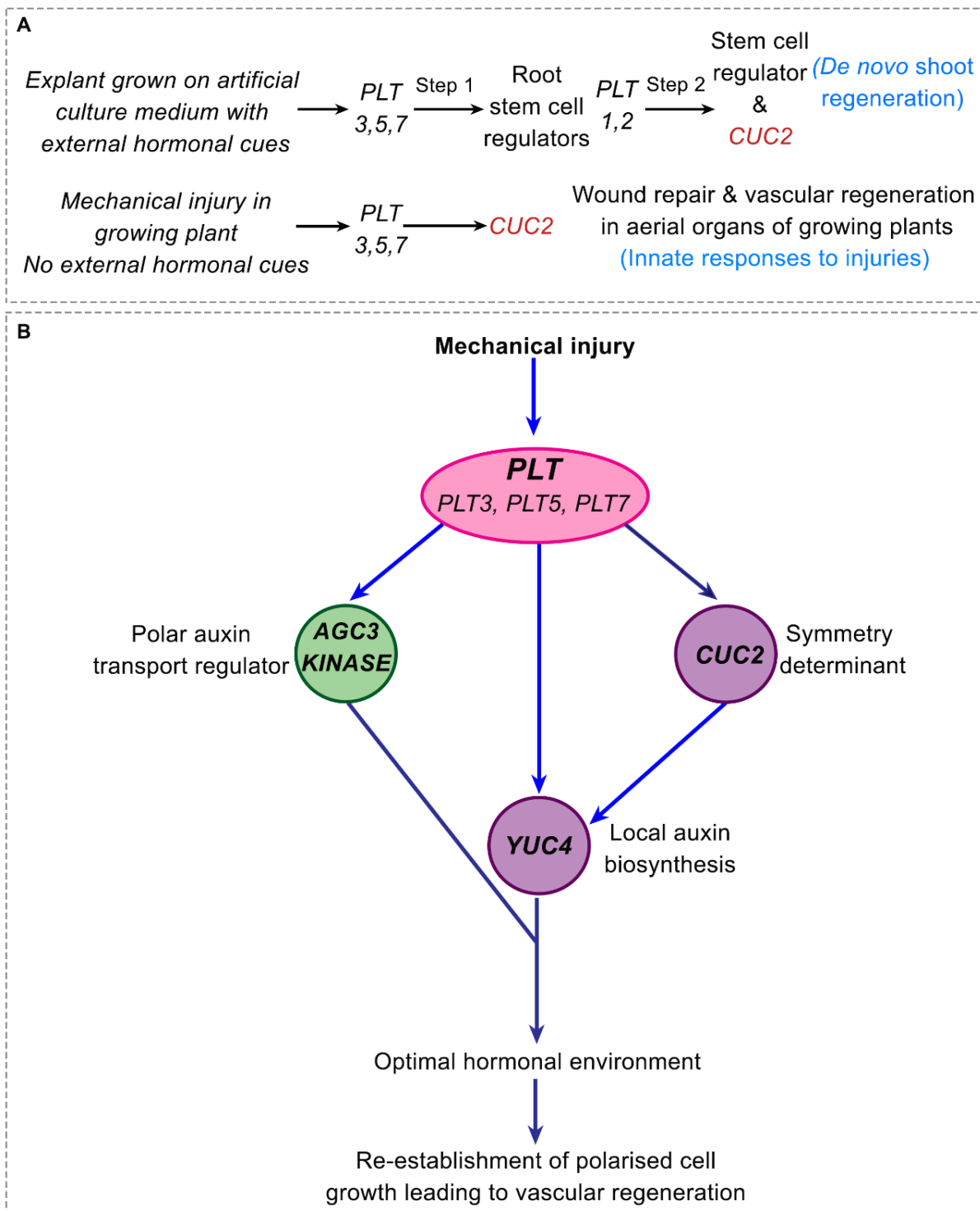


**Figure 3.35 Distinct *PLT*-regulated pathways in mechanical injury response versus tissue culture mediated shoot regeneration**

(A) Flowchart depicting how *PLT*-regulated root stem cell regulators and *PLT*-regulated *CUC2* modules function independently to initiate innate responses to injuries, unlike their sequential involvement in tissue-culture-induced shoot regeneration. (B) Schematic representation of the mechanistic module of *PLT* transcription factors activating symmetry determinant *CUC2* and *AGC3* kinases to generate an optimal auxin environment to aid in re-establishment of polarized growth of vascular cells. Regulatory interactions marked using light blue arrows emerged only from present study and was not known previously in any regeneration context.

### 3.3.8 Dynamic response of early vascular markers during leaf vein regeneration

To investigate the cellular reprogramming involved in regeneration, we examined the response of early vascular markers, namely *PXY* (*PHLOEM INTERCALATED WITH XYLEM*) and *WOX4* (*WUSCHEL-RELATED HOMEODOMAIN 4*), to injury (Figure 3.36, 3.37). *WOX4* and *PXY* are two key components involved in the *TDIF* (*TRACHEARY ELEMENT DIFFERENTIATION INHIBITORY FACTOR*) signalling pathway in plants, particularly in *Arabidopsis thaliana*. This pathway plays a crucial role in regulating vascular development, including procambial cell proliferation and differentiation<sup>141</sup>.

The reporter lines were tracked in real time for uninjured and injured samples from the time of injury. In the uninjured leaves, the expression of these markers reduced upon age, as these cells gradually differentiate into xylem and phloem (Figure 3.36A-D', 3.37A-B'). We observed dynamic changes in expression patterns following injury. Within 12 hours post injury, the *PXY* expression in the procambial cells (early vascular cells) near site of injury reduced, suggesting a loss of cell fate in these cells (Figure 3.36 F, F'). However, these cells regained expression by 24 hours post injury. Interestingly, at 48 hours post injury, patches of *PXY* expression were observed in a few nearby mesophyll cells, which do not have a vascular identity. This suggests that the mesophyll cells gained vascular identity. By 3 days post injury, there were many mesophyll cells expressing *PXY* marker in the shape of a D-loop between the disconnected vascular strands. In case of *WOX4* marker, high expression was detectable mainly in the cut ends of the vascular tissue, within 12 hours post injury and it persisted till 4 days.

The re-emergence of *PXY* expression in injured cells, including non-vascular cells, and the localized expression of *WOX4* at the cut ends highlight the dynamic cellular changes and potential transdifferentiation events that contribute to the regeneration of vascular tissue.

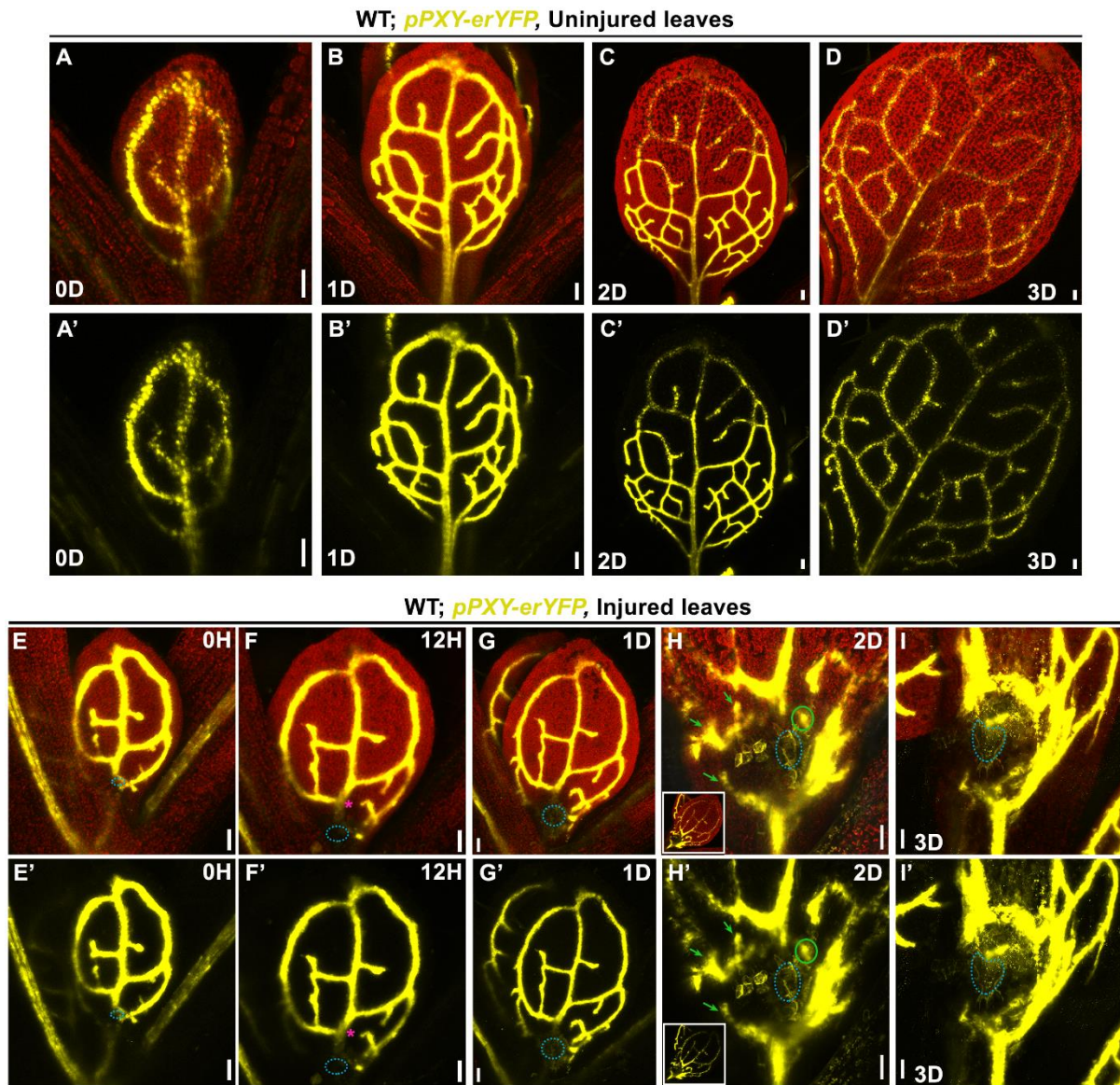


**Figure 3.36** *PXY* expression in uninjured and injured leaves

(A-D') Time lapse images showing expression of *pPXY-erYFP* (yellow) in growing uninjured leaves. A'-D' are corresponding YFP channel images for panels A-D. Red colour represents autofluorescence. Scale bar: 50 $\mu$ m. D: Day, H: Hour. Magenta asterisks in F and F' mark disappearance of *PXY* expression in the vascular tissue. Green arrows and green circle marks *PXY* expression in mesophyll cells. Blue dotted circle represent site of injury. WT: wildtype.

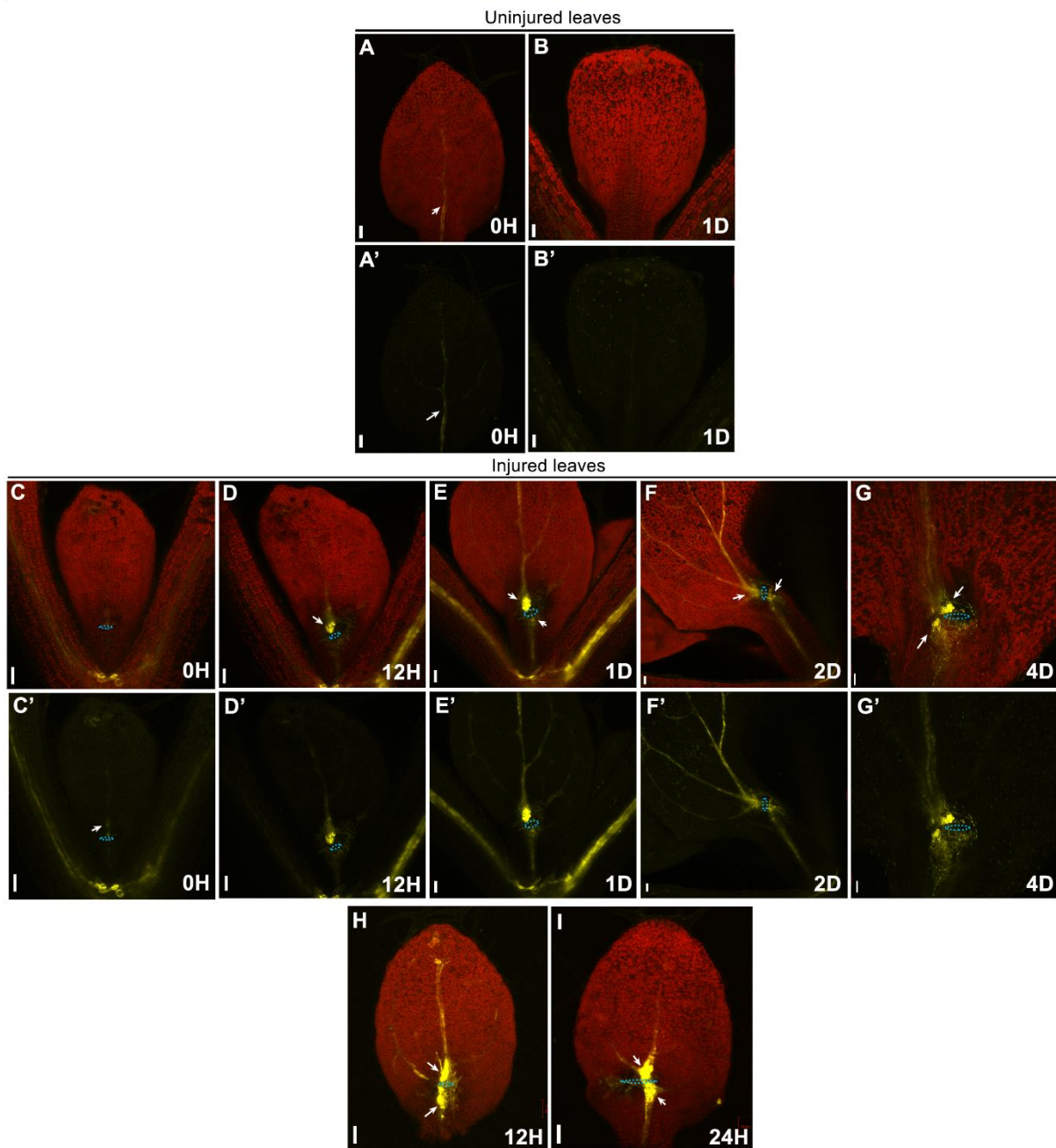


**Figure 3.37** *WOX4* expression in uninjured and injured leaves

(A-B') Expression pattern of *pWOX4-erYFP* (yellow) in uninjured leaves. Weak expression of *WOX4-YFP* was observed at 0H samples (A, A'). Expression of *WOX4-YFP* was not detected after 24 hours. (C-I) Expression of *WOX4-YFP* in injured leaves. Increased expression of *WOX4-YFP* at cut ends of vascular strand is marked by white arrows in time lapse (C-G') and time point images of injured leaves (H,I). Blue dotted circle mark site of injury. H: hour, D: day. Scale bar represents 50µm. Red colour represents chlorophyll autofluorescence. WT: wildtype.

### 3.4 Discussion

Many multicellular organisms display the ability to regrow tissues or organs that were either damaged or lost. Unlike animals where regeneration potential is restricted to specific

lineages, plants can repair and rebuild damaged tissues throughout the body. In this study, we have elucidated the mechanism of wound repair across the plant body and compared the regulation of vascular regeneration with its formation during the development of aerial organs. We made various kinds of injuries (mimicking those that a plant might encounter during its growth) in different parts of growing *Arabidopsis* plants and scored distinct regeneration responses such as local cell proliferation and tissue or organ regeneration. Our study shows the developmental-context sensitivity of a common set of PLETHORA transcription factors (PLT) in the decision making of local cell proliferation response only versus tissue/organ restoration across the body in response to injury. In addition to *PLT*, our study revealed a previously unrecognised role of *ANT* in vascular regeneration. Interestingly, *PLT*-like gene from rice, a morphologically diverse grass species, can rescue the wound repair defects in *Arabidopsis plt* mutant suggesting that the function of *PLT*-like genes is conserved between monocots and dicots. Taken together our study demonstrates a new role of the members of *PLT/ANT* gene family in conferring universal regeneration potential in plants in response to mechanical injuries.

Previously, *PLT* has been shown to act through root and shoot stem cell regulators in tissue-culture-mediated *in vitro* shoot regeneration. Activation of root stem cell regulators and assembly of shoot stem cell regulator by *PLT* are required to reinstate the correct cell-fate in the *plt* mutant callus and thus indirectly regaining the expression levels of thousands of genes. These changes at a global scale lead to *in vitro* regeneration of shoot progenitors in response to external hormonal cues<sup>97</sup> (Radhakrishnan et al., Unpublished data). In striking contrast to *in vitro* shoot regeneration, *PLT* does not act through root or shoot stem cell regulators like *WUS* for repairing the damaged tissues of a growing plant. Rather, *PLT* acts through *CUC2* in this process by directly activating its expression (Figure 3.35A). We find that the *PLT-CUC2* module-dependent control of local auxin biosynthesis is essential for wound repair and vascular regeneration in damaged aerial organs. Interestingly, *PLT* and *CUC2* acts in a feedforward loop to activate the expression of auxin biosynthesis gene *YUC4*. Like many other biological processes where feedforward loop operates for increasing the flux like in metabolic pathways<sup>142</sup>. The regulatory feedforward loop described here ensures the necessary increase in auxin flux following injury, which in turn leads to restoration of damaged tissues (Figure 3.35B). A regulatory feedback loop between auxin flux and polarization of auxin efflux carriers (PIN) has been proposed as a key regulatory mechanism of shoot branching, phyllotaxis and vascular tissue differentiation<sup>123,143–148</sup>. It is likely that that *PLT-CUC2*-dependent re-establishment of

the wound size-sensitive feedback regulation between PIN polarity and auxin flux as shown in our mathematical modelling drives vascular regeneration in damaged growing leaves (Figure 3.12, Section 3.2.11). Taken together, our study has revealed that *PLT-CUC2*-dependent local hormonal environment and cell polarization as the key underlying mechanism of vascular regeneration in growing aerial organs (Figure 3.35B).

The effective auxin response has been suggested to be instrumental in plant regeneration in several different contexts, while the molecular mechanisms generating this response during reprogramming remained unknown<sup>62,75,97,115,123,149</sup>. Here, we show that *PLT-CUC2* is as a core regulatory module for generation of essential auxin response following injury partly by controlling local hormone production. Recently it has been shown that local auxin-signalling maximum specifies the stem-cell organiser of vascular cambium in root<sup>138</sup>.

The expression pattern of early vascular markers PXY and WOX4 upon injury strongly indicate cellular reprogramming occurring at the cut ends of the vascular strands and in the surrounding mesophyll cells. Moreover, they provide valuable insights into the potential involvement of both cell division and transdifferentiation processes during the regeneration of vascular tissues. It is tempting to speculate that *PLT-CUC2* dependent control of local auxin production repairs the damaged leaf vascular tissue by influencing the leaf cambium stem cell activity. Future study is required to test this possibility.

The interplay between the mechanisms of development and of regeneration can be seen in both plants and animals. In neonatal mice, limb digit tip regeneration requires the regulators of early limb development<sup>150</sup>. Similarly, regeneration of primary root tip that originates during embryogenesis requires the regulators of embryonic root<sup>115,116</sup>. Though such interplay between the mechanisms of development and of regeneration is not unexpected, a key question is whether an organ's ability to repair wound can be separated from its normal developmental program. Interestingly, vascular regeneration in *plt3;plt5-2;plt7* mutant leaf is impaired but not the venation pattern and vascular tissue development. *PLT* is known to regulate aerial organ positioning along the plant body axis but not the stem development or leaf venation<sup>90,127,151</sup>. This provides compelling evidence that impaired regeneration responses in aerial organs of *plt3;plt5-2;plt7* mutant is not an indirect effect of their growth or development. Similarly, vascular regeneration in *cuc2* loss of function mutant is severely impaired but not the vascular development. Thus our study demonstrates the exclusive role of the *PLT* transcription module (*PLT* activated *CUC2*) specifically in controlling regeneration of leaf vascular but not in its development. It thus distinguishes the regulation of tissue regeneration

in aerial organs from regulation of its development during plant growth. These findings open up a new possibility of engineering wound repair in growing aerial organs without interfering with their normal developmental programs.

In the process of unravelling the mechanism of vascular regeneration we established a new system to study communication between, and reunion of mechanically disconnected tissues in a growing leaf. The regenerating leaf vascular strands grow in contact with spongy parenchyma and mesophyll cells. It is tempting to speculate that combinatorial contacts guide the orientation of the cell division plane in the newly re-specified vascular cells either by imposing appropriate mechanical forces or by providing biochemical cues<sup>152</sup>. While activation signals originating from surrounding mesophyll cells can guide the polarity driven growth of the regenerating vascular strand, distress signals from damaged cells are likely to keep regenerating strands away from the site of injury (Figure 3.38).

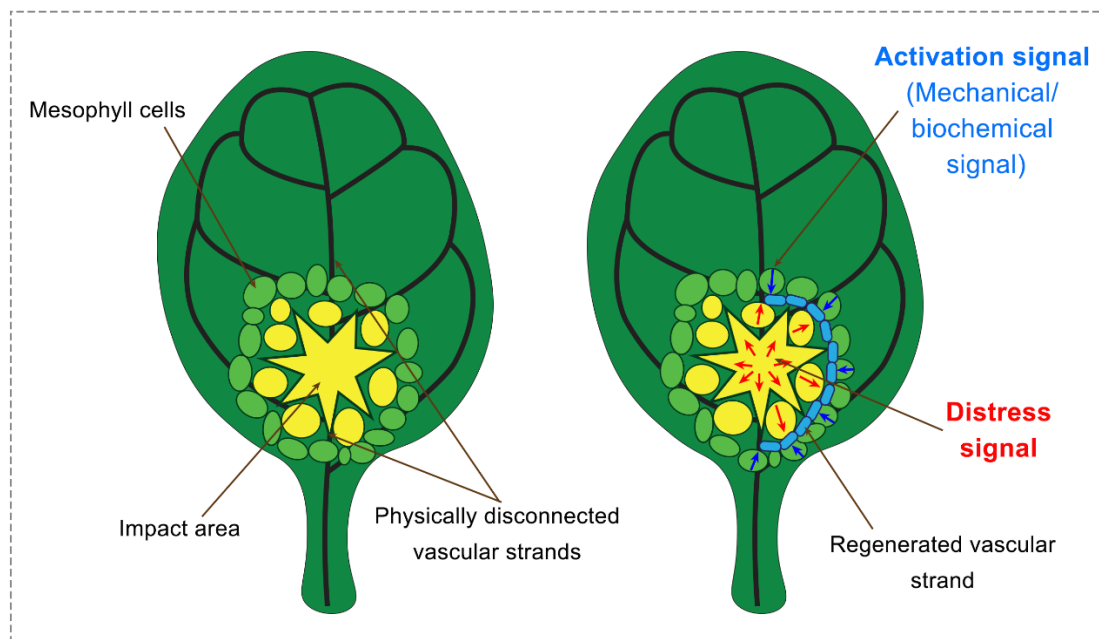


**Figure 3.38 Two seemingly opposite forces work in collaboration to guide the path of vascular tissue reunion**

Vascular regeneration in growing leaf can be used as a model to study the communication and reunion between the tissues that are physically disconnected. Activation signals (blue arrow) from surrounding healthy mesophyll cells (green cells) can guide the polarity driven growth of new vascular cells (blue elongated cells) while distress signals (red arrows) from damaged parenchyma cells (yellow cells) are likely to keep regenerating strands away from the site of injury. These two seemingly opposite signals can act in collaboration to guide the vascular strand reunion.

In summary, we present a comprehensive study of wound repair and tissue regeneration in response to mechanical injury in aerial organs growing in the normal developmental-context. The study unravels a new role for the conserved transcription factors, PLT/ANT and CUC2 in

this process. Furthermore, our study reveals *PLT-CUC2* regulatory axis dependent control of local hormonal environment and cell polarization as a key regulatory mechanism conferring universal regeneration potential to plant tissues in response to injury, and distinguishes regulation of tissue regeneration from its formation during development.

## ***Chapter 4***

# **Regulation of contact-stimulated *de novo* root regeneration from detached leaves**

The work described in this chapter is published in:

**Shanmukhan, A. P., Mathew, M. M., Aiyaz, M., Varaparambathu, V., Kareem, A., Radhakrishnan, D., & Prasad, K. (2021).** Regulation of touch-stimulated *de novo* root regeneration from Arabidopsis leaves. *Plant Physiology*, 187(1), 52-58.

## 4.1 Introduction

Leaves display versatile regenerative capabilities among various aerial organs of plants. Whether through natural means, mechanical injury, or tissue culture, leaves have the ability to regenerate. A notable example of natural regeneration from leaves is the ability of *Kalanchoe* leaves from different species to regenerate entire plants<sup>153</sup>. Plant regeneration can be broadly categorised as tissue-culture based or mechanical-injury induced, depending on the stimulus. Tissue culture-mediated regeneration involves small leaf explants that can generate entire shoots and root systems with the help of hormonal supplements. Mechanical injury-induced regeneration occurs through the incised mid-vein of a growing leaf that remains attached, as well as the cut end of detached leaves. While mid-vein regeneration in growing leaves has only recently been studied, regenerative responses at the cut end of detached leaves have been investigated for several years<sup>23,38,47,77,94</sup>. In studies involving *Arabidopsis*, it has been observed that adventitious roots can emerge from the cut end of detached leaves, either at the base of the leaf blade or the petiole, through DNRR<sup>77,94</sup>. This ability of a tissue part to produce an organ with a different identity than its parent tissue is intriguing. However, the response at the cut end of a detached *Arabidopsis* leaf is not limited to DNRR, as callus formation for wound healing also occurs.

The available data did not provide clarity on whether the decision between callus formation and DNRR is random or if external factors influence one over the other. Therefore, it was crucial to investigate the different regenerative responses to the same injury in the same organ. Through various experimental methods, we demonstrate that the key factor favouring DNRR over callus formation is the direct physical contact of the cut end with any solid or liquid surface. Interestingly, the plant hormone auxin shows increased accumulation in response to contact near wound site. Additionally, we show that *PLETHORA* (*PLT*) genes are essential and sufficient for promoting DNRR.

## 4.2 Materials and methods

### 4.2.1 Growth conditions

*Arabidopsis thaliana* seeds were sterilized by treating them with 70% ethanol and 20% bleach. Afterward, they underwent seven rinses with sterile distilled water. The seeds were then placed on half-strength Murashige-Skoog (MS) medium (pH 5.7) containing 0.7% agar.

They were vertically grown in an environment with continuous white light at a density of 45  $\mu\text{mol}/\text{m}^2/\text{s}$ , maintaining 22°C and a relative humidity of 70%.

#### **4.2.2 Seed sterilization and plating**

Please refer section 2.2.2 in chapter 2.

#### **4.2.3 *De novo* root regeneration assay**

All plants were cultivated on a hormone-free half-strength MS-Agar medium (Sigma-Aldrich). To investigate the regenerative responses of detached leaves, 7-day-old seedlings were selected, and the first pair of leaves was carefully removed using Vannas straight scissors. The excised leaves, along with their petioles, were then placed on hormone-free half-strength MS agar medium containing 0.7% agar. The detached leaves were positioned with either the abaxial side (lower surface) or the adaxial side (upper surface) facing the agar medium. When the abaxial side of the leaf was in contact with the medium or cut end, *de novo* roots were observed to develop. On the other hand, if the cut end of the leaf was exposed or the adaxial side faced the medium surface, a local wound healing response in the form of callus formation was observed. Both types of regeneration responses were evaluated 10 days after the excision.

#### **4.2.4 Split plate experiment**

A hormone-free solid MS-Agar medium (0.7%) was prepared and poured into the upper half of a pre-sterilized square petri dish (Himedia). The petri dish was divided in half using a pre-sterilized insulator. The lower half of the dish was filled with a hormone-free solid Agar-only medium also with a concentration of 0.7%. The detached leaves were positioned with the abaxial side (lower surface) facing downwards, spanning across the divided middle section of the dish. The distal region of the leaf was in contact with the MS-Agar medium, while the cut end of the leaf with its petiole made contact with the Agar-only medium. The leaf explants were then cultured in the dish, and their regeneration was assessed on the 10<sup>th</sup> day.

#### **4.2.5 Leaf pressed into media experiment**

Hormone-free 0.7% solid MS-Agar medium was prepared and poured into a pre-sterilized square petri dish. After the medium cooled down, the detached leaves were positioned with the adaxial side (upper surface) facing downwards and pressed into the medium, ensuring that the cut end of the leaf made contact with the agar surface. The leaf explants were then cultured in the dish, and their regeneration was evaluated on the 10th day.

#### **4.2.6 Agar block experiment**

Hormone-free solid MS-Agar medium (0.7%) was poured into a pre-sterilized square petri dish. After cooling, a thin strip of parafilm was placed across the MS-Agar medium. The detached leaves were positioned with the adaxial side (upper surface) facing downwards, ensuring that only the distal region of the leaves made contact with the MS-Agar medium. The cut end and petiole of the leaves were insulated from the medium by the parafilm strip. Hormone-free Agar-only blocks were placed on the cut ends of the leaves, effectively sandwiching the cut ends of the petioles between the parafilm and the Agar-only block. The leaf explants were then cultured in the dish, and their regeneration was assessed on the 10th day.

#### **4.2.7 DNRR in water and soil**

To induce DNRR, the leaves were placed with their abaxial side (lower surface) down, allowing them to float on liquid MS-medium. For callus formation from the cut end, the leaves were positioned with their adaxial side (upper surface) down, also floating on liquid MS-medium. In experiments conducted with soil, the leaves were placed on the soil surface with their abaxial side down to promote DNRR. For callus formation from the cut end, the leaves were positioned with their adaxial side down and the petiole facing upwards in the air.

#### **4.2.8 Quantification of auxin levels**

Liao et al. (2015) introduced a single reporter called R2D2, which combines the RPS5A-driven DII fused to n3×VENUS and RPS5A-driven mDII fused to ntdTomato on a single transgene. This reporter is used to quantify auxin accumulation by measuring the ratio of green signal relative to magenta signal. To quantify R2D2, the software ImageJ was used to analyze a specific region of interest (ROI). A rectangular area measuring 500x130 pixels located above the cut end of the leaf was selected, and the intensity of each nucleus within this area was measured. The ratio between the grey value of each nucleus in the magenta channel (mDII-ntdtomato) and the green channel (DII-Venus) was calculated to analyze the level of auxin.

#### **4.2.9 Real-Time quantitative PCR (RT-qPCR)**

The primers for RT-qPCR for *INDOLE-3-ACETIC ACID9 (IAA9)* and *MONOPTEROS (MP/ARF5)* were used as these genes were shown to have upregulated expression in response to increased auxin levels<sup>154,155</sup>.

qIAA9-FP: CACCACTTTCACCTCTTGGTCAATG

qIAA9-RP: AACAAAGCATCCAGTCACCATCC

qARF5-FP: GGGTCAGTCGGGAGATCAAT

qARF5-RP: CCTTACGCATCCCACAAACT

#### 4.2.10 Plant materials

*Arabidopsis thaliana* ecotype Columbia (Col-0) was used as WT for the study. The genetic backgrounds and translational fusion constructs used for the study were *plt3;plt5-2;plt7* and *PLT1::PLT1-vYFP*, *PLT2::PLT2-vYFP*, *PLT3::PLT3-vYFP*, *PLT5::PLT5-vYFP*, *PLT7::PLT7-vYFP*, *CUC2::CUC2-vYFP* and *35S::PLT7-GR<sup>47</sup>* and *PLT7::PLT1-vYFP<sup>97</sup>*, *PLT5::CUC2-vYFP* was generated using Multisite Gateway recombination system.

#### 4.2.11 Confocal and brightfield imaging

The imaging techniques used in this study were conducted following the methods described by Kareem et al. (2015)<sup>97</sup>. Confocal imaging of leaf samples was performed using a Zeiss LSM 880 confocal laser-scanning microscope, while brightfield images were acquired using a Leica M205 FA fluorescence stereo microscope. To visualize the cell boundaries of detached leaf samples during confocal imaging, propidium iodide (Sigma-Aldrich) at a concentration of 20 µg/ml was used for staining. Imaging was conducted using 10× air and 20× air objectives, and the acquired images were processed using Zeiss ZEN black software. Schematics were created using Adobe Illustrator CC 2018, and image compilation was done using Adobe Photoshop CS6.

Specific imaging parameters were set for different fluorescence markers. For lines expressing YFP (*PLT1-YFP*, *PLT2-YFP*, *PLT3-YFP*, *PLT5-YFP*, *PME-YFP*, *YUC4-YFP*, and *CUC2-YFP*), a laser power of 50% with excitation at 514 nm was used. The band width for YFP detection ranged from 519 nm to 540 nm, and the gain was set at 650. For GFP (*pWOX5-GFP*), a laser power of 40% with excitation at 488nm was used, and the band width for GFP detection ranged from 490 nm to 510 nm, with a gain of 700. Auto fluorescence was collected within the bandwidth of 650 nm to 750 nm with a gain of 550. During R2D2 imaging, RFP was excited at 561 nm with a laser power of 50%, and the band width for RFP detection ranged from 575nm to 588 nm, with a gain of 700. YFP was excited at 514 nm with a laser power of 50%, and the band width for YFP detection ranged from 519 nm to 540 nm, with a gain of 750. The settings for propidium iodide stained samples were the same as those for samples containing RFP.

#### 4.2.12 Statistical analysis

The regeneration assay utilized Pearson's  $\chi^2$  test, while the R2D2 quantification and qRT-PCR results were analysed using the Welch Two Sample *t*-test. Additional information regarding p-values, sample sizes, types of error, and the number of experiments conducted can be found in the figure legends associated with the respective results.

### 4.3 Results

#### 4.3.1 Leaves show distinct regeneration responses from the cut end

To investigate regeneration responses, we removed the first pair of true leaves from 7 day old seedlings. These detached leaves were then incubated in hormone-free half-strength Murashige and Skoog (MS) media for a duration of 10 days. Half of the leaf explants were positioned with the abaxial side facing the media, while the other half had the adaxial side facing the media. The responses of the leaves were observed and recorded after 10 days.

When the leaves were placed with their abaxial side down and the cut end of the petiole in contact with the hormone-free solid Murashige and Skoog-Agar medium (MS-agar medium), we observed *de novo* root regeneration, which is consistent with previous studies<sup>77,94</sup> (Figure 4.1, A, A', B, B'). Only 33% (n = 93) of the leaves were able to regenerate mature roots, while the remaining leaves did not exhibit *de novo* root regeneration or callus formation (Figure 4.1, E). However, when the leaves were placed with their adaxial side down and the petiole exposed to the air, root regeneration did not occur. Instead, callus formation was observed at the cut end in 62% of the samples (n = 95; Figure 4.1, C, C', D, D', E).

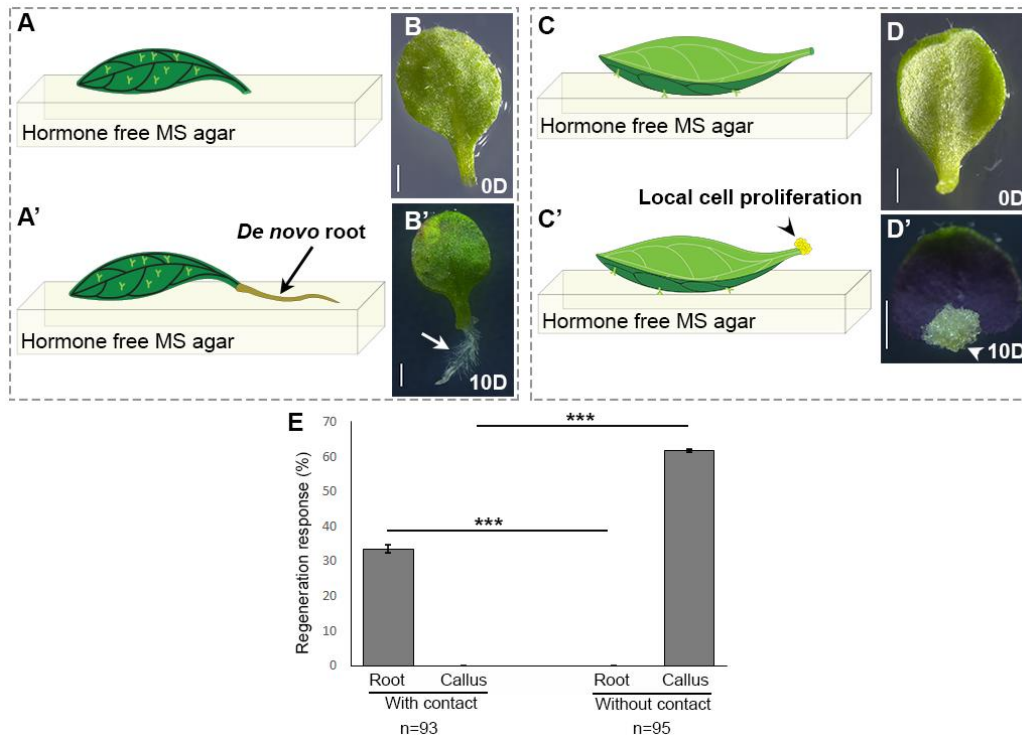


**Figure 4.1 Wound healing response and contact-dependent *de novo* root regeneration at the cut end of a detached leaf**

(A, A') A detached leaf when placed abaxial side down on the hormone-free solid MS-agar media (MS-agar media) results in the formation of *de novo* root. (B, B') Stereo-microscopic images of the detached leaf placed abaxial side down that regenerated *de novo* roots. (C, C') A detached leaf when placed adaxial side down on the MS-agar media results in the formation of callus. (D, D') Stereo-micrographs of the detached leaf placed adaxial side down that resulted in callus formation. (E) Graph showing distinct regeneration response [root ( $***P = 2.24 \times 10^{-08}$ , Pearson's  $\chi^2$  test) and callus ( $***P = 2.2 \times 10^{-16}$ , Pearson's  $\chi^2$  test)] with (n = 93, e = 4) and without (n = 95, e = 4) contact with agar. Error bars represent s.e.m. The black and white arrows indicate *de novo* regenerated root. Black and white arrow heads mark local cell proliferation from cut end of the leaf. Scale bars represent 1 mm. n, sample size; D, days post cut.

#### 4.3.2 Identification of factors involved in distinct regeneration response in detached leaf

Upon initial examination, three factors appeared to differ between the two responses: (i) Nutrient availability at the cut end (minimal MS and sucrose), (ii) orientation of the leaf on the MS-agar (abaxial or adaxial), and (iii) physical contact of the cut end with the agar surface.

To address the absorption of nutrients during *de novo* root regeneration (DNRR), we designed a split-plate experiment. The top half of the plate contained MS-agar, while the bottom half contained nutrient-free agar-only. These two media were separated by a thin strip of overhead projector (OHP) sheet to prevent nutrient diffusion. The leaves were placed with their abaxial side down, so that only the proximal region of the cut end with the petiole in contact with the agar-only surface. The distal region of the leaves remained in contact with the surface of the MS-agar, allowing minimal nutrient transport for their sustenance and growth

(Figure 4.2B and C). It was observed that leaves cannot survive when placed solely on nutrient-free agar (Figure 4.2A). Interestingly, 20.78% (n = 154) of the leaf explants exhibited DNRR from the cut end that was in contact with the surface of the agar-only media, while the remaining leaves did not exhibit DNRR or callus formation.

To examine the influence of leaf orientation, we conducted an experiment where the leaves were positioned with their adaxial side facing downwards on the MS-agar media. Carefully, the leaves were pressed into the media without additional damage to ensure that the cut end came into contact with the agar surface (Figure 4.2D, E). Interestingly, despite the fact that leaf orientation typically promotes callus formation, we observed that 34.2% (n = 76) of the leaves exhibited DNRR in this configuration. This finding suggests that leaf orientation is not a determining factor that distinguishes the distinct regenerative response in leaves.

In agar block experiment, the leaves were placed with the upper side down, and the cut ends were lacking nutrients, making contact with the surface of an agar-only block (Figure 4.2F, G). It was observed that 17.86% (n = 65) of the leaves displayed DNRR in this arrangement. Furthermore, the possibilities of DNRR were explored when the cut end made contact with other materials such as water and soil (Figure 4.2H-O). Leaves oriented abaxial-side down demonstrated DNRR in both liquid medium and soil. However, leaves oriented adaxial-side down only produced callus and no DNRR<sup>95</sup>. These results were consistent with the observations from solid MS-agar (Figure 4.1, B' and D').

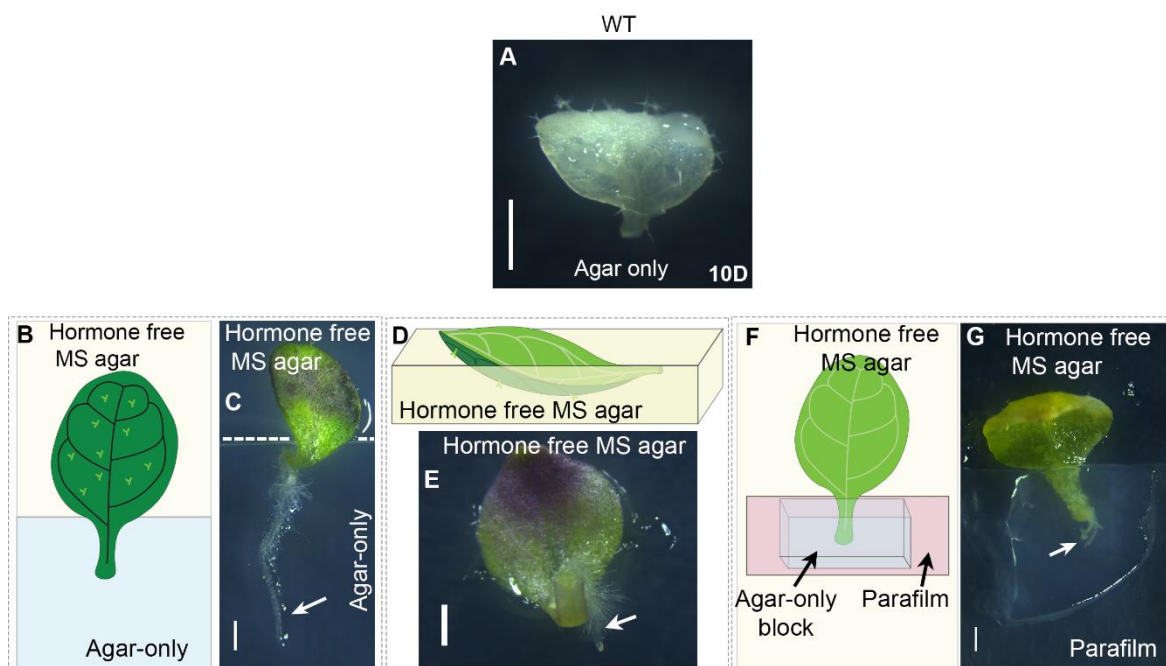


**Figure 4.2 Response of detached leaves when placed on different surfaces**

(A) Response of detached leaf when placed on agar-only media. (B), Schematic depicting a “split-plate”

where the top half of MS-agar medium is insulated from hormone-free solid agar-only medium (agar-only medium). The leaf is placed abaxial side down with its distal end in contact with the MS-agar medium and its cut end contacting the agar-only medium. (C) Stereo-micrographs of the leaf showing DNRR on the split plate. (D) Schematic showing the detached leaf being pressed into the media with its adaxial side down. (E) Stereo-micrograph of the leaf showing DNRR after being pressed into the medium. (F) Schematic illustrating the experimental set-up where the cut end contacts agar-only block but is insulated from MS-agar media. Here, the detached leaf is placed adaxial side down on MS-agar medium, and the cut end is sandwiched between a thin parafilm strip and an agar-only block. (G) Stereo micrograph of leaf showing DNRR after the cut end being sandwiched between parafilm and agar-only block. The black and white arrows indicate *de novo* regenerated root. White arrowheads represent callus formation from cut end. Scale bars represent 1 mm. D, days post cut.

The presence of water is crucial for the survival and regeneration of leaves. However, it is not just the availability of water, but the direct physical contact of water with the cut end of leaves that initiates DNRR. When the leaves are allowed to float on water with the upper side down and the cut end in the air, they do not undergo DNRR. Instead, they form callus at the cut end<sup>95</sup>. It is noteworthy that the entire leaves, including the petioles, remain green and healthy enough to develop callus without wilting. The direct contact of water with *Arabidopsis* leaves leads to an increase in the expression of several genes involved in touch responses<sup>156–158</sup>. This indicates that water can indeed trigger touch-induced physiological responses in plants. However, further studies are needed to determine which specific touch-responsive genes are upregulated during DNRR and their functions. Overall, these findings support the hypothesis that the contact with a solid or liquid surface is the primary factor that distinguishes the two regenerative responses at the cut end of a detached leaf, namely adventitious-rooting and callus-formation.

#### **4.3.3 Contact stimulated increase in auxin level at the cut end of the petiole**

Auxin is known to play a role in various regenerative processes<sup>159</sup>. To investigate its involvement, we used a sensitive marker called R2D2 to assess the auxin levels in the two distinct regenerative responses observed at the cut end of the detached leaf<sup>160</sup>. Our findings revealed that the auxin level was higher when the cut end was in contact with the agar surface compared to when it did not contact the agar (Figure 4.3, Figure 4.4). We consistently observed a similar increase in auxin level when the cut end made physical contact with soil as well<sup>95</sup>. Furthermore, the contact-induced elevation in auxin level was supported by a slight upregulation in the expression of auxin responsive genes such as INDOLE-3-ACETIC ACID INDUCIBLE 9 (1AA9) and MONOPTEROS (MP/ARF5) as determined by RT-qPCR (Figure 4.3F). The findings highlight the significance of physical contact and auxin accumulation in determining the regenerative outcome at the cut end of detached leaves.

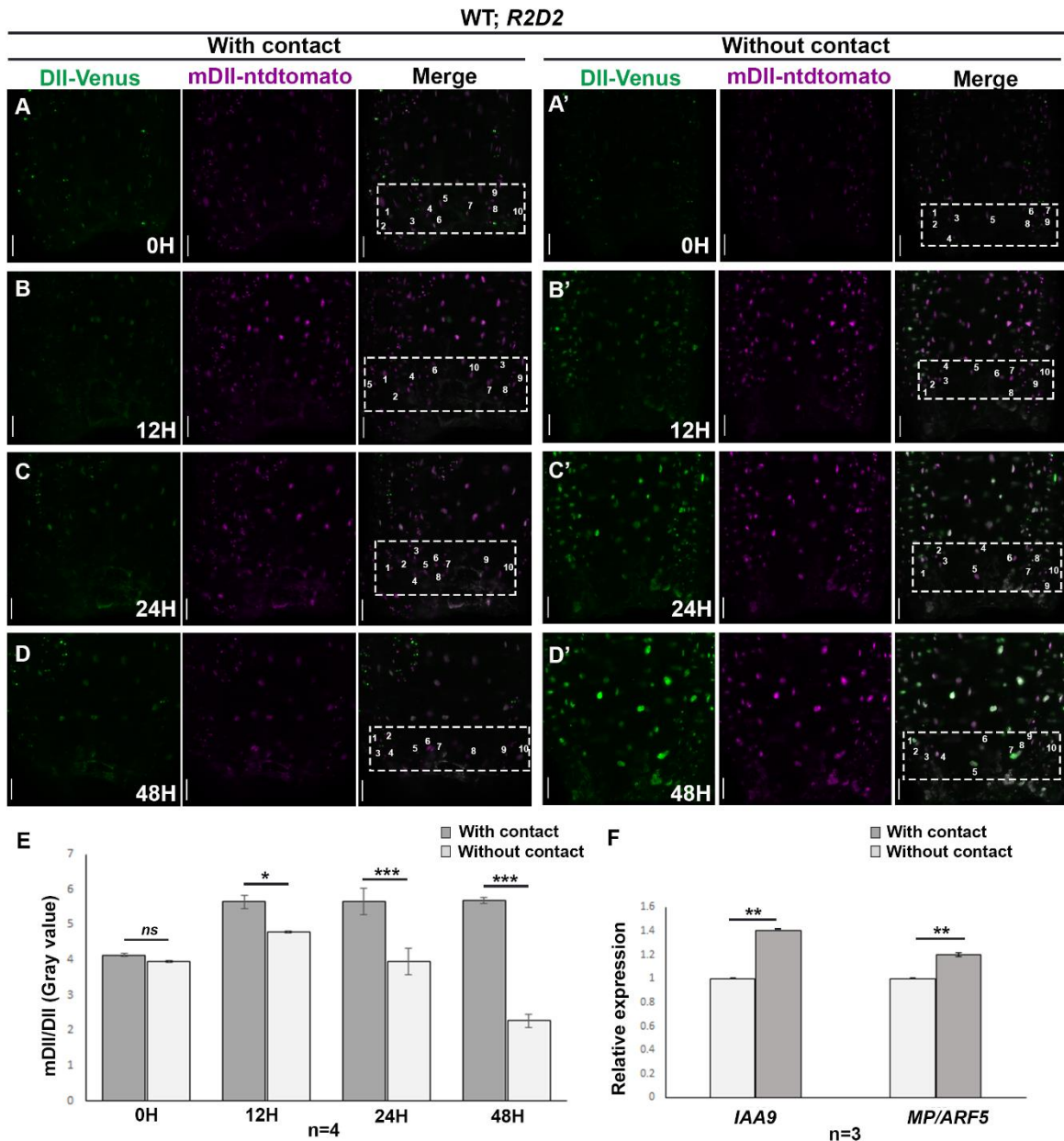


**Figure 4.3 Contact-dependent differential auxin response near the cut ends of detached leaves**

(A-D, A'-D') Time lapse images showing expression pattern of auxin sensor R2D2 in cut ends of detached leaves which are in contact (A-D) and not in contact (A'-D') with surface of the MS-agar medium. During time lapse, sequential imaging of the same leaves was done at regular intervals. Decrease in DII-Venus signal (green) indicates the increase in auxin levels. The numbers in the merge panel show nuclei used for quantification. (E) Graph showing differential auxin levels in the cut ends of petioles that is in contact with a surface against those that did not contact the surface, at 0 h (ns,  $P = 0.8577$ , Welch two sample t test), 12 h ( $*P = 0.04185$ , Welch two sample t test), 24 h ( $***P = 0.0001166$ , Welch two sample t test), and 48 h ( $***P = 3.144 \times 10^{-05}$ , Welch two sample t test;  $n = 4$ ,  $e = 2$ ). Here, the quantification of auxin level was done using 10 individual nuclei (labelled 1-10) from each leaf. (F) Mild upregulation in the expression of auxin response genes IAA9 ( $**P = 0.00251$ , Welch's two-sample t test) and ARF5 ( $**P = 0.00883$ , Welch's two-sample t test) (RT-qPCR) transcript levels in detached leaves upon contact with MS-agar media. Each experiment was performed with three biological replicates and each biological replicate contain six leaves. Error bar represents s.e.m. Scale bar: 50  $\mu\text{m}$ , n: sample size, e: number of experiments, H: hours post cut.

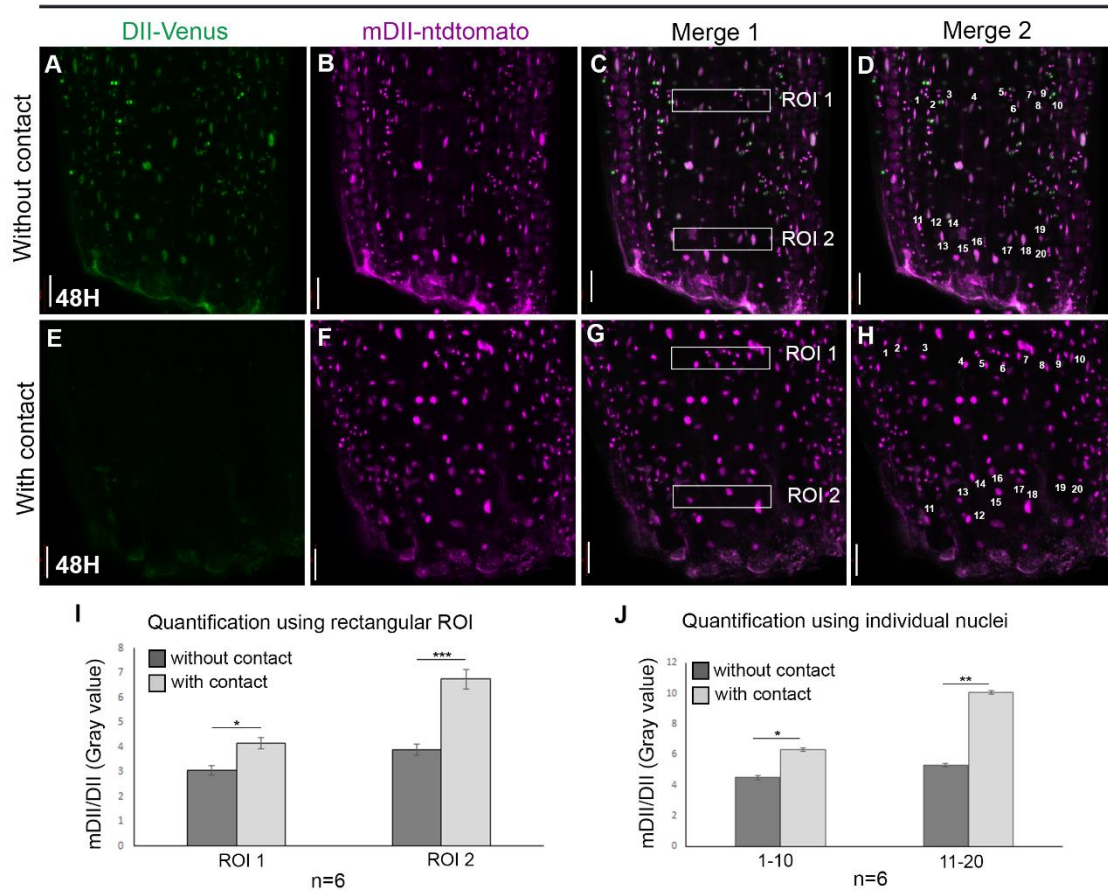


**Figure 4.4 Quantification of auxin levels at the cut ends of detached leaves placed on MS-agar medium**

(A-H) Expression pattern of auxin sensor R2D2 in cut ends of detached leaves which are in contact (A-D) and not in contact (E-H) with the surface of MS-Agar solid medium at 48 hours post cut. Auxin level was quantified from the Region of interest (ROI, marked by white rectangle) near cut end of the petiole (ROI 1) and away from the cut end (ROI 2) that contacted and did not contact media, as shown in Merge 1 panel. R2D2 expression pattern was also quantified using individual nuclei near the cut end (nuclei 11-20) and away from the cut end (nuclei 1-10), as shown in Merge 2 panel. (I, J) Graphs representing quantification of auxin level near and away from the cut end using rectangular ROI (I) and individual nuclei (J). Note the increase in auxin level as indicated by decrease in DII-Venus (green) signal. Scale bar: 50 $\mu$ m, H: hours post cut. Error bars represent s.e.m. WT: wildtype.

#### 4.3.4 PLT3, PLT5 and PLT7 are necessary as well as sufficient for contact-mediated DNRR

We examined the expression of transcriptional regulators that could potentially show varying levels of expression when the cut end of the leaf made contact with the surface. Based on their well-established role in plant regeneration, we specifically analysed PLT3, PLT5, and PLT7 (PLT3-YFP, PLT5-YFP, PLT7-YFP) in a WT background for our analysis<sup>47,97</sup>. After examining the expression pattern of PLT7 at 24 hours and 48 hours following the injury, we observed significant YFP expression in several cells near the cut end when it was in continuous

contact with the MS-agar surface during both time points (Figure 4.5, A–C). In contrast, when the cut end was not in contact with the MS-agar, the YFP expression was weak and limited to only a few cells (Figure 4.5D–F). At 7 days post injury, the PLT7 expression was found throughout the petiole in both the cases. PLT7 expression was also detected in the callus formed when the cut end did not make contact with the surface (Figure 4.5 G, H). Similar patterns of differential expression were observed for PLT3 and PLT5 at later time points near the cut end (Figure 4.6). It is important to note that all the leaf explants were subsequently cultured on hormone-free solid MS-agar media.

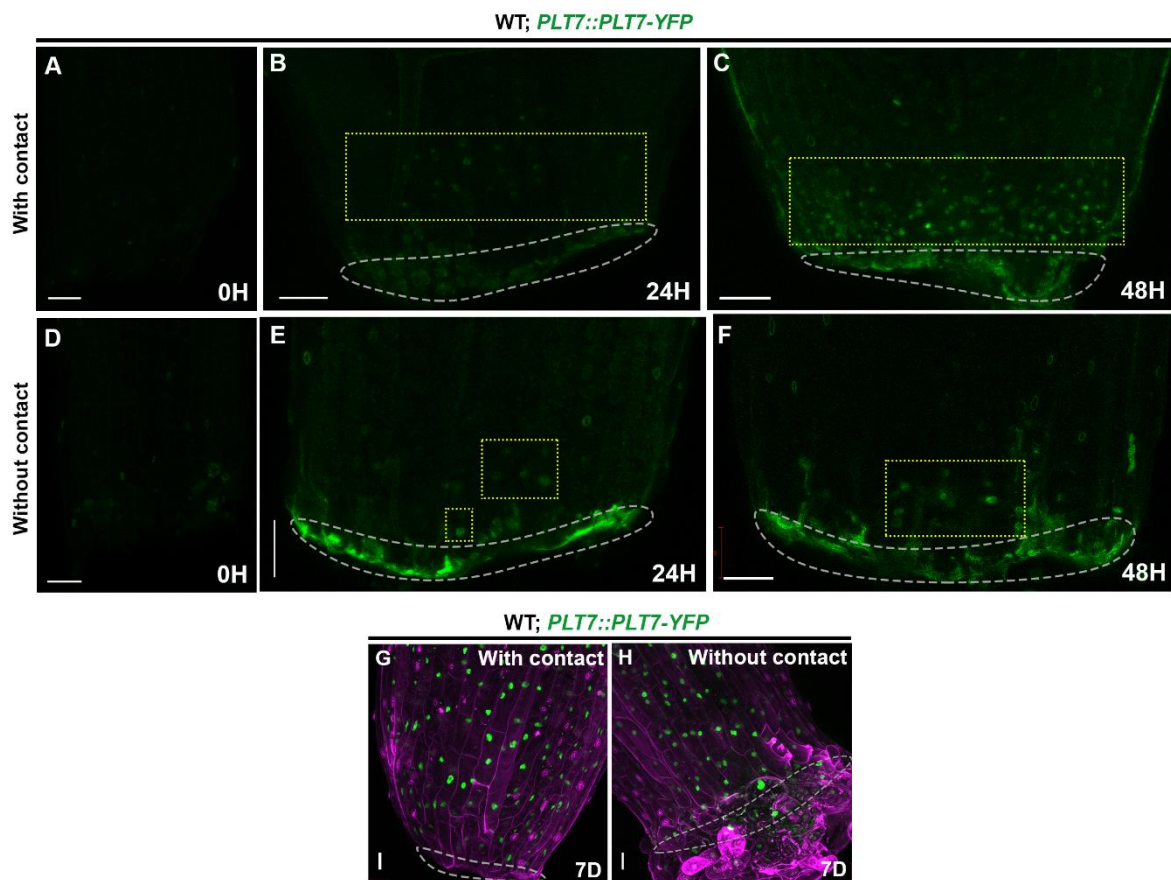


**Figure 4.5 PLT7 expression pattern in the cut end of leaf petiole**

(A–F) *PLT7::PLT7-vYFP* expression (green) when the cut end is in continuous contact with the MS-agar (A–C) and when the cut end fails to contact the medium (D–F). Yellow dotted area indicates regions with YFP; Note that the green fluorescence seen at the cut end is not the true signal, but rather the reflection from damage. A–F shows brightness-adjusted YFP-channel. (G) *PLT7::PLT7-vYFP* (green) expression at cut end of the leaf when it is in contact with MS-Agar media at 7D post injury. (H) *PLT7::PLT7-vYFP* (green) expression at cut end of petiole when it is not in contact with MS-Agar media at 7D post injury. It should be noted that a difference in PLT7 expression between the leaves where cut end contacted and did not contact the surface, is seen only at early time points as seen in A–F, but not at later time point as seen here. Grey dashed area encloses cut end of the leaf. Scale bar: 50µm, H: Hour D: Day.

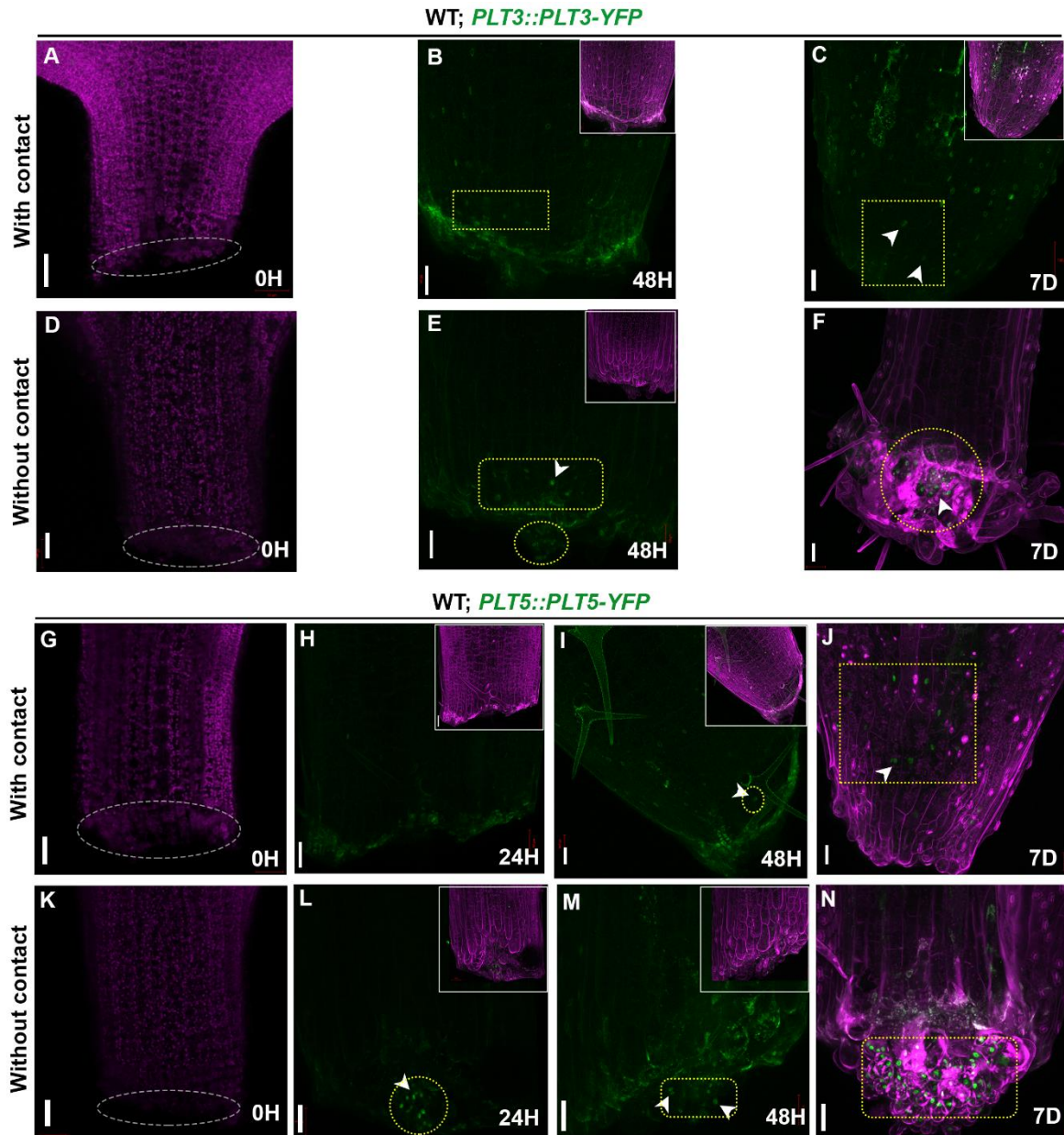


**Figure 4.6 Expression pattern of PLT3 and PLT5 in cut ends of detached leaves**

(A-C) *PLT3::PLT3-vYFP* (green) expression at 0H-48H-7D time points at the cut end of the petiole when it is in contact with media. (D-F) *PLT3::PLT3-vYFP* (green) expression at 0H-48H-7D time points at the cut end of the petiole when it is not in contact with media. (G-J) *PLT5::PLT5-vYFP* expression at 0H-24H-48H-7D time points at the cut end of the petiole when it is in contact with media. (K-N) Expression of *PLT5::PLT5-vYFP* at 0H-24H-48H-7D time points at cut ends of the detached leaf when there is no contact with media. Scale bar: 50µm (A-P), 1mm (Q-S). Yellow dashed area indicates regions with YFP; white arrowheads indicate YFP expression; Grey dashed area encloses the cut end of the leaf. Magenta colour denotes chlorophyll autofluorescence and propidium iodide. H: hours post cut, D: days post cut.

Since PLT3, PLT5, and PLT7 exhibited different expression patterns in response to with contact and without-contact conditions, we examined the response of the *plt3;plt5-2;plt7* triple mutant under these conditions. Interestingly, leaves from the triple mutant failed to show

any DNRR or formation of root primordium-like structures, even when the cut end was in contact with the MS-agar surface (Figure 4.7 A-C). Instead, the *plt* triple mutant produced a micro-callus at the cut site (Figure 4.7D). This micro-callus consisted of proliferating cells that lacked root-specific markers such as PLT1, PLT2, and WOX5 (Figure 4.7E-G), indicating a lack of root identity in these cells.

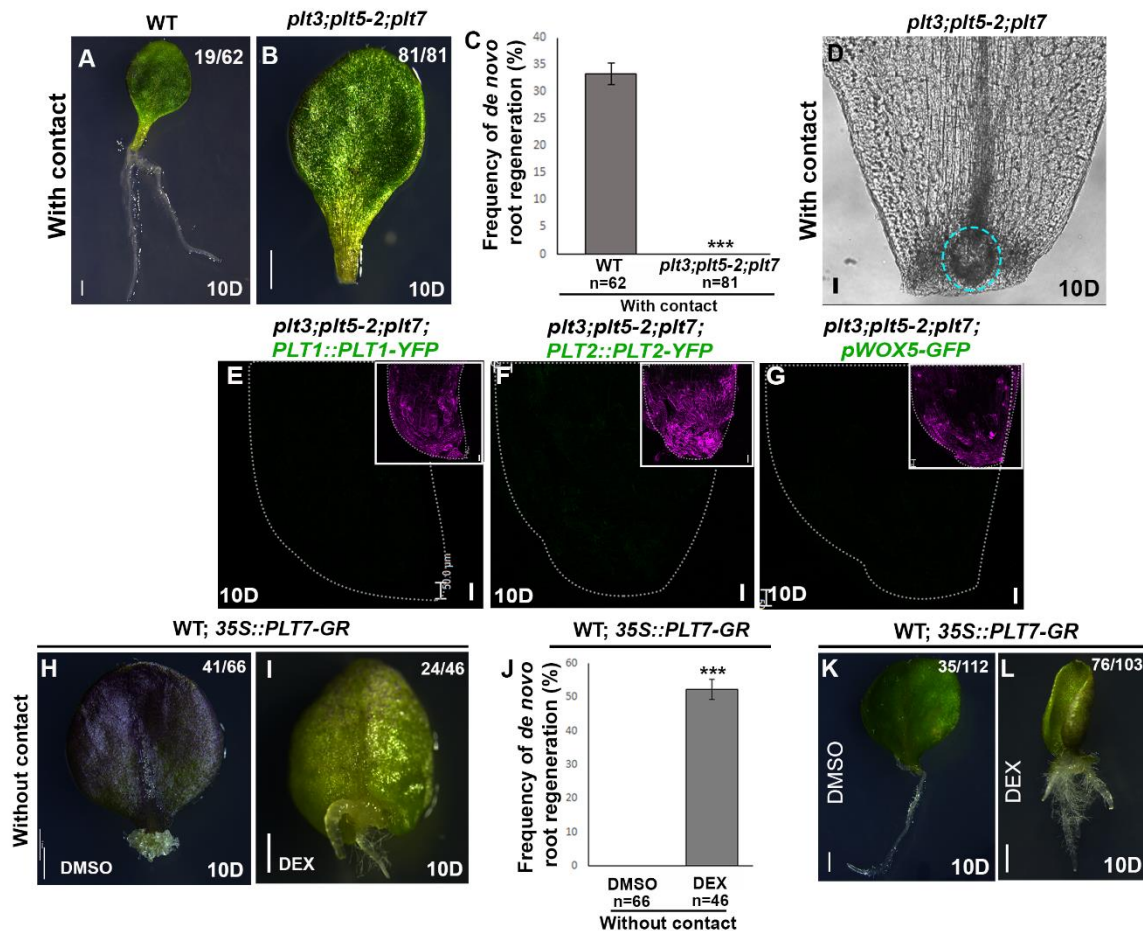


**Figure 4.7 PLTs are necessary and sufficient for contact-mediated DNRR from the cut end of the detached leaves**

(A, B) WT leaf explants exhibit DNRR (A) while *plt3;plt5-2;plt7* mutant (B) shows neither callus formation nor DNRR even when the cut end contacts the MS-agar medium. (C), Frequency of DNRR in WT and *plt3;plt5-2;plt7* mutant (\*\*\*)  $P$ -value = 0.0007431, Pearson's  $\chi^2$  test). (D) Brightfield image shows the absence of root primordia from vascular tissue near the cut end of *plt3;plt5-2;plt7* mutant leaf. The blue dashed area encircles the microcallus (E-G) Expression of *PLT1::PLT1-YFP* (E), *PLT2::PLT2-YFP* (F) and *pWOX5-GFP* (G) is not detectable in *plt3;plt5-2;plt7* mutant leaf even at 10 days post excision. By this time, mature roots would already be regenerated from the cut ends of WT leaves unlike this mutant (A, B). In WT, PLT1, PLT2 and WOX5 expression is confined at the regenerating root tip (data not shown). In striking contrast, there is no expression of PLT1, PLT2 and WOX5 even after 10 days as seen in Figure 4.8E-G. The grey dotted lines indicate the outline of the leaf petiole. Inset shows the same petioles with autofluorescence and propidium iodide. Note that neither YFP nor GFP signal is observed in the mutant. Magenta colour denotes chlorophyll autofluorescence and propidium iodide. (H, I), overexpression with *35S::PLT7-GR* yields DNRR even when the cut end fails to contact the MS-agar medium. DMSO was used as control. (J) Frequency of

DNRR upon overexpression of *35S::PLT7-GR* in WT leaves (\*\**P*-value =  $7.009 \times 10^{-12}$ , Pearson's  $\chi^2$  test). (K,L) Overexpression of *35S::PLT7-GR* causes multiple root formation from the cut end of leaf when it is in contact with media. Error bars represent s.e.m. for I, L, and M. n, sample size; e, number of experiments; H, hours post cut; D, days post cut. Scale bars: 50  $\mu\text{m}$  (A–F), 1 mm (G, H, J, K).

Intriguingly, when *PLT7* was overexpressed (WT; *35S::PLT7-GR*), DNRR was induced at a frequency of 52.2% (n = 46), even in the absence of contact with the MS-agar (Figure 4.7H–J). Additionally, *PLT7* overexpression enhanced DNRR efficiency under contact conditions (Figure 4.7K, L). This suggests that *PLT7* overexpression can bypass the necessity of the contact with surface. Together, our data indicate that *PLT* genes are essential as well as sufficient for DNRR.

#### **4.3.5 *PLT3*, *PLT5* and *PLT7* do not act via downstream targets known for other regenerative responses**

Previous studies reported that *PLT3*, *PLT5*, and *PLT7* function through different transcriptional regulatory modules in various regenerative responses. These include their involvement in tissue culture-induced shoot regeneration, where they act through root stem cell regulators *PLT1*, *PLT2*, and shoot promoting factor *CUC2*<sup>97</sup>. Additionally, the *PLT-CUC2* regulatory axis has been shown to participate in a coherent feed-forward loop that upregulates the local auxin biosynthesis gene *YUC4* during mechanical injury-induced vascular regeneration in growing plants<sup>47</sup>.

In our study, we used fluorescent-labelled live imaging to examine the expression patterns of *PLT1*, *PLT2*, and *CUC2* (*PLT1-YFP*, *PLT2-YFP*, *CUC2-YFP*) during DNRR in WT plants. We did not observe a rapid increase in the expression of these genes during DNRR (Figure 4.8A–F, K–M), but their expression was detected at later time points (Figure 4.8 G, H, N). In contrast, the *plt3;plt5-2;plt7* mutant leaves, which showed a defect in DNRR, did not exhibit the expression of *PLT1* or *PLT2*, genes that are typically expressed during the initiation of *de novo* root primordium (Figure 4.8I, J)<sup>94</sup>. Additionally, *CUC2-YFP* expression was not detectable in the *plt3; plt5-2;plt7* mutant at 7 days after injury (Figure 4.8O, P).

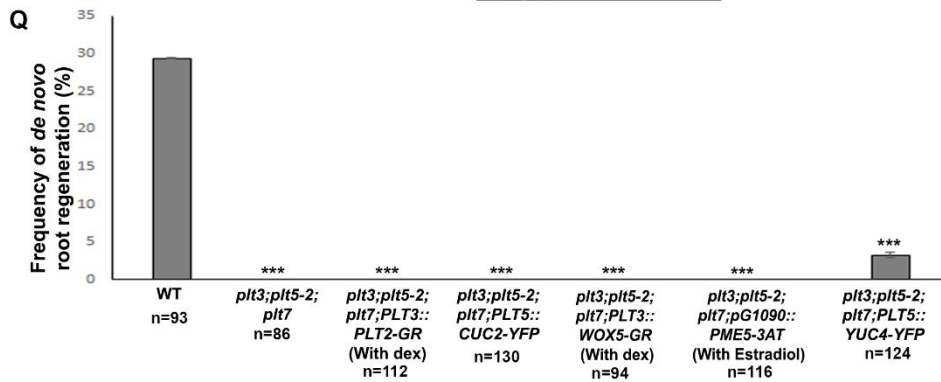
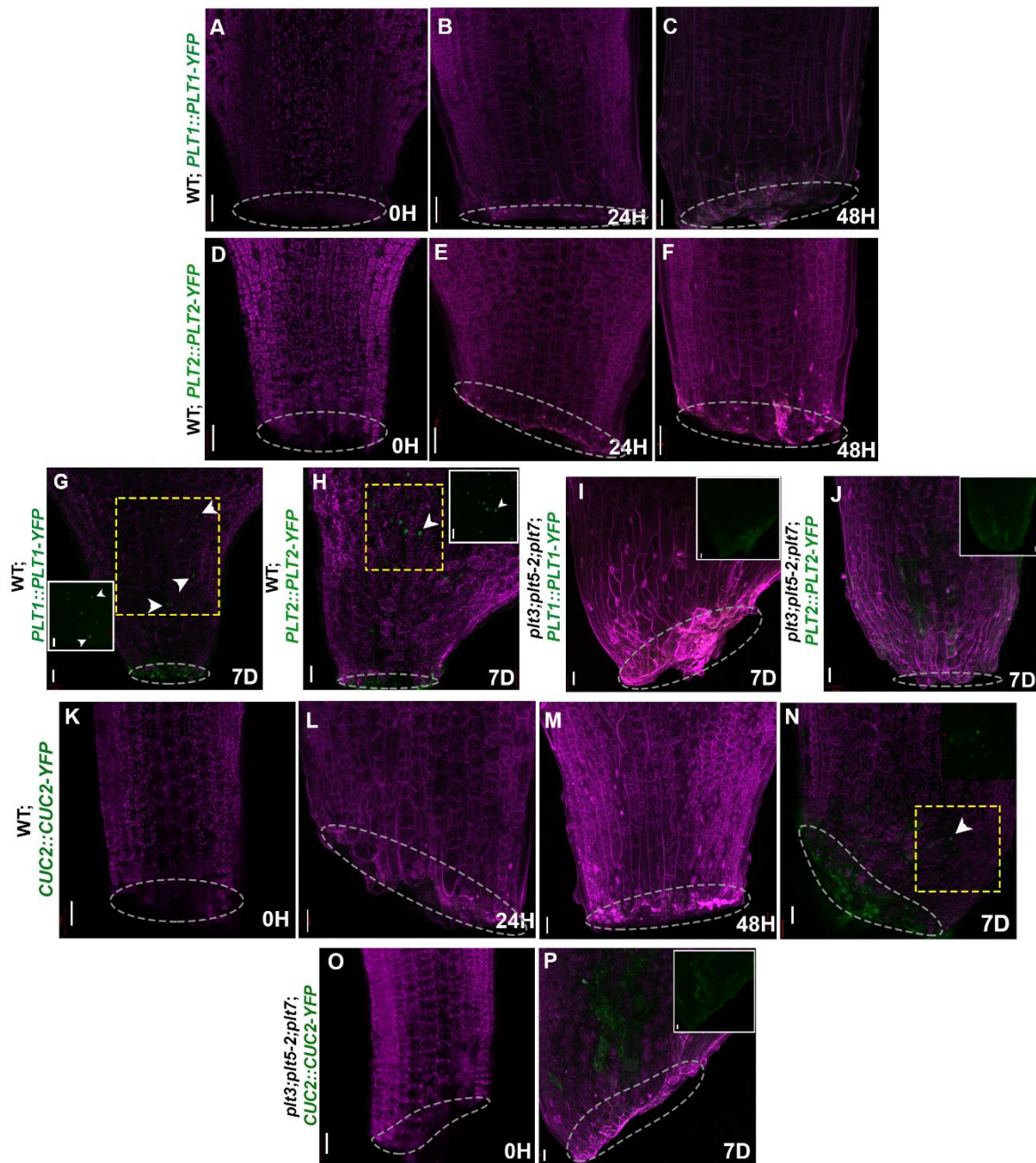


**Figure 4.8 Expression pattern of PLT1, PLT2 and CUC2 in the cut ends of detached leaves**

(A-C) Expression of *PLT1::PLT1-vYFP* (green) is not detectable in detached leaves of WT at 0H, 24H and 48H post cut. (D-F) *PLT2::PLT2-vYFP* (green) expression is not detectable 0H, 24H, and

48H post cut in detached leaves of WT. (G,H) Expression of *PLT1::PLT1-YFP* (green) (G) and *PLT2::PLT2-YFP* (green) (H) in detached leaves of WT, marked by white arrowheads. Inset shows YFP channel. (I,J) Absence of *PLT1::PLT1-vYFP* (green) (I) and *PLT2::PLT2-YFP* (green) (J) in *plt3;plt5-2;plt7* mutant. Note that the green fluorescence seen in inset of (I) and (J) are reflection from the cut end and not the true signals. (K-N) *CUC2::CUC2-YFP* expression (green) in detached leaves of WT. Yellow dashed area indicates regions with true signal; white arrowheads indicate the signals; grey dashed area encloses cut end of the leaf. (O,P) *CUC2::CUC2-vYFP* expression was not observed in detached leaves of *plt3;plt5-2;plt7* mutant. (Q) Graph showing DNRR response in WT, *plt3;plt5-2;plt7* (\*\*\*)  $P$ -value =  $9.593 \times 10^{-08}$ , Pearson's  $\chi^2$  test), *plt3;plt5-2;plt7; PLT3::PLT2-GR* (with dex) (\*\*\*)  $P$ -value =  $9.56 \times 10^{-07}$ , Pearson's  $\chi^2$  test), *plt3;plt5-2;plt7; PLT5::CUC2-YFP* (\*\*\*)  $P$ -value =  $8.853 \times 10^{-11}$ , Pearson's  $\chi^2$  test), *plt3;plt5-2;plt7; PLT3::WOX5-GR* (with dex) (\*\*\*)  $P$ -value =  $2.631 \times 10^{-08}$ , Pearson's  $\chi^2$  test), *plt3;plt5-2;plt7; pG1090::PME-3AT* (With estradiol) (\*\*\*)  $P$ -value = 0.0007, Pearson's  $\chi^2$  test), and *plt3;plt5-2;plt7; PLT5::YUC4-YFP* (\*\*\*)  $P$ -value =  $9.638 \times 10^{-08}$ , Pearson's  $\chi^2$  test) leaves ( $n = 4$ ). Scale bar: 50 $\mu$ m, Magenta colour denotes chlorophyll autofluorescence and propidium iodide. H: hours post cut, D: days post cut.

The defect in lateral root (LR) emergence in *plt3;plt5-2;plt7* was rescued by overexpressing *PLT1* or *PLT2* under the *PLT7* or *PLT3* promoter<sup>43,161</sup>. However, overexpression of *CUC2*, *PLT2*, or *WOX5* under different promoters could not rescue the DNRR defect in *plt3;plt5-2;plt7* (*plt3;plt5-2;plt7; PLT5::CUC2-YFP*, *plt3;plt5-2;plt7; PLT3::PLT2-GR*, and *plt3;plt5-2;plt7; PLT3::WOX5-GR*), indicating that *PLT3*, *PLT5*, and *PLT7* do not regulate DNRR through the control of *CUC2*, *PLT2*, or *WOX5* (Figure 4.8Q).

Previous studies provided evidence that the production of auxin *via YUCCA* genes plays a critical role in the process of DNRR. The expression levels of *YUC1* and *YUC4* genes increase in mesophyll cells and hydathodes within four hours after injury, and in the vasculature of the petiole after two days, as observed through the use of GUS reporter lines<sup>162</sup>. In order to further investigate the expression pattern of *YUC4*, we employed a translational reporter line (WT; *YUC4::YUC4-YFP*) and examined its presence in the cut end of the petiole under with and without contact conditions. Surprisingly, we were unable to detect any expression of *YUC4-YFP* in any of these scenarios. This absence of detection could potentially be attributed to the requirement of *YUC4* being present at minimal levels for the regenerative response to occur. However, rare occurrences of DNRR were observed at an extremely low frequency when *YUC4* was overexpressed using the *PLT5* promoter (*PLT5::YUC4-YFP*) in *plt3;plt5-2;plt7* leaves (Figure 4.9 and Figure 4.8Q). These findings strongly suggest that the regulation of DNRR through *YUC4* is highly unlikely to be controlled by *PLT3*, *PLT5*, and *PLT7*.

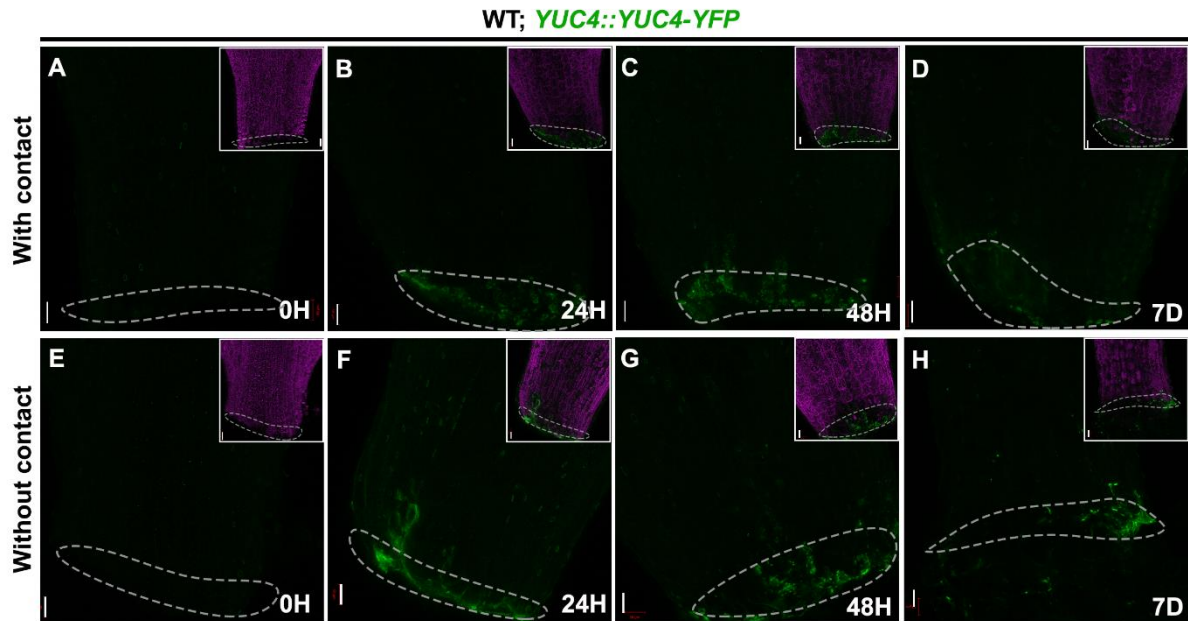


**Figure 4.9** Expression pattern of *YUC4* in the cut ends of detached leaves

(A-H) *YUC4::YUC4-YFP* expression (green) is not detected in the cut ends of detached leaves in WT at 0H, 12H, 24H and 48H after injury. (A-D) *YUC4-YFP* expression is not detected when the cut end of leaf is in contact with MS-agar media. (E-H) *YUC4-YFP* expression is not detectable when the cut end of petiole is protruding out of the medium. The cut end of the leaf petiole is indicated by grey dashed lines. Note that the green fluorescence seen at the cut end is not the true signal, but rather reflection from damage. Scale bar: 50 $\mu$ m, Magenta colour denotes chlorophyll autofluorescence and propidium iodide. H: hours post cut, D: days post cut.

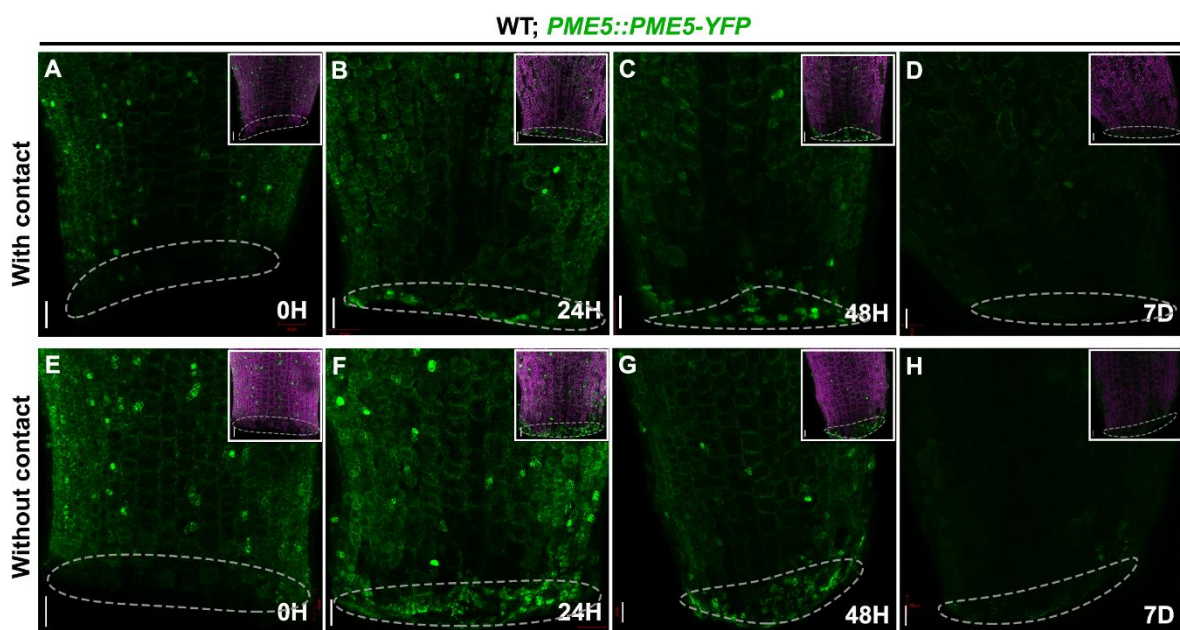


**Figure 4.10** Expression pattern *PME5* in cut ends of detached leaves

(A-D) Expression of *PME5::PME5-YFP* (green) in cut ends of detached leaves in contact with MS-Agar media. (E-H) Expression of *PME5-YFP* (green) when the cut ends of detached leaves are not in contact with media. Note that *PME5* is enriched in the cell wall. The cut end of the leaf petiole is indicated by grey dashed lines. Scale bar: 50 $\mu$ m, Magenta colour denotes chlorophyll autofluorescence

and propidium iodide. H: hours post cut, D: days post cut.

Furthermore, we examined the role of pectin methyl esterase (PME), a cell wall remodelling enzyme family known to induce adventitious rooting and LR initiation during normal development<sup>163,164</sup>. However, the expression of PME5-YFP was not upregulated during DNRR in the WT plants, and overexpression of PME (*plt3;plt5-2;plt7; pG1090::PME-3AT*) did not trigger DNRR in *plt3;plt5-2;plt7* (Figure 4.10 and Figure 4.8Q). Taken together, our findings suggest that DNRR requires a contact-driven regulatory module mediated by PLT3, PLT5, and PLT7, which is distinct from any previously reported regenerative or developmental pathway.

#### 4.4 Discussion

The cut end of a detached leaf exhibit two kinds of responses: DNRR and callus formation. In this study, we investigated the factors influencing distinct regeneration responses in detached leaves. The experiments involved placing detached leaves in different orientations and conditions to observe their regenerative responses. The results showed that when the cut end of a detached leaf was in direct physical contact with a solid or liquid surface, DNRR occurred. On the other hand, when the cut end was not in contact with any surface, callus formation was observed. Furthermore, the study investigated the role of auxin, a plant hormone, in the regenerative process. It was found that higher levels of auxin were detected when the cut end of the leaf was in contact with the agar surface. We also examined the expression of PLT3, PLT5, and PLT7 genes, which are known to be involved in plant regeneration. Significant expression of PLT7 was observed in cells near the cut end when it was in continuous contact with the agar surface. With the help of different genetic experiments, we found that PLT3, PLT5 and PLT7 are required and for DNRR. Moreover, PLT7 overexpression can bypass the requirement of contact for DNRR. Next we looked for downstream regulators for the PLT genes. Towards this we tested whether the genes that are previously known to be downstream regulators for PLT3, PLT5 and PLT7 in other regeneration and developmental contexts. Our findings suggest that DNRR requires a contact-driven regulatory module mediated by PLT, which operates independently from previously reported regenerative or developmental pathways.

These findings suggest that similar mechanisms may be operating in other plants like *Dracaena fragrans*, *Peperomia pellucida*, *Episcia cupreata*, *Hoya carnosa*, and *Saintpaulia ionantha*, where organ formation from the cut ends of detached leaves is observed. While the

exact mechanism underlying DNRR from leaves remains unknown, it is possible that it involves a signalling cascade triggered by mechano-sensing in response to the contact. Previous research had shown that osmotic pressure play a crucial role in the regeneration of specific cell types in roots, indicating the importance of mechano-sensing in the regeneration process<sup>165</sup>. However, other factors should also be taken into consideration. Contact with the surface may facilitate the release of inhibitors that impede DNRR, which would otherwise accumulate at the cut end. It will be interesting to investigate how contact with a surface affects the PLT-regulated genetic framework of DNRR in leaves.

## *Chapter 5*

# **CUC2 mediated regulation of PIN1 localization during *de novo* shoot regeneration**

Part of the work described in this chapter is published in:

Varapparambath, V.\*, Mathew, M.M.\*, **Shanmukhan, A.P.\***, Radhakrishnan, D., Kareem, A., Verma, S., Ramalho, J.J., Manoj, B., Vellandath, A.R., Aiyaz, M., Radha, R.K., Landge, A.N., Mahonen, A.P., Heisler, M.G., Weijers, D., Prasad, K. (2022). Mechanical conflict caused by a cell-wall-loosening enzyme activates *de novo* shoot regeneration. *Developmental Cell*, 57(17), pp.2063-2080.

\* Equal contribution

## 5.1 Introduction

Tissue culture-mediated regeneration is a widely used technique for propagating plants, allowing the regeneration of complete organisms from a mass of cells. Plant tissue culture involves various methods such as somatic embryogenesis, transdifferentiation, and callus-mediated regeneration<sup>97,99,166–169</sup>. Among these methods, callus-mediated regeneration is particularly valuable for studying how cells organize themselves in a multicellular context. It takes advantage of the unique ability of plant cells to become any type of cell and generates entire shoot and root systems through *de novo* organogenesis. In this process, shoot or root explants are cultured *in vitro* with the addition of hormones<sup>170</sup>. *De novo* organogenesis serves as the foundation for clonal propagation, which finds extensive applications in horticulture and crop-genome editing.

Callus-mediated regeneration involves the culture of shoot or root explants *in vitro* with hormonal supplements. *De novo* shoot regeneration is a sequential process influenced by the interplay of plant hormones, such as auxin and cytokinin, and specific transcription factors<sup>85,97,171,172</sup>. When an explant, which can be any part of the plant, is treated with auxin-rich callus induction media, it leads to the formation of a mass of pluripotent cells known as callus. This callus is analogous to the blastema in animals<sup>173</sup>. Subsequently, the pluripotent callus is then provided with cytokinin-rich cues for shoot induction, resulting in the formation of *de novo* shoots. However, only a small population of cells from the pluripotent callus can progress into shoot meristems, which eventually develop into a complete shoot system (Figure 5.1)<sup>96,174–176</sup>.

The shoot stem cell regulator *WUSCHEL* (*WUS*) is expressed sporadically in the region where shoot formation is expected within the callus<sup>96,174,177</sup>. The uneven expression of *WUS* and other factors that promote shoot development in the callus, along with the stochastic nature of shoot meristem formation, suggests that the callus is heterogeneous<sup>98,176</sup>. One important question arises: how are specific cells within the callus chosen as progenitors, and what drives their progression towards becoming shoot meristems? Unlike in the development of a plant embryo, where meristems are formed based on the integration of the apical-basal polarity axis<sup>178</sup>, *de novo* shoot regeneration lacks pre-patterning cues for the positioning of prospective meristems. This is because shoot progenitors formed in tissue culture-induced callus, unlike those in somatic embryogenesis<sup>166</sup>, do not involve embryo formation<sup>179,180</sup>.

Our studies have shown that the polar localization pattern of the auxin efflux transporter *PINFORMED1* (*PIN1*) in developing progenitors plays a crucial role in shoot meristem regeneration. We have observed that this polar localization pattern is functionally significant as it helps in the removal of auxin hormone from the progenitor cells by actively transporting it away from them. Further analysis showed that *CUP SHAPED COTYLEDON 2* (*CUC2*) influence *PIN1* polarity in progenitors non cell autonomously by regulating *XTH9* (*XYLOGLUCAN ENDOTRANSGLUCOSYLASE / HYDROLASE*).

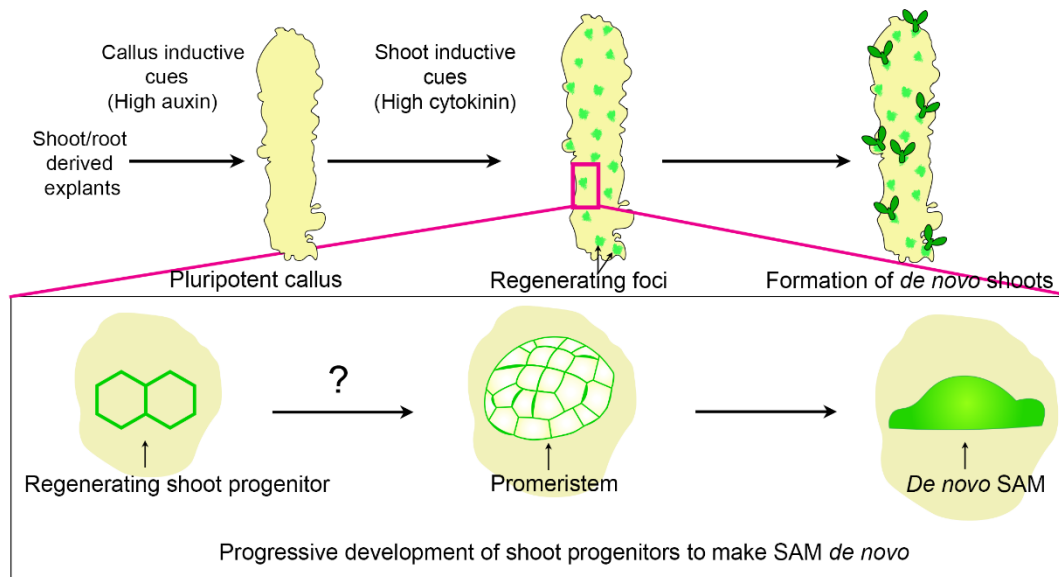


**Figure 5.1 Schematic representation of progressive development of *PIN1* (green) marked shoot progenitor to make *de novo* shoot apical meristem (SAM)**

## 5.2 Materials and Methods

### 5.2.1 Plant materials

*Arabidopsis thaliana* Columbia ecotype was used as a WT for this study. The mutants and transgenic lines used in the study are *cuc2-3*<sup>129</sup>, WT; *R2D2*<sup>160</sup>, WT; *PIN1::PIN1-GFP*, *cuc2-3*; *PIN1::PIN1-GFP* (this study) and WT; *pG1090:XVE::YUC4-YFP* (this study). Transgenic lines were generated by introducing plasmid construct into the C58 *Agrobacterium* strain and transformed into WT or mutant background of *Arabidopsis* by floral-dipping method<sup>131</sup>.

### 5.2.2 Plasmid construction and molecular cloning

The sequence of interest was amplified from total genomic DNA using the CTAB method. Polymerase chain reaction (PCR) was performed with Phusion polymerase (NEB-Biolabs) using specific conditions for each sequence. The amplification was carried out with 10uM sequence-specific paired primers (Table 5.1) using the BIO-RAD C1000 Touch<sup>TM</sup> thermal

cycler. The entry clones were propagated in the DH5 $\alpha$  strain of E.coli using single gateway cloning system. To create the *XTH9::XTH9:vYFP* construct, the 2.3Kb upstream regulatory element of *XTH9* and the 1.176Kb *XTH9* sequence were separately cloned. The yellow fluorescent protein (YFP) sequence was incorporated as a reporter. For *XTH9* knockdown, a 337bp exon sequence was amplified from cDNA using specific primers and inserted into the sense and antisense vectors through the single gateway cloning system. The sense and antisense *XTH9* sequences were cloned under the pG1090 inducible promoter<sup>181</sup> in the pCAMBIA-based R4R3 destination vector. Similarly gYUC4, gIPT5 and gCKX3 were combined with pG1090 and vYFP to make *pG1090::YUC4-YFP*, *pG1090::IPT5-YFP* and *pG1090::CKX3-YFP* respectively. The promoter was cloned in pGEM-TP4P1R, the gene in pGEMteasy221, and the reporter or terminator in pGEMteasyP2RP3<sup>182</sup>. The entry clones were combined in the pCAMBIA3100-based destination vector using the multisite recombination gateway cloning system (Invitrogen).

<b>Primer</b>	<b>Sequence</b>
gYUC4 FP	GGGGACAAGTTTGTACAAAAAAGCAGGCTGTATGGGCACTT GTAGAGA
gYUC4 RP	GGGGACCACTTTGTACAAGAAAGCTGGGTTGGATTTATTGA AATGAAGATGA
gIPT5 FP	GGGGACAAGTTTGTACAAAAAAGCAGGCTGTATGAAGCCAT GCATGACGGCTCTAAGACAAGTG
gIPT5 RP	GGGGACCACTTTGTACAAGAAAGCTGGGTTCCGGGAAATCG CCGCCACGGCGG
gCKX3 FP	GGGGACAAGTTTGTACAAAAAAGCAGGCTGTATGGCGAGTT ATAATCTTCGTTTACAAGTTTCG
gCKX3 RP	GGGGACCACTTTGTACAAGAAAGCTGGGTTACTCGAGTTTA TTTTTTGAAATATATTTTGTCCC
pXTH9 FP	GGGGACAAGTTTGTATAGAAAAGTTGTTTGATTATGGAGAT GCTGATTG
pXTH9 RP	GGGGACTGCTTTTTTTGTACAACTTGTTTTTTTTTTAACTTAT CTCTCTAAATAAATC

gXTH9 FP	GGGGACAAGTTTGTACAAAAAAGCAGGCTGTATGGTCGGTA TGGATTTGTTCAAATGTGT
gXTH9 RP	GGGGACCACTTTGTACAAGAAAGCTGGGTTCAAATGACGAT GATGTTGGCACTCAAGAGG
XTH9 dsRNAi FP	AGTTCTATCTCGAGGGTTGTCTCTTGTGGTGAAGCT
XTH9dsRNAi RP	TACATAATGGATCCCTCTGTTTCCAACCTCCGTTTAC
cXTH9 FP	GGGGACAAGTTTGTACAAAAAAGCAGGCTGTATGGTCGGTA TGGATTTGTTCAAATGTGT
cXTH9 RP	GGGGACCACTTTGTACAAGAAAGCTGGGTTCAAATGACGAT GATGTTGGCACTCAAGAGG

**Table 5.1 Primers used in the study**

### 5.2.3 Plant growth conditions

Please refer Chapter 4, Section 4.2.1 for details.

### 5.2.4 Microscopic live imaging

The Leica M205FA stereo microscope was used to capture bright-field images of *de novo* shoots derived from calli. Confocal laser scanning microscopy was performed using the Zeiss LSM 880 and Leica TCS SP5 II confocal laser-scanning microscopes, following the previously described methods<sup>47,97</sup>. Live imaging of callus tissue was conducted using a 40x water dipping objective, while time-point images of the root were obtained using a 20x air objective. The progenitors were located using a 10x air objective, and images were captured using a 40x water dipping objective.

To perform live imaging of the callus tissue, a small piece of green callus was detached from the explant and placed in a 35 mm sterile petri dish containing SIM media or SIM media supplemented with steroids, using melted agar to fix the sides of the callus onto the SIM media. This ensured that the callus piece remained in place during live imaging using the 40x water dipping objective. The progenitors were tracked until they matured into meristems. Each stage of a progenitor was captured using the same settings as day 1 of progenitor spotting. The stage of the progenitor was determined based on the number of superficial progenitor cells present.

During imaging, the settings used were as follows: 50% laser power of Argon with excitation wavelengths of 488nm (for GFP), 514nm (for YFP), and 561nm (for PI); master gain

set between 600 and 800; pinhole range adjusted between 50 and 200; frame size set to 1,024 by 1,024 pixels; line averaging adjusted to two; and digital zoom set to 0.6. The master gain and pinhole adjustments varied depending on the samples being imaged. Z-stack images were acquired with intervals of either 5 $\mu$ m or 1 $\mu$ m, and autofluorescence was captured at a wavelength of 633nm. Propidium iodide (PI) at a concentration of 20 $\mu$ g/ml, filtered for sterilization, was used to stain the cell walls.

### **5.2.5 Regeneration assay**

The regeneration assay was conducted following the protocol described in the previous study by Kareem et al. (2015). The root explants used in the study were collected from 7-day-old plants, specifically 7 days post-germination (dpg), which were grown on 1/2MS medium containing 2.15g of MS salt, 10g of sucrose, and 0.7% plant-based agar. The explants were initially incubated on callus induction medium (CIM) containing 3.2g of Gamborg B5 salt mixture, 20g of D-Glucose, 0.5g of MES hydrate, 1ml of 1000x Gamborg's vitamin solution, and 0.7% plant-based agar. The hormones used in CIM were 0.5mg/ml of 2,4-D and 0.05mg/ml of kinetin. After an 8-day incubation on CIM, the explants were transferred to shoot induction medium (SIM) and incubated for 30 days. SIM consisted of 4.3g of MS salt, 10g of sucrose, 0.5g of MES hydrate, 1mL of 1000x Gamborg's vitamin solution, 1 $\mu$ g/ml of d-Biotin, and 0.7% plant-based agar. As an external hormonal inductive cue, SIM was supplemented with 10mM trans-zeatin. After the 30-day incubation on SIM, the number of shoots per explant was counted.

### **5.2.6 Estradiol treatment for live imaging and regeneration assay**

SIM was supplemented with Estradiol (5mM) to control gene over-expression or silencing. The progenitors located using confocal based live imaging were treated with liquid SIM supplemented with 5 $\mu$ M Estradiol by direct local application on the progenitors for 20 minutes (short pulse). The transiently treated samples were washed with sterile milliQ post treatment and transferred onto solid SIM supplemented with 5 $\mu$ M estradiol for sustained induction, or solid simply SIM for further incubation. For the regeneration assay 24 hour induction or continuous induction was provided by incubating the callus in estradiol containing SIM. The calli are transferred to SIM without estradiol post induction.

### 5.2.7 PIN1 polarity quantification

The Fiji software's multipoint and angle tools were employed to quantify the polarity of PIN1 from a specific cell membrane region in both productive progenitors and pseudo-progenitors, as described previously<sup>183</sup>. Propidium iodide staining was utilized to identify the cell boundary, and a centroid was calculated using the central mark inside the cell. A connecting line was established between the centroid and a point placed at the top, parallel to the centroid, with the top point designated as the 0° angle point. The Multipoint tool was employed to select pixels from the cell membrane and measure the intensity of localized PIN1-GFP fluorescence. The angles of the multipoint, ranging from 0° to 360°, were used to measure the mean intensity gray values at each multipoint, with the number of multipoints varying depending on the cell wall area. This process was conducted on a total of 94 cells from 6 productive progenitors and 73 cells from 6 pseudo-progenitors, with a subset of Z-stack images selected for PIN1 quantification. The resulting mean intensity grayscale values and corresponding angles were depicted as a scatter plot, and the polarization angle was identified based on peak values in graph.

Additionally, another method was employed to evaluate PIN1 polarity by analysing the arc, curvature of the cell, and protein localization on the membrane using the Blue to Yellow standard LUTs tools in ZEN2.3 SP1 black edition image processing software. Z-stack images of 1µm maximum intensity projection were utilized to examine the polarity orientation within the cell, and the polarity of cells was indicated in the cells. For more details, please refer (Mathew, 2023)<sup>184</sup>.

### 5.2.8 Auxin quantification

To quantify the auxin concentration in the progenitor cells, a single reporter called R2D2 (consisting of RPS5A-driven DII fused to n3xVENUS and RPS5A-driven mDII fused to ntdTomato)<sup>160</sup>. This reporter line was combined with a PIN1 translational fusion construct in the WT plants (WT; *PIN1::PIN1-GFP*). The purpose was to measure the auxin levels in the region of interest (ROI) by analysing the reduction in DII signal (yellow) compared to the red signal fused with mDII. The quantification of auxin accumulation was performed within the circular area of the nucleus in both the progenitor cells and the surrounding non-progenitor cells of productive and pseudo-progenitors.

To measure the intensity of the reporter fluorescence, the maximum intensity projection technique was used to calculate the mean intensity gray value of the reporter fluorescence from

the images. We used Colour Histogram tool in ImageJ/Fiji software to determine the intensity of the reporter fluorescence. The grayscale value of the ROI in mDII-ntdtomato (red signal) and DII-Venus (yellow signal) was calculated for each nucleus within each category. These values were then graphically represented to compare the auxin accumulation in the progenitor cells versus the surrounding cells in productive progenitors, as well as in pseudo-progenitors<sup>95,185</sup>.

### 5.2.9 Statistical analysis

One way ANOVA followed by Tukey HSD post hoc test was used for regeneration assay. Statistical analysis for auxin quantification was performed using Mann-Whitney U test. Kruskal-Wallis one-way ANOVA was used to analyse the quantification of PIN1. R programming was used for all the statistical analysis.

## 5.3 Results

### 5.3.1 Two distinct shoot progenitors are formed in the callus upon shoot inductive cues

When shoot inductive cues are provided to a pluripotent callus, a specific group of cells within the callus respond to these cues and undergo self-organization to give rise to shoot progenitors. The shoot progenitors subsequently develop into shoot meristems. A recent study has demonstrated that shoot progenitors originate from the middle layer of the callus in response to shoot inductive cues<sup>186</sup>. The polar auxin efflux carrier PIN1 serves as a marker for identifying shoot progenitors. Previous studies indicated that PIN1 expression occurs at various stages preceding shoot meristem formation, including the late progenitor or dome-shaped promeristem stages (Figure 5.1)<sup>96,97</sup>. However, limited information was available regarding the early stages of shoot progenitor development. By utilizing a transgenic line expressing PIN1-GFP (WT; *PIN1::PIN1-GFP*), we were able to detect different stages of PIN1-expressing cell clusters within the callus (Figure 5.2A).

To gain insights into the self-organization of progenitor cells leading to shoot meristem formation (Figure 5.1), we employed real-time tracking of the pluripotent callus using the PIN1-GFP marker and confocal-based live imaging. It was observed that early-stage progenitors consisting of 2-10 cells expressing PIN1 were located beneath the surface of the callus (n=34) (Figure 5.2B-C). Additionally, the irregular topology of the callus presented challenges in the real-time detection and tracking of progenitors. We successfully tracked numerous progenitors within the callus and found that PIN1-GFP was detected in the

membranes of 2-4 celled progenitors (n = 29) (Figure 5.2D-H), while progenitors at the 1-cell stage were rarely observed (n = 4) (Figure 5.2I-M).

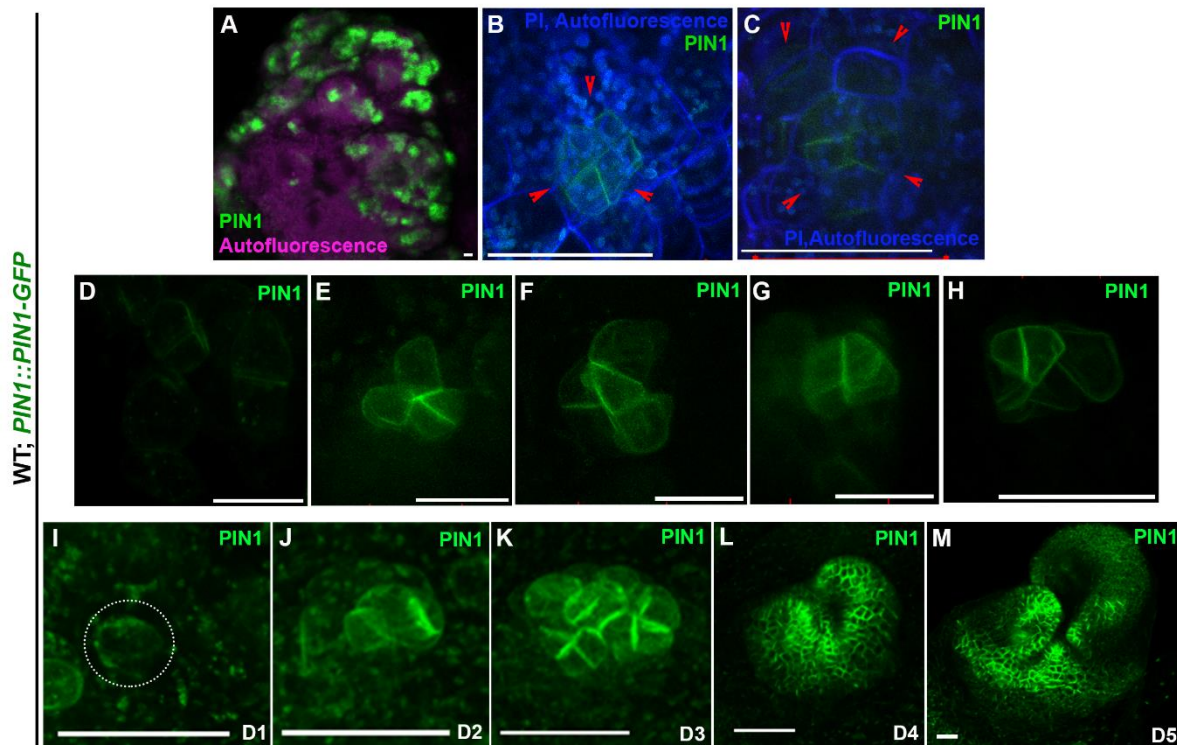


**Figure 5.2 Different stages of PIN1 marked shoot progenitors**

(A) Representative image of callus captured at 10x magnification, reveals several progenitor cells in different stages, marked with PIN1-GFP (green). (B, C) Representative images displaying 2- to 4-celled (B) and 8- to 10-celled (C) progenitor cells marked with PIN1-GFP (indicated by red arrowheads) (n=34). (D-H) Representative images showing 2- to 4-celled progenitor cells marked with PIN1-GFP (green) (n=24). (I-M) Representative real-time live imaging demonstrating the progression of a single progenitor cell into a shoot meristem (n=4). The PIN1-GFP-marked single-celled progenitor is indicated by a white dotted circle (I). In response to shoot-inducing signals, it develops into a functional shoot meristem by day 5 (D5) of progenitor spotting (n=211) (M). In panel A, magenta colour represents chlorophyll autofluorescence, and in images B and C, blue colour represents chlorophyll autofluorescence. Scale bar: 50 $\mu$ m, n: number of progenitors, D: day. WT: wildtype.

We discovered that not all progenitors progress into shoot meristems (Figures 5.1 and 5.2). As we followed the development of these progenitors, we observed two distinct categories based on their fate:

1. Productive progenitors: These are the progenitors that successfully transition into functional shoot meristems (n, number of PIN1-marked foci = 211/287) (Figure 5.3A-C).
2. Pseudo-progenitors: These progenitors fail to complete the transformation into shoot meristems and undergo abortion during the process (n = 76/287) (Figure 5.3D-F).

Upon closer examination, we noticed that productive progenitors exhibit specific morphological characteristics. They consist of a group of small, polygonal-shaped cells with compact arrangement (Figure 5.3A). On the other hand, pseudo-progenitors are comprised of larger, bubble-shaped cells that are loosely packed (Figure 5.3D, E).

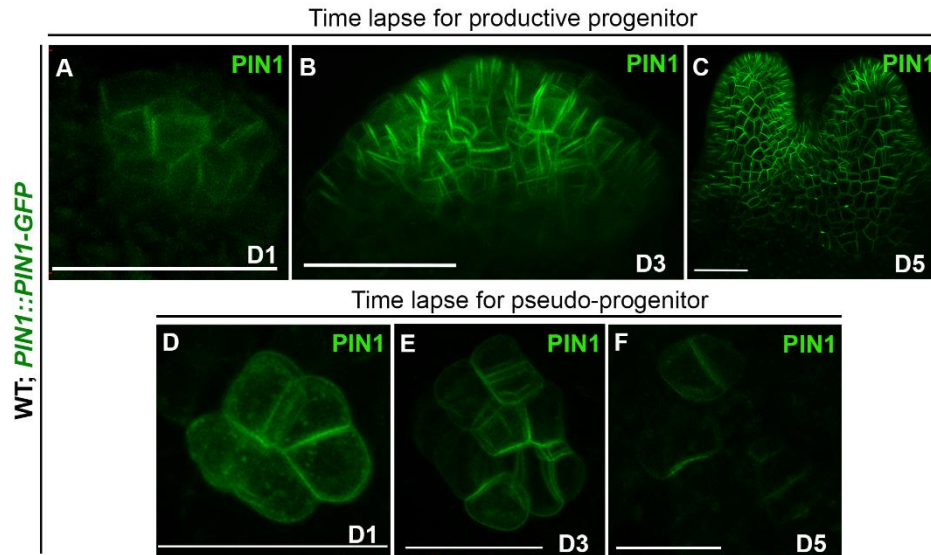


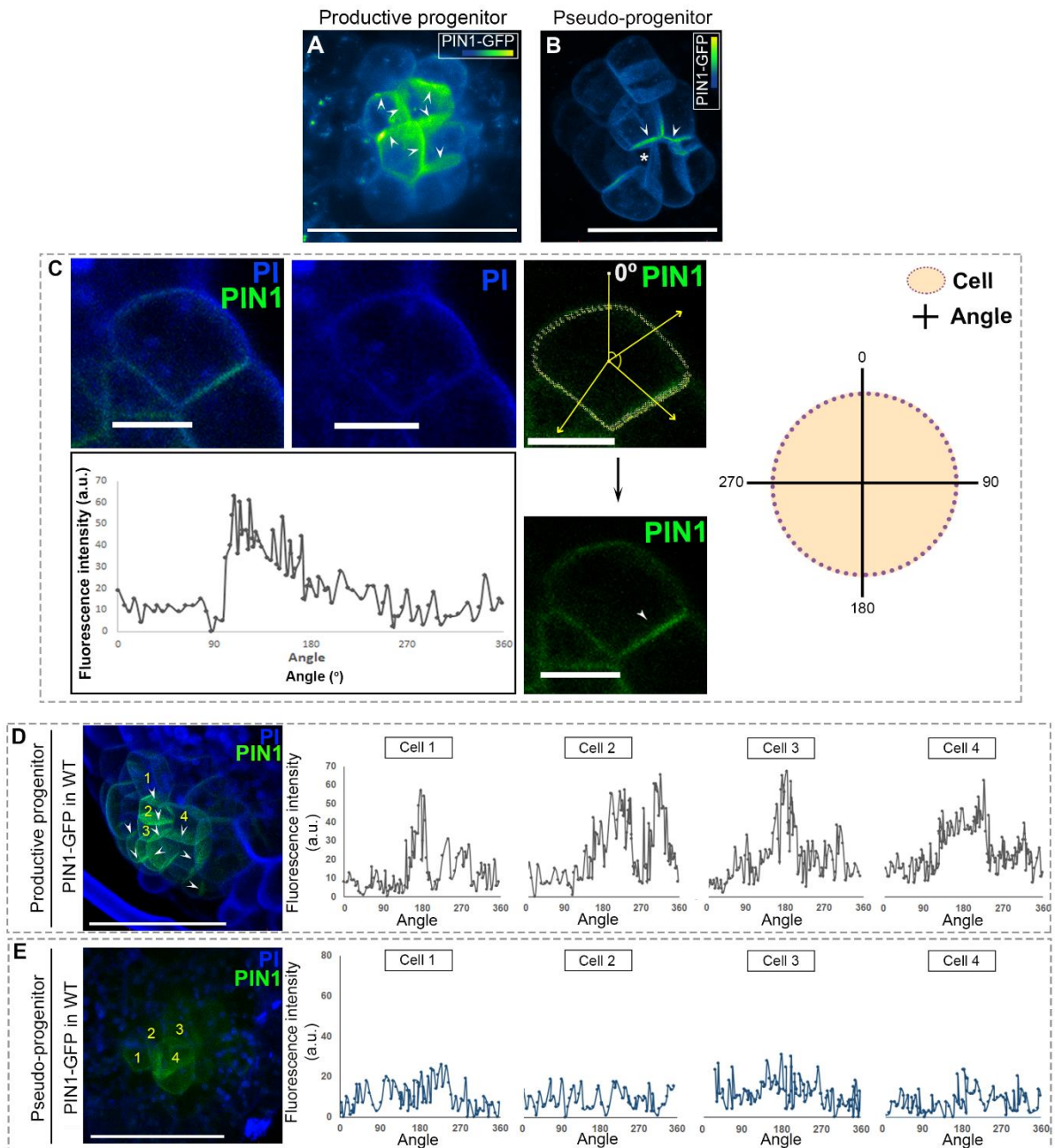
**Figure 5.3 Time lapse for productive and pseudo-productive progenitor**

(A-C) Sequential images captured over time for the development of a productive progenitor. (D-F) Successive images taken at different time points illustrating the development of a pseudo-progenitor. The green colour represents PIN1-GFP expression. Scale bar: 50  $\mu$ m, D: Day. WT: wildtype.

### 5.3.2 The localization pattern of polarity proteins correlates with *de novo* shoot meristem formation.

Apart from the differences in morphology between progenitor and pseudo-progenitor cells, their distinction can also be made based on the localization pattern of PIN1. We conducted both qualitative and quantitative analyses to assess the intensity of PIN1-GFP in these cells (Figure 5.4). In the qualitative approach, we employed a blue-to-yellow gradient pseudo-colour scheme to visualize the PIN1-GFP signal. Blue represented the lowest intensity, while yellow represented the highest intensity of PIN1-GFP. Our observations revealed that productive progenitor cells exhibited high PIN1-GFP intensity with preferential polar localization in each cell, with the polarity oriented towards the neighbouring cells or outside the progenitor. On the other hand, pseudo-progenitors displayed low intensity of PIN1-GFP uniformly distributed in most cells, except for a few cells where the polarity was directed inward within the progenitor (Figure 5.4A, B). To validate the polarity, we employed a quantitative approach where we separately measured the signal intensity on each side of the progenitor cells and plotted them along with their orientation (Figure 5.4C). The intensity of PIN1 expression in the cell

membrane of productive progenitors was found to be higher compared to that of pseudo-progenitors (Figure 5.4D, E). The peak of expression in the graph corresponds to the wall with highest PIN1-GFP expression.



Images by Mabel M M and Anju P S, quantification by Vijina VP and Anju P S

**Figure 5.4 Quantitative and qualitative analysis of PIN1 polarity in productive progenitors and pseudo-progenitors**

(A, B) Images of a representative productive progenitor ( $n = 12$ ) and pseudo-progenitor ( $n = 7$ ) without propidium iodide (PI) staining, displaying the fluorescence intensity of PIN1-GFP. The colour spectrum ranges from blue (low intensity) to yellow (high intensity). The white asterisk indicates the intercellular space. (C) Quantitative method used to assess the fluorescence intensity of PIN1-GFP on the cell membrane and determine the directionality of PIN1 polarization. (D, E) Depicted images of a

productive progenitor and pseudo-progenitor with PI-stained cell walls. The white arrowheads indicate the direction of PIN1-GFP polarization (left). The graph represents the fluorescence intensity of PIN1-GFP along the membrane of annotated cells (1, 2, 3, and 4, marked in yellow). Statistical analysis using the Kruskal-Wallis test showed non-significant differences for productive progenitor cells (ns,  $P = 0.1163$ ) ( $x = 94$  cells) and pseudo-progenitor cells (ns,  $P = 0.1764$ ) ( $x = 73$  cells). However, a significant difference was observed between productive progenitor and pseudo-progenitor cells ( $***P = 0.000$ ), as confirmed by the Kruskal-Wallis test followed by post-hoc Dunn's test. The peak indicates the wall with the highest PIN1-GFP fluorescence (right).  $x$ : number of cells used for analysis. The scale bar corresponds to 50  $\mu\text{m}$ . WT: wildtype.

Through both approaches, we discovered that productive progenitor cells exhibited distinct localization of PIN1-GFP on their membrane. In each cell, there was a noticeable accumulation of PIN1 either away from the progenitor or towards its neighbouring cell (Figure 5.4A, D). Despite variations in the number of cells displaying PIN1 localization either sideward or outward, the overall pattern remained consistent among the productive progenitors we examined. Pseudo progenitor cells ( $n=10$ ), on the other hand, displayed low expression of PIN1-GFP and weak localization on the cell membrane (Figure 5.4B, E). Unlike productive progenitors (Figure 5.4A, D), these cells did not demonstrate a discernible polarization pattern. Eventually, the pseudo progenitors terminated their development before reaching the 15-20 celled stage, as indicated by the disappearance of the PIN1-GFP signal (Figure 5.3D-F). In contrast, the productive progenitors continued to proliferate and formed a promeristem consisting of approximately 100-120 cells (Figure 5.3A, B). Subsequently, they progressed to develop shoots (Figure 5.3C). We were able to distinguish between productive and pseudo-progenitors when they reached a size of 6-15 cells.

### **5.3.3 Specific localization of PIN1 promotes differential pattern of auxin distribution in productive progenitors and its surrounding cells**

Subsequently, we investigated the functional significance of the PIN1 localization pattern during shoot regeneration. As PIN1 is a polar auxin efflux transporter, we hypothesised that the distinct PIN1 localization pattern (Figure 5.4) could generate varying concentrations of auxin between the progenitor cells and the surrounding cells. To test this hypothesis, we utilized an auxin-sensitive marker called DII-Venus mDII-ntdtomato (R2D2)<sup>160</sup> and quantified the levels of auxin within the progenitor cells and the adjacent non-progenitor cells by measuring mDII-ntdtomato / DII-Venus (Figure 5.5, 5.6).

Supporting our proposal, we discovered that the productive progenitors (20-celled) ( $n=25$ ), characterized by the distinct PIN1 localization pattern, exhibited lower levels of auxin compared to their neighbouring cells (Figure 5.5A, C). In contrast, the pseudo-progenitors (12-

15 celled) (n=19) with weak membrane localization of PIN1 displayed auxin levels similar to their neighbouring cells (Figure 5.5B, D). The productive progenitor cells had relatively low auxin level compared to the pseudo progenitor cells (Figure 5.5E). Additionally, we observed auxin accumulation throughout the calli of *pin1-1* or *plt3;plt5-2;plt7* mutants, which failed to express PIN1-GFP. Both these mutants are defective in shoot regeneration<sup>97,187</sup>. These findings indicate a correlation between the PIN1 localization pattern and the abundance of auxin in the progenitors (Figure 5.6).

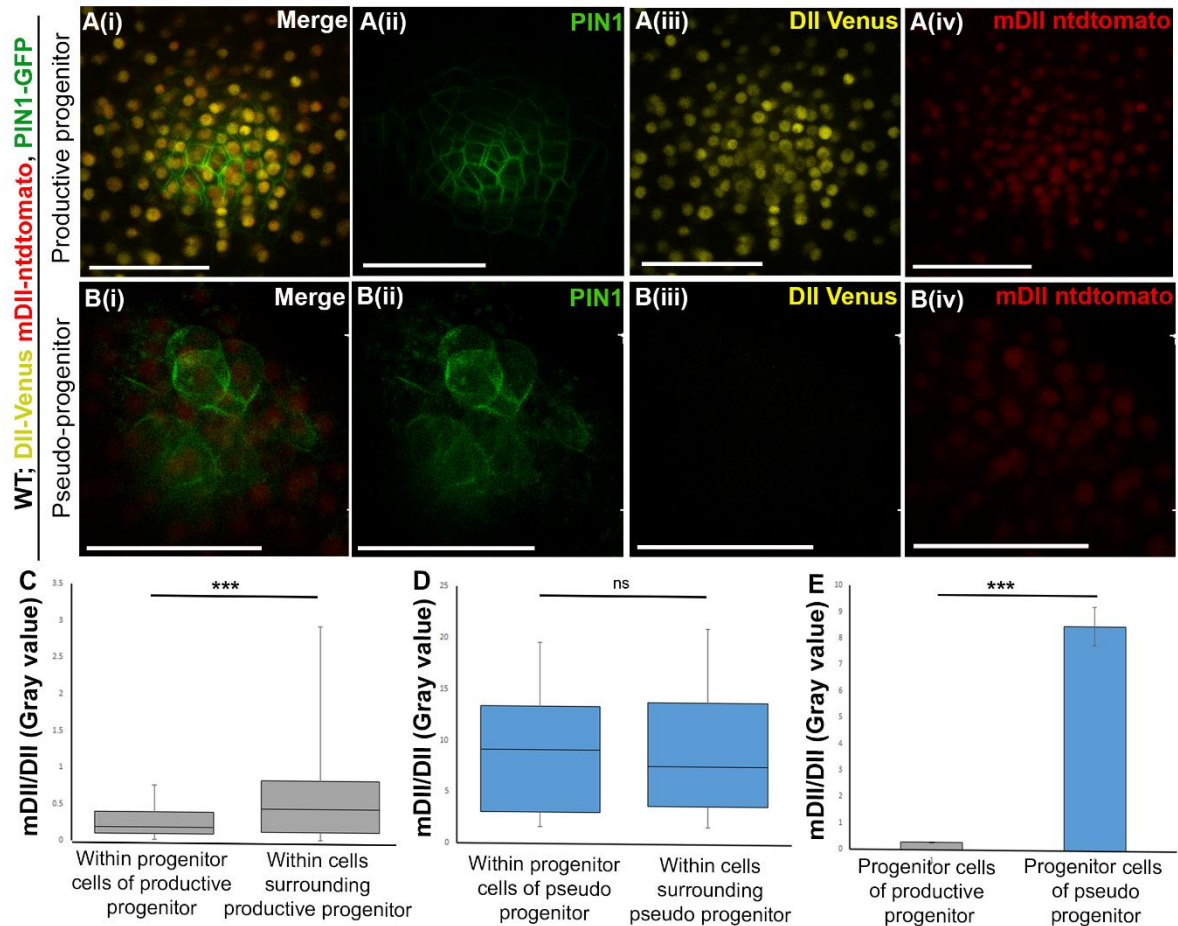


**Figure 5.5 Response of auxin sensor R2D2 in productive and pseudo-progenitor**

(A(i)-B(iv)): Representative images for the expression pattern of DII-Venus mDII-ntdtomato (R2D2) in a productive progenitor and a pseudo-progenitor. The productive progenitor (20-celled) exhibited low auxin levels (n=25) compared to its surrounding cells (A(i)-A(iv)). In contrast, the pseudo-progenitor (15-celled) displayed high and comparable auxin levels to its surrounding cells (B(i)-B(iv)). The merged image (A(i), B(i)) shows the expression patterns of both R2D2 and PIN1-GFP, where the GFP channel specifically highlights the localization of PIN1-GFP (green) in the progenitor (A(ii), B(ii)), the YFP channel represents DII-Venus (yellow) (A(iii), B(iii)), and the RFP channel displays mDII-ntdtomato (red) (A(iv), B(iv)) for DII-Venus mDII-ntdtomato (R2D2). (C) A graph depicting the mDII/DII (R2:D2) ratio, which correlates with lower auxin levels within the PIN1-marked cells of a productive progenitor compared to its surrounding cells (\*\*\* $P=0.000025$ , Mann-Whitney U test). (D) Graph illustrates the mDII/DII (R2:D2) ratio, indicating comparable auxin levels within the PIN1-marked cells of a pseudo-progenitor and its surrounding cells (ns,  $P=0.547264$ , Mann-Whitney

U test). (E) A graph demonstrates the mDII/DII (R2:D2) ratio, indicating lower auxin levels within the PIN1-marked cells of a productive progenitor ( $n=98$ ,  $0.27 \pm 0.021$ ) compared to the PIN1-marked cells of a pseudo-progenitor ( $n=53$ ,  $8.523 \pm 0.734$ ) (\*\* $P=0.0001$ , Unpaired t test). Scale bar: 50  $\mu\text{m}$ . WT: wildtype.

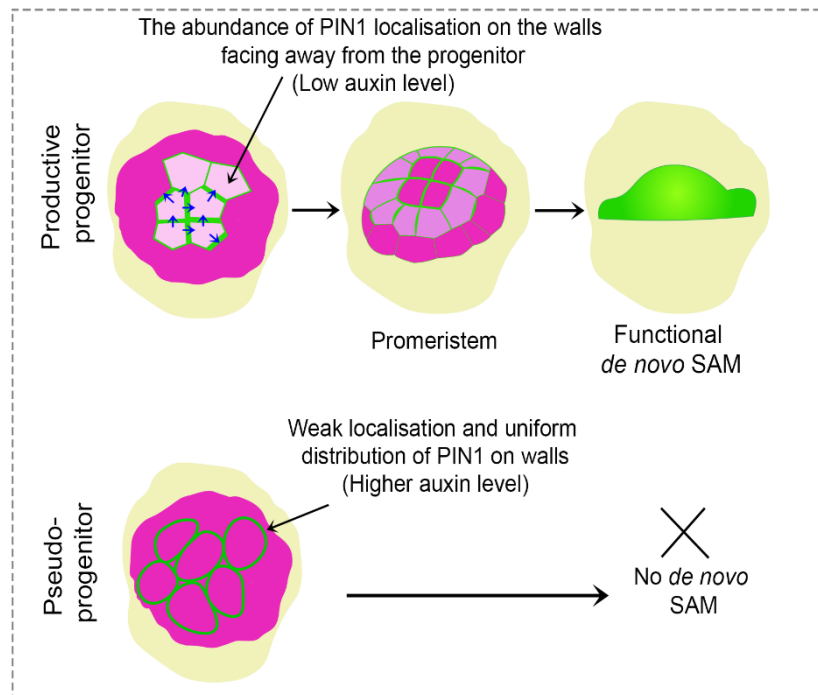


**Figure 5.6 Schematic representation of the role of PIN1 localization pattern in regulating auxin distribution during *de novo* shoot regeneration**

The diagram illustrates the auxin distribution pattern in productive and pseudo-productive progenitors. The pattern of localization of PIN1 onto the cell membrane generates a region of low auxin concentration in the progenitor cells. In contrast, the pseudo-progenitors, which has weak and uniform distribution of PIN1, exhibit high accumulation of auxin. Magenta colour represents auxin, green represent PIN1 and Blue arrow marks direction of PIN1 polarity. Pale yellow colour represents callus.

### 5.3.4 Excess of auxin in the callus impairs *de novo* shoot regeneration

To validate our observations, we conducted experiments to observe the effects of excess auxin in the callus. We employed a transgenic line with *pG1090:XVE::YUC4-vYFP*, to overexpress the auxin biosynthesis gene *YUC4*. We chose different time points for the overexpression based on the first shoot formed in the callus. The first shoot emerges around the 8<sup>th</sup> to 10<sup>th</sup> day of incubating the callus on SIM. So we decided to induce the callus with estradiol to overexpress on 1<sup>st</sup>, 3<sup>rd</sup>, 5<sup>th</sup>, 8<sup>th</sup> day and continuously for 30 days on SIM. The callus was induced for 24 hours in estradiol containing SIM.

Upon overexpression, we observed a significant reduction in shoot formation across all treatment conditions (Figure 5.7). Shoot formation was reduced to 13% when the level of auxin was increased during the initial days of SIM incubation (Figure 5.7A, B, G). Shoot formation

was further reduced on subsequent days of treatment. Continuous or later-stage induction of auxin completely abolished shoot formation on SIM (Figure 5.7). The relatively higher number of shoots observed in the initial treatment can be attributed to the callus tissue recovering from the rapid increase in auxin levels during the course of SIM incubation. However, the absence of shoot formation upon continuous overexpression of auxin indicates that a high concentration of auxin hinders successful *de novo* shoot formation. This is likely because the development of a shoot meristem requires a local minimum of auxin, as observed during normal shoot meristem development<sup>188</sup>. An elevated amount of auxin throughout the explant inhibits the formation of these local auxin minima, leading to the failure to form shoots. Interestingly, all induced explants produced roots during SIM incubation. The formation of roots in response to *YUC4* overexpression could be attributed to the pre-existing root identity of the callus, which is further enhanced by the enrichment of auxin.

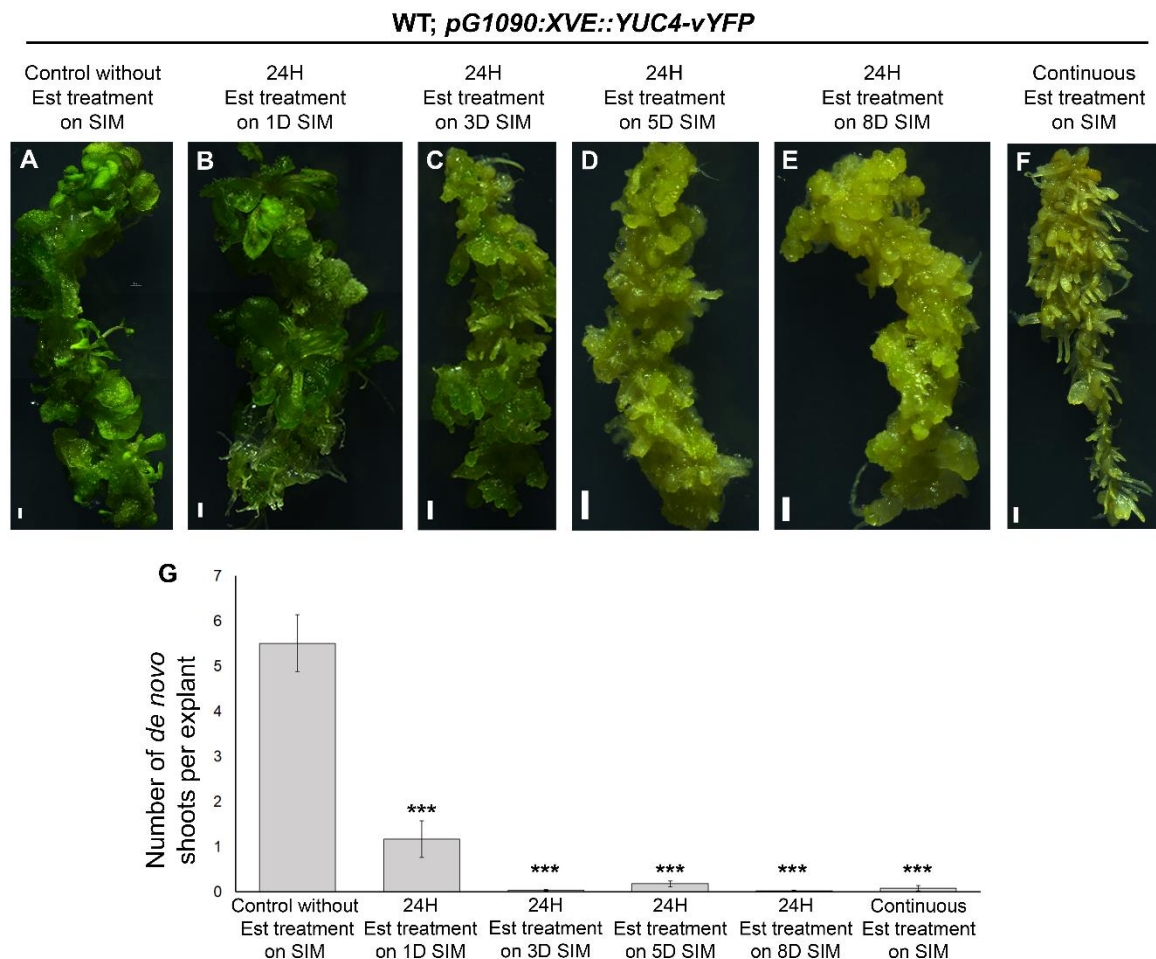


**Figure 5.7 Overexpression of auxin biosynthesis gene *YUC4* in the callus can abolish *de novo* shoot regeneration**

(A-F) Regeneration assay with estradiol inducible *G1090:XVE::YUC4-vYFP* in WT. Representative stereo images of callus on 30<sup>th</sup> Day of SIM incubation. (A) Control without estradiol treatment during SIM incubation. (B-F) *YUC4* overexpression was induced with estradiol for 24H on 1<sup>st</sup> day (B), 3<sup>rd</sup> day

(C), 5<sup>th</sup> day (D), 8<sup>th</sup> day (E) and continuous (F) estradiol treatment from 1<sup>st</sup> to 30<sup>th</sup> day of SIM incubation. (G) Graphical representation of the shoot regeneration assay. There was a significant reduction of shoot regeneration efficiency upon YUC4 overexpression. Statistical test used: One way ANOVA (F value = 328.668399,  $P$ -value =  $4.44089 \times 10^{-16}$ ) followed by Tukey HSD post hoc test ((Control vs 1D, Control vs 3D, Control vs 5D, Control vs 8D and Control vs continuous,  $P$ -value =  $1.17 \times 10^{-10}$ ), 2D vs 3D,  $P$ -value = 0.008796; 2D vs 5D,  $P$ -value = 0.02872; 2D vs 8D,  $P$ -value = 0.007457; 2D vs continuous,  $P$ -value = 0.02974; 3D vs 5D,  $P$ -value = 0.9905; 3D vs 8D,  $P$ -value = 1; 3D vs continuous,  $P$ -value = 0.9999; 5D vs 8D,  $P$ -value = 0.9835; 5D vs continuous,  $P$ -value = 0.9997; 8D vs continuous,  $P$ -value = 0.9997), Error bar represents s.e.m. WT: Wildtype, Scale bar: 1mm, H: hour, D: day.

### 5.3.5 CUC2 is required for the maintenance of PIN1 polarity in shoot progenitors

In Chapter 3, we established the significance of the PLT-CUC2 regulatory module in maintaining PIN1 cell polarity during vascular regeneration. We investigated whether this module is also functional in polarity maintenance during *de novo* shoot regeneration. Previous studies demonstrated that the *plt3;plt5-2;plt7* mutant, which fails to express PIN1, is unable to form shoot progenitors or develop shoots<sup>97</sup>. Therefore, we focused on *CUC2*, a shoot-promoting factor important for *de novo* shoot regeneration<sup>97</sup>. Furthermore, *CUC2* is known to be involved in PIN1 polarity convergence during leaf serration formation. In this context, *CUC2* is required for correct PIN1 polarization, and it can influence PIN1-dependent auxin activity<sup>139,189</sup>.

To explore the pattern of PIN1 localization in the progenitors of *cuc2* mutant, we utilized a PIN1 translational reporter line in the *cuc2-3* mutant. The pattern of PIN1 expression in the progenitor of *cuc2-3* mutant was similar to that of a pseudo progenitor in WT. PIN1 expression appeared hazy in the cytoplasm of progenitor cells. There was weak localization on the cell membrane and polarization was rarely observed in the cells, unlike the distinct pattern of polarization in productive progenitor cells in WT (Figure 5.8A, B). In addition to the defective PIN1 localization in the progenitor cells, we observed that there is a decline in the number of progenitors formed in the mutant callus (Figure 5.8C). The *cuc2-3* mutant displayed significant reduction in the shoot regeneration efficiency compared to WT<sup>187</sup>. These results highlight the importance of *CUC2* in maintaining PIN1 polarity for the successful conversion of shoot progenitor to shoot meristem.

Furthermore, *CUC2* expression was detectable in the immediate neighbouring cells of productive progenitors, specifically excluding the progenitor cells expressing PIN1<sup>187</sup>. This observation suggests that *CUC2* may be involved in regulating PIN1 polarity in a non-cell autonomous manner, facilitating the progression of progenitors. The disrupted PIN1 polarity in the progenitor cells of the *cuc2-3* mutant, along with the distribution pattern of *CUC2* expression in the regenerating callus of WT, supports the hypothesis that *CUC2* plays a non-

cell autonomous role in the regulation of PIN1 polarity during progenitor development.

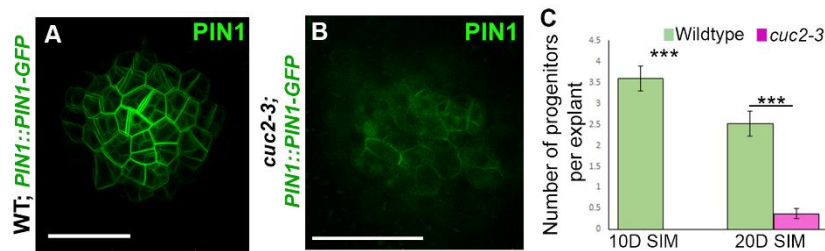


**Figure 5.8 CUC2 influence maintenance of PIN1 polarity in shoot progenitors**

(A, B) The expression of PIN1-GFP (green) in shoot progenitors in WT (A) and *cuc2-3* mutant (B) background. (C) Graphical representation comparing the formation of progenitors in the WT and *cuc2-3* mutant on the 10<sup>th</sup> and 20<sup>th</sup> days of SIM incubation. Welch two-sample *t*-test was used to check statistical significance. For the 10<sup>th</sup> Day: WT [n = 112, 3.6 ± 0.2905], *cuc2-3* [n = 216, 0 ± 0], \*\*\**P* = 1.009x10<sup>-8</sup>. For the 20<sup>th</sup> Day: WT [n = 92, 2.521739 ± 0.300264], *cuc2-3* [n = 114, 0.372093 ± 0.118187], \*\*\**P* = 6.248x10<sup>-5</sup>. WT: Wildtype, n: sample number, Scale bar: 50 μm.

### 5.3.6 CUC2 regulates *XTH9* for maintaining PIN1 polarity in progenitors

In order to understand the factors influencing the localization of PIN1 in regenerating progenitors, we conducted a comparative-transcriptome analysis. We compared transgenic lines that were capable of producing progenitors but incapable of progressing into a shoot meristem, lines that produced progenitors capable of progressing into a functional shoot meristem, and lines that generated an increased number of progenitors capable of forming meristems. Through this analysis and subsequent validations, we discovered that CUC2 regulates the expression of *XTH9* (done by Vijina VP)<sup>187</sup>.

Further, we examined the PIN1 expression pattern in the progenitors formed in *xth9* mutant compared to the progenitors in WT. The productive progenitors in the WT callus maintained their PIN1 localization pattern and progressed into shoot. However, the progenitors in the *xth9* were similar to pseudo progenitors in WT. These progenitor cells showed delocalized and reduced PIN1 expression and were unable to progress to a shoot meristem (done by Mabel M.M.). Moreover, the *xth9* mutants showed a reduction in regeneration efficiency<sup>187</sup>.

### 5.3.7 *XTH9* shows differential expression patterns in productive and pseudo progenitors

We were surprised by the influence of *XTH9* on *de novo* shoot regeneration, as its known role is to promote cell expansion and loosening, which would be expected to favour the formation of pseudo progenitors. To elucidate this contradiction, we closely monitored the spatio-temporal pattern of *XTH9* expression. For visualization, we utilized a transgenic reporter line containing the *XTH9::XTH9-vYFP* (*XTH9*-YFP) construct and the *PIN1::PIN1-*

*GFP* (PIN1-GFP) construct to track the expression pattern of XTH9 in progenitors.

Remarkably, the XTH9-YFP expression was not detected within the PIN1-GFP marked cells of productive progenitors. Instead, it exhibited robust expression in the neighbouring non-progenitor cells, like a shell encapsulating the progenitor (Figure 5.9 A–K). This distinct expression pattern was particularly prominent during the initial stages of progenitor development when the progenitor consisted of 5 to 10 cells. At this stage, a layer of XTH9-YFP expressing cells covered the surface of the progenitor (Figure 5.9 A-C, G, H, J, K). Upon examining deeper optical sections within the callus, the expression of XTH9 formed a ring-like pattern surrounding the PIN1-GFP marked progenitor (Figure 5.9 G(iv), G(v), H(iv), H(v), I(iv), and I(v)). As the progenitor progressed and increased in cell number (15–70 cells), the PIN1-GFP marked progenitor cells emerged from beneath the overlaying cells, while XTH9-YFP expression became confined to the immediate vicinity of the progenitor, also in a ring-like fashion (Figure 5.9A, D, and E). In the formation of a mature shoot, XTH9-YFP was observed along the periphery of the meristem and at the base of emerging leaf primordia. Notably, it remained undetectable in the centre of the meristem (Figure 5.9F).

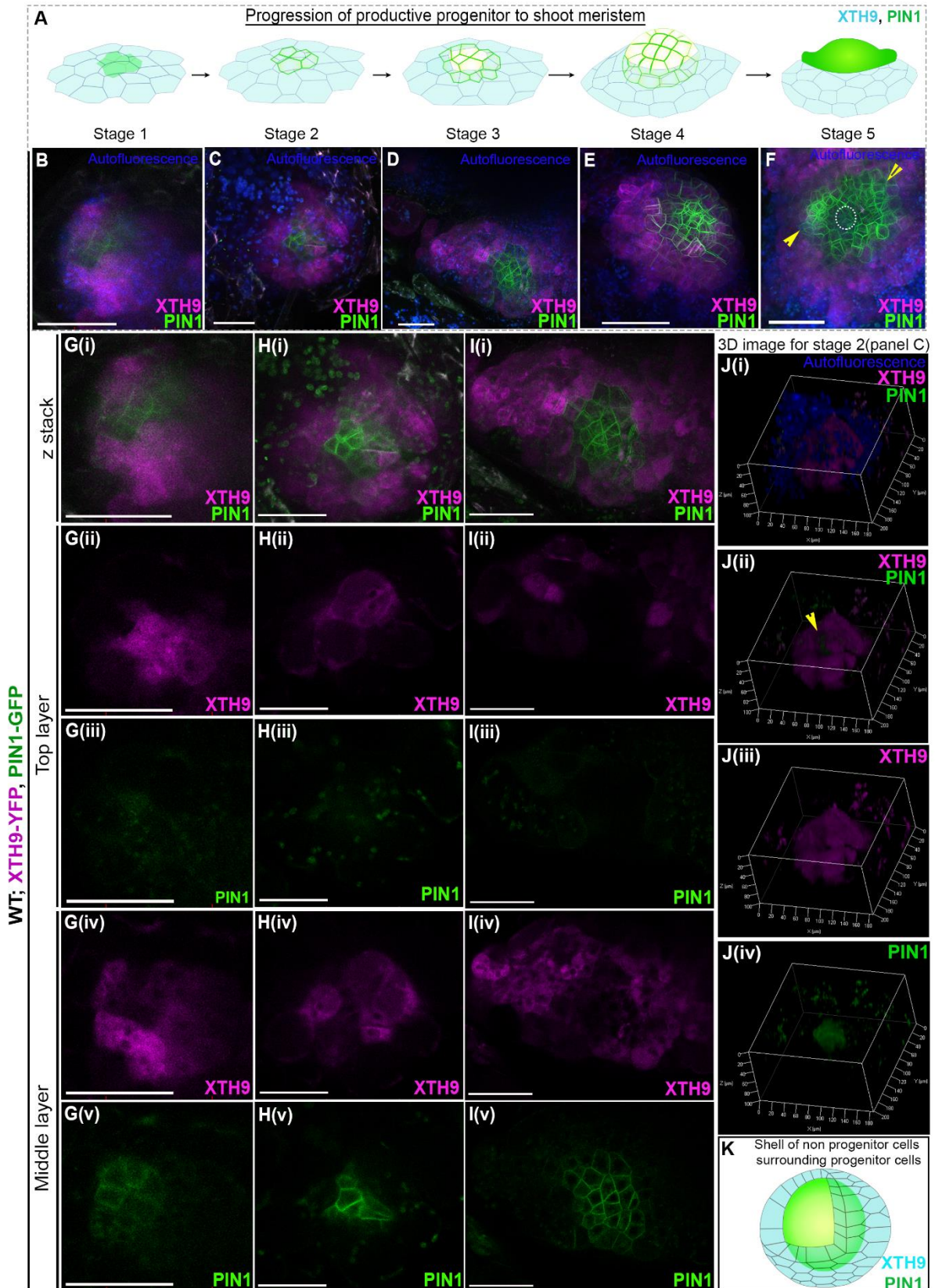


**Figure 5.9 Expression pattern of XTH9 in productive progenitors**

(A) Schematic representation of different stages of progression of productive progenitors into shoot. Light blue colour represents XTH9 expression and green represents PIN1. (B-F) Representative

confocal images of different stages of progenitor to shoot conversion. Yellow arrowhead in F marks emerging leaf primordia. Magenta: XTH9 expression, Green: PIN1 expression, Dark blue: autofluorescence. (G (i)-(v)) z stack, top layer and middle layer images of Stage 1 progenitor with XTH9 expression. (H(i)-(v)) z stack, top layer and middle layer images of Stage 2 progenitor with XTH9 expression. (I (i)-(v)) z stack, top layer and middle layer images of Stage 3 progenitor with XTH9 expression. (J (i)-(iv)) 3D representation of stage 2 progenitor. (K) Schematic representation of productive progenitor with shell of XTH9 expression in the surrounding cells. Green puncta in H(i), H(iii) and H(v) GFP is bleed-through from chlorophyll autofluorescence. Scale bar: 50µm. WT: wildtype.

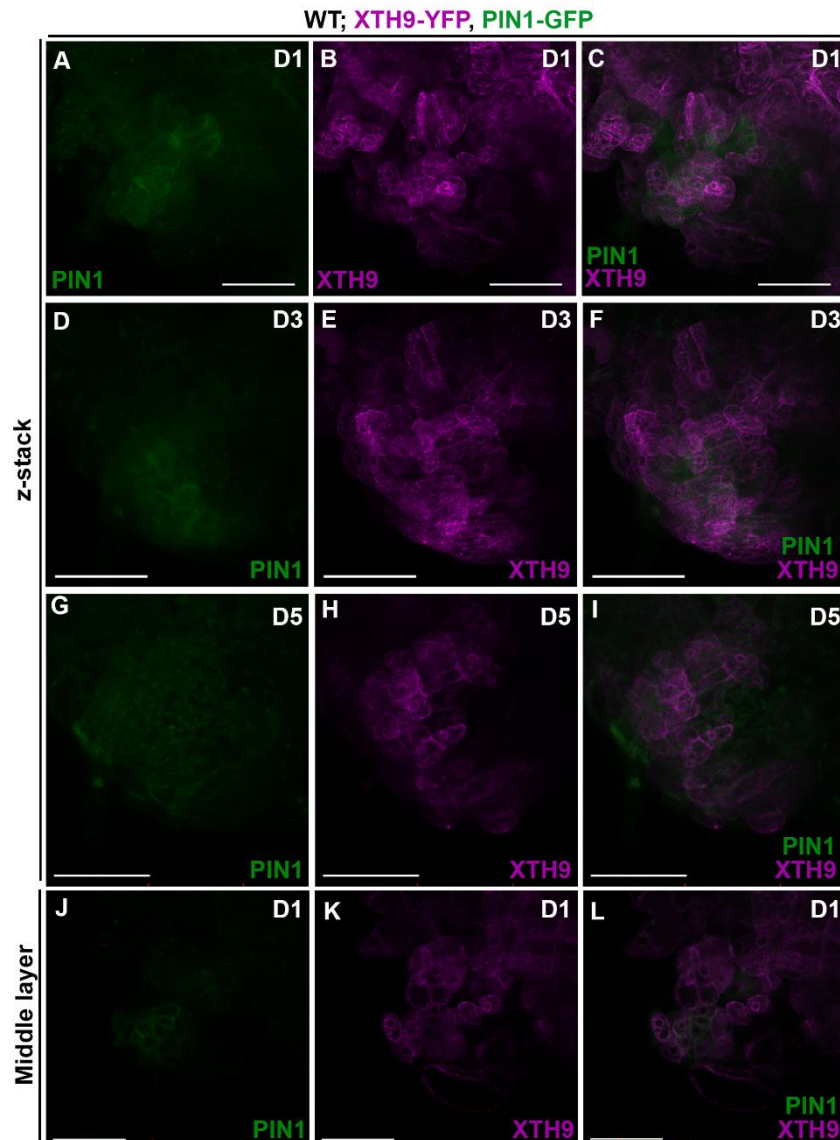


**Figure 5.10 Expression pattern of XTH9 in pseudo progenitors**

(A-I) Time lapse imaging of pseudo progenitor development. (J-L) Middle layer of progenitor at D1. XTH9 expression is present inside the PIN1 expressing progenitor cells as well as surrounding non progenitor cells. XTH9: magenta, PIN1: green. D: Day, Scale bar: 50µm. WT: wildtype.

In contrast to productive progenitors, pseudo progenitors showed a distinct pattern where XTH9-YFP and PIN1-YFP did not have mutually exclusive domains. Instead, XTH9 exhibited abundant expression within the cells marked by PIN1, specifically in pseudo

progenitors consisting of 10 to 12 cells (n = 20) (Figure 5.10). These pseudo progenitors were ultimately aborted, as evidenced by the disappearance of PIN1-GFP expression (Figure 5.10). Hence, while XTH9 expression in non-progenitor cells promoted the growth of progenitors, its presence within the progenitor cells had the opposite effect, contributing to their failure to progress and ultimately resulting in their abortion.

### **5.3.8 XTH9 regulates PIN1 polarity non cell autonomously in productive progenitors**

To further investigate the physiological significance of the XTH9 expression pattern, we conducted experiments to assess the impact of altering XTH9 function on the progression of progenitors into meristems. Through the inducible downregulation of XTH9 (WT; *pG1090:XVE::XTH9-dsRNAi*) in the callus either throughout the incubation on shoot induction medium (SIM) or transiently during the onset of progenitor formation, we observed a severe reduction in shoot regeneration<sup>187</sup>.

Interestingly, even a brief 20-minute pulse of transient XTH9 downregulation at approximately 6-celled or 15-celled progenitor stages resulted in the complete abolition of their progression (n = 26) (Figure 5.11A-G). However, late-stage progenitors consisting of 25 or more cells or promeristems were still capable of progressing into meristems despite XTH9 downregulation (Figure 5.11H-K). These findings clearly demonstrate the crucial role of XTH9 during the early stages of progenitor development, highlighting its necessity for the progression of progenitors into functional meristems.

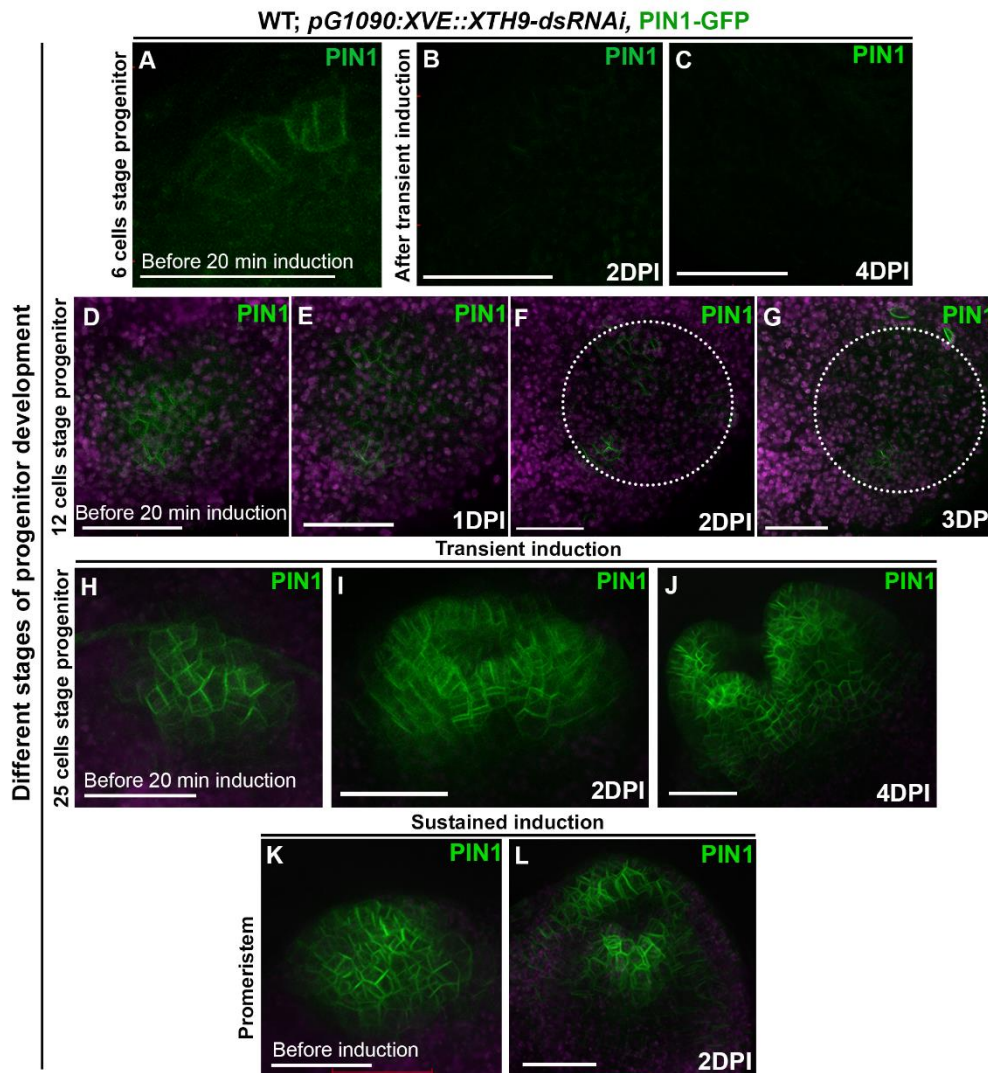


**Figure 5.11 Downregulation of XTH9 affect PIN1 polarity and progenitor development**

(A-C) Transient downregulation of XTH9 in 6 cell stage progenitor through inducible RNAi line WT; *pG1090:XVE::XTH9-dsRNAi*. PIN1 expression (green) was lost in response to induction for 20 minutes and progenitor development was aborted. (D-E) Transient downregulation of XTH9 in 12-celled productive progenitor. The progenitor progression was aborted. Magenta colour represents chlorophyll autofluorescence. Scale bar: 50  $\mu$ m, DPI: day post induction. WT: wildtype.

The inducible overexpression of XTH9 (WT; *pG1090:XVE::XTH9-vYFP*) during the onset of progenitors in SIM callus abolished the regeneration of shoots<sup>187</sup>. However, transient overexpression of XTH9 did not completely impede their progression. Instead, it caused a temporary delocalization of PIN1 and delay in the progression of progenitors to shoot for two days (Figure 5.12A, B). Subsequently, PIN1 localization returned to the cell membrane, and the progenitor cells resumed their development into a mature meristem by the 7<sup>th</sup> day after the induction (Figure 5.12A-H). This demonstrates that the XTH9 activity can be reversed, emphasizing the importance of precise timing and location of XTH9 expression in controlling the pattern of PIN1 localization during the formation of shoot meristems.

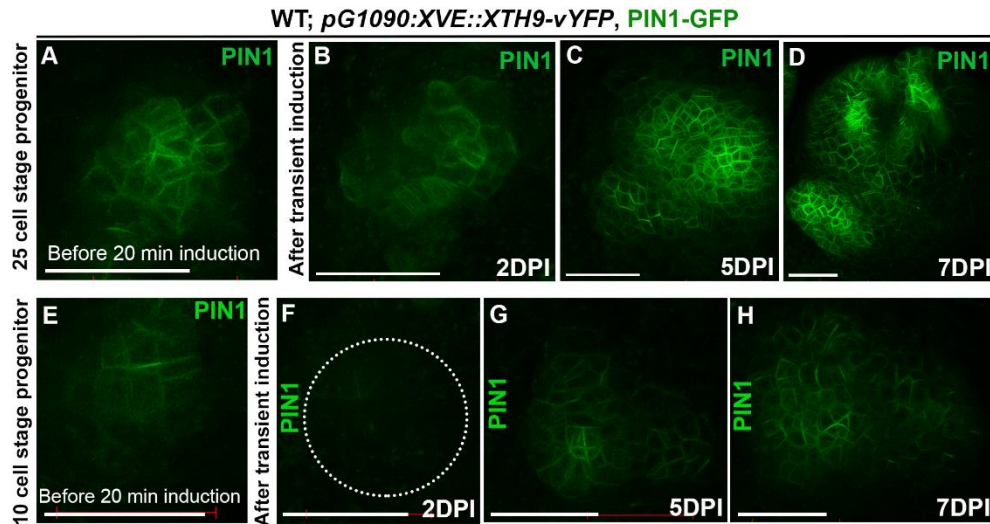


**Figure 5.12 Overexpression of XTH9 affect PIN1 polarity and progenitor development**

(A-D) Transient overexpression of XTH9 using estradiol inducible WT; *pG1090: XVE::XTH9-vYFP* in 25 cell progenitor. Upon induction, PIN1 was delocalized and it regains its membrane localization in subsequent days after the removal of estradiol induction. (E-H) Time-lapse imaging of 10 cell stage progenitor upon transient XTH9 overexpression. DPI: days post induction. Scale bar: 50 $\mu$ m. WT: wildtype.

### 5.3.9 Influence of cytokinin in *de novo* shoot regeneration

The *XTH9-CUC2* axis for *de novo* shoot formation is activated upon external hormonal inductive cues. The plant hormone cytokinin is a major component used in shoot induction medium for *de novo* shoot regeneration. We checked the influence of cytokinin levels during different stages of *de novo* shoot meristem formation. Towards this, we overexpressed cytokinin biosynthesis gene *IPT5* (*ISOPENTENYLTRANSFERASE 5*) and degradation gene *CKX3* (*CYTOKININ OXIDASE 3*) on 1<sup>st</sup>, 3<sup>rd</sup>, 5<sup>th</sup> and 8<sup>th</sup> day of incubation of callus on SIM along with continuous and control (mock) treatments. For this, we used estradiol inducible overexpression lines of cytokinin biosynthesis gene *IPT5* and cytokinin degradation gene *CKX3*.

The overexpression of cytokinin biosynthesis gene *IPT5* during the initial stages of SIM treatment resulted in a decrease in regeneration efficiency. However, when *IPT5* overexpression was induced during later stages and maintained continuously, it led to an enhancement in shoot formation (Figure 5.13A-G). This indicates that cytokinin is required during the later stages of *de novo* shoot development, consistent with its role in normal shoot development in plants. However, an excess of cytokinin inhibits the early stages of *de novo* shoot formation.

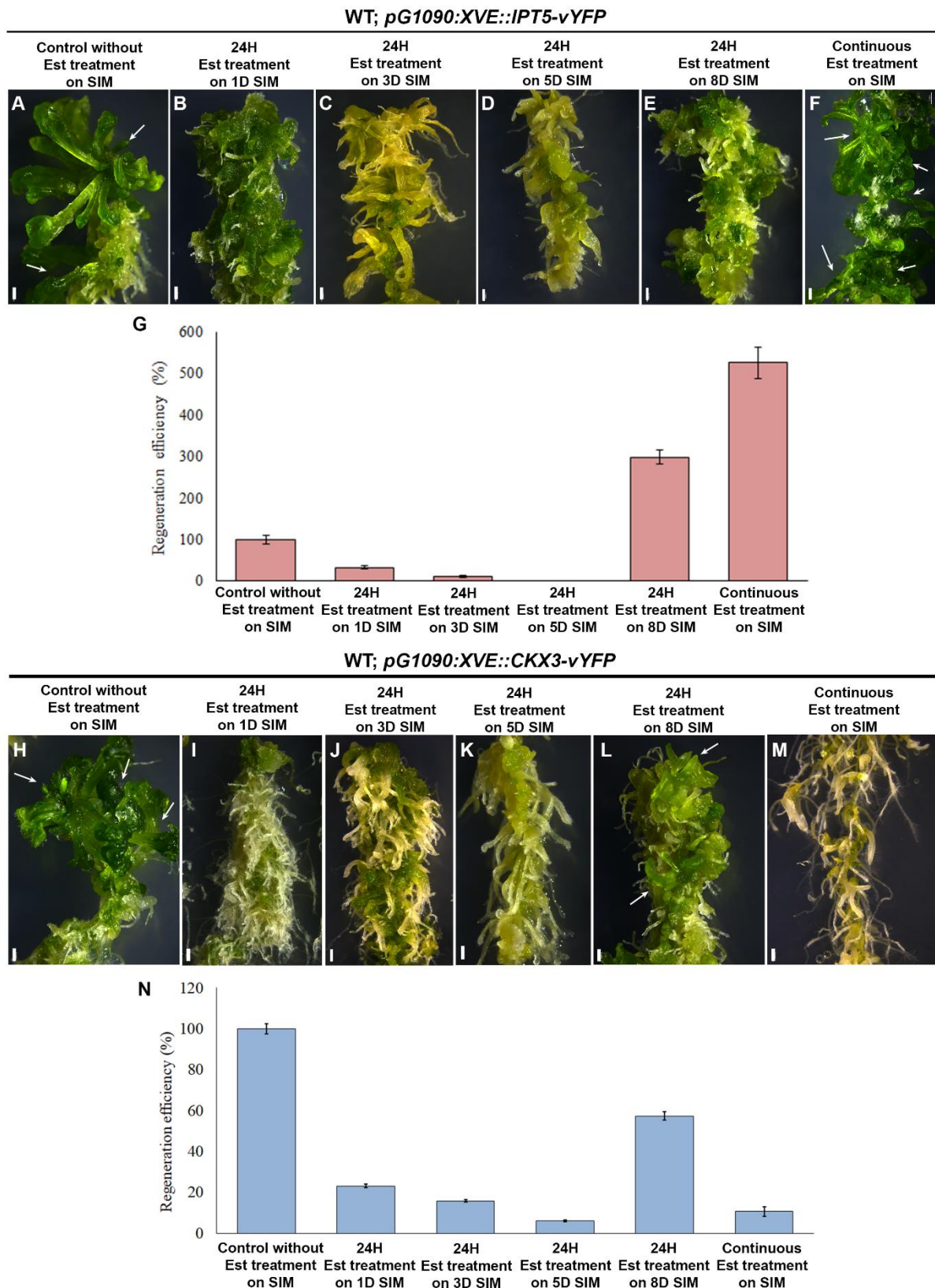


**Figure 5.13 Effect of modulation of cytokinin levels on de novo shoot regeneration (preliminary data)**

(A-G) Overexpression of cytokinin biosynthesis gene using the biosynthesis gene IPT5 in wildtype (WT; *pG1090:XVE::IPT5-vYFP*). The treatments are 24H induction on D1, D3, D5, D8 and continuous

overexpression on callus incubated on SIM. (A-F) Representative stereo images of callus on 30<sup>th</sup> day of incubation on SIM for different treatments. Graph representing regeneration efficiency for different treatments in comparison to uninduced control (preliminary data). (H-N) Overexpression of cytokinin degradation gene CKX3 at different time points of SIM incubation (WT; *pG1090:XVE::IPT5-vYFP*). (H-M) Representative images of callus after each treatment. (N) Graphical representation of shoot regeneration assay (preliminary data). White arrows mark *de novo* shoot. Error bars represent standard deviation. Scale bar: 1mm, D = Day, WT: wildtype.

In the regeneration assay using the overexpression of the cytokinin degradation gene CKX3, an excessive rooting response was observed in the explants (Figure 5.13H-I). This excessive rooting may be attributed to an imbalance in the ratio of auxin and cytokinin resulting from cytokinin degradation. The reduction in shoot regeneration is more noticeable during the initial days of SIM treatment, which aligns with the findings from the regeneration assay involving IPT5 overexpression. These observations suggest that both excessively high and low concentrations of cytokinin can have negative effects during the initiation of regeneration. However, once the cells have committed to the newly acquired shoot fate, a reduction in cytokinin level does not halt shoot regeneration. On the other hand, an increase in cytokinin levels can enhance shoot regeneration by ensuring the completion of shoot development. These results imply that a balanced level of cytokinin during the progenitor onset is essential for regeneration (Figure 5.13). It would be interesting to explore how endogenous cytokinin influence activation of *CUC2-XTH9* axis for PIN1 marked progenitor formation for *de novo* shoot regeneration.

## 5.4 Discussion

Regeneration is a crucial process for the growth and survival of organisms. Plants, with their totipotent nature, serve as an excellent system for studying regeneration. Tissue culture-mediated regeneration takes advantage of the totipotency of plant cells, allowing researchers to investigate the development of organ systems from cells lacking positional information. In this study, the emergence of shoots from callus was found to be asynchronous, with shoot progenitors arising at different locations and stages within the callus. Through live imaging, two types of progenitors were identified: productive and pseudo progenitors. Productive progenitors could develop into shoot meristems, while pseudo progenitors were unable to do so. The distribution of PIN1, involved in auxin efflux transport, differed between productive and pseudo progenitors. Productive progenitors exhibited polar localization of PIN1, whereas pseudo progenitors had non-polar distribution. Furthermore, productive progenitors maintained a lower level of auxin compared to surrounding cells, while pseudo progenitors had high auxin levels in both progenitor and surrounding cells. This suggested that the polar orientation of

PIN1 in productive progenitors facilitated the pumping of auxin outside the progenitor cells, maintaining a minimum auxin level necessary for shoot initiation. The study also demonstrated that shoot progenitors require a local minimum of auxin for successful conversion into shoots. Disruption of auxin minimum formation, as confirmed by ectopic overexpression of the auxin biosynthesis gene *YUC4*, resulted in the inhibition of shoot regeneration. These findings highlight the importance of cell polarity and auxin distribution in *de novo* shoot meristem regeneration, emphasizing the need for auxin minimum foci for progenitor formation and outgrowth. The study underscores cell polarity as a critical factor in the self-organization of shoot meristem from a heterogeneous population of cells.

We found that the shoot promoting factor, *CUC2* influences cell polarity non cell autonomously by regulating the expression of *XTH9*, a gene involved in cell wall loosening. Manipulating *XTH9* expression affects PIN1 localization and the progression of progenitors. Precise timing and location of *XTH9* expression are crucial for controlling PIN1 localization and successful shoot meristem formation. These findings shed light on the regulatory mechanisms involved in PIN1 polarity maintenance during shoot regeneration and provide insights into molecular factors governing the process.

The morphology of productive and pseudo progenitor cells differs, with productive progenitors displaying smaller, tightly packed polygonal cells, while pseudo progenitors have larger, loosely packed circular cells. This raises questions about the impact of cell morphology on organ development and its relationship with cell polarity.

Further investigations revealed that cell mechanics play a critical role in progenitor development. There was a clear distinction in cell geometry between the progenitor cells expressing PIN1 and their neighbouring non-progenitor cells. Progenitor cells were smaller in size and divided more frequently than the adjacent non progenitor cells. Progenitor cells exhibited isodiametric growth, while the surrounding cells expanded tangentially. The expansion of the neighbouring cells could be explained by the unique expression pattern of a cell wall loosening enzyme called *XTH9*, which formed a shell around the PIN1-expressing progenitor cells. The non-uniform cell division and differential growth pattern creates a push and pull and thereby creates a mechanical conflict between progenitor and non-progenitor cells. The pattern of microtubule distribution in the progenitor and surrounding cells is an evidence for mechanical conflict. In other words, to maintain geometry of cells for shoot meristem emergence, necessary mechanical stress need to be maintained between progenitor vs non progenitor cells. It is evident by distribution of cell wall loosening enzyme *XTH9*, distinct

growth rate, and microtubule orientation pattern in the progenitor and neighbouring non progenitor cells<sup>187</sup>.

The results indicated a feedback mechanism between PIN1-expressing progenitor cells and the adjacent non-progenitor cells expressing XTH9 or CUC2. This feedback is crucial for creating the correct biochemical cues necessary for maintaining low auxin levels and activating essential genes. It also generates a mechanical feedback, highlighting the importance of the *CUC2-XTH9* axis-driven mechanical conflict for initiating *de novo* shoot meristems. The findings suggest that three core modules, namely mechanical properties, cell shape, and biochemical properties of cells, operate in a feedback loop that is central to the morphogenesis of shoot apical meristem, particularly in the absence of tissue patterning cues<sup>187,190</sup>.

## *Chapter 6*

### **Conclusion**

Regeneration is crucial for the survival and growth of organisms. Plants exhibit remarkable capabilities to regenerate and restore tissues and organs that have been lost or damaged due to injury. The intrinsic mechanisms involved in tissue repair and regeneration in plants are complex and not fully understood. Although recent studies have made progress in understanding the mechanisms of tissue restoration in response to injury in underground plant organs, our understanding of the molecular mechanisms involved in aerial organs is still limited and requires further exploration.

**Chapter 2** presents a novel vascular regeneration assay in leaves that was developed to study tissue repair mechanisms in growing plants. The chapter provides a detailed procedure to perform leaf injury and analyse the regeneration of the vascular system. The study emphasizes the significance of wound size, leaf age, injury location, and environmental factors such as light in the ability of the leaf to restore its vascular system.

The study described in **Chapter 3** focuses on investigating the mechanisms underlying plant regeneration, specifically in the context of wound repair and vascular regeneration in aerial organs. We utilized the leaf vascular regeneration assay described in **Chapter 2** and several other mechanical injuries on aerial organs of the plant to mimic injuries naturally occurring during growth. We examined regeneration responses such as local cell proliferation and tissue or organ regeneration and identified the role of *PLT* and *CUC2* transcription factors in regulating these processes. Our study also reveals a previously unrecognized role of *ANT* in vascular regeneration. *PLT* directly bind to the *CUC2* promoter and regulates *CUC2* expression to initiate downstream signalling events for wound repair and vascular regeneration. The successful rescue of vascular regeneration defects in *plt* triple mutant by reconstituting *CUC2* expression supports the critical role of *CUC2* in vascular regeneration and importance of the *PLT-CUC2* regulatory module. The study explores the role of *PLT* and *CUC2* in activating the transcription of local auxin biosynthesis gene, *YUC4* in a feedforward loop that creates an optimal hormonal environment for tissue repair and regeneration. The rescue of vascular regeneration defects through the reconstitution of *YUC4* expression in *plt* and *cuc2* mutants further highlights the importance of this regulatory module. Overall, the results described in **Chapter 3** provides insights into the interdependent roles of *PLT*, *CUC2*, and *YUC4* in cellular reprogramming, vascular regeneration, and wound repair. The transcription factors *PLT* and *CUC2* act in a coherent feed-forward loop to activate *YUC4* for auxin biosynthesis, creating an optimal hormonal environment for vascular regeneration. It emphasizes their contribution to

the molecular mechanisms underlying wound repair and tissue regeneration in growing aerial organs.

The study described in **Chapter 4** demonstrates that the physical contact of the cut end of a leaf with a solid or liquid surface is a key factor influencing the regenerative response. *De novo* root regeneration occurs when the cut end is in contact with a growing surface or a liquid medium, while callus formation occurs when the cut end is exposed to air or not in contact with any surface. The presence of auxin was higher when the cut end of the leaf was in contact with the agar surface, as opposed to when there was no contact with the agar. The study also highlights the role of *PLT* genes in mediating contact dependent regenerative responses. Additionally, it was revealed that *PLT* genes, which are crucial for *de novo* root regeneration, regulate this process through a distinct mechanism separate from their role in other regenerative responses.

**Chapter 5** of the thesis focuses on exploring the importance of PIN1 polarization and the factors influencing PIN1 polarity in shoot progenitors during *de novo* shoot meristem formation. The shoot progenitor initiation in callus is stochastic, and there are two distinct types of progenitors: productive and pseudo progenitors. Productive progenitors have a preferential localization of PIN1 along the cell membrane, indicating polar localization, while pseudo progenitors have a weak, uniform distribution of PIN1 without polarization. The study also demonstrates a distinction in auxin distribution between productive and pseudo progenitors and their surrounding cells. Productive progenitors exhibit a relative minima of auxin within the progenitor cells compared to non-progenitor cells, while pseudo progenitors have high auxin levels in both progenitor and surrounding cells. Disruption of the local minima, as observed in pseudo progenitors, inhibits shoot regeneration. The study provides evidence that cell polarity, specifically the unique polarity pattern created by PIN1 expression in progenitor cells to generate local auxin minima, is crucial for the self-organization of shoot meristem. Furthermore, the study discussed in **Chapter 5** investigates the effects of changes in cytokinin levels on *de novo* shoot regeneration and finds that excess or insufficient levels of cytokinin during progenitor onset can abolish shoot regeneration efficiency.

From our understanding from **Chapter 3**, we explored whether *PLT-CUC2* module can influence PIN1 polarity in progenitors. The *plt* mutant did not produce any shoot progenitors and *cuc2-3* mutants showed defective PIN1 polarity in their progenitors. To understand the factors influencing PIN1 localization, a comparative-transcriptome analysis was conducted, which reveals the regulation of *XTH9* expression by *CUC2* (carried out by Vijina VP). The

study demonstrates that downregulation of *XTH9* results in delocalized and reduced PIN1 expression similar to pseudo progenitors and leads to reduced regeneration efficiency. Manipulating the *XTH9* function affects the pattern of PIN1 localization and the successful formation of shoot meristems during shoot regeneration. In summary, **Chapter 5** provides insights into the intricate regulatory mechanisms involved in PIN1 polarity maintenance during shoot regeneration. It highlights the role of cell polarity, auxin distribution, and the *PLT-CUC2* regulatory module in *de novo* shoot meristem formation. The study also emphasizes the importance of precise timing and location of *XTH9* expression for controlling PIN1 localization and successful shoot meristem development during tissue culture-mediated shoot regeneration.

Overall, the study highlights the role of the *PLT-CUC2* regulatory module in different regenerative contexts. During vascular regeneration in growing leaves in response to mechanical injury, the *PLT-CUC2* module facilitates PIN1 polarization to generate necessary auxin flux for vascular regeneration around the site of injury. In tissue culture mediated *de novo* shoot regeneration, the *PLT-CUC2* module helps in PIN1 polarization to pump out auxin from the progenitor cells, generating local auxin minima in the developing shoot progenitors. Our findings indicate that *CUC2* is involved in non-cell autonomous regulation of PIN1 polarity in progenitor cells during *de novo* shoot regeneration. Conversely, in vein regeneration, the regulation of PIN1 polarity appears to be cell autonomous. However, additional investigation is needed to gain a better understanding of the cell autonomous mechanism by which *CUC2* regulates PIN1 for vascular regeneration. Taken together, *PLT-CUC2* module performs a common physiological function by controlling PIN1 polarization and auxin distribution, enabling the successful regeneration of plant tissues in response to mechanical injury in growing aerial organs or tissue culture-induced shoot regeneration.

## *Chapter 7*

### **References**

- (1) Hoffmeister, S.; Schaller, H. C. A New Biochemical Marker for Foot-Specific Cell Differentiation in Hydra. *Wilhelm Rouxs Arch. Dev. Biol.* **1985**, *194*, 453–461.
- (2) Gierer, A.; Berking, S.; Bode, H.; David, C. N.; Flick, K.; Hansmann, G.; Schaller, H.; Trenkner, E. Regeneration of Hydra from Reaggregated Cells. *Nature. New Biol.* **1972**, *239*, 98–101.
- (3) Vieira, W. A.; Wells, K. M.; McCusker, C. D. Advancements to the Axolotl Model for Regeneration and Aging. *Gerontology* **2020**, *66* (3), 212–222.
- (4) Morgan, T. H. Regeneration and Liability to Injury. *Science* **1901**, *14* (346), 235–248.
- (5) White, C. P. Regeneration of the Tail in the Common Lizard (*L. Vivipara*) after Autotomy. *Rep. Br. Assoc. Adv. Sci.* **1915**, *257*, 472–473.
- (6) Griswold, R.-M. E. Investigation of Barbel Regeneration in the Catfish *Ameiurus Nebulosus*. **1972**.
- (7) Harrison, P. J.; Cate, H. S.; Steullet, P.; Derby, C. D. Amputation-induced Activity of Progenitor Cells Leads to Rapid Regeneration of Olfactory Tissue in Lobsters. *J. Neurobiol.* **2003**, *55* (1), 97–114.
- (8) Gilbert, E. A. B.; Delorme, S. L.; Vickaryous, M. K. The Regeneration Blastema of Lizards: An Amniote Model for the Study of Appendage Replacement. *Regeneration* **2015**, *2* (2), 45–53.
- (9) Ponfick, V. A. Surgery of the Liver. *Lancet* **1890**, *1*, 881.
- (10) Koniaris, L. G.; McKillop, I. H.; Schwartz, S. I.; Zimmers, T. A. Liver Regeneration. *J. Am. Coll. Surg.* **2003**, *197* (4), 634–659.
- (11) Mao, S. A.; Glorioso, J. M.; Nyberg, S. L. Liver Regeneration. *Transl. Res.* **2014**, *163* (4), 352–362.
- (12) Broussonet, M. Observations Sur La Régénérations de Quelques Parties Du Corps Des Poissons. *Hist IAcad Roy Sci.* **1786**.
- (13) Broussonet, M. R. Memoir on the Regeneration of Certain Parts of the Bodies of Fishes. *Lit. Mag. Br. Rev.* **1789**, *3*, 111–113.
- (14) Reddien, P. W. The Cellular and Molecular Basis for Planarian Regeneration. *Cell* **2018**, *175* (2), 327–345.
- (15) Sena, G.; Wang, X.; Liu, H.-Y.; Hofhuis, H.; Birnbaum, K. D. Organ Regeneration Does Not Require a Functional Stem Cell Niche in Plants. *Nature* **2009**, *457* (7233), 1150–1153.
- (16) Hauvermale, A. L.; Sanad, M. N. Phenological Plasticity of Wild and Cultivated Plants [Online First], IntechOpen. Retrived <https://www.intechopen.com/online-first/phenological-plasticity-of-wild-and-cultivated-plants> **2019**.
- (17) Reuhs, B. L.; Kim, J. S.; Matthysse, A. G. Attachment of *Agrobacterium Tumefaciens* to Carrot Cells and Arabidopsis Wound Sites Is Correlated with the Presence of a Cell-Associated, Acidic Polysaccharide. *J. Bacteriol.* **1997**, *179* (17), 5372–5379.
- (18) Mousavi, S. A.; Chauvin, A.; Pascaud, F.; Kellenberger, S.; Farmer, E. E. GLUTAMATE RECEPTOR-LIKE Genes Mediate Leaf-to-Leaf Wound Signalling. *Nature* **2013**, *500* (7463), 422–426.

- (19) Tuteja, N.; Sopory, S. K. Chemical Signaling under Abiotic Stress Environment in Plants. *Plant Signal. Behav.* **2008**, *3* (8), 525–536.
- (20) Braam, J. In Touch: Plant Responses to Mechanical Stimuli. *New Phytol.* **2005**, *165* (2), 373–389.
- (21) Van den Berg, C.; Willemsen, V.; Hage, W.; Weisbeek, P.; Scheres, B. Cell Fate in the Arabidopsis Root Meristem Determined by Directional Signalling. *Nature* **1995**, *378* (6552), 62–65.
- (22) Reinhardt, D.; Frenz, M.; Mandel, T.; Kuhlemeier, C. Microsurgical and Laser Ablation Analysis of Interactions between the Zones and Layers of the Tomato Shoot Apical Meristem. **2003**.
- (23) Ikeuchi, M.; Ogawa, Y.; Iwase, A.; Sugimoto, K. Plant Regeneration: Cellular Origins and Molecular Mechanisms. *Development* **2016**, *143* (9), 1442–1451.
- (24) Galliot, B.; Crescenzi, M.; Jacinto, A.; Tajbakhsh, S. Trends in Tissue Repair and Regeneration. *Development* **2017**, *144* (3), 357–364.
- (25) Lancerotto, L.; Orgill, D. P. Mechanoregulation of Angiogenesis in Wound Healing. *Adv. Wound Care* **2014**, *3* (10), 626–634.
- (26) Nühse, T. S. Cell Wall Integrity Signaling and Innate Immunity in Plants. *Front. Plant Sci.* **2012**, *3*, 280.
- (27) Wolf, S.; Hématy, K.; Höfte, H. Growth Control and Cell Wall Signaling in Plants. *Annu. Rev. Plant Biol.* **2012**, *63*, 381–407.
- (28) Hamant, O.; Heisler, M. G.; Jonsson, H.; Krupinski, P.; Uyttewaal, M.; Bokov, P.; Corson, F.; Sahlin, P.; Boudaoud, A.; Meyerowitz, E. M. Developmental Patterning by Mechanical Signals in Arabidopsis. *science* **2008**, *322* (5908), 1650–1655.
- (29) Heil, M.; Ibarra-Laclette, E.; Adame-Alvarez, R. M.; Martínez, O.; Ramirez-Chavez, E.; Molina-Torres, J.; Herrera-Estrella, L. How Plants Sense Wounds: Damaged-Self Recognition Is Based on Plant-Derived Elicitors and Induces Octadecanoid Signaling. *PLoS One* **2012**, *7* (2), e30537.
- (30) Heil, M.; Land, W. G. Danger Signals–Damaged-Self Recognition across the Tree of Life. *Front. Plant Sci.* **2014**, *5*, 578.
- (31) Toyota, M.; Spencer, D.; Sawai-Toyota, S.; Jiaqi, W.; Zhang, T.; Koo, A. J.; Howe, G. A.; Gilroy, S. Glutamate Triggers Long-Distance, Calcium-Based Plant Defense Signaling. *Science* **2018**, *361* (6407), 1112–1115.
- (32) Choi, W.-G.; Miller, G.; Wallace, I.; Harper, J.; Mittler, R.; Gilroy, S. *Orchestrating Rapid Long-distance Signaling in Plants with Ca<sup>2+</sup>, ROS and Electrical Signals*; Wiley Online Library, 2017; Vol. 90, pp 698–707.
- (33) Seo, S.; Katou, S.; Seto, H.; Gomi, K.; Ohashi, Y. The Mitogen-activated Protein Kinases WIPK and SIPK Regulate the Levels of Jasmonic and Salicylic Acids in Wounded Tobacco Plants. *Plant J.* **2007**, *49* (5), 899–909.
- (34) Schulze, A.; Zimmer, M.; Mielke, S.; Stellmach, H.; Melnyk, C. W.; Hause, B.; Gasperini, D. Wound-Induced Shoot-to-Root Relocation of JA-Ile Precursors Coordinates Arabidopsis Growth. *Mol. Plant* **2019**, *12* (10), 1383–1394.

- (35) Shannon, E. K.; Stevens, A.; Edrington, W.; Zhao, Y.; Jayasinghe, A. K.; Page-McCaw, A.; Hutson, M. S. Multiple Mechanisms Drive Calcium Signal Dynamics around Laser-Induced Epithelial Wounds. *Biophys. J.* **2017**, *113* (7), 1623–1635.
- (36) Li, T.; Yan, A.; Bhatia, N.; Altinok, A.; Afik, E.; Durand-Smet, P.; Tarr, P. T.; Schroeder, J. I.; Heisler, M. G.; Meyerowitz, E. M. Calcium Signals Are Necessary to Establish Auxin Transporter Polarity in a Plant Stem Cell Niche. *Nat. Commun.* **2019**, *10* (1), 726.
- (37) Xu, J.; Hofhuis, H.; Heidstra, R.; Sauer, M.; Friml, J.; Scheres, B. A Molecular Framework for Plant Regeneration. *Science* **2006**, *311* (5759), 385–388.
- (38) Zhang, G.; Zhao, F.; Chen, L.; Pan, Y.; Sun, L.; Bao, N.; Zhang, T.; Cui, C.-X.; Qiu, Z.; Zhang, Y. Jasmonate-Mediated Wound Signalling Promotes Plant Regeneration. *Nat. Plants* **2019**, *5* (5), 491–497.
- (39) Van Den Berg, C.; Willemsen, V.; Hendriks, G.; Weisbeek, P.; Scheres, B. Short-Range Control of Cell Differentiation in the Arabidopsis Root Meristem. *Nature* **1997**, *390* (6657), 287–289.
- (40) Sanchez-Corrionero, A.; Perez-Garcia, P.; Cabrera, J.; Silva-Navas, J.; Perianez-Rodriguez, J.; Gude, I.; del Pozo, J. C.; Moreno-Risueno, M. A. Stem Cell Activity and Regeneration in Roots Require Non-Cell Autonomous Regulation from the Ground Tissue. *bioRxiv* **2019**.
- (41) Moreno-Risueno, M. A.; Sozzani, R.; Yardımcı, G. G.; Petricka, J. J.; Vernoux, T.; Blilou, I.; Alonso, J.; Winter, C. M.; Ohler, U.; Scheres, B. Transcriptional Control of Tissue Formation throughout Root Development. *Science* **2015**, *350* (6259), 426–430.
- (42) Marhava, P.; Hoermayer, L.; Yoshida, S.; Marhavý, P.; Benková, E.; Friml, J. Re-Activation of Stem Cell Pathways for Pattern Restoration in Plant Wound Healing. *Cell* **2019**, *177* (4), 957-969. e13.
- (43) Durgaprasad, K.; Roy, M. V.; Venugopal, A.; Kareem, A.; Raj, K.; Willemsen, V.; Mähönen, A. P.; Scheres, B.; Prasad, K. Gradient Expression of Transcription Factor Imposes a Boundary on Organ Regeneration Potential in Plants. *Cell Rep.* **2019**, *29* (2), 453-463. e3.
- (44) Matosevich, R.; Cohen, I.; Gil-Yarom, N.; Modrego, A.; Verna, C.; Scarpella, E.; Efroni, I. A Dynamic Pattern of Local Auxin Sources Is Required for Root Regeneration. *bioRxiv* **2019**, 783480.
- (45) Santuari, L.; Sanchez-Perez, G. F.; Luijten, M.; Rutjens, B.; Terpstra, I.; Berke, L.; Gorte, M.; Prasad, K.; Bao, D.; Timmermans-Hereijgers, J. L. The PLETHORA Gene Regulatory Network Guides Growth and Cell Differentiation in Arabidopsis Roots. *Plant Cell* **2016**, *28* (12), 2937–2951.
- (46) Asahina, M.; Azuma, K.; Pitaksaringkarn, W.; Yamazaki, T.; Mitsuda, N.; Ohme-Takagi, M.; Yamaguchi, S.; Kamiya, Y.; Okada, K.; Nishimura, T. Spatially Selective Hormonal Control of RAP2. 6L and ANAC071 Transcription Factors Involved in Tissue Reunion in Arabidopsis. *Proc. Natl. Acad. Sci.* **2011**, *108* (38), 16128–16132.
- (47) Radhakrishnan, D.; Shanmukhan, A. P.; Kareem, A.; Aiyaz, M.; Varappambathu, V.; Toms, A.; Kerstens, M.; Valsakumar, D.; Landge, A. N.; Shaji, A. A Coherent Feed-Forward Loop Drives Vascular Regeneration in Damaged Aerial Organs of Plants Growing in a Normal Developmental Context. *Development* **2020**, *147* (6), dev185710.

- (48) Morgan, T. H. *Further Experiments on the Regeneration of the Tail of Fishes*; 1902.
- (49) Zhou, W.; Lozano-Torres, J. L.; Blilou, I.; Zhang, X.; Zhai, Q.; Smant, G.; Li, C.; Scheres, B. A Jasmonate Signaling Network Activates Root Stem Cells and Promotes Regeneration. *Cell* **2019**, *177* (4), 942–956. e14.
- (50) Kral, N.; Hanna Ougolnikova, A.; Sena, G. Externally Imposed Electric Field Enhances Plant Root Tip Regeneration. *Regeneration* **2016**, *3* (3), 156–167.
- (51) Saucet, S. B.; Van Ghelder, C.; Abad, P.; Duval, H.; Esmenjaud, D. Resistance to Root-knot Nematodes *Meloidogyne* Spp. in Woody Plants. *New Phytol.* **2016**, *211* (1), 41–56.
- (52) Marhavý, P.; Kurenda, A.; Siddique, S.; Dénervaud Tendon, V.; Zhou, F.; Holbein, J.; Hasan, M. S.; Grundler, F. M.; Farmer, E. E.; Geldner, N. Single-cell Damage Elicits Regional, Nematode-restricting Ethylene Responses in Roots. *EMBO J.* **2019**, *38* (10), e100972.
- (53) Iwase, A.; Mitsuda, N.; Koyama, T.; Hiratsu, K.; Kojima, M.; Arai, T.; Inoue, Y.; Seki, M.; Sakakibara, H.; Sugimoto, K. The AP2/ERF Transcription Factor WIND1 Controls Cell Dedifferentiation in Arabidopsis. *Curr. Biol.* **2011**, *21* (6), 508–514.
- (54) Heyman, J.; Cools, T.; Canher, B.; Shavialenka, S.; Traas, J.; Vercauteren, I.; Van den Daele, H.; Persiau, G.; De Jaeger, G.; Sugimoto, K. The Heterodimeric Transcription Factor Complex ERF115–PAT1 Grants Regeneration Competence. *Nat. Plants* **2016**, *2* (11), 1–7.
- (55) Mähönen, A. P.; Tusscher, K. ten; Siligato, R.; Smetana, O.; Díaz-Triviño, S.; Salojärvi, J.; Wachsman, G.; Prasad, K.; Heidstra, R.; Scheres, B. PLETHORA Gradient Formation Mechanism Separates Auxin Responses. *Nature* **2014**, *515* (7525), 125–129.
- (56) Fromm, J.; Lautner, S. Electrical Signals and Their Physiological Significance in Plants. *Plant Cell Environ.* **2007**, *30* (3), 249–257.
- (57) Canales, J.; Henriquez-Valencia, C.; Brauchi, S. The Integration of Electrical Signals Originating in the Root of Vascular Plants. *Front. Plant Sci.* **2018**, *8*, 2173.
- (58) Flaishman, M. A.; Loginovsky, K.; Lev-Yadun, S. Regenerative Xylem in Inflorescence Stems of Arabidopsis Thaliana. *J. Plant Growth Regul.* **2003**, *22*, 253–258.
- (59) Chano, V.; López, R.; Pita, P.; Collada, C.; Soto, Á. Proliferation of Axial Parenchymatic Xylem Cells Is a Key Step in Wound Closure of Girdled Stems in Pinus Canariensis. *BMC Plant Biol.* **2015**, *15* (1), 1–14.
- (60) Pang, Y.; Zhang, J.; Cao, J.; Yin, S.-Y.; He, X.-Q.; Cui, K.-M. Phloem Transdifferentiation from Immature Xylem Cells during Bark Regeneration after Girdling in *Eucommia Ulmoides* Oliv. *J. Exp. Bot.* **2008**, *59* (6), 1341–1351.
- (61) Zhang, J.; Gao, G.; Chen, J.-J.; Taylor, G.; Cui, K.-M.; He, X.-Q. Molecular Features of Secondary Vascular Tissue Regeneration after Bark Girdling in *Populus*. *New Phytol.* **2011**, *192* (4), 869–884.
- (62) Melnyk, C. W.; Schuster, C.; Leyser, O.; Meyerowitz, E. M. A Developmental Framework for Graft Formation and Vascular Reconnection in Arabidopsis Thaliana. *Curr. Biol. CB* **2015**, *25* (10), 1306–1318. <https://doi.org/10.1016/j.cub.2015.03.032>.

- (63) Sachs, T. On the Determination of the Pattern of Vascular Tissue in Peas. *Ann. Bot.* **1968**, 32 (4), 781–790.
- (64) Sachs, T. The Control of the Patterned Differentiation of Vascular Tissues. *Adv. Bot. Res.* **1981**, 9, 151–262. [https://doi.org/10.1016/S0065-2296\(08\)60351-1](https://doi.org/10.1016/S0065-2296(08)60351-1).
- (65) Jacobs, W. P. The Role of Auxin in Differentiation of Xylem around a Wound. *Am. J. Bot.* **1952**, 301–309.
- (66) Sachs, T. Cell Polarity and Tissue Patterning in Plants. **1991**.
- (67) Mitchison, G. J. A Model for Vein Formation in Higher Plants. *Proc. R. Soc. Lond. B Biol. Sci.* **1980**, 207 (1166), 79–109.
- (68) SACHS, T. Polarity and the Induction of Organized Vascular Tissues. *Ann. Bot.* **1969**, 33 (2), 263–275. <https://doi.org/10.1093/oxfordjournals.aob.a084281>.
- (69) Hess, T.; Sachs, T. The Influence of a Mature Leaf on Xylem Differentiation. *New Phytol.* **1972**, 71 (5), 903–914.
- (70) Simon, S. Experimentelle Untersuchungen Über Die Entstehung von Gefassverbindungen. *Ber Dtsch Bot Ges* **1908**, 26, 364–396.
- (71) Swamy, B. G. L. Wound Healing Responses in Monocotyledons. II. Responses to Chemical Treatments. **1975**.
- (72) Hu, B.; Zhang, G.; Liu, W.; Shi, J.; Wang, H.; Qi, M.; Li, J.; Qin, P.; Ruan, Y.; Huang, H. Divergent Regeneration-competent Cells Adopt a Common Mechanism for Callus Initiation in Angiosperms. *Regeneration* **2017**, 4 (3), 132–139.
- (73) Aloni, R.; Plotkin, T. Wound-Induced and Naturally Occurring Regenerative Differentiation of Xylem in Zea Mays L. *Planta* **1985**, 163, 126–132.
- (74) Todd, T. On the Process of Reproduction of the Members of the Aquatic Salamander. *Quart J Sci Arts Lib* **1823**, 16, 84–86.
- (75) Melnyk, C. W.; Gabel, A.; Hardcastle, T. J.; Robinson, S.; Miyashima, S.; Grosse, I.; Meyerowitz, E. M. Transcriptome Dynamics at Arabidopsis Graft Junctions Reveal an Intertissue Recognition Mechanism That Activates Vascular Regeneration. *Proc. Natl. Acad. Sci. U. S. A.* **2018**, 115 (10), E2447–E2456. <https://doi.org/10.1073/pnas.1718263115>.
- (76) Verna, C.; Ravichandran, S. J.; Sawchuk, M. G.; Linh, N. M.; Scarpella, E. Coordination of Tissue Cell Polarity by Auxin Transport and Signaling. *Elife* **2019**, 8, e51061.
- (77) Chen, X.; Qu, Y.; Sheng, L.; Liu, J.; Huang, H.; Xu, L. A Simple Method Suitable to Study de Novo Root Organogenesis. *Front. Plant Sci.* **2014**, 5, 208.
- (78) Liu, J.; Sheng, L.; Xu, Y.; Li, J.; Yang, Z.; Huang, H.; Xu, L. WOX11 and 12 Are Involved in the First-Step Cell Fate Transition during de Novo Root Organogenesis in Arabidopsis. *Plant Cell* **2014**, 26 (3), 1081–1093. <https://doi.org/10.1105/tpc.114.122887>.
- (79) De Klerk, G.-J.; Van Der Krieken, W.; de Jong, J. C. Review the Formation of Adventitious Roots: New Concepts, New Possibilities. *Vitro Cell. Dev. Biol.-Plant* **1999**, 35, 189–199.

- (80) Bellini, C.; Pacurar, D. I.; Perrone, I. Adventitious Roots and Lateral Roots: Similarities and Differences. *Annu. Rev. Plant Biol.* **2014**, *65*, 639–666.
- (81) Perez-Garcia, P.; Moreno-Risueno, M. A. Stem Cells and Plant Regeneration. *Dev. Biol.* **2018**, *442* (1), 3–12.
- (82) Sang, Y. L.; Cheng, Z. J.; Zhang, X. S. Plant Stem Cells and de Novo Organogenesis. *New Phytol.* **2018**, *218* (4), 1334–1339.
- (83) Xu, L. De Novo Root Regeneration from Leaf Explants: Wounding, Auxin, and Cell Fate Transition. *Curr. Opin. Plant Biol.* **2018**, *41*, 39–45.
- (84) Druege, U.; Hilo, A.; Pérez-Pérez, J. M.; Klopotek, Y.; Acosta, M.; Shahinnia, F.; Zerche, S.; Franken, P.; Hajirezaei, M. R. Molecular and Physiological Control of Adventitious Rooting in Cuttings: Phytohormone Action Meets Resource Allocation. *Ann. Bot.* **2019**, *123* (6), 929–949.
- (85) Ikeuchi, M.; Favero, D. S.; Sakamoto, Y.; Iwase, A.; Coleman, D.; Rymen, B.; Sugimoto, K. Molecular Mechanisms of Plant Regeneration. *Annu. Rev. Plant Biol.* **2019**, *70*, 377–406.
- (86) Mironova, V.; Xu, J. A Single-Cell View of Tissue Regeneration in Plants. *Curr. Opin. Plant Biol.* **2019**, *52*, 149–154.
- (87) Druege, U.; Franken, P.; Hajirezaei, M. R. Plant Hormone Homeostasis, Signaling, and Function during Adventitious Root Formation in Cuttings. *Front. Plant Sci.* **2016**, *7*, 381.
- (88) Liu, W.; Zhang, Y.; Fang, X.; Tran, S.; Zhai, N.; Yang, Z.; Guo, F.; Chen, L.; Yu, J.; Ison, M. S. Transcriptional Landscapes of de Novo Root Regeneration from Detached Arabidopsis Leaves Revealed by Time-Lapse and Single-Cell RNA Sequencing Analyses. *Plant Commun.* **2022**, *3* (4), 100306.
- (89) Liu, J.; Sheng, L.; Xu, Y.; Li, J.; Yang, Z.; Huang, H.; Xu, L. WOX11 and 12 Are Involved in the First-Step Cell Fate Transition during de Novo Root Organogenesis in Arabidopsis. *Plant Cell* **2014**, *26* (3), 1081–1093.
- (90) Prasad, K.; Grigg, S. P.; Barkoulas, M.; Yadav, R. K.; Sanchez-Perez, G. F.; Pinon, V.; Blilou, I.; Hofhuis, H.; Dhonukshe, P.; Galinha, C.; Mähönen, A. P.; Muller, W. H.; Raman, S.; Verkleij, A. J.; Snel, B.; Reddy, G. V.; Tsiantis, M.; Scheres, B. Arabidopsis PLETHORA Transcription Factors Control Phyllotaxis. *Curr. Biol. CB* **2011**, *21* (13), 1123–1128. <https://doi.org/10.1016/j.cub.2011.05.009>.
- (91) Aida, M.; Beis, D.; Heidstra, R.; Willemsen, V.; Blilou, I.; Galinha, C.; Nussaume, L.; Noh, Y.-S.; Amasino, R.; Scheres, B. The PLETHORA Genes Mediate Patterning of the Arabidopsis Root Stem Cell Niche. *Cell* **2004**, *119* (1), 109–120.
- (92) Nowack, M. K.; Harashima, H.; Dissmeyer, N.; Bouyer, D.; Weimer, A. K.; De Winter, F.; Yang, F.; Schnittger, A. Genetic Framework of Cyclin-Dependent Kinase Function in Arabidopsis. *Dev. Cell* **2012**, *22* (5), 1030–1040.
- (93) Scofield, S.; Jones, A.; Murray, J. A. The Plant Cell Cycle in Context. *J. Exp. Bot.* **2014**, *65* (10), 2557–2562.
- (94) Bustillo-Avenidaño, E.; Ibáñez, S.; Sanz, O.; Sousa Barros, J. A.; Gude, I.; Perianez-Rodríguez, J.; Micol, J. L.; Del Pozo, J. C.; Moreno-Risueno, M. A.; Pérez-Pérez, J. M. Regulation of Hormonal Control, Cell Reprogramming, and Patterning during De

- Novo Root Organogenesis. *Plant Physiol.* **2018**, *176* (2), 1709–1727.  
<https://doi.org/10.1104/pp.17.00980>.
- (95) Shanmukhan, A. P.; Mathew, M. M.; Aiyaz, M.; Varaparambathu, V.; Kareem, A.; Radhakrishnan, D.; Prasad, K. Regulation of Touch-Stimulated de Novo Root Regeneration from Arabidopsis Leaves. *Plant Physiol.* **2021**, *187* (1), 52–58.
- (96) Gordon, S. P.; Heisler, M. G.; Reddy, G. V.; Ohno, C.; Das, P.; Meyerowitz, E. M. Pattern Formation during de Novo Assembly of the Arabidopsis Shoot Meristem. **2007**.
- (97) Kareem, A.; Durgaprasad, K.; Sugimoto, K.; Du, Y.; Pulianmackal, A. J.; Trivedi, Z. B.; Abhayadev, P. V.; Pinon, V.; Meyerowitz, E. M.; Scheres, B. PLETHORA Genes Control Regeneration by a Two-Step Mechanism. *Curr. Biol.* **2015**, *25* (8), 1017–1030.
- (98) Radhakrishnan, D.; Kareem, A.; Durgaprasad, K.; Sreeraj, E.; Sugimoto, K.; Prasad, K. Shoot Regeneration: A Journey from Acquisition of Competence to Completion. *Curr. Opin. Plant Biol.* **2018**, *41*, 23–31.
- (99) Atta, R.; Laurens, L.; Boucheron-Dubuisson, E.; Guivarc’h, A.; Carnero, E.; Giraudat-Pautot, V.; Rech, P.; Chriqui, D. Pluripotency of Arabidopsis Xylem Pericycle Underlies Shoot Regeneration from Root and Hypocotyl Explants Grown in Vitro. *Plant J.* **2009**, *57* (4), 626–644.
- (100) Hau-Hsuan Hwang; Manda Yu; Erh-Min Lai. Agrobacterium-Mediated Plant Transformation: Biology and Applications. *Arab. Book* **2017**, *2017* (15).  
<https://doi.org/10.1199/tab.0186>.
- (101) Shanmukhan, A. P.; Mathew, M. M.; Radhakrishnan, D.; Aiyaz, M.; Prasad, K. Regrowing the Damaged or Lost Body Parts. *Curr. Opin. Plant Biol.* **2020**, *53*, 117–127.
- (102) Kuchen, E. E.; Fox, S.; Reuille, P. B.; Kennaway, R.; Bensmihen, S.; Avondo, J. Generation of Leaf Shape through Early Patterns of Growth and Tissue Polarity. *Science* **2012**, *335*. <https://doi.org/10.1126/science.1214678>.
- (103) Scarpella, E.; Marcos, D.; Friml, J.; Berleth, T. Control of Leaf Vascular Patterning by Polar Auxin Transport. *Genes Dev.* **2006**, *20* (8), 1015–1027.
- (104) Scarpella, E.; Meijer, A. H. Pattern Formation in the Vascular System of Monocot and Dicot Plant Species. *New Phytol.* **2004**, *164* (2), 209–242.
- (105) Sachs, T.; Hassidim, M. Mutual Support and Selection between Branches of Damaged Plants. *Vegetatio* **1996**, *127*, 25–30.
- (106) Rolland-Lagan, A.-G.; Prusinkiewicz, P. Reviewing Models of Auxin Canalization in the Context of Leaf Vein Pattern Formation in Arabidopsis. *Plant J.* **2005**, *44* (5), 854–865.
- (107) Pervin, M. S.; Itoh, G.; Talukder, M. S. U.; Fujimoto, K.; Morimoto, Y. V.; Tanaka, M.; Ueda, M.; Yumura, S. A Study of Wound Repair in Dictyostelium Cells by Using Novel Laserporation. *Sci. Rep.* **2018**, *8* (1), 7969.
- (108) Yun, M. H. Changes in Regenerative Capacity through Lifespan. *Int. J. Mol. Sci.* **2015**, *16* (10), 25392–25432.
- (109) Nelson, N.; Yocum, C. F. Structure and Function of Photosystems I and II. *Annu Rev Plant Biol* **2006**, *57*, 521–565.

- (110) Franklin, K. A. Shade Avoidance. *New Phytol.* **2008**, *179* (4), 930–944.
- (111) Smith, H. Phytochromes and Light Signal Perception by Plants—an Emerging Synthesis. *Nature* **2000**, *407* (6804), 585–591.
- (112) Meng, L.; Mestdagh, H.; Ameye, M.; Audenaert, K.; Höfte, M.; Van Labeke, M.-C. Phenotypic Variation of Botrytis Cinerea Isolates Is Influenced by Spectral Light Quality. *Front. Plant Sci.* **2020**, *11*, 1233.
- (113) Salvador-Recatalà, V. New Roles for the GLUTAMATE RECEPTOR-LIKE 3.3, 3.5, and 3.6 Genes as on/off Switches of Wound-Induced Systemic Electrical Signals. *Plant Signal. Behav.* **2016**, *11* (4), e1161879. <https://doi.org/10.1080/15592324.2016.1161879>.
- (114) Nguyen, C. T.; Kurenda, A.; Stolz, S.; Chételat, A.; Farmer, E. E. Identification of Cell Populations Necessary for Leaf-to-Leaf Electrical Signaling in a Wounded Plant. *Proc. Natl. Acad. Sci. U. S. A.* **2018**, *115* (40), 10178–10183. <https://doi.org/10.1073/pnas.1807049115>.
- (115) Xu, J.; Hofhuis, H.; Heidstra, R.; Sauer, M.; Friml, J.; Scheres, B. A Molecular Framework for Plant Regeneration. *Science* **2006**, *311*. <https://doi.org/10.1126/science.1121790>.
- (116) Efroni, I.; Mello, A.; Nawy, T.; Ip, P.-L.; Rahni, R.; DelRose, N.; Powers, A.; Satija, R.; Birnbaum, K. D. Root Regeneration Triggers an Embryo-like Sequence Guided by Hormonal Interactions. *Cell* **2016**, *165* (7), 1721–1733. <https://doi.org/10.1016/j.cell.2016.04.046>.
- (117) Reinhardt, D.; Frenz, M.; Mandel, T.; Kuhlemeier, C. Microsurgical and Laser Ablation Analysis of Leaf Positioning and Dorsovenral Patterning in Tomato. *Development* **2004**, *132* (1), 15–26. <https://doi.org/10.1242/dev.01544>.
- (118) SACHS, T. The Role of the Root in the Induction of Xylem Differentiation in Peas. *Ann. Bot.* **1968**, *32* (2), 391–399. <https://doi.org/10.1093/oxfordjournals.aob.a084216>.
- (119) Sachs, T. Cell Polarity and Tissue Patterning in Plants. *Development* **1991**, *113* (Supplement 1).
- (120) Asahina, M.; Azuma, K.; Pitaksaringkarn, W.; Yamazaki, T.; Mitsuda, N.; Ohme-Takagi, M.; Yamaguchi, S.; Kamiya, Y.; Okada, K.; Nishimura, T.; Koshiha, T.; Yokota, T.; Kamada, H.; Satoh, S. Spatially Selective Hormonal Control of RAP2.6L and ANAC071 Transcription Factors Involved in Tissue Reunion in Arabidopsis. *Proc. Natl. Acad. Sci. U. S. A.* **2011**, *108* (38), 16128–16132. <https://doi.org/10.1073/pnas.1110443108>.
- (121) Flaishman, M. A.; Loginovsky, K.; Lev-Yadun, S. Regenerative Xylem in Inflorescence Stems of Arabidopsis Thaliana. *J. Plant Growth Regul.* **2003**, *22* (3), 253–258. <https://doi.org/10.1007/s00344-003-0030-y>.
- (122) Pitaksaringkarn, W.; Matsuoka, K.; Asahina, M.; Miura, K.; Sage-Ono, K.; Ono, M.; Yokoyama, R.; Nishitani, K.; Ishii, T.; Iwai, H.; Satoh, S. XTH20 and XTH19 Regulated by ANAC071 under Auxin Flow Are Involved in Cell Proliferation in Incised Arabidopsis Inflorescence Stems. *Plant J.* **2014**, *80* (4), 604–614. <https://doi.org/10.1111/tpj.12654>.

- (123) Mazur, E.; Benková, E.; Friml, J. Vascular Cambium Regeneration and Vessel Formation in Wounded Inflorescence Stems of Arabidopsis. *Sci. Rep.* **2016**, *6* (1), 33754. <https://doi.org/10.1038/srep33754>.
- (124) Iwase, A.; Ohme-Takagi, M.; Sugimoto, K. WIND1: A Key Molecular Switch for Plant Cell Dedifferentiation. *Plant Signal. Behav.* **2011**, *6* (12), 1943–1945. <https://doi.org/10.4161/psb.6.12.18266>.
- (125) Ikeuchi, M.; Shibata, M.; Rymen, B.; Iwase, A.; Bagman, A.-M.; Watt, L.; Coleman, D.; Favero, D. S.; Takahashi, T.; Ahnert, S. E.; Brady, S. M.; Sugimoto, K. A Gene Regulatory Network for Cellular Reprogramming in Plant Regeneration. *Plant Cell Physiol.* **2018**, *59* (4), 765–777. <https://doi.org/10.1093/pcp/pcy013>.
- (126) Dhonukshe, P.; Huang, F.; Galvan-Ampudia, C. S.; Mähönen, A. P.; Kleine-Vehn, J.; Xu, J.; Quint, A.; Prasad, K.; Friml, J.; Scheres, B. Plasma Membrane-Bound AGC3 Kinases Phosphorylate PIN Auxin Carriers at TPRXS (N/S) Motifs to Direct Apical PIN Recycling. *Development* **2010**, *137* (19), 3245–3255.
- (127) Pinon, V.; Prasad, K.; Grigg, S. P.; Sanchez-Perez, G. F.; Scheres, B. Local Auxin Biosynthesis Regulation by PLETHORA Transcription Factors Controls Phyllotaxis in Arabidopsis. *Proc. Natl. Acad. Sci.* **2013**, *110* (3), 1107 LP–1112.
- (128) Krizek, B. A. AINTEGUMENTA-LIKE Genes Have Partly Overlapping Functions with AINTEGUMENTA but Make Distinct Contributions to Arabidopsis Thaliana Flower Development. *J. Exp. Bot.* **2015**, *66* (15), 4537–4549.
- (129) Hibara, K.; Karim, M. R.; Takada, S.; Taoka, K.; Furutani, M.; Aida, M.; Tasaka, M. Arabidopsis CUP-SHAPED COTYLEDON3 Regulates Postembryonic Shoot Meristem and Organ Boundary Formation. *Plant Cell* **2006**, *18* (11), 2946–2957.
- (130) Nikovics, K.; Blein, T.; Peaucelle, A.; Ishida, T.; Morin, H.; Aida, M.; Laufs, P. The Balance between the MIR164A and CUC2 Genes Controls Leaf Margin Serration in Arabidopsis. *Plant Cell* **2006**, *18* (11), 2929–2945.
- (131) Clough, S. J.; Bent, A. F. Floral Dip: A Simplified Method for Agrobacterium-mediated Transformation of Arabidopsis Thaliana. *Plant J.* **1998**, *16* (6), 735–743.
- (132) Díaz-Triviño, S.; Long, Y.; Scheres, B.; Blilou, I. Analysis of a Plant Transcriptional Regulatory Network Using Transient Expression Systems. *Plant Gene Regul. Netw. Methods Protoc.* **2017**, 83–103.
- (133) Yamaguchi, N.; Winter, C. M.; Wu, M.-F.; Kwon, C. S.; William, D. A.; Wagner, D. PROTOCOLS: Chromatin Immunoprecipitation from Arabidopsis Tissues. *Arab. Book American Soc. Plant Biol.* **2014**, 12.
- (134) Mitchison, G. J.; Hanke, D. E.; Sheldrake, A. R. The Polar Transport of Auxin and Vein Patterns in Plants [and Discussion]. *Philos. Trans. R. Soc. B Biol. Sci.* **1981**, *295* (1078), 461–471. <https://doi.org/10.1098/rstb.1981.0154>.
- (135) Scarpella, E.; Barkoulas, M.; Tsiantis, M. Control of Leaf and Vein Development by Auxin. *Cold Spring Harb. Perspect. Biol.* **2010**, *2* (1), a001511.
- (136) Rolland-Lagan, A.-G.; Prusinkiewicz, P. Reviewing Models of Auxin Canalization in the Context of Leaf Vein Pattern Formation in Arabidopsis. *Plant J.* **2005**, *44* (5), 854–865. <https://doi.org/10.1111/j.1365-313X.2005.02581.x>.

- (137) Mitchison, G. J. A Model for Vein Formation in Higher Plants. *Proc. R. Soc. B Biol. Sci.* **1980**, *207* (1166), 79–109. <https://doi.org/10.1098/rspb.1980.0015>.
- (138) Smetana, O.; Mäkilä, R.; Lyu, M.; Amiryousefi, A.; Sánchez Rodríguez, F.; Wu, M.-F.; Solé-Gil, A.; Leal Gavarrón, M.; Siligato, R.; Miyashima, S.; Roszak, P.; Blomster, T.; Reed, J. W.; Broholm, S.; Mähönen, A. P. High Levels of Auxin Signalling Define the Stem-Cell Organizer of the Vascular Cambium. *Nature* **2019**, *565* (7740), 485–489. <https://doi.org/10.1038/s41586-018-0837-0>.
- (139) Bilborough, G. D.; Runions, A.; Barkoulas, M.; Jenkins, H. W.; Hasson, A.; Galinha, C.; Laufs, P.; Hay, A.; Prusinkiewicz, P.; Tsiantis, M. Model for the Regulation of Arabidopsis Thaliana Leaf Margin Development. *Proc. Natl. Acad. Sci.* **2011**, *108* (8), 3424–3429.
- (140) O'Malley, R. C.; Huang, S. C.; Song, L.; Lewsey, M. G.; Bartlett, A.; Nery, J. R.; Galli, M.; Gallavotti, A.; Ecker, J. R. Cistrome and Epicistrome Features Shape the Regulatory DNA Landscape. *Cell* **2016**, *165* (5), 1280–1292.
- (141) Hirakawa, Y.; Kondo, Y.; Fukuda, H. TDIF Peptide Signaling Regulates Vascular Stem Cell Proliferation via the WOX4 Homeobox Gene in Arabidopsis. *Plant Cell* **2010**, *22* (8), 2618–2629.
- (142) Kuchel, P. W.; Easterbrook-Smith, S.; Gysbers, V.; Guss, J. M. *Schaum's Outline of Biochemistry*; McGraw-Hill Education, 2009.
- (143) Jönsson, H.; Heisler, M. G.; Shapiro, B. E.; Meyerowitz, E. M.; Mjolsness, E. An Auxin-Driven Polarized Transport Model for Phyllotaxis. *Proc. Natl. Acad. Sci.* **2006**, *103* (5), 1633–1638.
- (144) Smith, R. S.; Guyomarc'h, S.; Mandel, T.; Reinhardt, D.; Kuhlemeier, C.; Prusinkiewicz, P. A Plausible Model of Phyllotaxis. *Proc. Natl. Acad. Sci.* **2006**, *103* (5), 1301–1306.
- (145) Bayer, E. M.; Smith, R. S.; Mandel, T.; Nakayama, N.; Sauer, M.; Prusinkiewicz, P.; Kuhlemeier, C. Integration of Transport-Based Models for Phyllotaxis and Midvein Formation. *Genes Dev.* **2009**, *23* (3), 373–384.
- (146) Schuetz, M.; Smith, R.; Ellis, B. Xylem Tissue Specification, Patterning, and Differentiation Mechanisms. *J. Exp. Bot.* **2013**, *64* (1), 11–31.
- (147) Fujita, H.; Kawaguchi, M. Spatial Regularity Control of Phyllotaxis Pattern Generated by the Mutual Interaction between Auxin and PIN1. *PLoS Comput. Biol.* **2018**, *14* (4), e1006065.
- (148) De Rybel, B.; Adibi, M.; Breda, A. S.; Wendrich, J. R.; Smit, M. E.; Novák, O.; Yamaguchi, N.; Yoshida, S.; Van Isterdael, G.; Palovaara, J. Integration of Growth and Patterning during Vascular Tissue Formation in Arabidopsis. *Science* **2014**, *345* (6197), 1255215.
- (149) Efroni, I.; Birnbaum, K. D. The Potential of Single-Cell Profiling in Plants. *Genome Biol.* **2016**, *17* (1), 65. <https://doi.org/10.1186/s13059-016-0931-2>.
- (150) Han, M.; Yang, X.; Farrington, J. E.; Muneoka, K. Digit Regeneration Is Regulated by Msx1 and BMP4 in Fetal Mice. *Dev. Camb. Engl.* **2003**, *130* (21), 5123–5132. <https://doi.org/10.1242/dev.00710>.
- (151) Prasad, K.; Grigg, S. P.; Barkoulas, M.; Yadav, R. K.; Sanchez-Perez, G. F.; Pinon, V.; Blilou, I.; Hofhuis, H.; Dhonukshe, P.; Galinha, C.; Mahonen, A. P.; Muller, W. H.;

- Raman, S.; Verkleij, A. J.; Snel, B.; Reddy, G. V.; Tsiantis, M.; Scheres, B. Arabidopsis PLETHORA Transcription Factors Control Phyllotaxis. *Curr. Biol. CB* **2011**, *21* (13), 1123–1128. <https://doi.org/10.1016/j.cub.2011.05.009>.
- (152) Sugioka, K.; Bowerman, B. Combinatorial Contact Cues Specify Cell Division Orientation by Directing Cortical Myosin Flows. *Dev. Cell* **2018**, *46* (3), 257–270.e5. <https://doi.org/10.1016/j.devcel.2018.06.020>.
- (153) Smith, G. F.; Figueiredo, E.; Van Wyk, A. E. *Kalanchoe (Crassulaceae) in Southern Africa: Classification, Biology, and Cultivation*; Academic Press, 2019.
- (154) Wang, H.; Jones, B.; Li, Z.; Frasse, P.; Delalande, C.; Regad, F.; Chaabouni, S.; Latche, A.; Pech, J.-C.; Bouzayen, M. The Tomato Aux/IAA Transcription Factor IAA9 Is Involved in Fruit Development and Leaf Morphogenesis. *Plant Cell* **2005**, *17* (10), 2676–2692.
- (155) Wójcikowska, B.; Gaj, M. D. Expression Profiling of AUXIN RESPONSE FACTOR Genes during Somatic Embryogenesis Induction in Arabidopsis. *Plant Cell Rep.* **2017**, *36*, 843–858.
- (156) Braam, J.; Davis, R. W. Rain-, Wind-, and Touch-Induced Expression of Calmodulin and Calmodulin-Related Genes in Arabidopsis. *Cell* **1990**, *60* (3), 357–364.
- (157) Van Aken, O.; De Clercq, I.; Ivanova, A.; Law, S. R.; Van Breusegem, F.; Millar, A. H.; Whelan, J. Mitochondrial and Chloroplast Stress Responses Are Modulated in Distinct Touch and Chemical Inhibition Phases. *Plant Physiol.* **2016**, *171* (3), 2150–2165.
- (158) Van Moerkercke, A.; Duncan, O.; Zander, M.; Šimura, J.; Broda, M.; Vanden Bossche, R.; Lewsey, M. G.; Lama, S.; Singh, K. B.; Ljung, K. A MYC2/MYC3/MYC4-Dependent Transcription Factor Network Regulates Water Spray-Responsive Gene Expression and Jasmonate Levels. *Proc. Natl. Acad. Sci.* **2019**, *116* (46), 23345–23356.
- (159) Mathew, M. M.; Prasad, K. Model Systems for Regeneration: Arabidopsis. *Development* **2021**, *148* (6), dev195347.
- (160) Liao, C.-Y.; Smet, W.; Brunoud, G.; Yoshida, S.; Vernoux, T.; Weijers, D. Reporters for Sensitive and Quantitative Measurement of Auxin Response. *Nat. Methods* **2015**, *12* (3), 207–210.
- (161) Du, Y.; Scheres, B. PLETHORA Transcription Factors Orchestrate de Novo Organ Patterning during Arabidopsis Lateral Root Outgrowth. *Proc. Natl. Acad. Sci.* **2017**, *114* (44), 11709–11714.
- (162) Chen, J.; Somta, P.; Chen, X.; Cui, X.; Yuan, X.; Srinives, P. Gene Mapping of a Mutant Mungbean (*Vigna Radiata* L.) Using New Molecular Markers Suggests a Gene Encoding a Yuc4-like Protein Regulates the Chasmogamous Flower Trait. *Front. Plant Sci.* **2016**, *7*, 830.
- (163) Guénin, S.; Mareck, A.; Rayon, C.; Lamour, R.; Assoumou Ndong, Y.; Domon, J.-M.; Sénéchal, F.; Fournet, F.; Jamet, E.; Canut, H. Identification of Pectin Methyltransferase 3 as a Basic Pectin Methyltransferase Isoform Involved in Adventitious Rooting in Arabidopsis Thaliana. *New Phytol.* **2011**, *192* (1), 114–126.

- (164) Wachsman, G.; Zhang, J.; Moreno-Risueno, M. A.; Anderson, C. T.; Benfey, P. N. Cell Wall Remodeling and Vesicle Trafficking Mediate the Root Clock in Arabidopsis. *Science* **2020**, *370* (6518), 819–823.
- (165) Hoermayer, L.; Montesinos, J. C.; Marhava, P.; Benková, E.; Yoshida, S.; Friml, J. Wounding-Induced Changes in Cellular Pressure and Localized Auxin Signalling Spatially Coordinate Restorative Divisions in Roots. *Proc. Natl. Acad. Sci.* **2020**, *117* (26), 15322–15331.
- (166) Kadokura, S.; Sugimoto, K.; Tarr, P.; Suzuki, T.; Matsunaga, S. Characterization of Somatic Embryogenesis Initiated from the Arabidopsis Shoot Apex. *Dev. Biol.* **2018**, *442* (1), 13–27.
- (167) Radoeva, T.; Albrecht, C.; Piepers, M.; de Vries, S.; Weijers, D. Suspensor-Derived Somatic Embryogenesis in Arabidopsis. *Development* **2020**, *147* (13), dev188912.
- (168) Rosspopoff, O.; Chelysheva, L.; Saffar, J.; Lecorgne, L.; Gey, D.; Caillieux, E.; Colot, V.; Roudier, F.; Hilson, P.; Berthomé, R. Direct Conversion of Root Primordium into Shoot Meristem Relies on Timing of Stem Cell Niche Development. *Development* **2017**, *144* (7), 1187–1200.
- (169) Kareem, A.; Radhakrishnan, D.; Sondhi, Y.; Aiyaz, M.; Roy, M. V.; Sugimoto, K.; Prasad, K. De Novo Assembly of Plant Body Plan: A Step Ahead of Deadpool. *Regeneration* **2016**, *3* (4), 182–197.
- (170) Weigel, D.; Glazebrook, J. *Arabidopsis: A Laboratory Manual*; cold Spring Harbor laboratory press, 2002.
- (171) Cheng, Z. J.; Wang, L.; Sun, W.; Zhang, Y.; Zhou, C.; Su, Y. H.; Li, W.; Sun, T. T.; Zhao, X. Y.; Li, X. G. Pattern of Auxin and Cytokinin Responses for Shoot Meristem Induction Results from the Regulation of Cytokinin Biosynthesis by AUXIN RESPONSE FACTOR3. *Plant Physiol.* **2013**, *161* (1), 240–251.
- (172) Wu, L.-Y.; Shang, G.-D.; Wang, F.-X.; Gao, J.; Wan, M.-C.; Xu, Z.-G.; Wang, J.-W. Dynamic Chromatin State Profiling Reveals Regulatory Roles of Auxin and Cytokinin in Shoot Regeneration. *Dev. Cell* **2022**, *57* (4), 526–542. e7.
- (173) Birnbaum, K. D.; Alvarado, A. S. Slicing across Kingdoms: Regeneration in Plants and Animals. *Cell* **2008**, *132* (4), 697–710.
- (174) Lardon, R.; Wijnker, E.; Keurentjes, J.; Geelen, D. The Genetic Framework of Shoot Regeneration in Arabidopsis Comprises Master Regulators and Conditional Fine-Tuning Factors. *Commun. Biol.* **2020**, *3* (1), 549.
- (175) Lee, K.; Seo, P. J. Dynamic Epigenetic Changes during Plant Regeneration. *Trends Plant Sci.* **2018**, *23* (3), 235–247.
- (176) Motte, H.; Vercauteren, A.; Depuydt, S.; Landschoot, S.; Geelen, D.; Werbrouck, S.; Goormachtig, S.; Vuylsteke, M.; Vereecke, D. Combining Linkage and Association Mapping Identifies RECEPTOR-LIKE PROTEIN KINASE1 as an Essential Arabidopsis Shoot Regeneration Gene. *Proc. Natl. Acad. Sci.* **2014**, *111* (22), 8305–8310.
- (177) Zhang, T.-Q.; Lian, H.; Zhou, C.-M.; Xu, L.; Jiao, Y.; Wang, J.-W. A Two-Step Model for de Novo Activation of WUSCHEL during Plant Shoot Regeneration. *Plant Cell* **2017**, *29* (5), 1073–1087.

- (178) Capron, A.; Chatfield, S.; Provard, N.; Berleth, T. Embryogenesis: Pattern Formation from a Single Cell. *Arab. Book* **2009**, 2009 (7).
- (179) Duclercq, J.; Sangwan-Norreel, B.; Catterou, M.; Sangwan, R. S. De Novo Shoot Organogenesis: From Art to Science. *Trends Plant Sci.* **2011**, 16 (11), 597–606.
- (180) Phillips, G. C.; Garda, M. Plant Tissue Culture Media and Practices: An Overview. *Vitro Cell. Dev. Biol.-Plant* **2019**, 55, 242–257.
- (181) Zuo, J.; Niu, Q.-W.; Chua, N.-H. An Estrogen Receptor-based Transactivator XVE Mediates Highly Inducible Gene Expression in Transgenic Plants. *Plant J.* **2000**, 24 (2), 265–273.
- (182) Shimotohno, A.; Heidstra, R.; Blilou, I.; Scheres, B. Root Stem Cell Niche Organizer Specification by Molecular Convergence of PLETHORA and SCARECROW Transcription Factor Modules. *Genes Dev.* **2018**, 32 (15–16), 1085–1100.
- (183) Nakayama, N.; Smith, R. S.; Mandel, T.; Robinson, S.; Kimura, S.; Boudaoud, A.; Kuhlemeier, C. Mechanical Regulation of Auxin-Mediated Growth. *Curr. Biol.* **2012**, 22 (16), 1468–1476.
- (184) Mathew, M. M.; Shanmukhan, A. P.; Varappambath, V.; Prasad, K. Protocol for Real-Time Imaging, Polar Protein Quantification, and Targeted Laser Ablation of Regenerating Shoot Progenitors in Arabidopsis. *STAR Protoc.* **2023**, 4 (2), 102184.
- (185) Salvi, E.; Rutten, J. P.; Di Mambro, R.; Polverari, L.; Licursi, V.; Negri, R.; Ioio, R. D.; Sabatini, S.; Ten Tusscher, K. A Self-Organized PLT/Auxin/ARR-B Network Controls the Dynamics of Root Zonation Development in Arabidopsis Thaliana. *Dev. Cell* **2020**, 53 (4), 431–443. e23.
- (186) Zhai, N.; Xu, L. Pluripotency Acquisition in the Middle Cell Layer of Callus Is Required for Organ Regeneration. *Nat. Plants* **2021**, 7 (11), 1453–1460.
- (187) Varappambath, V.; Mathew, M. M.; Shanmukhan, A. P.; Radhakrishnan, D.; Kareem, A.; Verma, S.; Ramalho, J. J.; Manoj, B.; Vellandath, A. R.; Aiyaz, M. Mechanical Conflict Caused by a Cell-Wall-Loosening Enzyme Activates de Novo Shoot Regeneration. *Dev. Cell* **2022**, 57 (17), 2063–2080. e10.
- (188) Hofmann, N. R. *The Importance of Being Absent: Auxin Minima Are Required for Axillary Meristem Formation*; American Society of Plant Biologists, 2014.
- (189) Abley, K.; Sauret-Güeto, S.; Marée, A. F.; Coen, E. Formation of Polarity Convergences Underlying Shoot Outgrowths. *eLife* **2016**, 5, e18165. <https://doi.org/10.7554/eLife.18165>.
- (190) Hamant, O. Shoot Meristem Progenitors Emerge from Mechanical Heterogeneities. *Dev. Cell* **2022**, 57 (17), 2043–2044.